UNIVERSITY OF CALIFORNIA SAN DIEGO
SAN DIEGO STATE UNIVERISTY

Catalytic Methodologies for Sulfenylation of Arenes and Tryptophan-Containing Peptides

A Dissertation submitted in partial satisfaction of the requirements
for the degree Doctor of Philosophy

in

Chemistry

by

Zachary Edahn Brown

Committee in charge:

University of California San Diego
Professor Joseph O'Connor
Professor Robert Pomeroy

San Diego State University
Professor Jeffrey L. Gustafson, Chair
Professor B. Mikael Bergdahl
Professor Marina Kalyuzhnaya

2025

The Dissertation of Zachary Edahn Brown is approved, and it is acceptable in quality and form for publication on microfilm and electronically.

Chair

University of California San Diego
San Diego State University

2025

DEDICATION

To my family for always being there for me and supporting me no matter what direction my life takes. To my loving fiancé Madeline for being my rock and roll. To my crazy dog Xena for always keeping me on my toes.

TABLE OF CONTENTS

LIST OF FIGURES

LIST OF TABLES

ACKNOWLEDGEMENTS

I want to start by thanking my family for always being my foundation and always lifting me up even through times that I have felt so low. Grad school has been an absolute journey. I have learned an unbelievable amount since I first walked on campus as a young grad student. I have learned more than I thought I would about myself. I want to thank Jeff for being patient with me and guiding me through this journey even though it has been less than typical. I appreciate your help and your advice along the way. If situations were different for me, I would have been out there in New York with you pioneering this new chapter in your career with you. Thank you for keeping me on, helping me from across the country, and for fighting for Beeta, Bahar, Mariam and I to have a space to finish our research. We owe you a six pack at least!

Thank you, Mom, for being the absolute rock in my life and pushing me to be the better person that I want to be. I appreciate you more than you could possibly know. It's about time I start paying you back for all you have done for me. I wouldn't be here standing the man I am today if it weren't for all the hard work and love you have put into me. Thank you, Dad, for being there for me and for being a strong role model, and for teaching me how to be tough when I need to be. You work so hard and yet you stay so cool. That's pretty sweet. You have helped me so much through the years and I can't thank you enough. I love you guys!

To Maddie my dear I love you and thank you for supporting me the last couple years. I wish we could have met sooner but hey the rest of our lives doesn't sound so bad. I am looking forward to starting this next chapter in our lives together and to start making new memories with you. Life is going to throw us some curve balls but I know we will hit them out of the park. I wouldn't be such a happy man if it weren't for you so thank you for being here with me, right where I need you. I love you!

I want to thank all my friends from San Diego and beyond for all fun we have had over the last many years. Thanks Daniel for always being there for me and especially for your guidance lately and your future guidance. I'm looking forward to joining the work life with you. Thanks Ryan for being the good guy that you are and for setting me straight when I needed it. Nic I miss you man I hope you're doing well and that your program is going well for you. I will never forget those years that we all had together. Love you guys!

Thank you Greg for your mentorship and for all your help over the last few years. You really made an impact on me and my research. It has been a pleasure working with you and getting to know you, and I hope we can one day work together again. Let's keep in touch and go on a hike soon!

Chapter 2, in part, is a reformatted reprint of the material as it appears in the following manuscript: Nalbandian, C. J.; Brown, Z. E.; Alvarez, E.; Gustafson, J. L Lewis Base/Bronsted Acid Dual-Catalytic C-H Sulfenylation of Aromatics *Org. Lett.* **2018**, *20* (11), 3211-3214. The dissertation author was the secondary investigator and author of this paper. Chapter 2, in part, contains unpublished material in which the dissertation author is the primary investigator and author of this material.

Chapter 3, in full, is currently being prepared for submission for publication of the material. Brown, Z. E.; Elliott, G.; Gustafson, J. L. Peptide Stapling Via Selective Sulfenylation of Tryptophan. The dissertation author was the primary researcher and author of this material.

VITA

2016 Bachelor of Science in Biochemistry, California State University Channel Islands

2025 Doctor of Philosophy in Chemistry, University of California San Diego/San Diego State University

PUBLICATIONS

1. Brown, Zachary E.; Elliot, Greg; Gustafson, Jeffrey L. Peptide Stapling Via Selective Sulfenylation of Tryptophan. *Manuscript in Progress.* **2025**

2. Cardenas, Mariel M.; Nguyen, Ashley D.; Brown, Zachary E.; Heydari, Beeta; Heydari, Bahar; Vaidya, S.; Gustafson, J. L. Atropisomerism as an inspiration for new chemistry. *Arkivoc*. **2021**, *i*, 20-47.

3. Nalbandian, Christopher. J.; Brown, Zachary. E.; Alvarez, Erik.; Gustafson, Jeffrey. L Lewis Base/Bronsted Acid Dual-Catalytic C-H Sulfenylation of Aromatics *Org. Lett.* **2018**, *20* (11), 3211-3214.

FIELD OF STUDY

Major Field: Chemistry (Organic)
Studies in Development of Sulfenylation Methodologies for Chemical Biology
Professor Jeffrey L. Gustafson

ABSTRACT OF THE DISSERTATION

Catalytic Methodologies for Sulfenylation of Arenes and Tryptophan-Containing Peptides

by

Zachary Edahn Brown

Doctor of Philosophy in Chemistry

University of California San Diego, 2025
San Diego State University, 2025

Professor Jeffrey L. Gustafson, Chair

Sulfur-based reactivity and peptide macrocyclization provide complementary opportunities for controlling molecular structure and function. In this work, we report a unified investigation spanning electrophilic aromatic sulfenylation, regioselective Lewis base catalysis, and the development of a tryptophan-directed peptide stapling platform. We first describe a mild and general Lewis Base/Brønsted acid system that promotes rapid C–H sulfenylation of arenes using N-thiosuccinimide reagents. Kinetic analysis reveals that electron-rich sulfide products

enable autocatalysis, whereas electron-poor systems require exogenous Lewis base catalysis. These findings inform the design of chiral indane-derived selenide catalysts that overcome innate para preference and deliver enhanced ortho selectivity, establishing that C–S bond formation can be directed through rational Lewis base tuning. Building on this mechanistic foundation, we next explore the unique chemical behavior of tryptophan, an electronically rich, structurally privileged, and interface-enriched amino acid, as a site-selective anchor for biomolecular modification. Leveraging its inherent C2 nucleophilicity, we introduce a metal-free Lewis base/Brønsted acid-catalyzed tryptophan sulfenylation strategy using PEG-based N-thiosuccinimide linkers to achieve *i,i+4* macrocyclization. This Trp–Trp stapling platform exhibits broad compatibility, preserves native cysteine and lysine residues, and effectively stabilizes α-helical structure across both established and unexplored peptide–protein interaction targets. Together, these studies provide new insights into electrophilic sulfenylation mechanisms, regioselective Lewis base catalysis, and the underused potential of tryptophan as a covalent handle, culminating in a versatile new approach for peptide stapling and molecular design.

Chapter 1

Introduction to Sulfenylation and the Importance of Tryptophan as a Powerful Biological Target

1.1 Abstract

Sulfur-based transformations and amino acid–specific reactivity represent two powerful and complementary frontiers in modern chemical research. Sulfenylation chemistry has advanced rapidly as a highly versatile method for constructing C–S bonds and accessing a broad landscape of sulfur-derived functional groups with profound implications for drug design, catalysis, and materials science. Its evolution from traditional electrophilic sulfenylating reagents to innovative metal-catalyzed, radical, and photochemical C–H activation strategies reflects the growing need for precise, efficient, and modular pathways to embed sulfur into complex molecular frameworks. In parallel, tryptophan has emerged as an equally compelling target whose indole-based structure imparts unique electronic, photophysical, and biological properties to proteins. Although rare in proteomes, tryptophan residues are selectively deployed by nature to mediate molecular recognition, electron transfer, and conformational control, making them valuable anchors for chemical modification, bioconjugation, and mechanistic exploration. Together, these two areas illustrate how deep understanding of heteroatom chemistry and amino acid–specific reactivity can enable precise manipulation of biomolecules and small molecules alike. By bridging advancements in selective sulfur installation with insights into the strategic use of tryptophan in biological systems, this combined perspective highlights emerging opportunities for the deliberate, site-specific modification of both synthetic and biological scaffolds. The intersection of sulfenylation methodologies with tryptophan-targeted chemistry offers a conceptual framework for designing next-generation molecular tools, therapeutic agents,

and materials that capitalize on the rich reactivity and functional importance of sulfur and indole chemistry.

1.2 Sulfenylation

Sulfenylation, the formation of carbon–sulfur (C–S) bonds by transfer of a sulfenyl fragment to an organic substrate, has become one of the most powerful and versatile transformations in modern synthetic chemistry. The significance of sulfenylation lies not only in the construction of thioethers but also in the access it provides to a wide family of sulfur-containing functional groups, sulfoxides, sulfones, sulfonamides, sulfenates, and heterocyclic motifs that play central roles in medicinal chemistry, agrochemicals, catalysis, and materials science[1,2]. Over the last two decades, advances in sulfur-based reagent design, C–H activation chemistry, and radical or photochemical pathways have dramatically expanded the scope and selectivity of sulfenylation reactions, enabling sulfur installation at virtually any molecular position, including unactivated C(sp^2)–H and C(sp^3)–H bonds[3–6]. Because sulfur is larger, more polarizable, and capable of more oxidation states than oxygen, the choice to sulfenylate a molecule, or etherify it, has profound implications for molecular shape, electronics, conformational control, and pharmacokinetics[7,8]. These unique features have made sulfur a privileged heteroatom in drug molecules, with approximately one quarter of FDA-approved small-molecule therapeutics containing at least one sulfur atom[9,10].

Historically, sulfenylation chemistry began with classical electrophilic sulfur reagents such as sulfenyl chlorides, disulfides, and thiols[11]. Sulfenyl chlorides in particular, though often reactive and unstable, provided straightforward routes to aryl and heteroaryl thioethers through electrophilic aromatic substitution[12]. However, their harshness and instability limited

applicability in complex-molecule synthesis. Modern sulfenylating reagents, such as N-thiosuccinimides, sulfonyl hydrazides, and sulfenyl ammonium salts, offer significantly improved stability, modularity, and safety[13–15]. Sulfonyl hydrazides, for instance, are now widely used because they are air-stable, odorless thiol surrogates that can generate electrophilic sulfur species under oxidative or radical conditions[16]. Their broad application to heteroarenes such as indoles, pyrroles, and benzothiophenes reflects the generality of sulfenylation methodologies[17].

A milestone in the evolution of sulfenylation chemistry is the development of direct C–H sulfenylation, eliminating the need for pre-functionalization. Transition-metal catalysis has enabled the C–H activation of arenes and heteroarenes adjacent to directing groups, where palladium[18], copper[19], iron[20], and ruthenium[21] complexes have been used to facilitate selective C–S bond formation. In particular, palladium-catalyzed sulfenylation of 2-arylpyridines has become a cornerstone transformation, relying on chelation-assisted C–H activation to deliver sulfides with predictable regioselectivity[22]. The ability to achieve C–H sulfenylation without metals is also noteworthy: metal-free conditions using hypervalent iodine reagents[23], peroxides[24], or photoredox catalysis[25] have dramatically reduced environmental and operational burdens.

Among heterocycles, indoles occupy a privileged position in sulfenylation chemistry due to the inherent nucleophilicity of their C3 position[26]. Early methods relied on sulfenyl chlorides or disulfides, but modern strategies employ thiol surrogates activated photochemically[27], electrochemically[28], or by radical initiators[29]. These advances have enabled late-stage functionalization of complex natural products and drug-like scaffolds bearing multiple competing nucleophilic sites. The resulting 3-sulfenylindoles are versatile building blocks with biological activities including antiviral, anticancer, anti-inflammatory, and enzyme-inhibitory properties[30,31]. Similar advances have been made in the sulfenylation of benzothiazoles[32],

quinolines[33], quinazolines[34], pyridines[35], and thiophenes[36], highlighting the broad reach of sulfenylation across aromatic systems.

The sulfenylation of C(sp^3)–H bonds presents greater challenges because of the inertness of aliphatic C–H bonds and the potential for overoxidation or undesired β-elimination. Nevertheless, photoredox catalysis has enabled α-C–H sulfenylation of amines[37], ethers[38], and carbonyl compounds[39]. Amine α-sulfenylation is particularly attractive, as the resulting α-thioamines serve as intermediates in alkaloid synthesis, enzyme inhibitors, and sulfur-containing pharmaceuticals[40]. Metal-catalyzed approaches have also emerged: copper catalysts enable benzylic sulfenylation[41], while iron-based catalysts, more sustainable and abundant, can mediate radical C–H abstraction pathways for aliphatic sulfenylation[42].

A compelling aspect of sulfenylation chemistry is the breadth of downstream transformations accessible after sulfur installation. Thioethers can be oxidized to sulfoxides or sulfones, providing dramatic changes in polarity, conformation, and hydrogen-bonding ability[43]. Sulfoxides introduce a stereogenic sulfur center, enabling chiral control and asymmetric synthesis[44]. Sulfones, powerful electron-withdrawing groups, can activate adjacent carbons toward deprotonation and alkylation[45]. Moreover, sulfur-containing intermediates can be converted into sulfonamides via oxidative or nucleophilic pathways, expanding their relevance in drug design, as sulfonamide groups often enhance binding affinity and metabolic stability[46]. The ability to generate sulfur heterocycles such as thiazoles, thiadiazoles, thiophenes, or benzothiazoles from sulfenylated precursors further underscores the synthetic richness provided by sulfur chemistry[47,48].

The choice to use sulfur rather than oxygen in a synthetic transformation is rooted in sulfur's atomic and electronic properties. Sulfur's larger covalent radius relative to oxygen leads

to longer C–S bonds than C–O bonds, imparting greater flexibility and allowing access to molecular conformations not readily attainable with oxygen[49]. Sulfur's high polarizability and the presence of diffuse 3p orbitals contribute to stabilizing soft interactions such as chalcogen bonding and σ-hole interactions[50], which can enhance protein–ligand binding[51]. Critically, sulfur's ability to access oxidation states from −2 to +6 enables a diversity of functional group transformations unmatched by oxygen chemistry [53].

These molecular traits explain sulfur's prevalence in pharmaceuticals. Penicillin and cephalosporins rely on a sulfur-containing bicyclic core essential for antibacterial activity[54]. Dapsone, a classic sulfone antibiotic, exemplifies the influence of the sulfone group on lipophilicity and metabolic stability[55]. Proton pump inhibitors such as omeprazole, esomeprazole, and lansoprazole are sulfoxides whose activity depends on redox behavior at sulfur[56]. Modern anticancer drugs, including sunitinib, imatinib, dasatinib, and erlotinib, contain sulfonamides or thioethers that contribute to kinase selectivity and potency[57]. Sulfur's role extends to antivirals, antidiabetics, antihypertensives, and CNS agents[58,59]. The widespread incorporation of sulfur motifs across therapeutic classes is a direct reflection of the structural diversity and tunability enabled by sulfenylation chemistry.

Sulfenylation also parallels biological processes, particularly protein S-sulfenylation, where cysteine thiols are oxidized to sulfenic acids under oxidative stress[60]. These transient species function as regulatory switches, modulating enzyme activity, redox signaling, and protein–protein interactions[61]. This synergy between synthetic and biological sulfur chemistry highlights sulfur's fundamental importance in chemical biology.

Overall, sulfenylation represents more than a functionalization strategy, it is a gateway to the full landscape of sulfur chemistry. Its value lies in enabling fine-tuned modulation of

physical, electronic, and biological properties, providing access to diverse functional groups, and supporting the development of sophisticated molecular architectures. As methods continue to evolve toward milder, more selective, and more sustainable conditions, particularly through photocatalysis, electrochemistry, flow chemistry, and metal-free oxidative strategies, sulfenylation will continue to expand its role in synthesis, drug discovery, and materials science.

1.3 Tryptophan

Tryptophan occupies a uniquely influential position in both chemistry and biology. As the most structurally complex of the 20 canonical amino acids, tryptophan contains an indole ring system that endows proteins with distinctive electronic, structural, and spectroscopic properties[63]. Although it is the rarest amino acid in proteomes, often comprising less than 1% of total residues, its scarcity is not a reflection of unimportance. Instead, tryptophan's rarity reflects its high biosynthetic cost, intrinsic chemical reactivity, and specialized functional roles in proteins[64]. Evolution has conserved tryptophan not for abundance, but for precision: when proteins require strong aromatic interactions, redox capabilities, intrinsic fluorescence, or well-defined binding elements, tryptophan is chosen deliberately and sparingly[65].

Chemically, the indole ring is highly functional. Its electron-rich aromatic π-system enables deep conjugation, strong polarizability, and capacity for noncovalent interactions unmatched by other amino acids. The indole engages in π–π stacking, cation–π interactions, hydrogen bonding, hydrophobic contacts, and radical stabilization[66]. These interactions underpin why tryptophan is disproportionately represented in protein–protein interfaces, receptor binding sites, and membrane interactions, despite its low overall abundance[67]. In many proteins, tryptophan residues serve as anchoring points, orienting ligands or stabilizing transition states.

This functional specificity has made tryptophan an attractive target for chemical modification, bioconjugation, and mechanistic studies[68].

Another major reason researchers target tryptophan is its distinctive optical behavior. Tryptophan absorbs strongly around 280 nm and is responsible for the intrinsic fluorescence of many proteins[69]. This fluorescence is highly sensitive to microenvironment polarity, steric constraints, and conformational changes, enabling tryptophan to act as a natural probe of protein folding, binding, and structural dynamics[70]. Mutational and spectroscopic studies have shown that single tryptophan residues can report on global protein motions due to their large dynamic range and sensitivity to quenching, making them invaluable in mechanistic enzymology and biophysical chemistry[71].

Tryptophan is also integral to biological redox chemistry. Its high oxidation potential allows it to form relatively stable radical intermediates, a feature exploited in enzymatic electron-transfer chains and photochemical signaling proteins[72]. Proteins such as photolyases, oxidases, and peroxidases contain evolutionary conserved tryptophan "wires" that shuttle charge across long distances[73]. This reactivity has inspired chemists to examine tryptophan as a target for redox-active tagging, site-selective oxidation, and photocatalytic modulation in biological environments[74]. The high susceptibility of tryptophan to oxidative modification under physiological stress has also made it a key biomarker in oxidative biology and inflammation studies[75].

Although multiple amino acids can undergo chemical modification, tryptophan's unique electronic structure makes it particularly intriguing for selective bioconjugation. Whereas lysine or cysteine modifications often alter protein charge or disrupt catalytic activity, tryptophan sits at the intersection of reactivity and functional neutrality. Its indole ring can participate in mild

electrophilic aromatic substitutions, radical additions, or photochemical transformations without compromising backbone integrity[76]. These features have inspired the development of tryptophan-selective labeling methods that rely on intrinsic indole nucleophilicity, controlled single-electron oxidation, or reagent-specific affinity for the aromatic π-system[77].

Tryptophan's rarity in proteins further enhances its value as a selective handle for chemical modification. With few residues available, selective targeting becomes easier and more predictable, reducing heterogeneity in labeling or conjugation experiments[78]. This has proven invaluable in site-specific protein modification, where installing affinity tags, fluorophores, or drug-linker systems at uniquely placed tryptophan sites enables high-resolution mechanistic and structural studies[79]. Beyond its structural role in proteins, tryptophan occupies a central position in metabolism. It is the precursor to serotonin, melatonin, tryptamine, and numerous kynurenine-pathway metabolites, linking tryptophan levels to mood regulation, immune tolerance, inflammation, and neurodegeneration[80]. Enzymes that process tryptophan, such as indoleamine 2,3-dioxygenase or tryptophan hydroxylase have thus become major drug targets in oncology and neuroscience[81]. Even outside mammalian systems, tryptophan-derived indole alkaloids and secondary metabolites play essential ecological and biochemical roles, highlighting the breadth of tryptophan-centered chemistry[82].

Despite extensive study, several conceptual and methodological areas remain underdeveloped. One such area is site-selective modification of tryptophan in folded proteins, where targeting a specific tryptophan among multiple residues remains challenging[84]. Similarly, while C2 and C3 indole modifications are well established, N1- and C7-specific derivatization remain far less understood, with only limited strategies available[85]. A deeper understanding of

how protein environments tune indole reactivity would enable more precise chemical tools and probes.

Perhaps the greatest conceptual frontier lies in covalent targeting of tryptophan in drug design. While cysteine and lysine dominate covalent inhibitor development due to their nucleophilicity, the indole ring could serve as an orthogonal and more selective anchoring point, if chemists can design electrophiles that react with tryptophan under biologically relevant conditions[88]. Overall, tryptophan's rarity, unique reactivity, electronic richness, and versatile functional roles make it far more than just another amino acid—it is a strategic element of protein architecture and an exceptional chemical target. Its ability to mediate structural stability, electron transfer, molecular recognition, and optical signaling ensures that whenever a protein requires precision, nature selects tryptophan. As chemical biology continues to evolve, tryptophan's exceptional properties guarantee that it will remain at the forefront of mechanistic exploration, probe development, and next-generation protein modification strategies.

1.4 References

(1) Petrillo, D. E.; O'Brien, A. G. Modern Electrophilic Sulfenylation Strategies. *Chem. Rev.* **2021**, *121*, 9710–9741.

(2) Chauhan, P.; Mahajan, S.; Enders, D. Organocatalytic Sulfenylation. *Chem. Rev.* **2014**, *114*, 8807–8864.

(3) Kumar, R.; Sharma, U. Transition Metal-Catalyzed C–H Sulfenylation. *Chem. Soc. Rev.* **2021**, *50*, 11065–11125.

(4) Tang, S.; Wang, Z. Metal-Free C–H Sulfenylation. *Org. Lett.* **2018**, *20*, 6003–6007.

(5) Hou, S.; Peng, Y. Radical-Mediated Sulfur Transfer. *Angew. Chem. Int. Ed.* **2020**, *59*, 20195–20200.

(6) Shen, X.; Wang, J. Photoredox Sulfenylation. *Chem. Sci.* **2019**, *10*, 3110–3115.

(7) Ilardi, E. A.; Vitaku, E.; Njardarson, J. T. Data on Sulfur in Drugs. *J. Med. Chem.* **2014**, *57*, 2832–2842.

(8) Mullard, A. Trends in Sulfur-Based Drugs. *Nat. Rev. Drug Discov.* **2018**, *17*, 531–532.

(9) Vitaku, E.; Smith, D. T.; Njardarson, J. Analysis of FDA Drugs. *J. Med. Chem.* **2014**, *57*, 10257–10274.

(10) Feng, M.; Tang, B.; Liang, S. H.; Jiang, X. Sulfur in Drug Discovery. *Curr. Top. Med. Chem.* **2016**, *16*, 1200–1216.

(11) Kergomard, A. Sulfenyl Chlorides in Synthesis. *Tetrahedron* **1970**, *26*, 3161–3172.

(12) Oae, S.; Shinhama, K. Electrophilic Sulfenylation. *Org. React.* **1963**, *13*, 91–157.

(13) Chen, X.; Yi, H.; Lei, A. N-Sulfenylsuccinimides. *J. Am. Chem. Soc.* **2017**, *139*, 9094–9097.

(14) Shao, B.; Yuan, C. Sulfenyl Ammonium Salts. *Org. Lett.* **2017**, *19*, 62–65.

(15) Deng, Q.; Gong, J. Sulfonyl Hydrazides as Sulfur Sources. *J. Org. Chem.* **2018**, *83*, 1465–1475.

(16) Yu, X.; Chen, F. Sulfonyl Hydrazide Mechanisms. *JOC* **2019**, *84*, 6425–6436.

(17) Paira, M. Indole Sulfenylation Methods. *Asian J. Chem.* **2022**, *34*, 1213–1222.

(18) Lyons, T. W.; Sanford, M. S. Pd C–H Activation. *Chem. Rev.* **2010**, *110*, 1147–1169.

(19) Zhang, G.; Huang, H. Cu-Catalyzed Sulfuration. *JACS* **2013**, *135*, 12446–12449.

(20) Yoshikai, N. Fe-Catalyzed C–S Bond Formation. *Acc. Chem. Res.* **2019**, *52*, 2659–2670.

(21) Ackermann, L. Ru-Catalyzed C–H Activation. *Chem. Rev.* **2011**, *111*, 1315–1345.

(22) Engle, K. M.; Mei, T.-S. Directed C–H Activation. *ACS Catal.* **2012**, *2*, 89–119.

(23) Kita, Y. Iodine(III) Sulfenylation. *Chem. Commun.* **2015**, *51*, 994–1007.

(24) Xia, X.; Chen, J. Peroxide-Induced Sulfenylation. *Org. Biomol. Chem.* **2018**, *16*, 5713–5720.

(25) Romero, N.; Nicewicz, D. Photoredox Catalysis. *Chem. Rev.* **2016**, *116*, 10075–10166.

(26) Bandini, M. Indole Functionalization. *Chem. Rev.* **2014**, *114*, 1827–1847.

(27) Ye, Y.; Sanford, M. Visible-Light Sulfenylation. *JACS* **2013**, *135*, 4648–4651.

(28) Hicks, J.; Lam, K. Electrochemical Sulfenylation. *Angew. Chem.* **2016**, *55*, 14492–14496.

(29) Lei, A. Radical C–H Sulfenylation. *Nat. Commun.* **2018**, *9*, 1805.

(30) Gribble, G. Bioactive Indoles. *Chem. Soc. Rev.* **1999**, *28*, 335–346.

(31) Menichincheri, M. Indole Sulfides in Medicinal Chemistry. *J. Med. Chem.* **2016**, *59*, 4389–4404.

(32) Wu, W.; Jiang, H. Benzothiazole Sulfenylation. *Chem. Rev.* **2012**, *112*, 1747–1802.

(33) Seregin, I.; Gevorgyan, V. Quinolines in C–H Activation. *Chem. Soc. Rev.* **2007**, *36*, 1173–1193.

(34) Hesp, K. D.; Love, J. Quinoxalines and Sulfur. *JACS* **2015**, *137*, 1559–1565.

(35) Fischer, C.; Fu, G. Pyridine Functionalization. *JACS* **2005**, *127*, 4594–4595.

(36) Gulevich, A. Thiophene Chemistry. *Org. Lett.* **2012**, *14*, 1176–1179.

(37) Nicewicz, D. Radical α-Sulfenylation. *JACS* **2015**, *137*, 11270–11273.

(38) Knowles, R. Photoredox α-Oxy Sulfenylation. *Nat. Chem.* **2017**, *9*, 119–122.

(39) Chen, F.; Xiao, F. Carbonyl α-C–H Sulfenylation. *Org. Lett.* **2016**, *18*, 2722–2725.

(40) Lavilla, R. Thioamine Synthesis. *Chem. Rev.* **2011**, *111*, 3314–3374.

(41) Burns, N. Copper Benzylic Sulfenylation. *JACS* **2014**, *136*, 7223–7226.

(42) Iron Radical Methods. *Chem. Sci.* **2020**, *11*, 12070–12077.

(43) Bentley, R. Sulfoxides and Sulfones. *Chem. Rev.* **2005**, *105*, 677–682.

(44) Denmark, S.; C-S Stereocenters. *Acc. Chem. Res.* **2008**, *41*, 1486–1499.

(45) Liu, G. Sulfone Activation. *Adv. Synth. Catal.* **2019**, *361*, 170–184.

(46) Barrow, A. Sulfonamide Drug Chemistry. *J. Med. Chem.* **2019**, *62*, 10412–10429.

(47) Wipf, P. Thiazole Synthesis. *Chem. Rev.* **2002**, *102*, 1737–1760.

(48) Hall, D. Thiophene and Thiadiazole Methods. *Chem. Rev.* **2020**, *120*, 2879–2949.

(49) Huheey, J. Sulfur Properties. *Inorganic Chemistry*; Harper, **1993**.

(50) Politzer, P. Chalcogen Bonding. *J. Mol. Model.* **2017**, *23*, 197.

(51) Vargas-Bernal, R. Sulfur Interactions in Proteins. *Biochemistry* **2016**, *55*, 1870–1883.

(52) Martin, Y. Lipophilicity of Sulfur Groups. *J. Med. Chem.* **2005**, *48*, 287–298.

(53) Clayden, J. Organosulfur Mechanisms. *Chem. Rev.* **2011**, *111*, 6553–6569.

(54) Frère, J.-M. Penicillin Chemistry. *J. Antimicrob. Chemother.* **1995**, *35*, 1–19.

(55) Coleman, M. Dapsone Pharmacology. *J. Clin. Pharmacol.* **2001**, *41*, 719–732.

(56) Shin, J. Omeprazole Mechanism. *J. Clin. Gastroenterol.* **2013**, *47*, 543–548.

(57) Dar, A.; Imatinib and Sulfonamides. *Cancer Res.* **2011**, *71*, 636–645.

(58) Pushpakom, S. Thiazide Drugs. *Nat. Rev. Drug Discov.* **2019**, *18*, 41–58.

(59) De Clercq, E. Sulfur in Antivirals. *Med. Res. Rev.* **2013**, *33*, 1215–1270.

(60) Poole, L. Protein Sulfenylation. *Annu. Rev. Pharmacol.* **2015**, *55*, 429–457.

(61) Paulsen, C. Sulfenic Acids in Biology. *Nat. Chem. Biol.* **2012**, *8*, 57–64.

(62) Leonard, S. Redox Drug Design. *Chem. Sci.* **2019**, *10*, 10390–10400.

(63) Watanabe, K.; Schmidt, M. Tryptophan's Chemical Properties. *Chem. Rev.* **2020**, *120*, 1427–1512.

(64) Jordan, F.; Berry, A. Biosynthetic Cost of Aromatic Amino Acids. *Biochemistry* **2002**, *41*, 231–239.

(65) Liao, S.; Seebeck, F. Biological Roles of Tryptophan. *Biochemistry* **2017**, *56*, 3565–3574.

(66) Dougherty, D. Cation–π Interactions in Biology. *Acc. Chem. Res.* **2013**, *46*, 885–893.

(67) Bowie, J. Protein–Protein Interface Aromatic Hotspots. *Nat. Rev. Mol. Cell Biol.* **2001**, *2*, 790–796.

(68) Porter, N. Chemical Targeting of Tryptophan. *Biochem. J.* **2018**, *475*, 1231–1249.

(69) Lakowicz, J. Tryptophan Photophysics. *Principles of Fluorescence Spectroscopy*; Springer, **2006**.
(70) Vivian, J.; Callis, P. Tryptophan Fluorescence Sensitivity. *Biophys. J.* **2001**, *80*, 2093–2109.

(71) Eftink, M. Fluorescence Probes in Protein Folding. *Biophys. Chem.* **1997**, *62*, 53–66.

(72) Aubert, C. Tryptophan Radicals in Enzymes. *Acc. Chem. Res.* **2004**, *37*, 798–805.

(73) Stubbe, J. Long-Range Electron Transfer. *Chem. Rev.* **2003**, *103*, 2167–2201.

(74) Ravetz, B.; Knowles, R. Radical Activation of Indoles. *JACS* **2018**, *140*, 11202–11209.

(75) Davies, M. Oxidative Modification of Tryptophan. *Free Radic. Biol. Med.* **2016**, *100*, 105–115.

(76) Francis, M. Tryptophan-Selective Chemistries. *JACS* **2018**, *140*, 15078–15088.

(77) Itoh, T. Indole-Specific Bioconjugation Reagents. *Chem. Commun.* **2019**, *55*, 1183–1186.

(78) Chalker, J.; Davis, B. Advantages of Rare Residue Labeling. *JACS* **2011**, *133*, 17–19.

(79) Boutureira, O.; Bernardes, G. Protein Modification Strategies. *Chem. Rev.* **2015**, *115*, 2174–2195.

(80) Richard, D. Tryptophan Metabolic Networks. *Nat. Rev. Mol. Cell Biol.* **2009**, *10*, 23–35.

(81) Platten, M. IDO1 and Immune Suppression. *Nat. Rev. Cancer* **2019**, *19*, 385–398.

(82) Hayaishi, O. Indole and Kynurenine Pathways. *PNAS* **1971**, *68*, 264–267.

(83) Hildebrand, P. Indole Reactivity in Protein Microenvironments. *Biochemistry* **2014**, *53*, 4147–4160.

(84) Bode, J. Site-Selective Protein Modification Challenges. *Curr. Opin. Chem. Biol.* **2019**, *52*, 88–97.

(85) Korwar, S. Less-Explored Indole Positions. *Tetrahedron* **2020**, *76*, 130902.

(86) Gazit, E. Aromatic Peptides in Materials Chemistry. *Nat. Chem.* **2014**, *6*, 17–24.

(87) Amdursky, N. Tryptophan-Based Bioelectronics. *Adv. Mater.* **2017**, *29*, 1604423.

(88) Singh, J. Covalent Target Design. *Nat. Rev. Drug Discov.* **2011**, *10*, 307–317.

(89) Thorn-Seshold, O. Photoactivated Indole Targeting. *Chem. Sci.* **2019**, *10*, 10675–10682.

Chapter 2

Lewis Base/Bronsted Acid Dual Catalyzed Sulfenylation of Aromatics

2.1 Abstract

A Lewis base/Bronsted acid catalyzed aromatic sulfenylation is reported. These studies demonstrated that the incorporation of electron-rich sulfenyl groups proceeded in the absence of Lewis base, with kinetic studies indicating an autocatalytic mechanism. The incorporation of electron-poor sulfenyl groups demonstrated little autocatalysis necessitating the use of Lewis base. This method proved amenable to diverse arenes and heterocycles and was effective in the context of the late-stage functionalization of biologically active small molecules. These studies show further application of this chemistry towards regioselective sulfenylation of phenol, demonstrating ortho selectivity through the use of chiral Lewis base catalysts.

2.2 Introduction

Aryl and Alkyl sulfides are common motifs in drug discovery[1–3] and have seen use in polymer[4] and synthetic chemistry.[5–7] As such, the formation and transformation of carbon sulfur (C-S) bonds has recently received significant attention.[8,9] Typically, the introduction of aryl or alkyl sulfides has been achieved through cross-couplings via metal catalysis.[10–12] However, more recently, aromatic (C-H) sulfenylation, has been achieved via electrophilic aromatic substitution (S_EAr). Aromatic sulfenylation via S_EAr was originally achieved via sulfenyl halide intermediates generated in situ, however these methods can often result in a mixture of halogenated and sulfenylated products.[13,14] More recently, several groups have found sulfenyl halides can be generated in situ from N-thiosuccinimides using $MgBr_2$, however these methods

can suffer from a reliance on elevated temperatures, and often only work on the most electron-rich aromatics such as indoles.[15–18] In a recent advance, aromatic sulfenylation of arenes was achieved by employing super-stoichiometric quantities of trifluoroacetic acid (tfa) to activate N-thiosuccinimides, however the harshness of these conditions can limit the substrate scope to electron-rich arenes that are free of acid sensitive groups (Figure 2.1A).[19]

Recently, our lab disclosed a bifunctional catalyst consisting of a Lewis basic thiourea conjugated to a Bronsted acid that was able to affect the sulfenylation of aromatics under mild conditions,[20] however the scope of the reaction was limited to electron-rich azaheterocycles. Based on mechanistic studies from that work we hypothesized that sulfide and selenide ethers, which have been used as catalysts for the sulfenofunctionalization of alkenes,[21–25] might prove to be a more efficient catalyst as there would be no mechanism to stabilize the putative Lewis base/sulfenium adducts. The destabilized adducts would be expected to be more electrophilic and

thus perhaps more amenable to less electron-rich aromatics.

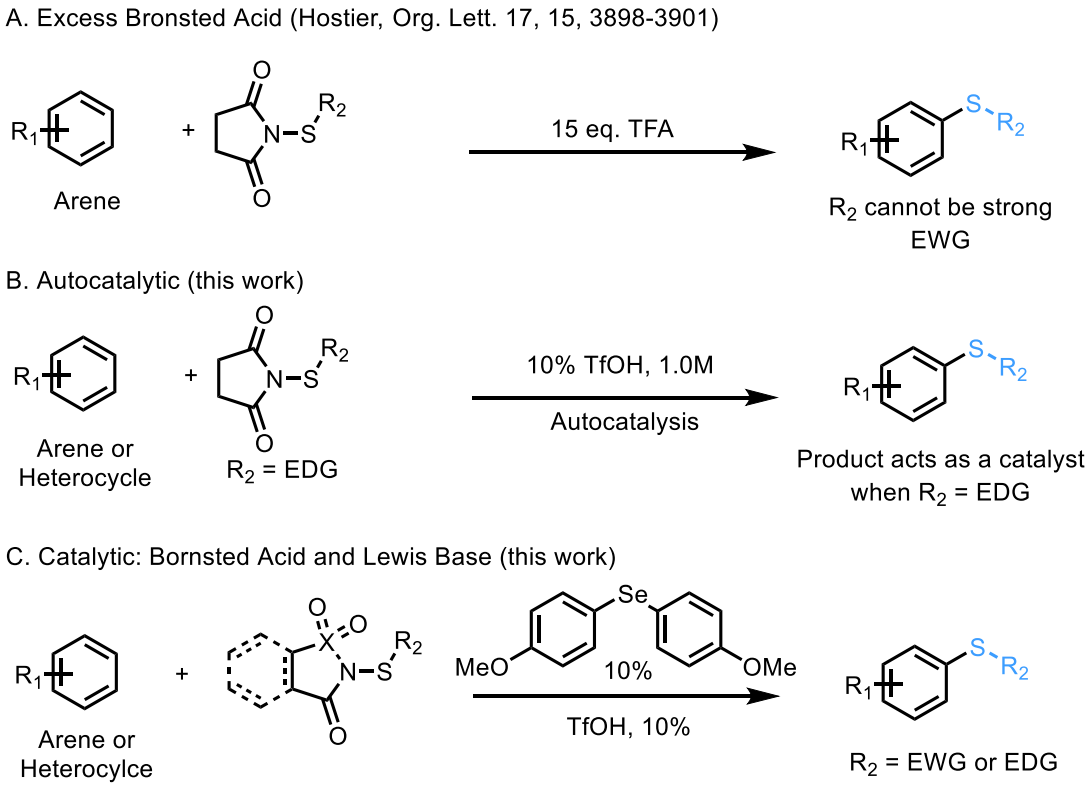

Figure 2-1 A.) Excess Bronsted acid sulfenylation of Arenes B.) Autocatalytic profile of sulfenylation C.) Catalytic: Bronsted acid and Lewis base sulfenylation.

2.3 Results and Discussion

We began our studies by evaluating different Lewis bases in the absence or presence of different acids for the sulfenylation of anisole (**1**) with reagent **2a** which possessed a methyl group that could be used as a handle to monitor the reaction conversion by ^{1}H NMR. We observed no reaction in the absence of catalyst (Table 2.1, entry 1), with 1 equivalent of tfa (Table 2.1, entry 2), in the presence of triphenylphosphine selenide with 1.0 equivalent of tfa (Table 2.1, entry 3),[20] or in the presence of diarylselenide **3** in the absence of tfa (Table 2.1 entry 4). Conversely, when catalyst **3** was combined with 1 equivalent of tfa, we observed good conversion to **4** at 6 hours (Table 2.1, entry 5).

Table 2-1 Optimization of reaction conditions with selenoether catalyst

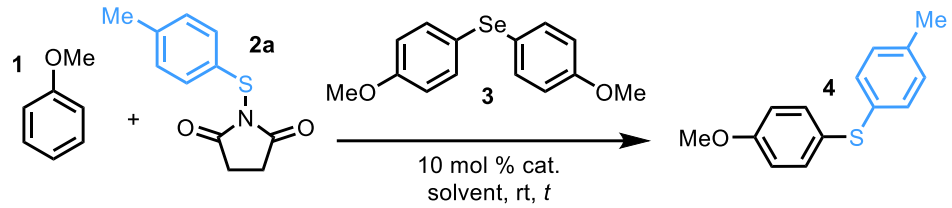

entry	catalyst	additive	molarity, M	time	[a]yield, %
1	none	none	0.2	6 h	0
2	none	1 equiv tfa	0.2	6 h	0
3	$SePPh_3$	1 equiv tfa	0.2	6 h	0
4	3	none	0.2	6 h	0
5	3	1 equiv tfa	0.2	6 h	82
6	3	1 equiv tfa	0.5	1 h	83
7	3	1 equiv tfa	1.0	10 min	88
8	3	10 mol % TfOH	1.0	10 min	89[b]
9	none	10 mol % TfOH	1.0	10 min	90[b]
10	none	1 equiv tfa	1.0	10 min	1
11	none	1 equiv tfa	1.0	3 h	85
12	4	1 equiv tfa	1.0	1 h	95

[a]Percent conversion by NMR represents an average of 3 trials using tms as an internal standard. Reactions were performed on 0.12 mmol, 0.3, or 0.6 mmol scale of **1** in 0.6 mL of $CDCl_3$.
[b]Isolated yield using $CHCl_3$ as solvent.

This could be improved by increasing the reaction concentration up to 1.0 M (Table 2.1, entry 7) to give nearly complete conversions on the minute time scale. Next, we sought to determine the effect of the strength of the acid additive, finding the combination of **3** with catalytic triflic acid also resulted in near complete conversion in 10 minutes (Table 2.1, entry 8). Surprisingly, 10 mol % triflic acid, in the absence of Lewis base also effected sulfenylation on a similar time scale. This led us to take a closer look at the reactions employing 1 equivalent of tfa without **3** at 1.0 M, wherein we observed no conversion to **4** at 10 minutes (Table 2.1, entry 10); however, near complete conversion at 1.0 M concentration took place after 3 hours (Table 2.1 entry 11). This lead us to investigate the role of product **4** in the reaction. When 10 mol % **4** is added as a catalyst (Table 2.1, entry 12), the reaction is notably faster than with no catalyst

yielding a conversion of 95% after 1 hour. Taken together this data suggests that while selenide ethers are more efficient catalysts, the resulting product sulfide, which is itself a Lewis base, can also catalyze the reactions; thus the reactions occurring in the absence of **3** are likely proceeding autocatalytically. To probe the potential for autocatalysis we performed preliminary kinetics experiments in which the reaction was monitored at three-minute increments by ^{1}H NMR with 1 equivalent tfa in the absence or presence (Figure 2.1) of catalyst **3**. As we suspected, the reaction without **3** displayed a considerable lag time before the rate picked up, indicative of autocatalysis. Conversely, the reaction with 10 mol % **3** displayed no lag time and was complete significantly sooner. While we were unable to obtain kinetics using triflic acid due to the short reaction time not being amenable to NMR kinetics, we feel that it is probable that autocatalysis is also a factor in this case.

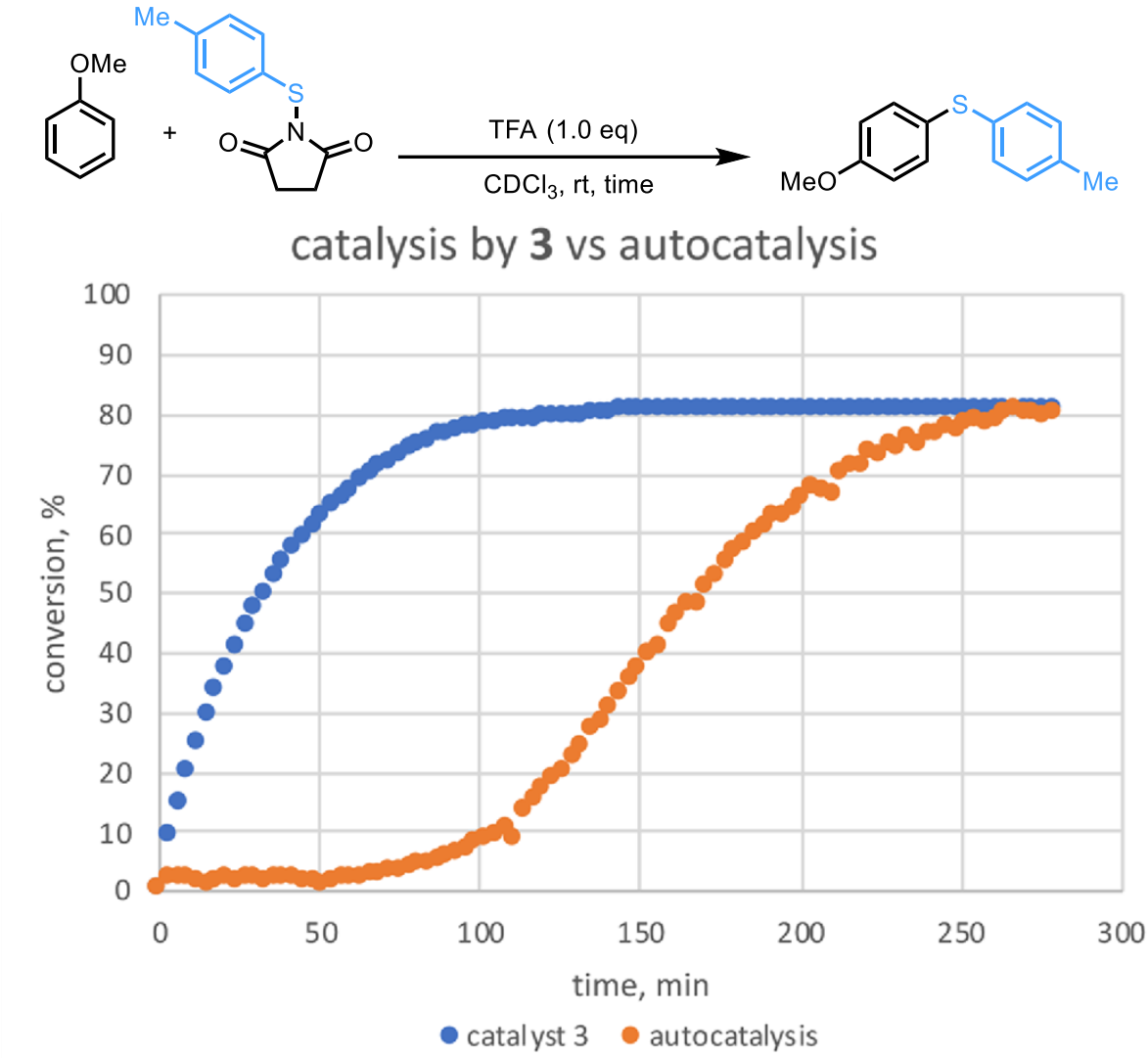

Figure 2-2 Catalyst **3** kinetics were obtained using conditions from Table 2.1 entry 10. Autocatalysis kinetics were obtained using conditions from Table 2.1 entry 6.

Next, we sought to evaluate the sulfenylation of different aromatics using reagent **2a** both in the presence and absence of **3** (Figure 2.3). Anisole (**1**), phenol, mesitylene, and 2-naphthol were all sulfenylated cleanly on the minute time scale using 10 mol % triflic acid, with the conversion being nearly indistinguishable with or without **3**. On the other hand, acetanilide, which is less electron-rich than the other evaluated substrates,[26] did display a dependence on

catalyst, as the corresponding product **8** was only observed in the presence of Lewis base catalyst **3**.

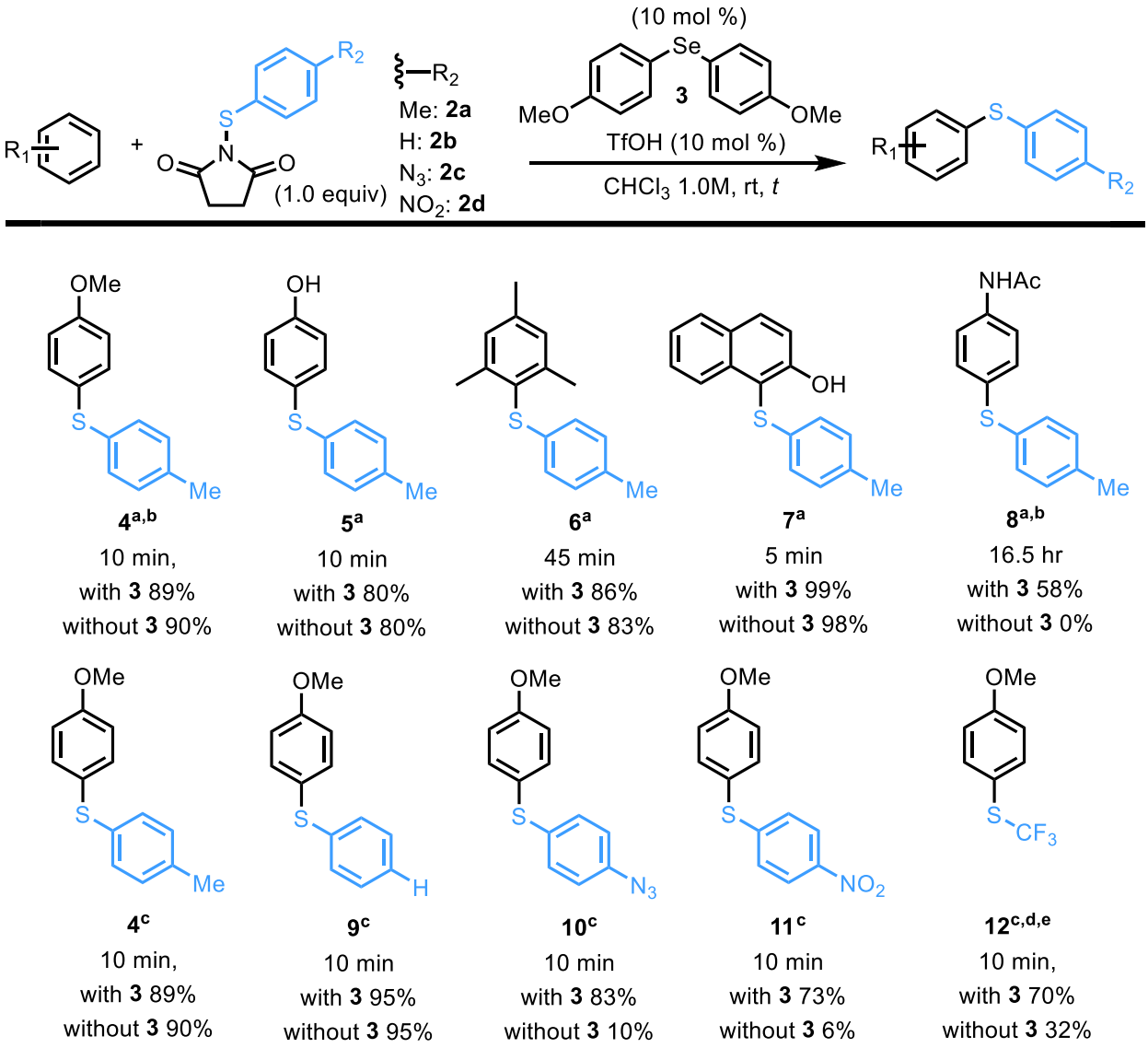

Figure 2-3 Comparison of several aromatic substrate classes with **3** and without **3**. [a]Isolated yield. [b]1.2 equiv sulfenylation reagent. [c]Conversions determined by ^{1}H NMR. [d]0.25 equiv TfOH. [e]Reagent **2e** was used.

We next set out to investigate the electronic effect of the substitution off the sulfur in the sulfenylation reagent. We accomplished this by evaluating the sulfenylation of **1** by ^{1}H NMR with sulfenylation reagents of varying electronic properties. Electron-rich reagents (**2a** and **2b**)

showed no difference in conversion to products (**4** or **9**) with or without **3**. When more electron-poor sulfenylation reagents (**2c**, **2d**, and **2e)** were used we observed a significant increase in conversion with **3**. For example, when **2c** is used we observe 83% sulfenylation to **10** in the presence of 10 mol % **3**, however only 10% conversion at the same time point without **3**. Similarly, with **2d** we observe 73% conversion to **11** with **3** and only 6% without **3**, and with **2e** we observe 70% conversion with catalyst and 32% without. These results can be justified as the products that possess electron-withdrawing groups (**10**, **11**, **12**) will have attenuated Lewis basicity leading to lessened autocatalysis.

We next sought to define the substrate scope of the selenide ether catalyzed sulfenylation reaction employing electron-poor N-thiosuccinimide reagents **2c** and **2e** (Figure 3.4). Reagent **2c** was chosen as the azido group possesses a wide range of applications, particularly those related to bioorthoganol conjugation chemistry.[27] Reagent **2e** was chosen as the SCF_3 group is becoming increasingly employed by medicinal chemists to modulate the lipophilicity and bioavailability of lead compounds, and as such the late-stage introduction of the SCF_3 group has become a sought-after strategy in synthetic chemistry.[28–30] The trends from Figure 2.3 proved to hold quite well across several different classes of aromatics, as we observed a significant increase in conversion when catalyst **3** was employed for each substrate evaluated. For example, in the absence of catalyst, less than 10% conversion was observed using **2c** for the sulfenylation of **1**, phenol, mesitylene, or the venerable NSAID naproxen. Conversely, the addition of 10 mol % **3** allowed for the isolation of the corresponding sulfides **10**, **13**, **14**, and **15** in yields ranging from 76-84% in under an hour.

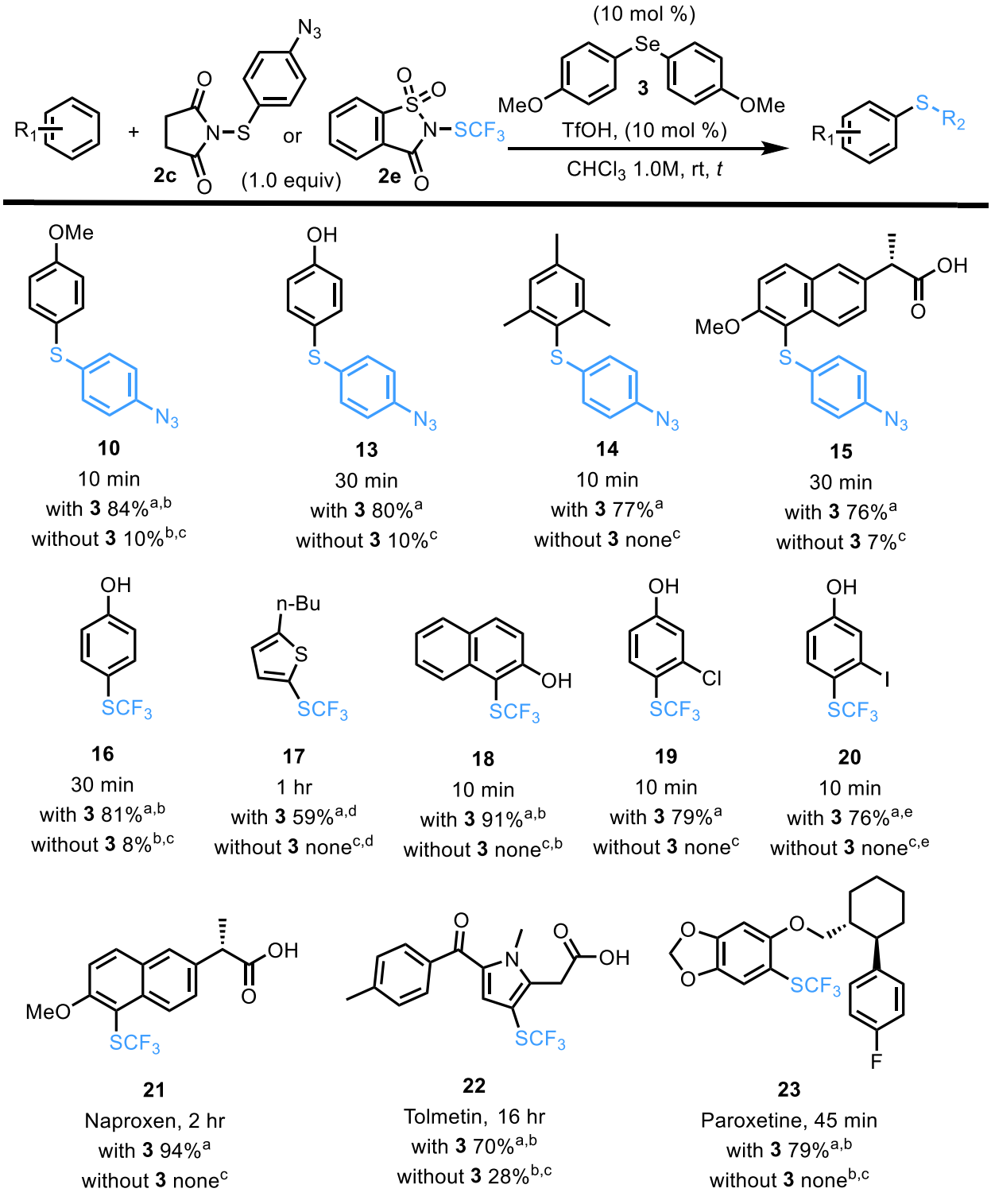

Figure 2-4 Substrate scope of trifluoromethylthiolation. [a]Isolated yield. [b]1.2 equiv **2c** or **2e**. [c]Conversions determined by ^{1}H NMR. [d]1.05 equiv **2e**. [e]Toluene was used as solvent.

The incorporation of the SCF_3 group using **2e** displayed a similar, if not more marked trend. Phenol derivative **16**, was isolated in 81% when 10 mol % **3** was employed and only 8% without **3**. Trifluoromethylthiolated thiophene **17** was isolated in 59% with 10 mol % **3** while we observed no conversion without **3**. Similarly, naphthol **18**, and phenol derivatives **19**, and **20** were isolated in 91%, 79%, and 76% yields, respectively with **3**, while each showed no conversion without **3**. Naproxen derivative **21** was also cleanly trifluoromethylthiolated in 94% with **3** while showing no conversion without **3**. Tolemetin another FDA-approved NSAID drug commonly used to treat pain from arthritis was functionalized in 70% yield in the presence of **3** however displayed a larger background reaction in the absence of **3** (28%).

Overall, we found this chemistry to be amenable to a wide range functional groups including phenols, carboxylic acids, heterocycles and protected amines. Free amines, however presented a problem, as we would often isolate *N*-sulfenylated products. This can be overcome by protecting the amine as we did with the FDA-approved selective serotonin reuptake inhibitor (SSRI) paroxetine, wherein we found mesylated paroxetine cleanly sulfenylated allowing for the isolation of **23**, in 79% yield with 10 mol % **3**, while we observed no conversion in the absence of **3**. In general, the substrates that reacted significantly in the absence of Lewis base were more electron-rich, and thus more innately reactive. Despite this, the fact that the resultant products (*i.e.* **12**, **22**) would be more Lewis basic and thus possess the potential for greater autocatalysis should not be overlooked.

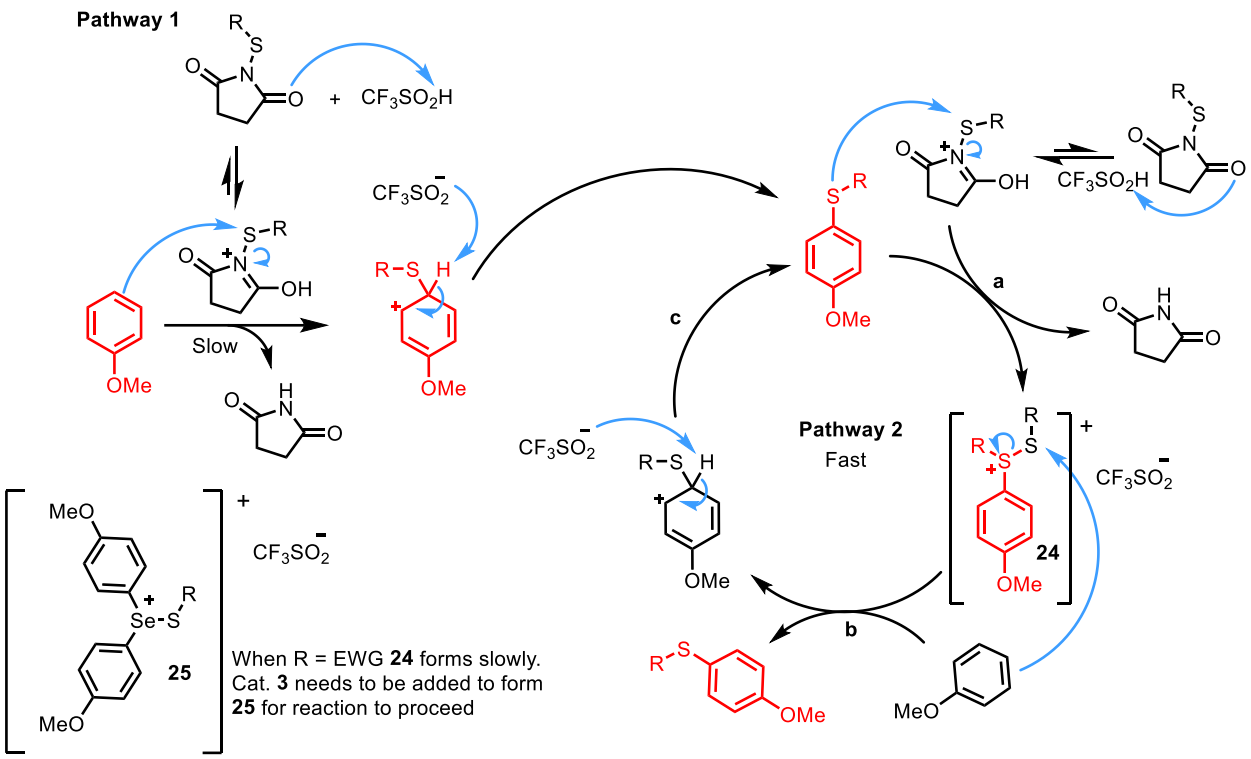

Figure 2-5 Mechanistic proposal for autocatalysis

The mechanistic proposal in Figure 2.5 summarizes our findings in this letter. The first pathway presented, pathway 1, is an acid-mediated mechanism where product formation happens slowly representing the lag period in the kinetic profile in Figure 2.2. When enough product has formed a second pathway, pathway 2, that involves Lewis base autocatalysis drives the reaction to completion represented by the dramatic increase of rate later on in the reaction. When the formed product is less electron-rich it will possess attenuated Lewis basicity and thus lessened autocatalysis, which can be overcome by the addition of a sufficiently Lewis basic catalyst such as **3**.

Following this work, we realized lack of regio selective control currently present in sulfenylation literature and wanted to expand on this field[21-25]. Statistically the ortho position

should be the preferred location due to there being twice as many reactive sites when compared

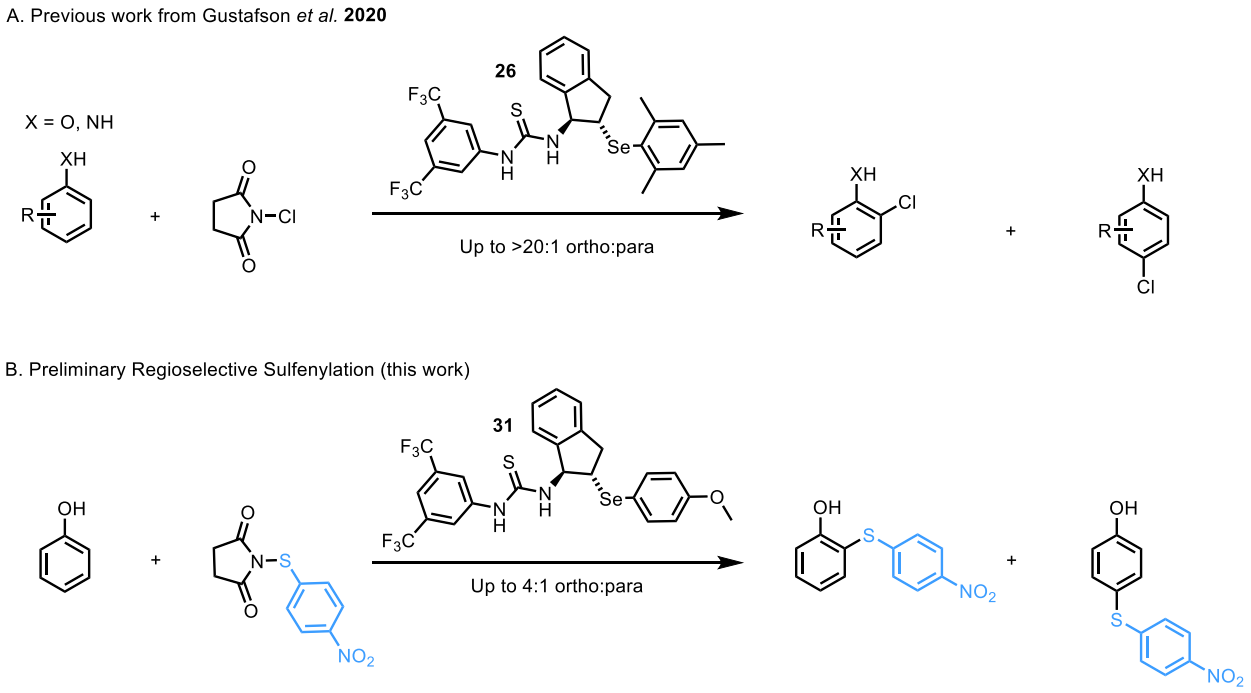

Figure 2-6 Previous work from the Gustafson lab and this work

to the para position. Although, due to steric hinderance the para site is the more reactive site. Our selenide ether catalyst **3** is nonselective so it tends to avoid the steric bulk and instead reacts at the para position. This is not due to control but purely due to the lack of steric hinderance about the para position. We wanted to design a catalyst that orients and controls the substrate and sulfenylating reagent to overcome steric hinderance and selectively sulfenylate at the ortho position.

A study recently published by the Gustafson lab,[31] illustrated in Figure 2.6**,** shows the ortho selective chlorination of phenols and anilines using a thiourea indane based selenide catalyst. This work was inspired by Zhao and coworkers[32] in which they were able to utilize

similar 1-amino indanol based catalysts in the context of diverse electrophilic olefin

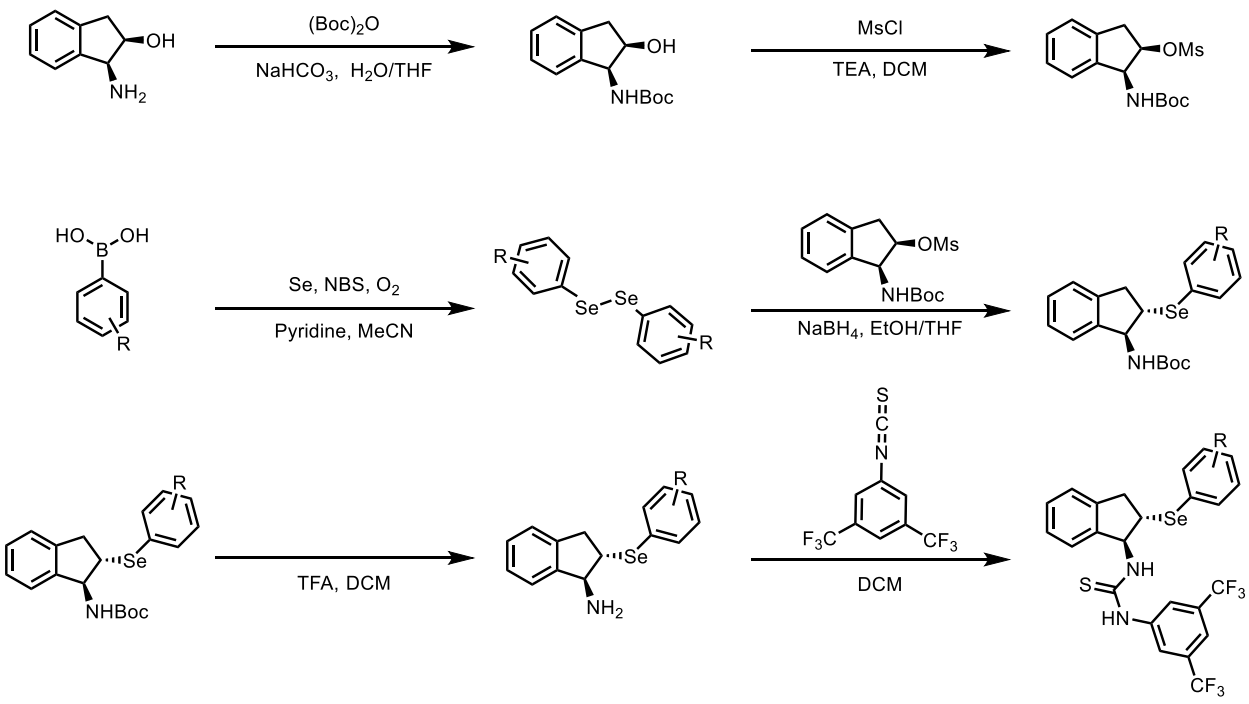

Figure 2-7 Synthetic strategy for the indane based selenoether catalysts

funcionalizations[32]. Andrew Dinh from the Gustafson group showed that with the use of a chiral seleno-indane based catalyst **26** he was able to regioselectively chlorinate the ortho position of a large variety of phenols and anilines with an ortho:para selectivity of greater than 20:1[31]. The method for this chemistry was Lewis base catalyzed electrophilic aromatic substitution using N-chlorosuccinime as the chlorinating agent. With this reactivity and similar chemistry to our own, we thought that this chemistry could potentially translate into regioselective sulfenylation of phenol. The synthetic strategy for these indane based catalysts is shown in Figure 2.7 starting from 1-amino indanol. With boc and mesyl protection the indanol is activated for nucleophilic attack from a reduced diselenide. The diselenide can be afforded through a wide variety of boronic acids. The resulting selenoether is deprotected with TFA and allowed to react with the isothiocyanate to yield the chiral indane based selenide catalysts.

When theorizing the conditions for this regioselective sulfenylation we had to carefully select the sulfenylating reagent. As shown in Figure 2.3, some of these sulfenylating reagents can induce autocatalysis with the product acting like an activated Lewis base catalyst. This had to be avoided so that it would not skew the measured ortho selectivity of the reaction as the sulfenylated product would act as a non-selective para dominant catalyst. With this thought we needed to choose a sulfenylating reagent that would deactivate the product and decrease the likelihood of the product acting as a Lewis base catalyst. The SCF_3 reagent seemed like a good choice but showed inconsistency with NMR reaction studies. We decided to go with the NO_2 reagent because it was a bench stable electron withdrawing sulfenylating reagent that showed consistent results when performing NMR studies.

These reactions were carried out in NMR tubes, so we took an initial NMR spectra of the reactions before the catalyst was added and then follow-up NMR spectra of the reaction after the chemistry was complete, using TMS as an internal standard. Early in the study, the ortho and para compounds were separated and purified to determine if there were chemical shifts that we could accurately measure from the crude reaction mixture. The para product would only show two unique aromatic phenol proton shifts due to its symmetry whereas the ortho selected product would show four unique phenol aromatic proton shifts. Based on the NMR data we concluded that a doublet at 7.53 ppm for the ortho product and a doublet at 6.93 ppm for the para product could be clearly measured to compare relative ortho:para selectivity of the catalyst. Phenol and the sulfenylating reagent were weighed into the NMR tube, diluted in $CDCl_3$ and stock solutions of the Lewis base catalyst and TFOH were pipetted into the tube. The NMR tube was capped shaken and allowed to react for 18 hours.

Table 2-2 Optimization for regioselective sulfenylation of phenol

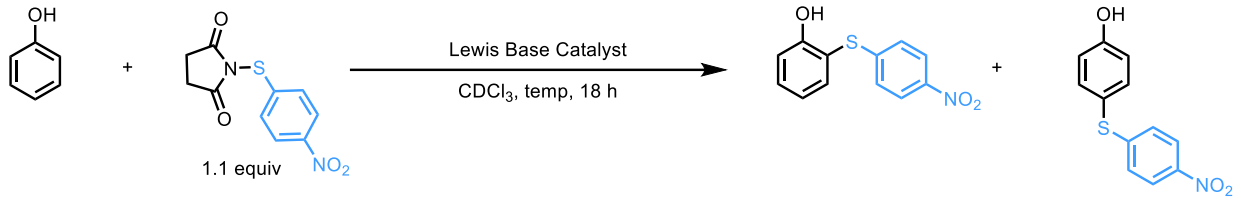

entry	catalyst	molarity, M	TfOH (mol %)	catalyst load (mol %)	temp (°C)	stirring	ratio (o:p)
1	**26**	0.1	10	1	rt	no	1.0:1.5
2	**26**	0.1	10	10	rt	no	1.0:5.0
3	**26**	0.05	10	1	rt	no	1.0:2.5
4	**26**	0.1	10	1	50	no	1.0:1.6
5	**26**	0.2	10	1	rt	no	1.0:1.1
6	**31**	0.1	10	1	rt	no	1.5:1.0
7	**31**	0.2	10	1	rt	no	2.3:1.0
8	**31**	0.05	10	1	rt	no	1.0:1.5
9	**31**	0.1	10	1	rt	yes	3.9:1.0
10	**31**	0.1	100	1	rt	no	N.C.

Upon choosing the sulfenylating reagent and determining efficacy of the NMR study the next step was to investigate the reactivity of Dinh's catalyst **25** in regioselective sulfenylation with our NO_2 sulfenylating reagent. Initial condition for catalyst investigation was the reaction was diluted to 0.1M in $CDCl_3$ at room temperature with a Lewis base catalyst load of 1 mol % and with TfOH added at 10 mol %. Under these initial conditions, Dinh's **25** catalyst showed para preference with a 1.0:1.5 ortho:para selectivity as shown in Table 2.2. I increased the Catalyst load from 1 mol % to 10 mol % and saw a steep decrease in ortho selectivity to 1.0:5.0, Table 2.2 entry 2. This pairs well with Seidel's conclusions that higher concentrations of thiourea

based catalysts can cause aggregation of the catalyst which alters its catalytic attributes[33]. I decreased the catalyst load back to 1 mol % and decreased the reaction concentration from 0.1M to 0.05M and saw a decrease in ortho selectivity to 1.0:2.5, Table 2.2 entry 3. I then test the effect of reaction temperature to see if an elevated temperature could increase the ortho selectivity, Table 2.2 entry 4. The increase in reaction temperature to 50^{o}C had little change on the ortho selectivity. I increased the reaction concentration to 0.2M at room temperature and saw an increase in ortho selectivity to 1.0:1.1. With this increase in selectivity, I determined that we could indeed increase the ortho selectivity and decided to test various chiral Lewis base catalysts to search for a pattern in selectivity to properly design an ortho selective Lewis base catalyst.

I tested various catalysts with sulfur and selenide Lewis base moieties under the initial conditions I used with Dinh's catalyst **25**, Table 2.2. The first pattern demonstrated in Figure 2.8 shows increased bulk around the selenide from methyl groups surrounding the selenide to isopropyl groups results in a decrease in ortho selectivity. This was not evident in Dinh's study likely due to the smaller size of the NCS chlorinating reagent. Our larger sulfenylating reagent seems to be too large to readily fit into the pocket holding the selenide. As you loosen the steric bulk around the selenide and switch to a naphthyl group off the selenide you see a slight increase in ortho selectivity to 1.0:1.3. I then tested the effect of the group off this thiourea switching from the bis-CF_3 **28** to bis-methyl **29** saw little change in ortho selectivity which I believe means that the electron density of the phenyl ring bound to the thiourea has little effect on its ability to coordinate phenol. I then lowered the steric bulk even further and tested the thioether **30** and saw a slight increase in ortho selectivity when compared to Dinh's catalyst **26.** With the same steric bulk, I switched the sulfur back to selenium **31** and increased its electron density by positioning a

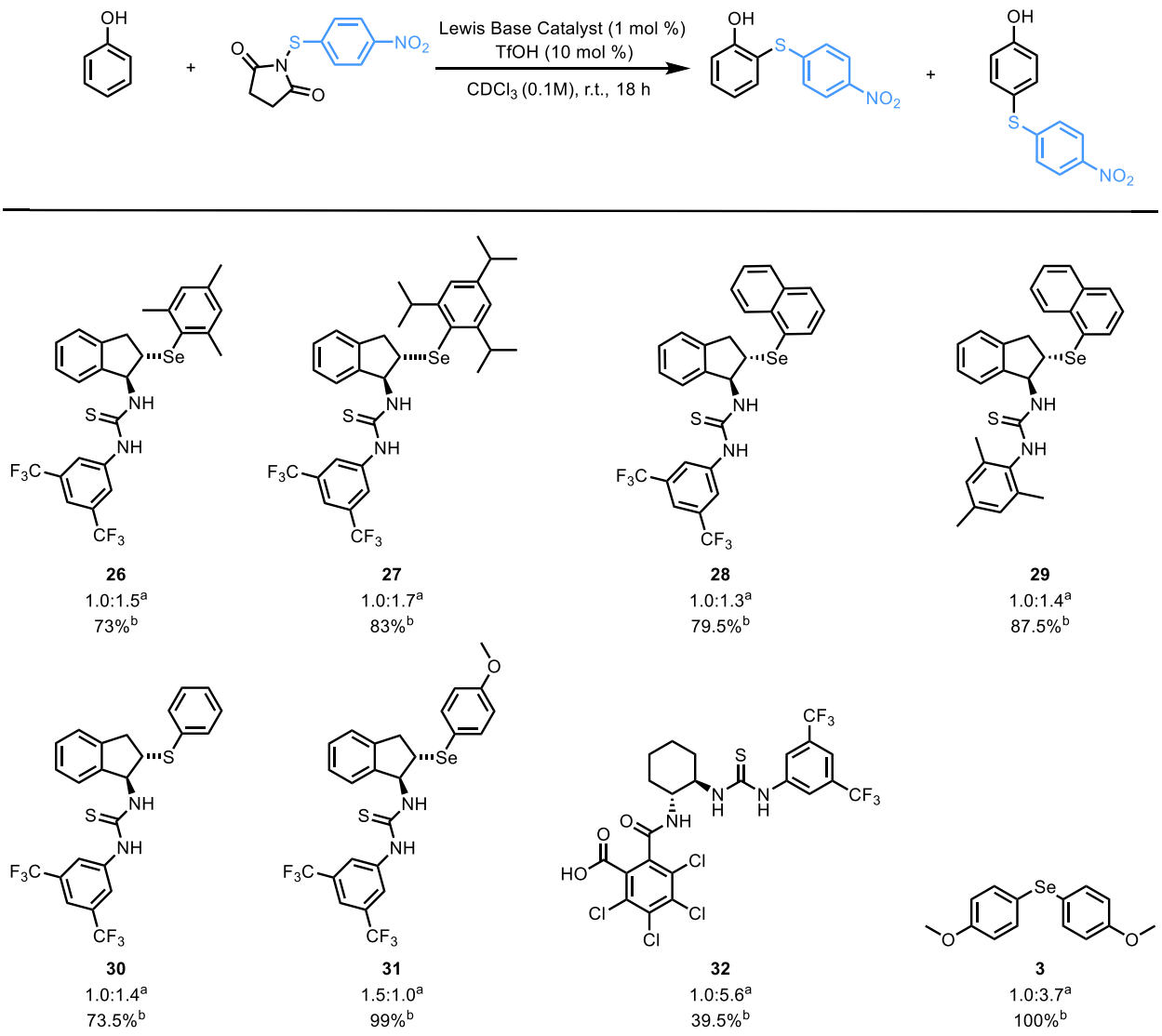

Figure 2-8 Testing various chiral selenide and sulfide Lewis base catalysts. [a]Ortho:para ratios were determined with crude NMR ratios shown in Supplemental Infomation. [b]Percent conversion determined through NMR studies using TMS as an internal standard.

methoxy substituent para to the selenide. This change greatly increased the ortho selectivity to 1.5:1.0 and was the first catalyst sampled that had a higher preference for ortho sulfenylation of phenol. I continued optimization with the 4-methoxy selenide **30**, Table 2.2 entries 6-10. I found that I was able to fit a micro stir bar into the NMR tubes and was able to stir the reaction at 1200 RPM. The stirring of the reaction greatly increased the ortho selectivity of **30** to 3.9:1.0 which is

roughly an 8-fold increase in ortho selectivity when compared to the innate selectivity demonstrated by the symmetric achiral selenide **3**, Figure 2.8.

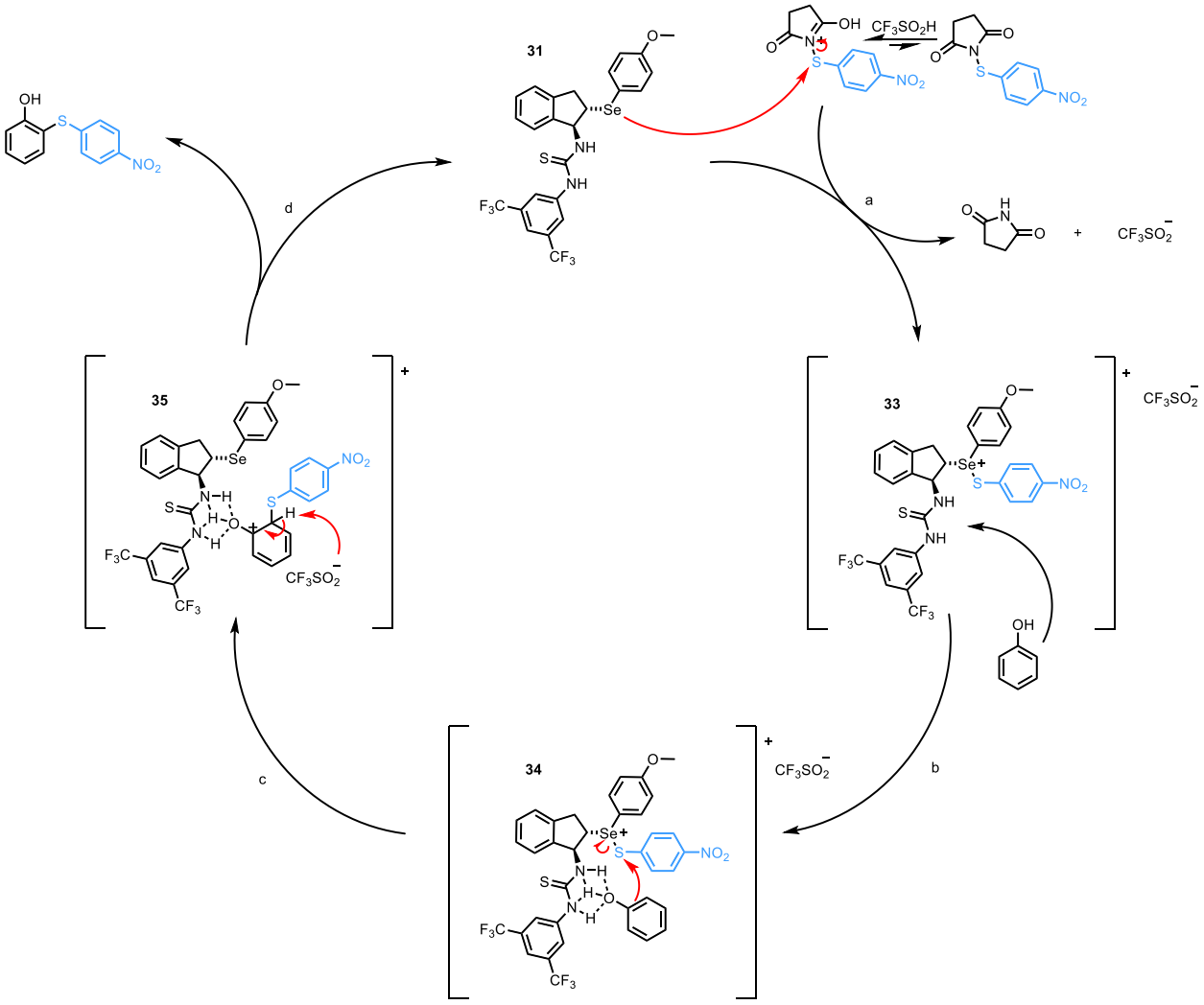

Figure 2-9 Mechanistic proposal for ortho sulfenylation of phenol

We propose a potential mechanism for the regioselective catalytic cycle in Figure 2.9. We theorize that triflic acid activates the N-thiosuccinimide sulfenylating reagent by protonating the carbonyl oxygen. Upon activation, it increases the electrophilic characteristic of the sulfur for the Lewis basic selenide to attack kicking off succinimide. This intermediate **33** then coordinates with phenol to position phenol with hydrogen bonding from the thiourea. The coordinated

catalyst phenol complex **34** positions the ortho position of phenol in close proximity to the electrophilic sulfur bound to the selenium. This close proximity allows for electrophilic aromatic substitution to occur with the phenyl ring attacking the sulfur and kicking off the selenium. We then propose triflate deprotonates the phenol in intermediate **35** driven by the restoration of aromaticity. This regenerates the Lewis base and the Bronsted acid catalysts yielding the ortho sulfenylated phenol product.

Through optimization of the reaction, we found a few interesting results. One interesting observation is that even though some reactions showed no ortho preference the reaction still went up to 88% completion illustrated in Figure 2.8. I theorize that the sulfur in the thiourea is performing a majority of the catalysis when the selenium is hidden behind steric bulk. I tested this hypothesis by testing catalyst **32** which contains only the thiourea Lewis basic location. The results from this test show the great para preference of this thiourea Lewis base with an ortho:para selectivity of 1.0:5.6 which had a higher preference for the para position when compared to catalyst **3.** I hypothesize that replacing the thiourea with a standard urea would greatly reduce the likelihood of Lewis base catalysis being conducted at this location.

2.4 Conclusions

In conclusion, we have studied the C-H sulfenylation of arenes via S_EAr. We found that the combination of a selenide ether with either 1.0 equivalent of tfa or 10 mol % TfOH resulted in rapid and robust conversions across several different arene classes, including several known bioactive compounds. When the product sulfide had electron-rich substitutions the reaction did not need a Lewis base catalyst as the reaction could proceed via an autocatalytic pathway. Conversely, electron-poor sulfides were reliant on the presence of a Lewis base catalyst. These

results represent a mild and efficient route for the addition of diverse sulfur containing functionalities into arenes. We also demonstrated catalyst designs for increasing the ortho selectivity of selenide Lewis base catalysts. More work needs to be done on optimizing the catalyst by increasing the concentrations of the reactions, increasing electron density around the selenide, and replacing the thiourea to a urea. With these preliminary results we showed that the new thiourea based selenide catalyst was able to perform an 8-fold increase in ortho selectivity compared to the previous selenoether **3**. This data shows great promise and is proof of concept that this sulfenylation chemistry can be properly controlled by a regioselective Lewis base catalyst.

2.5 Abbreviations

FDA, Food and Drug Administration; TFA, CF_3O_2H, trifluoroacetic acid; $MgBr_2$, magnesium bromide; S_EAr, Electrophilic aromatic substitution; TMS, tretramethylsilane; $CDCl_3$, deuterated chloroform; NMR, nuclear magnetic resonance; EDG, electron donating group; EWG, electron withdrawing group; TfOH, trifilic acid, trifluoromethanesulfonic acid; eq., equivalence; $CHCl_3$, chloroform; Me, methyl; H, hydrogen; N_3, azide; NO_2, nitro; NSAID, nonsteroidal anti-inflammatory drug; SSRI, selective serotonin reuptake inhibitor; RPM, revolutions per minute.

2.6 References

(1) Sader, H. S.; Johnson, D. M.; Jones, R. N. In Vitro Activities of the Novel Cephalosporin LB 11058 against Multidrug-Resistant Staphylococci and Streptococci. *Antimicrob. Agents Chemother.* **2004**, *48*, 53–62.

(2) Johannesson, P.; Lindeberg, G.; Johansson, A.; Nikiforovich, G. V; Gogoll, A.; Synnergren, B.; Le Greves, M.; Nyberg, F.; Karlen, A.; Hallberg, A. Vinyl Sulfide

Cyclized Analogues of Angiotensin II with High Affinity and Full Agonist Activity at the AT1 Receptor. *J. Med. Chem.* **2002**, *45*, 1767–1777.

(3) Marcantoni, E.; Massaccesi, M.; Petrini, M.; Bartoli, G.; Bellucci, M. C.; Bosco, M.; Sambri, L. A Novel Route to the Vinyl Sulfide Nine-Membered Macrocycle Moiety of Griseoviridin†. *J. Org. Chem.* **2000**, *65*, 4553–4559.

(4) Yoo, J.; Kuruvilla, D. J.; D'Mello, S. R.; Salem, A. K.; Bowden, N. B. New Class of Biodegradable Polymers Formed from Reactions of an Inorganic Functional Group. *Macromolecules* **2012**, *45*, 2292–2300.

(5) Liu, X.; An, R.; Zhang, X.; Luo, J.; Zhao, X. Enantioselective Trifluoromethylthiolating Lactonization Catalyzed by an Indane-Based Chiral Sulfide. *Angew. Chemie Int. Ed.* **2016**, *55*, 5846–5850.

(6) Kabir, M. S.; Lorenz, M.; Van Linn, M. L.; Namjoshi, O. A.; Ara, S.; Cook, J. M. A Very Active Cu-Catalytic System for the Synthesis of Aryl, Heteroaryl, and Vinyl Sulfides. *J. Org. Chem.* **2010**, *75*, 3626–3643.

(7) Wagner, A. M.; Sanford, M. S. Transition-Metal-Free Acid-Mediated Synthesis of Aryl Sulfides from Thiols and Thioethers. *J. Org. Chem.* **2014**, *79*, 2263–2267.

(8) Kazemi, M.; Shiri, L.; Kohzadi, H. Recent Advances in Aryl Alkyl and Dialkyl Sulfide Synthesis. *Phosphorus. Sulfur. Silicon Relat. Elem.* **2015**, *190*, 978–1003.

(9) Wang, L.; He, W.; Yu, Z. Transition-Metal Mediated Carbon-Sulfur Bond Activation and Transformations. *Chem. Soc. Rev.* **2013**, *42*, 599–621.

(10) Vasquez-Cespedes, S.; Ferry, A.; Candish, L.; Glorius, F. Heterogeneously Catalyzed Direct C-H Thiolation of Heteroarenes. *Angew. Chemie Int. Ed.* **2015**, *54*, 5772–5776.

(11) Beletskaya, I. P.; Ananikov, V. P. Transition-Metal-Catalyzed C−S, C−Se, and C−Te Bond Formation via Cross-Coupling and Atom-Economic Addition Reactions. *Chem. Rev.* **2011**, *111*, 1596–1636.

(12) Lee, C.-F.; Liu, Y.-C.; Badsara, S. S. Transition-Metal-Catalyzed C-S Bond Coupling Reaction. *Chem. – An Asian J.* **2014**, *9*, 706–722.

(13) Yadav, J. S.; Reddy, B. V. S.; Reddy, Y. J. A Rapid Synthesis of 3-Sulfenyl Indoles Using SelectfluorTM. *Tetrahedron Lett.* **2007**, *48*, 7034–7037.

(14) Schlosser, K. M.; Krasutsky, A. P.; Hamilton, H. W.; Reed, J. E.; Sexton, K. A Highly Efficient Procedure for 3-Sulfenylation of Indole-2-Carboxylates. *Org. Lett.* **2004**, *6*, 819–821.

(15) Tudge, M.; Tamiya, M.; Savarin, C.; Humphrey, G. R. Development of a Novel, Highly Efficient Halide-Catalyzed Sulfenylation of Indoles. *Org. Lett.* **2006**, *8*, 565–568.

(16) Gillis, H.; Greene, L.; Thompson, A. Preparation of Sulfenyl Pyrroles. *Synlett* **2008**, *2009*, 112–116.

(17) Matsugi, M.; Murata, K.; Nambu, H.; Kita, Y. An Efficient Sulfenylation of Aromatics Using Highly Active Quinone Mono O,S-Acetal Bearing a Pentafluorophenylthio Group. *Tetrahedron Lett.* **2001**, *42*, 1077–1080.

(18) Tian, H.; Zhu, C.; Yang, H.; Fu, H. Iron or Boron-Catalyzed C-H Arylthiation of Substituted Phenols at Room Temperature. *Chem. Commun.* **2014**, *50*, 8875– 8877.

(19) Hostier, T.; Ferey, V.; Ricci, G.; Gomez Pardo, D.; Cossy, J. Synthesis of Aryl Sulfides: Metal-Free C–H Sulfenylation of Electron-Rich Arenes. *Org. Lett.* **2015**, *17*, 3898–3901.

(20) Nalbandian, C. J.; Miller, E. M.; Toenjes, S. T.; Gustafson, J. L. A Conjugate Lewis Base-Bronsted Acid Catalyst for the Sulfenylation of Nitrogen Containing Heterocycles under Mild Conditions. *Chem. Commun.* **2017**, *53*, 1494–1497.

(21) Luo, J.; Zhu, Z.; Liu, Y.; Zhao, X. Diaryl Selenide Catalyzed Vicinal Trifluoromethylthioamination of Alkenes. *Org. Lett.* **2015**, *17*, 3620–3623.

(22) Zhu, Z.; Luo, J.; Zhao, X. Combination of Lewis Basic Selenium Catalysis and Redox Selenium Chemistry: Synthesis of Trifluoromethylthiolated Tertiary Alcohols with Alkenes. *Org. Lett.* **2017**, *19*, 4940–4943.

(23) Hartmann, E.; Denmark, S. E. Structural, Mechanistic, Spectroscopic, and Preparative Studies on the Lewis Base Catalyzed, Enantioselective Sulfenofunctionalization of Alkenes. *Helv. Chim. Acta* **2017**, *100*, e1700158–n/a.

(24) Luo, J.; Cao, Q.; Cao, X.; Zhao, X. Selenide-Catalyzed Enantioselective Synthesis of Trifluoromethylthiolated Tetrahydronaphthalenes by Merging Desymmetrization and Trifluoromethylthiolation. *Nat. Commun.* **2018**, *9*, 527.

(25) Denmark, S. E.; Hartmann, E.; P., K. J.; Wang, H. Mechanistic, Crystallographic, and Computational Studies on the Catalytic, Enantioselective Sulfenofunctionalization of Alkenes. *Nat Chem* **2014**, *6*, 1056–1064.

(26) McDaniel, D. H.; Brown, H. C. An Extended Table of Hammett Substitutent Constants Based on the Ionization of Substituted Benzoic Acids. *J. Org. Chem.* **1958**, *23*, 420–427.

(27) McKay, C. S.; Finn, M. G. Click Chemistry in Complex Mixtures: Bioorthogonal Bioconjugation. *Chem. Biol.* **2014**, *21*, 1075–1101.

(28) Barata-Vallejo, S.; Bonesi, S.; Postigo, A. Late Stage Trifluoromethylthiolation Strategies for Organic Compounds. *Org. Biomol. Chem.* **2016**, *14*, 7150–7182.

(29) Xu, C.; Ma, B.; Shen, Q. N-Trifluoromethylthiosaccharin: An Easily Accessible, Shelf-Stable, Broadly Applicable Trifluoromethylthiolating Reagent. *Angew. Chemie Int. Ed.* **2014**, *53*, 9316–9320.

(30) Shao, X.; Xu, C.; Lu, L.; Shen, Q. Shelf-Stable Electrophilic Reagents for Trifluoromethylthiolation. *Acc. Chem. Res.* **2015**, *48*, 1227–1236.

(31) Dinh, A. N.; Maddox S. M.; Vaidya S. D.; Saputra M. A.; Nalbandian C. J.; and Gustafson J. L. Catalyst-Controlled Regioselective Chlorination of Phenols and Anilines through a Lewis Basic Selenoether Catalyst *J. Org. Chem*, **2020** 85 (21), 13895-13905

(32) Liu, X.; Liang, Y.; Ji, J.; Luo, J.; Zhao, X. Chiral SelenideCatalyzed Enantioselective Allylic Reaction and Intermolecular Difunctionalization of Alkenes: E Fficient Construction of C-SCF 3 Stereogenic Molecules. *J. Am. Chem. Soc.* **2018**, 140, 4782−4786.

(33) Mittal, N.; Lippert, K. M.; De, C. K.; Klauber, E. G.; Emge, T. J.; Schreiner, P. R.; Seidel, D. A Dual-Catalysis Anion-Binding Approach to the Kinetic Resolution of Amines: Insights into the Mechanism via a Combined Experimental and Computational Study. *J. Am. Chem. Soc.* **2015**, 137, 5748−5758.

2.7 Supplemental Information

General Information

^{1}H and ^{13}C NMR spectra were recorded on Varian VNMRS 400 MHz, Varian Inova 500 MHz, Varian VNMRS 600 MHz, and Bruker Avance III 600 MHz spectrometers at room temperature. All chemical shifts were reported in parts per million (δ) and were internally referenced to residual protio solvents unless otherwise noted. Spectral data were reported as follows: chemical shift (multiplicity [singlet (s), doublet (d), triplet (t), quartet (q), quintet (quin), and multiplet (m)], coupling constants [Hz], integration). Carbon spectra were recorded with complete proton decoupling. Conventional mass spectra were obtained

using Advion Expression^{s} CMS (APCI, ASAP. All chemicals used were purchased from Sigma Aldrich, TCI, Frontier Scientific, Acros Organics, Strem, Oakwood, Matrix Scientific, Cambridge Isotope Laboratories, or Fisher and were used as received without further purification, unless specifically noted. All normal phase flash column chromatography (FCC) was performed using Grade 60 Silica Gel (230-400 mesh) purchased from Fisher Scientific. Preparative Thin Layer Chromatography (TLC) plates contained grade 60 silica gel coated with fluorescent indicator F_{254}. Catalysts were either purchased or prepared from known literature procedures or synthesized.

Bis(4-methoxyphenyl)selane (3)

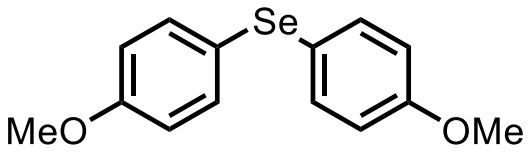

Procedure is based on preparation from reported literature: Verma, A.; Jana, S.; Durga Prasad, C.; Yadav, A.; Kumar, S. *Chem. Commun.* **2016**, *52* (22), 4179. The spectral data is in agreement with the reported literature: **^{1}H NMR** (500 MHz, $CDCl_3$)δ 7.44 – 7.37 (m, 4H), 6.83 – 6.79 (m, 4H), 3.78 (s, 6H).

General procedure for the preparation of *N*-thiosuccinimides (2a-2d)

Sulfuryl chloride (1.0 equivalent) was added drop wise to a solution of thiol (1.0 equivalent) and triethylamine (0.1 equivalents) in dichloromethane (1M) at 0 °C. After stirring for 15 minutes, the mixture was warmed to room temperature and stirred for 30 minutes and then cooled to 0 °C. The resulting solution was transferred drop wise via cannula to a solution of succinimide (1.0 equivalent) in dichloromethane (1M) and triethylamine (1.3

equivalents) at 0 °C, and the mixture was then warmed to room temperature over 1 hour. The solution was diluted with water and extracted with equal volume of dichloromethane before being dried over sodium sulfate. Evaporation of solvent gave crude product that was purified by using flash column chromatography.

1-(phenylthio)pyrrolidine-2,5-dione (2a)

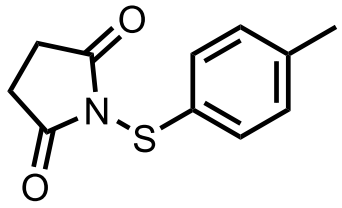

Procedure is based on preparation from reported literature. The spectral data is in agreement with the reported literature: Hostier, T.; Ferey, V.; Ricci, G.; Gomez Pardo, D.; Cossy, J. *Org. Lett.* **2015**, 17(15), 3898. **^{1}H NMR** (400 MHz, $CDCl_3$)δ 7.63 – 7.55 (m, 2H), 7.17 – 7.11 (m, 2H), 2.78 (d, *J* = 0.59 Hz, 4H), 2.33 (d, *J* = 0.76 Hz, 3H).

1-(phenylthio)pyrrolidine-2,5-dione (2b)

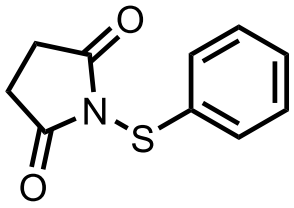

Procedure is based on preparation from reported literature. The spectral data is in agreement with the reported literature: Nalbandian, C.; Miller, E.; Toenjes, S.; Gustafson, J. L. *Chem. Commun.* **2017**, *53* (9), 1494. **^{1}H NMR** (400 MHz, $CDCl_3$) δ 7.74 – 7.50 (m, 2H), 7.46 – 7.27 (m, 3H), 2.81 (s, 4H).

1-((4-azidophenyl)thio)pyrrolidine-2,5-dione (2c)

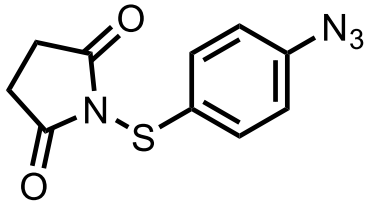

Procedure is based on preparation from reported literature. The spectral data is in agreement with the reported literature: Nalbandian, C.; Miller, E.; Toenjes, S.; Gustafson, J. L. *Chem. Commun.* **2017**, *53* (9), 1494. **^{1}H NMR** (400 MHz, $CDCl_3$) δ 7.75 – 7.66 (m, 2H), 7.01 – 6.96 (m, 2H), 2.79 (s, 4H).

1-((4-nitrophenyl)thio)pyrrolidine-2,5-dione (2d)

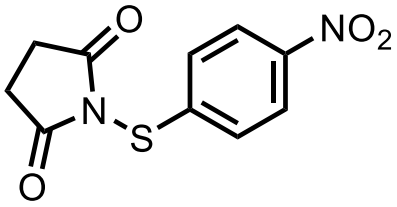

Procedure is based on preparation from reported literature. The spectral data is in agreement with the reported literature: Hostier, T.; Ferey, V.; Ricci, G.; Gomez Pardo, D.; Cossy, J. *Org. Lett.* **2015**, 17(15), 3898. **^{1}H NMR** (400 MHz, $CDCl_3$) δ 8.21 – 8.13 (m, 2H), 7.49 – 7.38 (m, 2H), 2.97 (s, 4H).

N-Trifluoromethylthiosaccharin (2e)

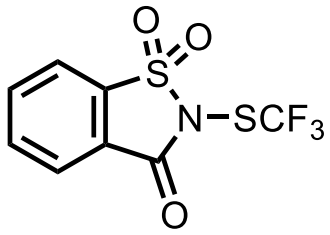

Procedure is based on preparation from reported literature. The spectral data is in agreement with the reported literature: Xu, C.; Ma, B.; Shen, Q. *Angew. Chemie Int. Ed.* **2014**, *53* (35), 9316. **^{1}H NMR** (500 MHz, $CDCl_3$) δ 8.19 (m, 1H), 8.07 – 7.97 (m, 2H), 7.93 (m, 1H). **^{19}F NMR** (470 MHz, $CDCl_3$) δ -47.70, -113.50 (Reference Standard $C_6H_5F_1$).

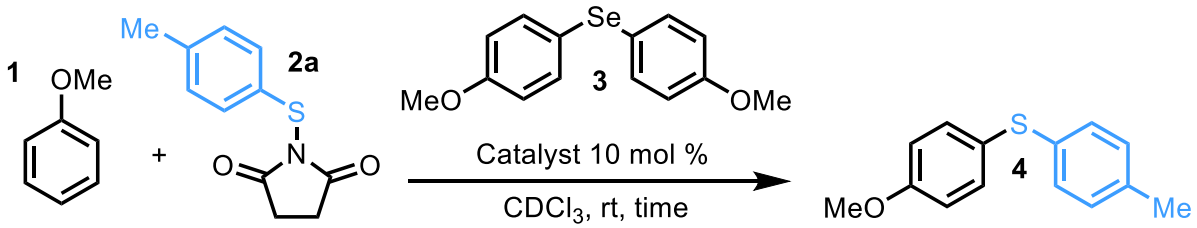

entry	catalyst	additive	molarity, M	time	[a]yield
1	3	1 equiv tfa	0.5	1 h	83
2	none	1 equiv tfa	1.0	3 h	85

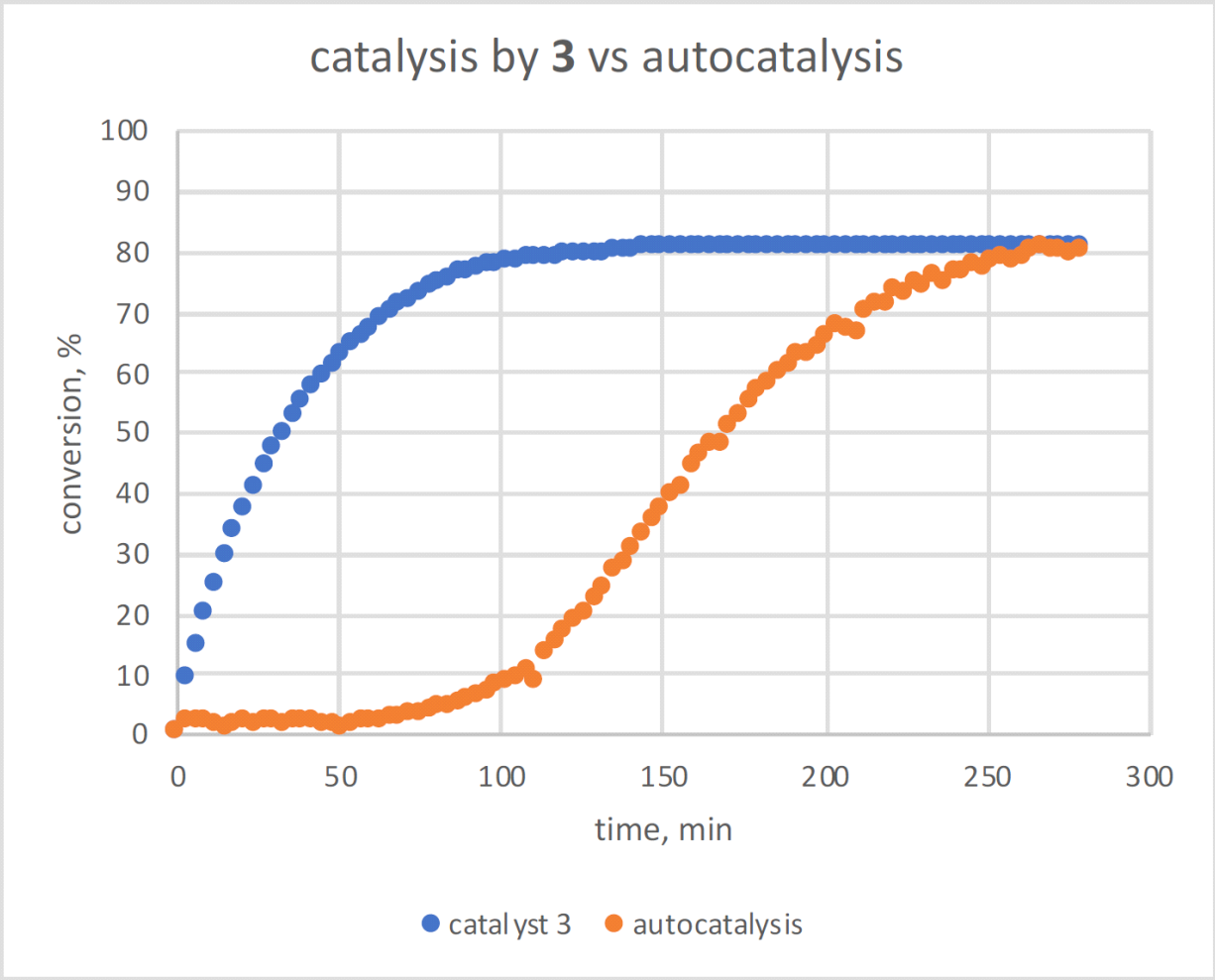

Figure 2-10 Time dependent NMR studies

General information for time dependent NMR studies

As a stock solution from $CDCl_3$, An NMR tube was added 0.3 mmol, **1**, 10 mol % catalyst **3**, 1.2 equivalent of **2a**, a total volume of 0.6 mL of $CDCl_3$ (0.5M in **1**), and 2 drops of tms (as an internal standard). An NMR was taken before tfa addition for internal standard calibration. 1 equivalent of tfa was then added, the NMR tube was inverted and placed in the NMR spectrometer. Spectra were recorded every 3 minutes for up to 5 hours. Yields were determined by internal standard with integration of product methyl peak (2.30 ppm; 3H). Entry 2 was carried out at 1.0M in **1** without catalyst **3.** (note: reaction times for kinetic studies are slightly longer. During kinetic studies NMR tubes are inverted once for mixing. Reactions from table 1 were inverted several times over the course of the reaction to emulate stirring.)

General procedure for the preparation of sulfenylated products (4-23)

A 2-dram vial, equipped with a stir bar, was charged with arene or heterocycle (1.0 equivalent) and catalyst (0.10 equivalents). Chloroform or toluene (1.0 M in arene or heterocycle) was added to the vial, followed by sulfenylating reagent (1.0-1.2) equivalents) and acid additive, Trifluoroacetic acid (tfa) (1.0 equivalents), or triflic acid (TfOH), (0.1 equivalents) the resulting solution was stirred at room temperature for 5 minutes to 16 hours. The reaction mixture was concentrated under reduced pressure and purified from crude mixture, or neutralized with DI water, 1 M HCl, or a saturated solution of sodium bicarbonate, and extracted with dichloromethane 3 times. The combined organic extracts were dried over anhydrous sodium sulfate, filtered and concentrated under reduced pressure. The crude product was purified by flash column chromatography on silica gel using a mixture

of hexanes-ethyl acetate, dichloromethane-methanol, or ethyl acetate-methanol as the eluent to afford the expected product. Isolated yields were determined on a 6-300 mg scale.

(4-methoxyphenyl)(*p*-tolyl)sulfane (4)

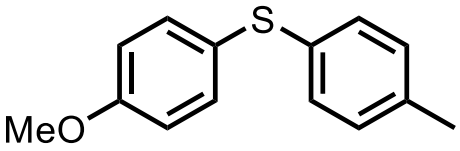

Following the general procedure: to anisole (124.4mg, 1.15 mmol) and 1.2 equivalent of **2a** the reaction was quenched with DI water after 10 min and the aqueous layer was extracted 3 times with dicholoromethane and the combined organic layers were dried with sodium sulfate filtered and was concentrated under reduced pressure. The crude product was purified by flash column chromatography using silica gel and pure hexanes to 1% ethyl acetate in hexanes as the eluent. The purified product was concentrated under reduced pressure to afford the expected product as a white solid (238.4mg, 90% yield).The spectral data is in agreement with the reported literature: Yoshida, S.; Sugimura, Y.; Hazama, Y.; Nishiyama, Y.; Yano, T.; Shimizu, S.; Hosoya, T. *Chem. Commun.* **2015**, *51* (93), 16613.**^{1}H NMR** (500 MHz, $CDCl_3$) δ 7.39 – 7.33 (m, 2H), 7.16 – 7.11 (m, 2H), 7.07 (d, *J* = 8.04 Hz, 2H), 6.91 – 6.82 (m, 2H), 3.81 (s, 3H), 2.30 (s, 3H).

4-(*p*-tolylthio)phenol (5)

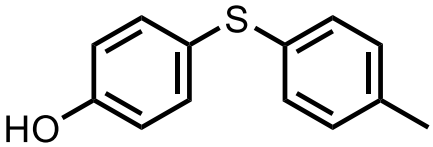

Following the general procedure: to phenol (60.7mg, 0.65 mmol) and 1.0 equivalent of

2a the reaction was concentrated under reduced pressure after 10 minutes. The crude product was purified by flash column chromatography using silica gel and pure hexanes to 10% ethyl acetate in hexanes as the eluent. The purified product was concentrated under reduced pressure to afford the expected product as a white solid (111.8mg, 80% yield). **^{1}H NMR** (500 MHz, $CDCl_3$) δ 7.35 – 7.30 (m, 2H), 7.19 – 7.14 (m, 2H), 7.11 – 7.06 (m, 2H), 6.84 – 6.78 (m, 2H), 5.11 (s, 1H), 2.32 (s, 3H).The spectral data is in agreement with the reported literature: Tian, H.; Zhu, C.; Yang, H.; Fu, H. *Chem. Commun.* **2014**, *50* (64), 8875.

Mesityl(*p*-tolyl)sulfane (6)

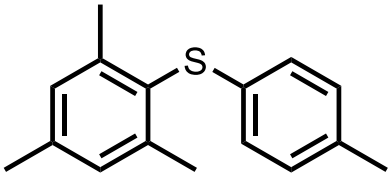

Following the general procedure: to mesitylene and 1.0 equivalent of **2a** (24.90mg, 0.207 mmol) the reaction was concentrated under reduced pressure after 45 minutes. The crude product was purified by flash column chromatography using silica gel and pure hexanes as the eluent. The purified product was concentrated under reduced pressure to afford the expected product as a white solid (43.2mg, 86% yield). **^{1}H NMR** (500 MHz, $CDCl_3$) δ 7.04 – 6.96 (m, 4H), 6.87 – 6.80 (m, 2H), 2.32 (s, 3H), 2.27 (s, 3H). The spectral data is in agreement with the reported literature: Anbarasan, P.; Neumann, H.; Beller, M. *Chem. Commun.* **2011**, *47* (11), 3233.

1-(*p*-tolylthio)naphthalen-2-ol (7)

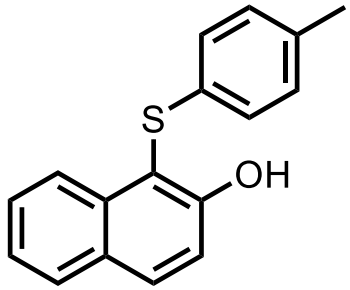

Following the general procedure: to 2-naphthol (30.27mg, 0.21mmol) and 1.0 equivalent of **2a** the reaction was concentrated under reduced pressure after 5 minutes. The crude product was purified by flash column chromatography using silica gel and pure hexanes as the eluent. The purified product was concentrated under reduced pressure to afford the expected product as a white solid (55.3mg, 99% yield).The spectral data is in agreement with the reported literature: Silva, L. T.; Azeredo, J. B.; Saba, S.; Rafique, J.; Bortoluzzi, A. J.; Braga, A. L. *European J. Org. Chem.* **2017**, *2017* (32), 4740. **^{1}H NMR** (500 MHz, $CDCl_3$) δ 8.29 (d, *J* = 8.46 Hz, 1H), 7.93 (d, *J* = 8.85 Hz, 1H), 7.85 (d, *J* = 8.07 Hz, 1H), 7.54 (t, *J* = 7.67 Hz, 1H), 7.39 (t, *J* = 8.17 Hz, 2H), 7.28 (s, 1H), 7.01 (q, *J* = 8.11 Hz, 4H), 2.28 (s, 3H).

4-(*p*-tolylthio)phenyl)acetanilide (8)

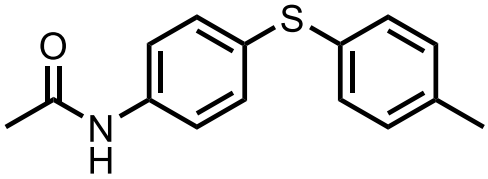

Following the general procedure: to acetanilide (39.7mg, 0.35mmol) and 1.2 equivalents of **2a** the reaction was concentrated under reduced pressure after 16.5 hours. The crude product was purified by flash column chromatography using silica gel and pure dichloromethane as the eluent. The purified product was concentrated under reduced pressure

to afford the expected product as a white solid (43.8mg, 58% yield).The spectral data is in agreement with the reported literature: Wang, H.; Jiang, L.; Chen, T.; Li, Y. *European J. Org. Chem.* **2010**, *2010* (12), 2324. **^{1}H NMR** (500 MHz, $CDCl_3$) δ 7.66 (s, 1H), 7.47 – 7.40 (m, 2H), 7.30 – 7.24 (m, 2H), 7.24 – 7.19 (m, 2H), 7.10 (d, *J* = 7.92 Hz, 2H), 2.32 (s, 3H), 2.15 (s, 3H).

(4-methoxyphenyl)(phenyl)sulfane (9)

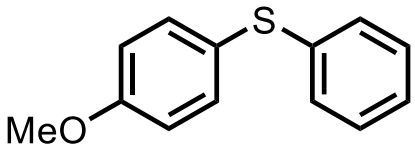

Followed general procedure for comparison studies. The spectral data is in agreement with the reported literature: Hostier, T.; Ferey, V.; Ricci, G.; Gomez Pardo, D.; Cossy, J. *Org. Lett.* **2015**, 17(15), 3898.

(4-azidophenyl)(4-methoxyphenyl)sulfane (10)

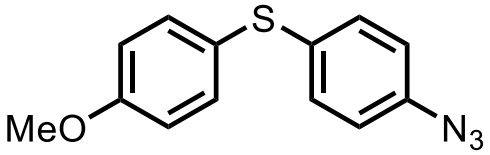

Following the general procedure: to anisole (10.4mg, 0.096mmol) and 1.2 equivalents of **2c** the reaction was concentrated under reduced pressure after 10 mins. The crude product was purified by flash column chromatography using silica gel and pure hexanes to 1% ethyl acetate in hexanes as the eluent. The purified product was concentrated under reduced pressure to afford the expected product as a white solid (20.8mg, 84% yield). **^{1}H NMR** (500 MHz, $CDCl_3$) δ 7.41 – 7.35 (m, 2H), 7.20 – 7.16 (m, 2H), 6.93 – 6.86 (m, 4H), 3.82 (s, 3H). **^{13}C NMR** (126 MHz, $CDCl_3$) δ 176.4, 142.7, 135.9 (3C), 129.7, 129.6, 120.8, 120.0

(3C), 114.0, 28.7. **LC-HRMS (EI): Calculated** $C_{13}H_{11}N_3OS$ $[M+1]^+$ 258.0702 m/z **Found:** 258.0649 m/z m/z.

(4-methoxyphenyl)(4-nitrophenyl)sulfane (11)

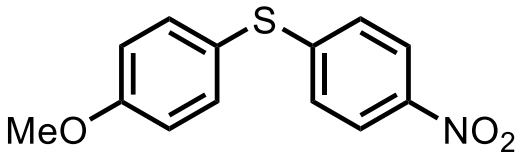

Followed general procedure for comparison studies. The spectral data is in agreement with the reported literature: Roy, S.; Sarma, M. J.; Kashyap, B.; Phukan, P. *Chem. Commun.* **2016**, *52* (6), 1170.

(4-methoxyphenyl)(trifluoromethyl)sulfane (12)

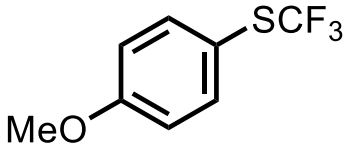

Followed general procedure for comparison studies The spectral data is in agreement with the reported literature: Pluta, R.; Nikolaienko, P.; Rueping, M. *Angew. Chemie Int. Ed.* **2014**, *53* (6), 1650.

4-((4-azidophenyl)thio)phenol (13)

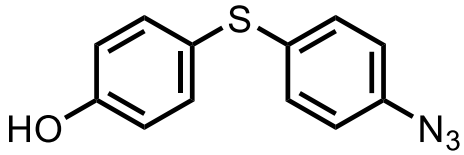

Following the general procedure: to phenol (10.3mg, 0.11mmol) and 1.0 equivalent of **2c** the reaction was concentrated under reduced pressure after 30 min. The crude product was

purified by flash column chromatography using silica gel and 20 % ethyl acetate in hexanes as the eluent. The purified product was concentrated under reduced pressure to afford the expected product as a white solid (21.4mg, 80% yield). **^{1}H NMR** (500 MHz, $CDCl_3$) δ 7.36 – 7.30 (m, 2H), 7.22 – 7.16 (m, 2H), 6.94 – 6.88 (m, 2H), 6.86 – 6.80 (m, 2H), 5.03 (s, 1H). **^{13}C NMR** (126 MHz, $CDCl_3$) δ 156.0, 138.2, 135.1(2C), 134.6, 130.5(2C), 125.1, 119.8(2C), 116.7(2C). **LC-HRMS (EI): Calculated** $C_{12}H_9N_3OS$ $[M-1]^-$ 242.0387 m/z **Found:** 242.0394 m/z.

(4-azidophenyl)(mesityl)sulfane (14)

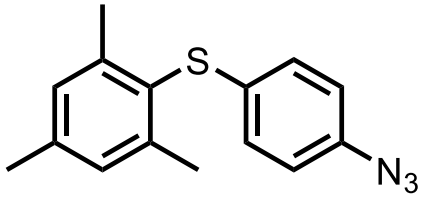

Following the general procedure: to mesitylene (16.2mg,0.135 mmol) and 1.0 equivalent of **2c** the reaction was concentrated under reduced pressure after 10 minutes. The crude product was purified by flash column chromatography using silica gel and pure hexanes as the eluent. The purified product was concentrated under reduced pressure to afford the expected product as a white solid (28mg, 77% yield). **^{1}H NMR** (500 MHz, $CDCl_3$) δ 7.01 (m, 2H), 6.93 – 6.88 (m, 2H), 6.87 – 6.82 (m, 2H), 2.38 (s, 6H), 2.32 (s, 3H). **^{13}C NMR** (126 MHz, $CDCl_3$) δ 143.7 (2C), 139.6, 136.6, 135.0, 129.6 (2C), 127.2 (2C), 127.1, 119.8 (2C), 21.8 (2C), 21.3. **LC-HRMS (EI): Calculated** $C_{15}H_{15}N_3S$ $[M+1]^+$ 270.1066 m/z. **Found:** 270.0943 m/z.

2-(4-azidophenyl)thio)-naproxen (15)

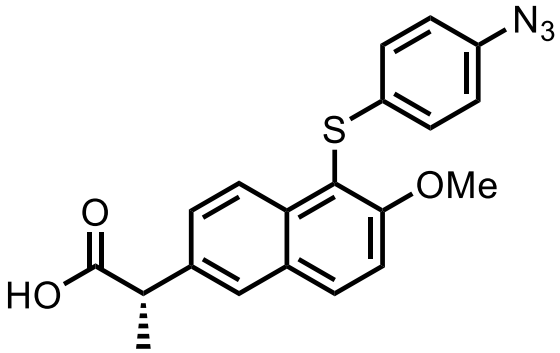

Following the general procedure: to naproxen (24.9mg, 0.108mmol) and 1.0 equivalent of **2c** the reaction was added dichloromethane and 1 M HCl in equal volume after 30 minutes. The aqueous layer was extracted 2 times with equal volume, the organic layers were combined, dried with sodium sulfate filtered and concentrated under reduced pressure. The crude product was purified by flash column chromatography using silica gel dichloromethane 100% to 5% methanol in dichloromethane as the eluent. The purified product was concentrated under reduced pressure to afford the expected product as white solid (31.2mg, 76% yield). **^{1}H NMR** (500 MHz, $CDCl_3$) δ ^{1}H NMR (500 MHz, Chloroform-*d*) δ 8.40 (d, *J* = 8.78 Hz, 1H), 7.97 – 7.89 (m, 1H), 7.74 (s, 1H), 7.47 (dd, *J* = 8.86, 1.92 Hz, 1H), 7.35 (d, *J* = 9.10 Hz, 1H), 7.06 – 6.98 (m, 2H), 6.85 – 6.75 (m, 2H), 3.95 (s, 3H), 3.89 (q, *J* = 7.15 Hz, 1H), 1.59 (d, *J* = 7.17 Hz, 3H).**^{13}C NMR** (101 MHz, $CDCl_3$) δ 180.0, 159.3, 137.0, 135.6, 135.6, 134.5, 132.2, 129.6 (2C), 128.3, 127.9, 126.8, 126.0, 119.6 (2C), 113.8, 113.2, 57.0, 45.1, 18.2. **LC-HRMS (EI): Calculated** $C_{20}H_{17}N_3O_3S^+$ [M-1]$^-$ 378.0912 m/z. **Found:** 378.0913 m/z.

4-((trifluoromethyl)thio)phenol (16)

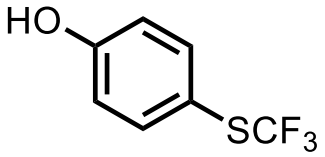

Following the general procedure: to phenol (15.7mg, 0.17mmol) and 1.2 equivalents of **2e** the reaction was concentrated under reduced pressure after 30 min. The crude product was purified by flash column chromatography using silica gel and 10% ethyl acetate in hexanes as the eluent. The purified product was concentrated under reduced pressure to afford the expected product as a white solid (26.7mg, 81% yield).The spectral data is in agreement with the reported literature: Xu, C.; Ma, B.; Shen, Q. *Angew. Chemie Int. Ed.* **2014**, *53* (35), 9316. **^{1}H NMR** (500 MHz, $CDCl_3$) δ 7.59 – 7.48 (m, 2H), 6.90 – 6.84 (m, 2H), 5.31 (s, 1H).

2-butyl-5-((trifluoromethyl)thio)thiophene (17)

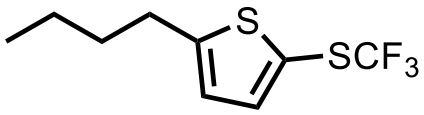

Following the general procedure: to n-butylthiophene (139 mg, 0.99 mmol) and 1.05 equivalents of **2e** the reaction was concentrated under reduced pressure after 1 hour. The crude product was purified by flash column chromatography using silica gel and pure hexanes as the eluent. The purified product was concentrated under reduced pressure to afford the expected product as a white solid (140.4mg, 59% yield). **^{1}H NMR** (400 MHz, $CDCl_3$) δ 7.24 (d, *J* = 3.7 Hz, 1H), 6.79 (dt, *J* = 3.6, 1.0 Hz, 1H), 2.87 – 2.80 (m, 2H), 1.73 – 1.63 (m, 2H), 1.41 (dq, *J* = 14.7, 7.4 Hz, 2H), 0.95 (t, *J* = 7.4 Hz, 3H). **^{13}C NMR** (126 MHz, $CDCl_3$) δ 155.7, 139.8, 129.8, 127.4, 125.5, 33.6, 30.4, 22.3, 13.9. **^{19}F NMR** (376

MHz, $CDCl_3$) δ -46.53, -76.55 (tfa). **(APCI): Calculated** C_9HFS^+[M]240.03. **Found:** 239.8 m/z.

1-((trifluoromethyl)thio)naphthalen-2-ol (18)

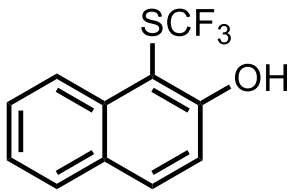

Following the general procedure: to 2-naphthol (70.0mg, 0.486mmol) and 1.2 equivalents of **2e** the reaction was concentrated under reduced pressure after 10 minutes. The crude product was purified by flash column chromatography using silica gel and pure hexanes as the eluent. The purified product was concentrated under reduced pressure to afford the expected product as a white solid (108.0mg, 91% yield). The spectral data is in agreement with the reported literature: Xu, C.; Ma, B.; Shen, Q. *Angew. Chemie Int. Ed.* **2014**, *53* (35), 9316 **^{1}H NMR** (500 MHz, $CDCl_3$) δ 8.41 – 8.32 (m, 1H), 7.94 (d, *J* = 8.94 Hz, 1H), 7.85 – 7.78 (m, 1H), 7.64 (ddd, *J* = 8.42, 6.91, 1.33 Hz, 1H), 7.44 (ddd, *J* = 8.02, 6.86, 1.13 Hz, 1H), 7.32 (d, *J* = 8.97 Hz, 1H), 6.96 (s, 1H).

3-chloro-4-((trifluoromethyl)thio)phenol (19)

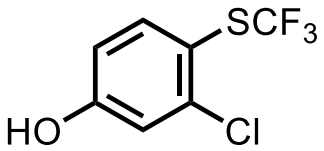

Following the general procedure: to 3-chlorophenol (51.0mg, 0.40mmol) and 1.0 equivalent of **2e** the reaction was concentrated under reduced pressure after 10 min. The crude product was purified by flash column chromatography using silica gel and 20% ethyl acetate in hexanes as the eluent. The purified product was concentrated under reduced

pressure to afford the expected product as a white solid (72.2mg, 79%yield). The spectral data is in agreement with the reported literature: Xu, C.; Ma, B.; Shen, Q. *Angew. Chemie Int. Ed.* **2014**, *53* (35), 9316. **^{1}H NMR** (500 MHz, $CDCl_3$) δ 7.62 (d, *J* = 8.5 Hz, 1H), 7.05 (d, *J* = 2.7 Hz, 1H), 6.79 (dd, *J* = 8.5, 2.7 Hz, 1H), 5.63 – 5.30 (m, 1H).

3-iodo-4-((trifluoromethyl)thio)phenol (20)

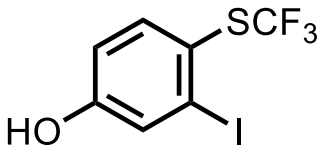

Following the general procedure: to 3-iodophenol (in toluene) (43.0mg, 0.20 mmol) and 1.0 equivalent of **2e** the reaction was concentrated under reduced pressure after 10 min. The crude product was purified by flash column chromatography using silica gel and 20% ethyl acetate in hexanes as the eluent. The purified product was concentrated under reduced pressure to afford the expected product as a white solid (51.2mg, 80% yield).The spectral data is in agreement with the reported literature: Xu, C.; Ma, B.; Shen, Q. *Angew. Chemie Int. Ed.* **2014**, *53* (35), 9316. **^{1}H NMR** (500 MHz, $CDCl_3$) δ 7.67 (d, *J* = 8.50 Hz, 1H), 7.49 (d, *J* = 2.76 Hz, 1H), 6.88 (dd, *J* = 8.50, 2.72 Hz, 1H), 5.35 (s, 1H).

2-Trifluoromethylthio-naproxen (21)

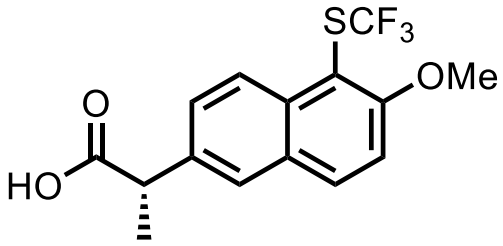

Following the general procedure: to Naproxen (24.3mg, 0.11mmol) and 1.0

equivalent of **2e** the reaction was added 1M HCl after 2 hours. The aqueous layer was extracted 2 times with equal volume, the organic layers were combined, dried with sodium sulfate filtered and concentrated under reduced pressure. The crude product was purified by flash column chromatography using silica gel and pure hexanes to 10% ethyl acetate in hexanes as the eluent. The purified product was concentrated under reduced pressure to afford the expected product as a white solid (32.8mg, 94% yield). **^{1}H NMR** (500 MHz, $CDCl_3$) δ 8.48 (d, *J* = 8.85 Hz, 1H), 7.97 (d, *J* = 9.02 Hz, 1H), 7.73 (d, *J* = 2.02 Hz, 1H), 7.58 (dd, *J* = 8.88, 1.86 Hz, 1H), 7.33 (d, *J* = 9.08 Hz, 1H), 4.04 (s, 3H), 3.94 – 3.87 (m, 1H), 1.61 (d, *J* = 7.14 Hz, 3H).**^{13}C NMR** (126 MHz, $CDCl_3$) δ 180.3, 160.8, 136.4, 135.8, 134.2(2C), 129.4, 128.3 (2C), 126.8 (2C), 125.8, 113.5, 57.0, 45.1, 18.2. **^{19}F NMR** (470 MHz, $CDCl_3$) δ - 2.47, -76.55(tfa). **LC-HRMS (EI): Calculated** $C_{15}H_{13}F_3O_3S$ $[M+1]^+$ 331.0616 m/z. **Found:** 331.0536 m/z.

3-Trifluoromethylthio-tolemtin (22)

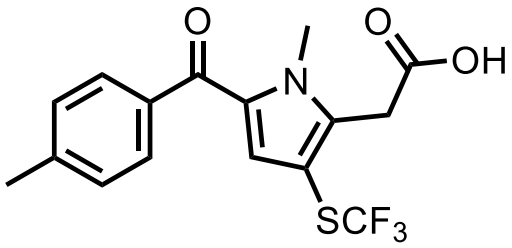

Following the general procedure: to Tolmetin (33.4mg, 0.13mmol) and 1.2 equivalents of **2e** the reaction was added 1M HCl after 16 hours. The aqueous layer was extracted 2 times with equal volume, the organic layers were combined, dried with sodium sulfate filtered and concentrated under reduced pressure. The crude product was purified by flash column chromatography using silica gel (washed with 10% volume triethylamine) 100% dichloromethane to 10% methanol in dichloromethane as the eluent. The purified product was

concentrated under reduced pressure to 5 ml of volume, washed with 5 ml 4M HCl. Combined organics were dried with sodium sulfate filtered and concentrated under reduced pressure to afford the expected product as an orange solid (32.5mg, 70% yield). **^{1}H NMR** (500 MHz, $CDCl_3$) δ 7.75 – 7.70 (m, 2H), 7.31 – 7.26 (m, 2H), 6.92 (s, 1H), 4.00 (s, 2H), 3.98 (s, 3H), 2.44 (s, 3H). **^{13}C NMR** (126 MHz, $CDCl_3$) 186.1, 173.9, 143.1, 139.6, 136.3, 131.9, 129.7 (2C), 129.1 (2C), 128.2, 102.0, 34.7, 30.5, 21.7. **^{19}F NMR** (376MHz, $CDCl_3$) δ -45.53, -76.55 (tfa). **LC-HRMS (EI): Calculated** $C_{16}H_{14}F_3NO_3S$ $[M+1]^+$ 358.0725 m/z **Found:** 358.0642 m/z.

N-Mesyl-2-trifluoromethylthio-paroxetine (23)

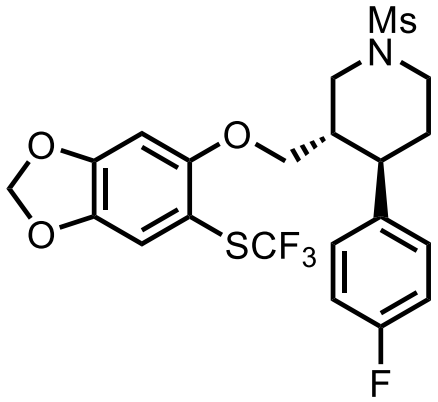

Following the general procedure: to N-mesylparoxetine (321.6mg, 0.789mmol) and 1.2 equivalents of **2e** the reaction was added dichloromethane and sodium bicarbonate in equal volume. The aqueous layer was extracted 2 times with equal volume, the organic layers were combined, dried with sodium sulfate filtered and concentrated under reduced pressure. The crude product was purified by flash column chromatography using silica gel hexanes 100% to 40% ethyl acetate in hexanes as the eluent. The purified product was concentrated under reduced pressure to afford the expected product as white solid (316.3mg, 79% yield). **^{1}H NMR** δ (500 MHz, $CDCl_3$) 7.18 – 7.13 (m, 2H), 7.00 (s, 1H), 7.00 – 6.94 (m, 2H), 6.27 (s, 1H), 5.93 (s, 2H), 4.03 (ddd, J = 11.93, 4.13, 1.91 Hz, 1H), 3.95 (ddt, J = 11.68,

4.83, 2.42 Hz, 1H), 3.67 (dd, *J* = 9.27, 2.45 Hz, 1H), 3.57 (dd, *J* = 9.29, 4.41 Hz, 1H), 2.98 (t, *J* = 11.45 Hz, 1H), 2.87 (td, *J* = 11.59, 5.13 Hz, 1H), 2.77 (td, *J* = 11.56, 3.70 Hz, 1H), 2.22 (ttd, *J* = 11.11, 4.18, 2.54 Hz, 1H), 2.01 – 1.90 (m, 2H). **^{13}C NMR** (126 MHz, $CDCl_3$) 162.7, 160.8, 156.4, 151.8, 141.7, 138.3, (quartet 133.3, 130.9, 128.4, 125.9) 128.9, 128.9, 117.1, 115.8, 115.6, 102.2, 95.7, 68.9, 49.0, 46.7, 42.8, 42.1, 34.3, 33.4.**^{19}F NMR** (376 MHz, $CDCl_3$) δ -43.86, -76.55 (tfa), 116.39. **LC-HRMS (EI): Calculated** $C_{21}H_{21}F_4NO_5S_2$ $[M+1]^+$ 508.0876 m/z **Found:**508.0765 m/z.

NMR Spectra

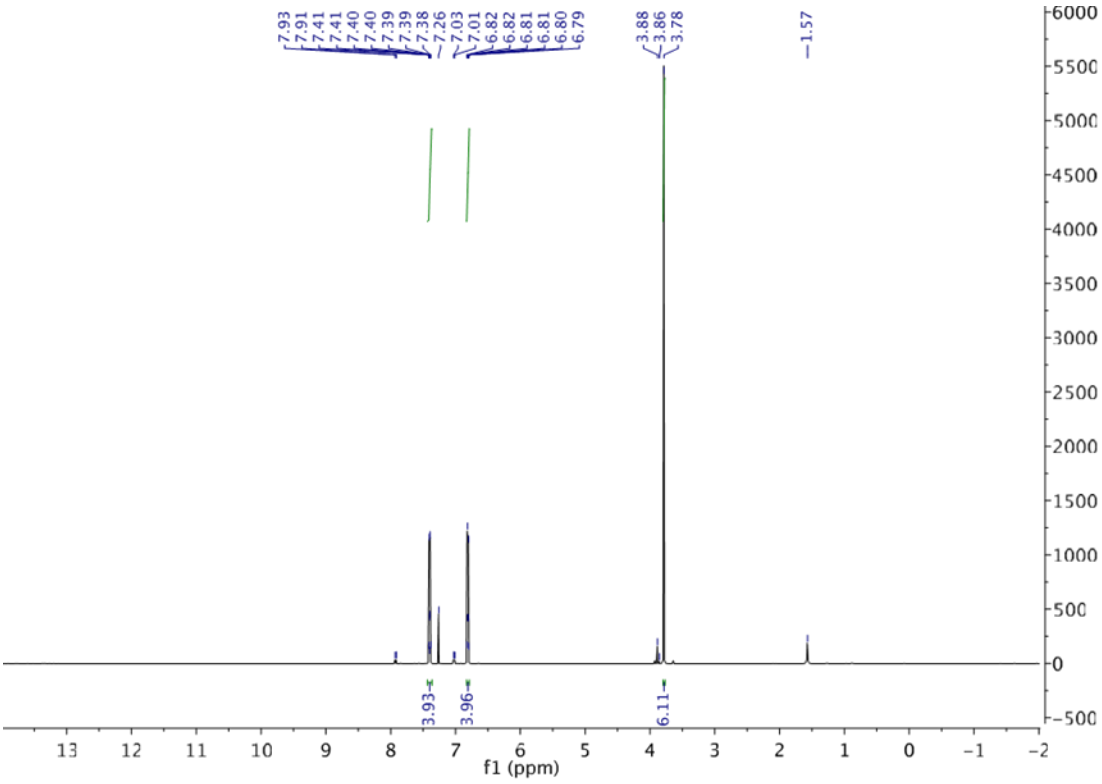

Figure 2-11 ^{1}H, ($CDCl_3$), 500 MHz, (**3**)

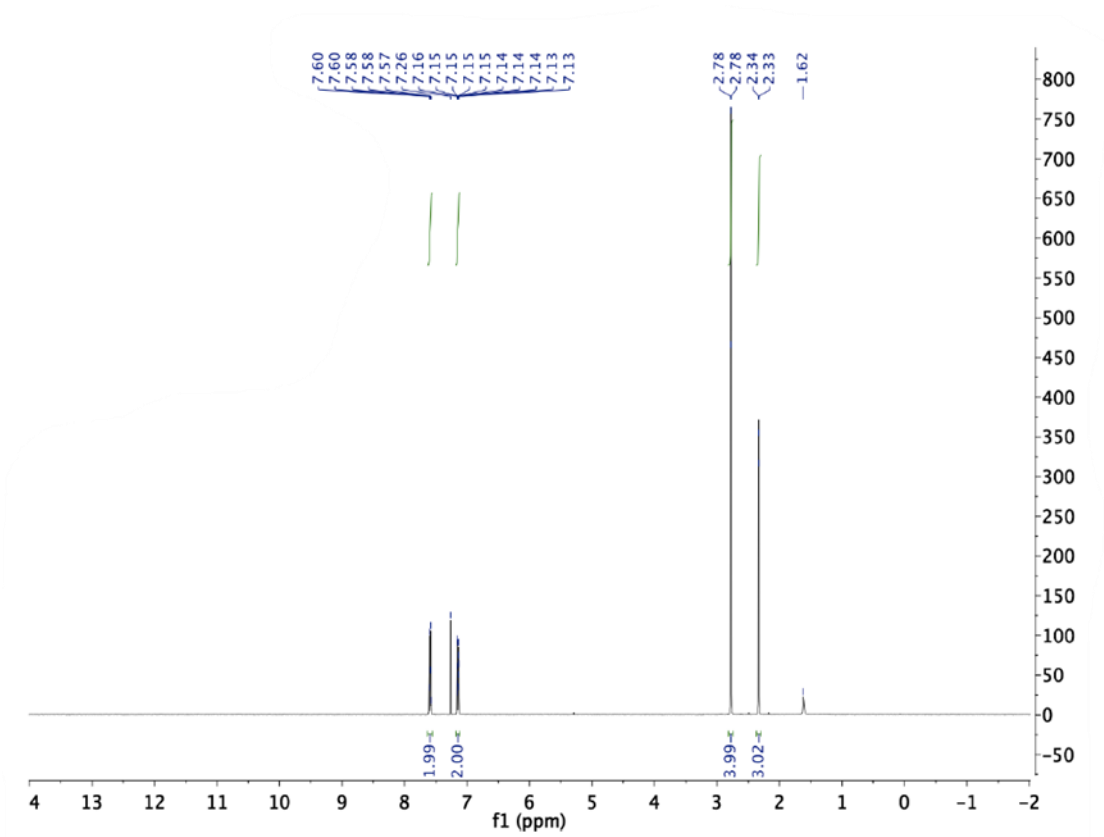

Figure 2-12 ^{1}H, ($CDCl_3$), 400 MHz, (**2a**)

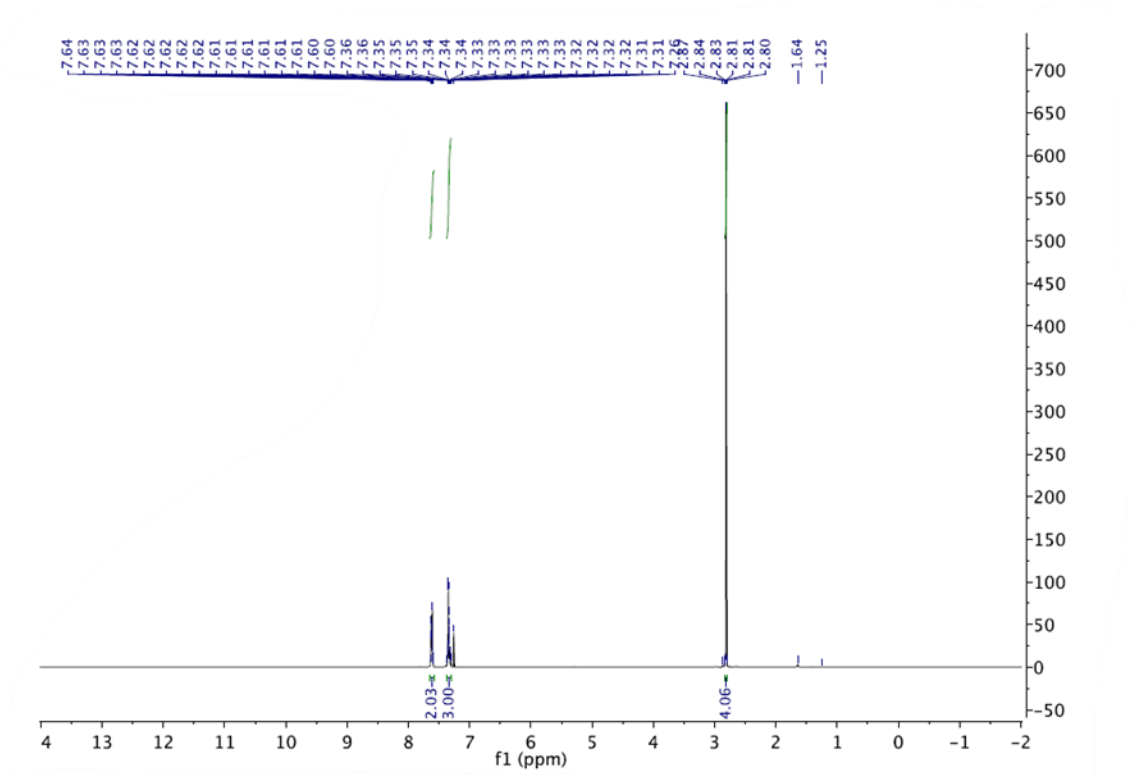

Figure 2-13 ^{1}H, ($CDCl_3$), 400 MHz, (**2b**)

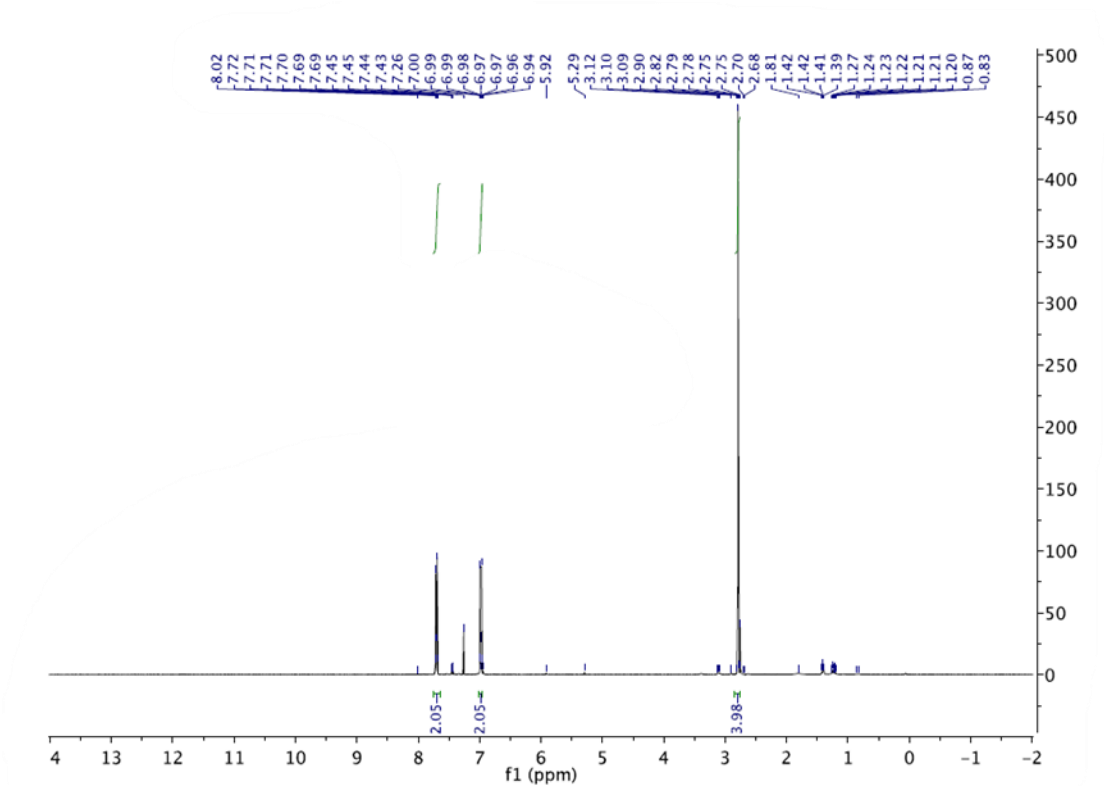

Figure 2-14 ^{1}H, $CDCl_3$, 400 MHz, (**2c**)

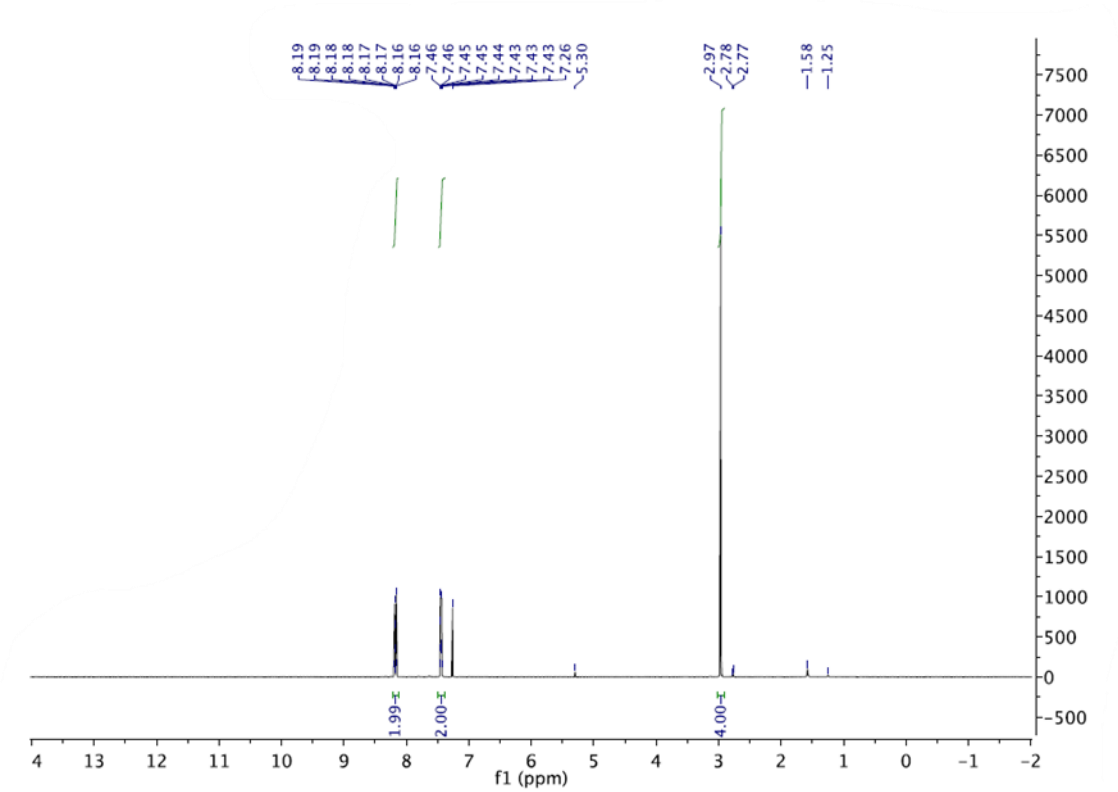

Figure 2-15 ^{1}H, ($CDCl_3$), 400 MHz, (**2d**)

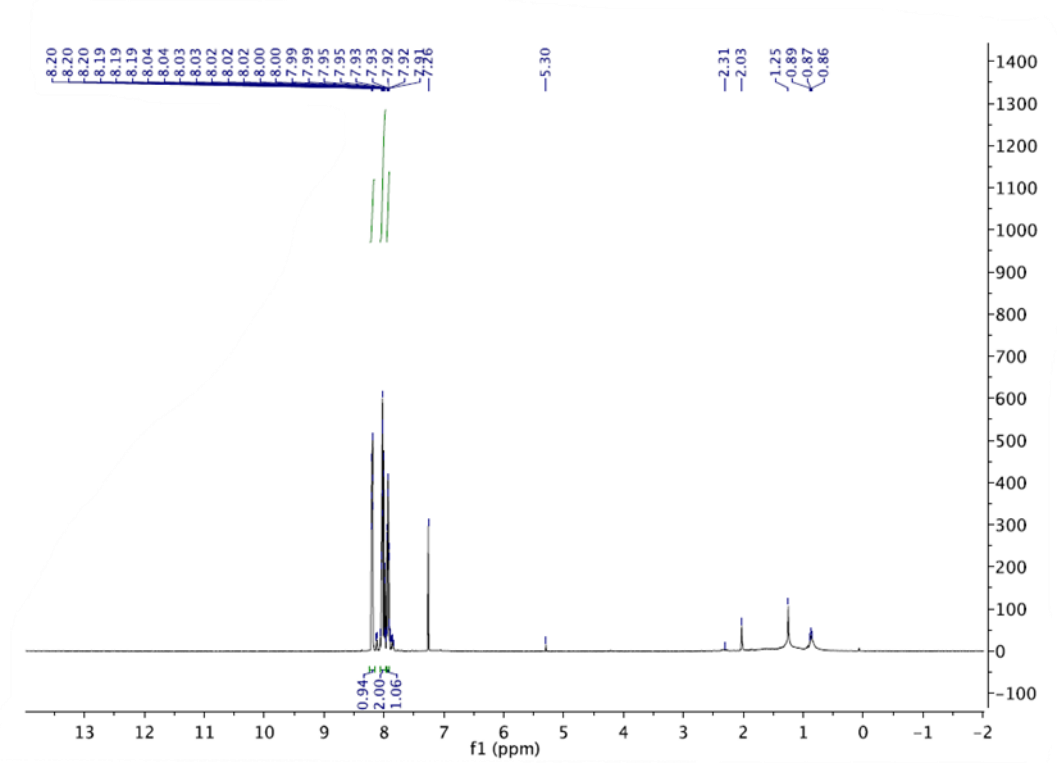

Figure 2-16 ^{1}H, $CDCl_3$, 500 MHz, (**2e**)

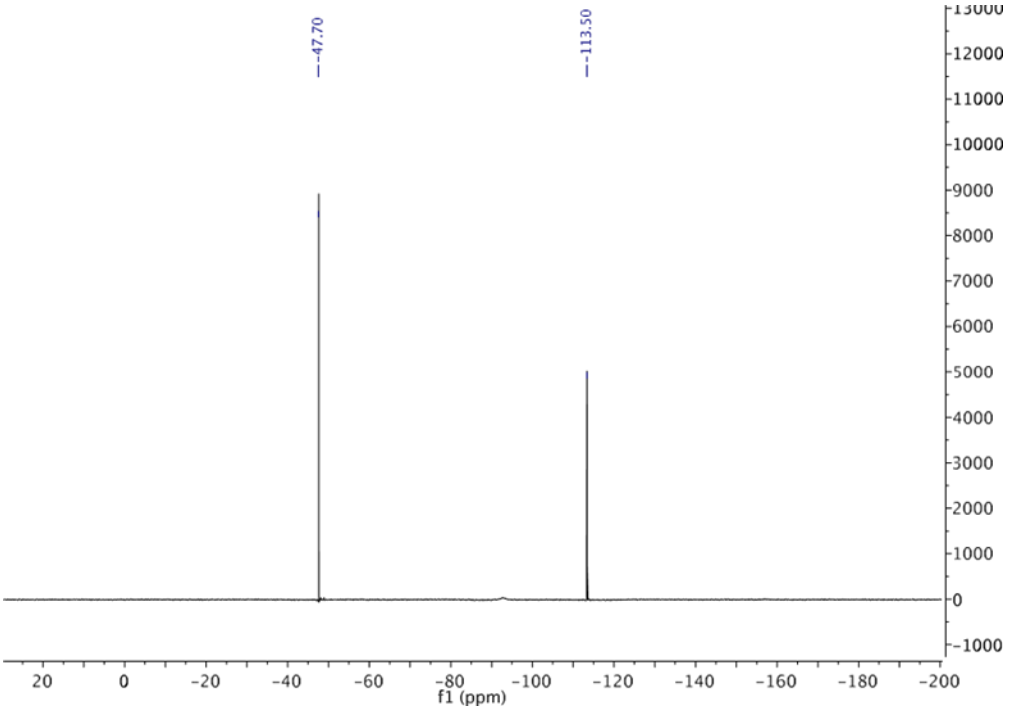

Figure 2-17 ^{19}F, $CDCl_3$, 470 MHz, (**2e**)

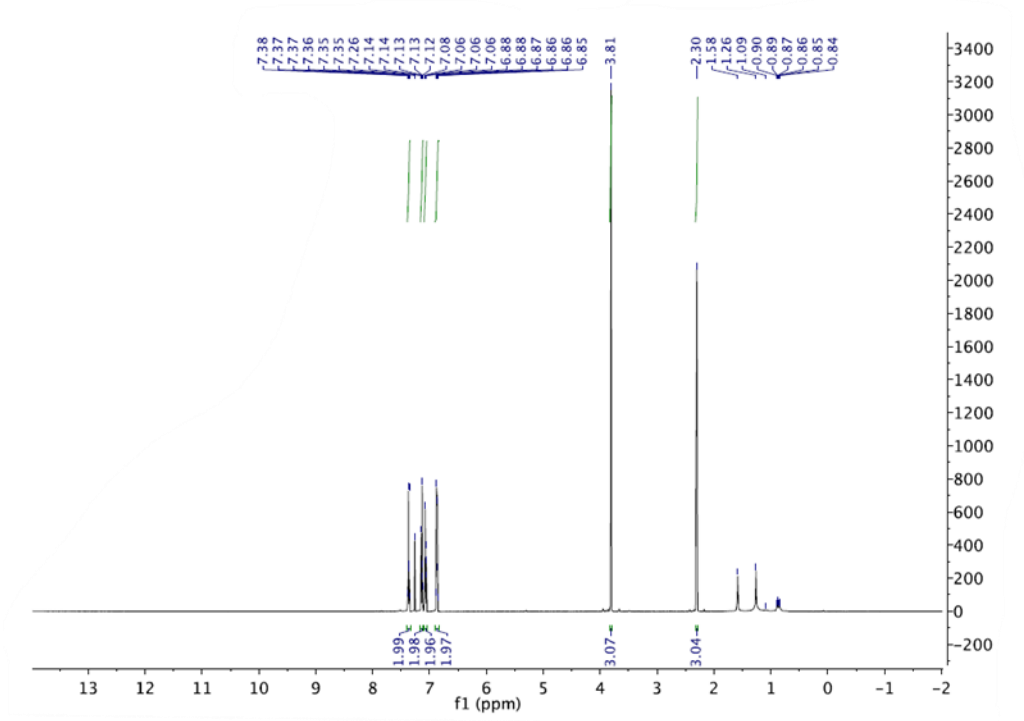

Figure 2-18 ^{1}H, $CDCl_3$, 500 MHz, (**4**)

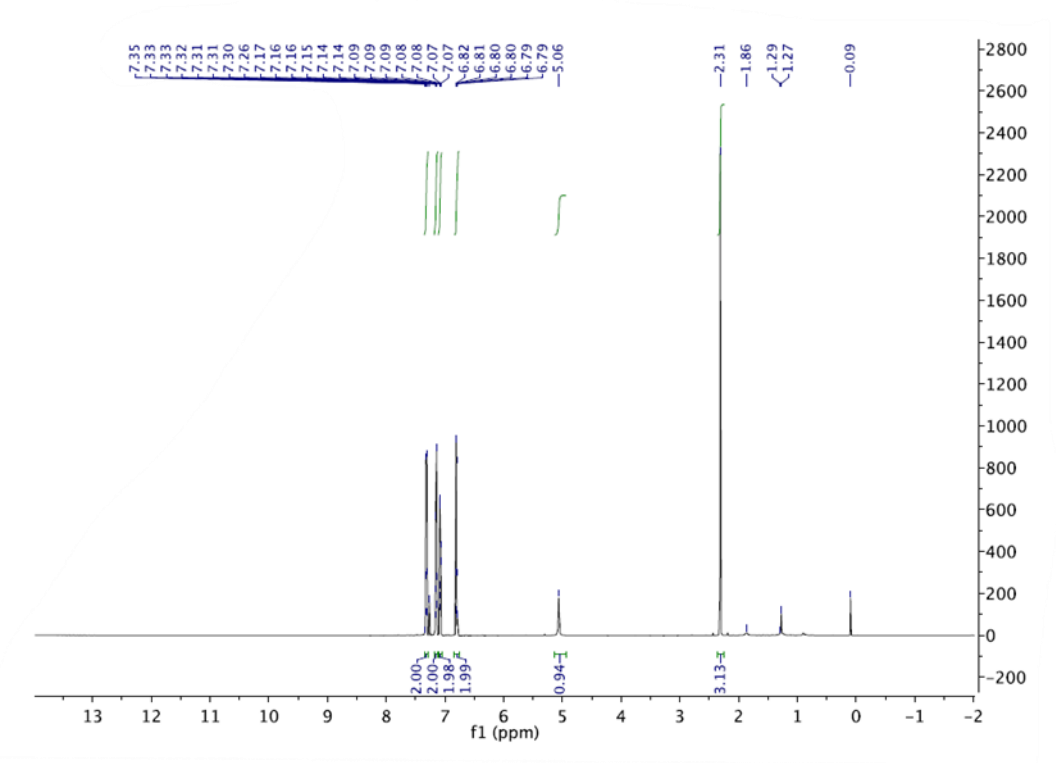

Figure 2-19 ^{1}H, $CDCl_3$, 500 MHz, (**5**)

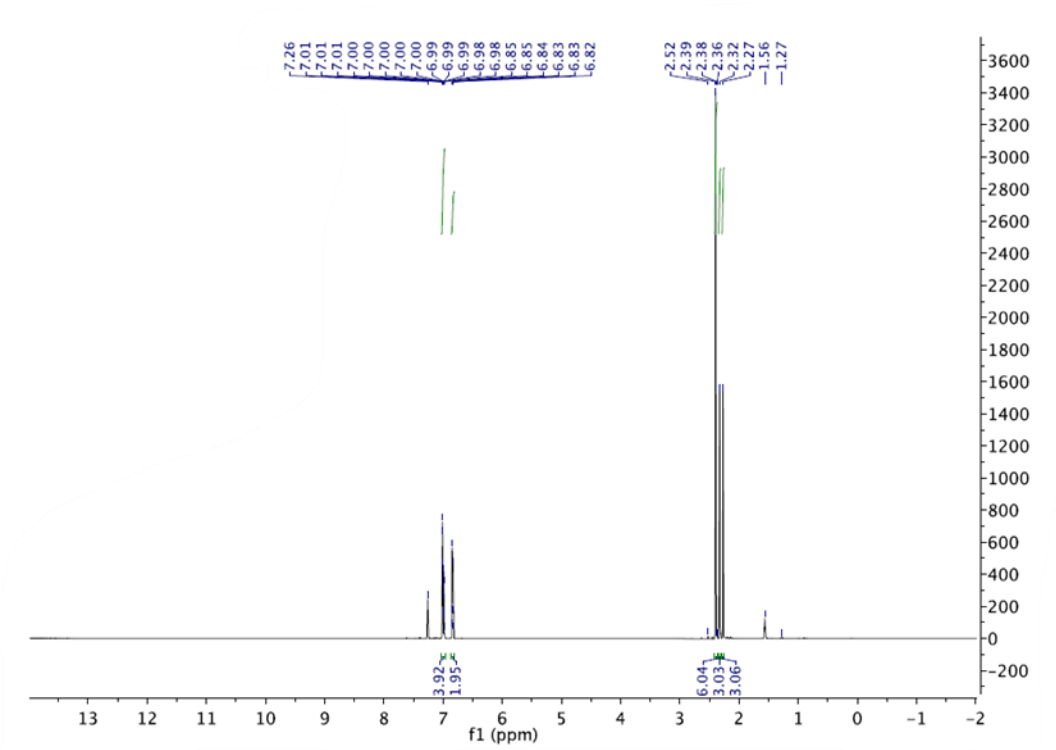

Figure 2-20 ^{1}H, $CDCl_3$, 500 MHz, (**6**)

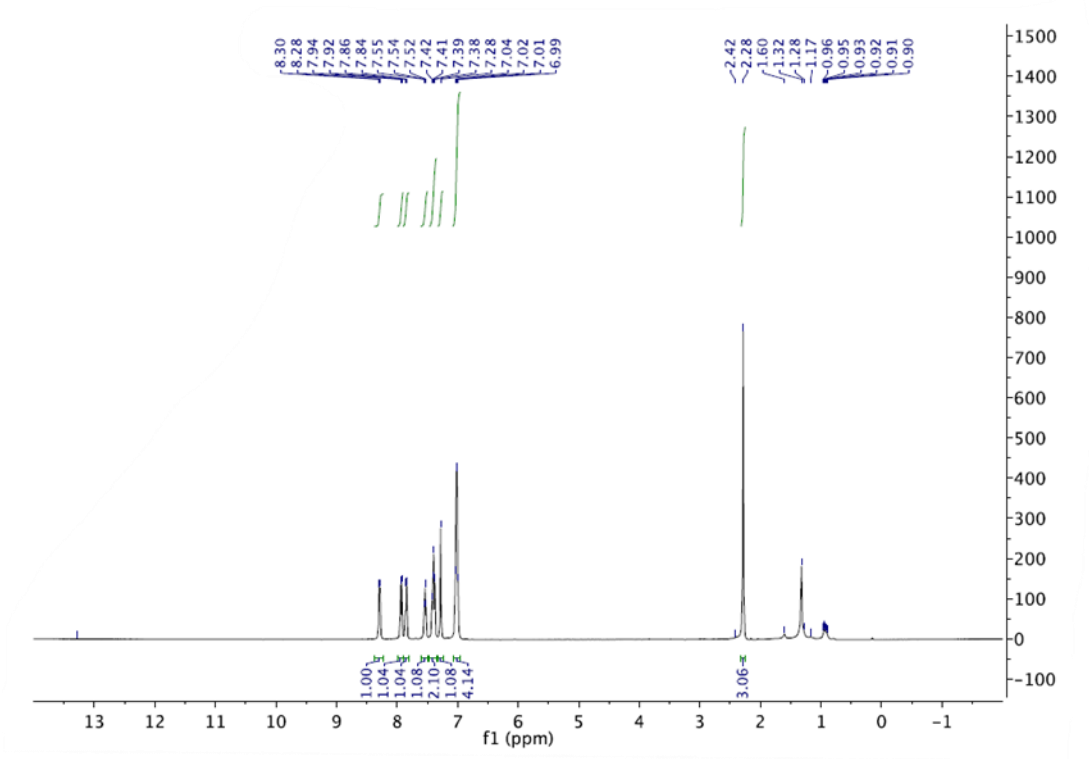

Figure 2-21 ^{1}H, $CDCl_3$, 500 MHz, (**7**)

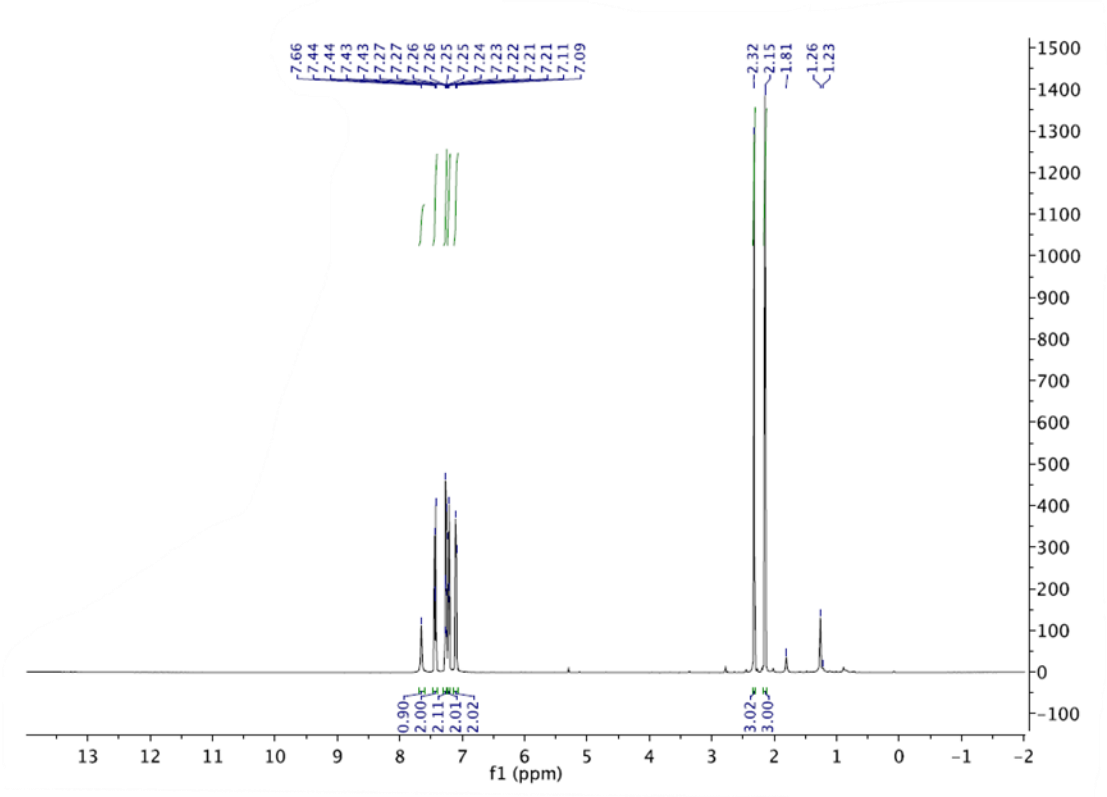

Figure 2-22 ^{1}H, $CDCl_3$, 500 MHz, (**8**)

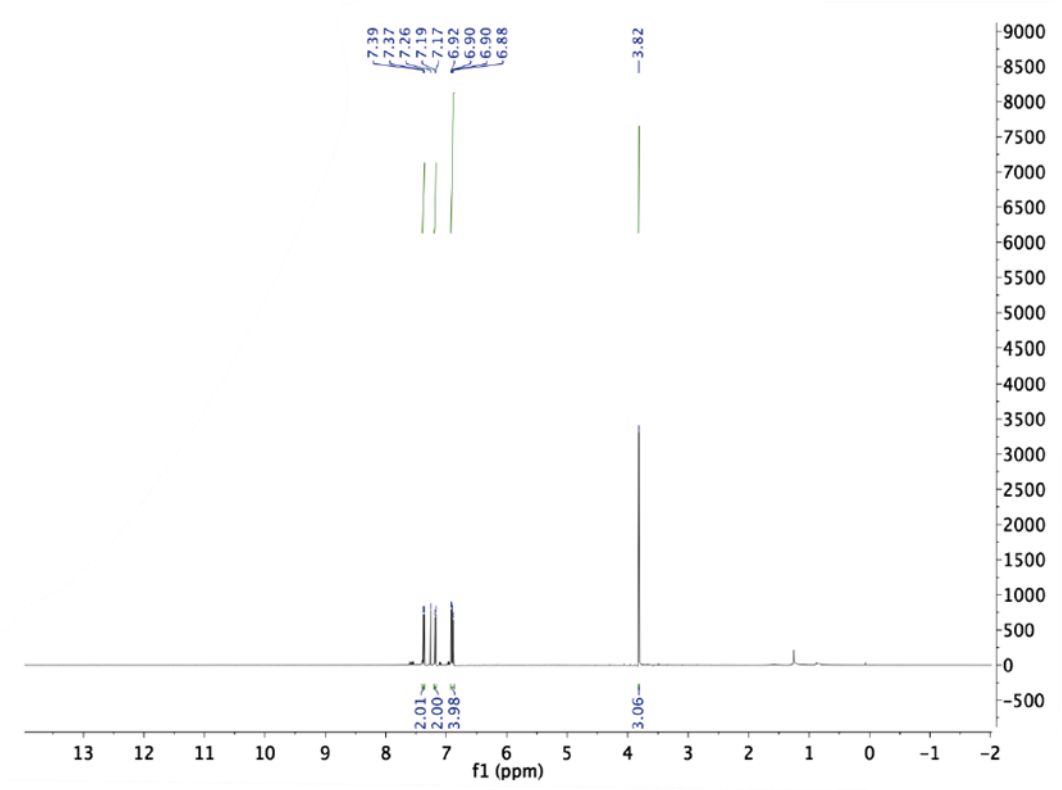

Figure 2-23 ^{1}H, $CDCl_3$, 500 MHz, (**10**)

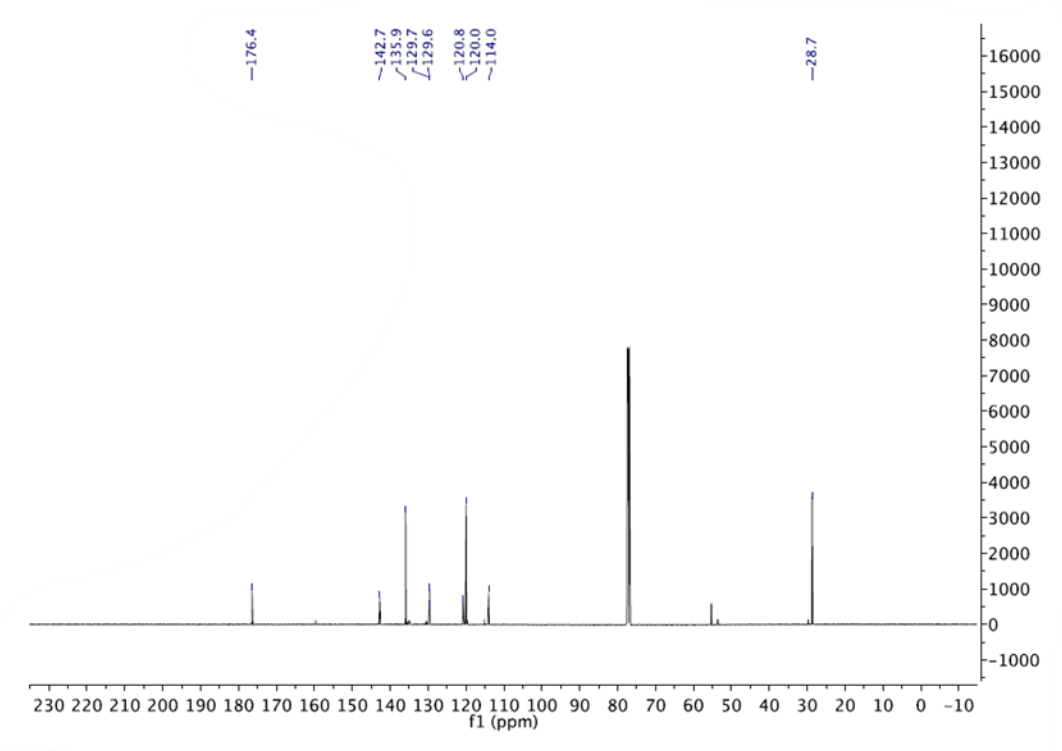

Figure 2-24 ^{13}C, $CDCl_3$, 126 MHz, (**10**)

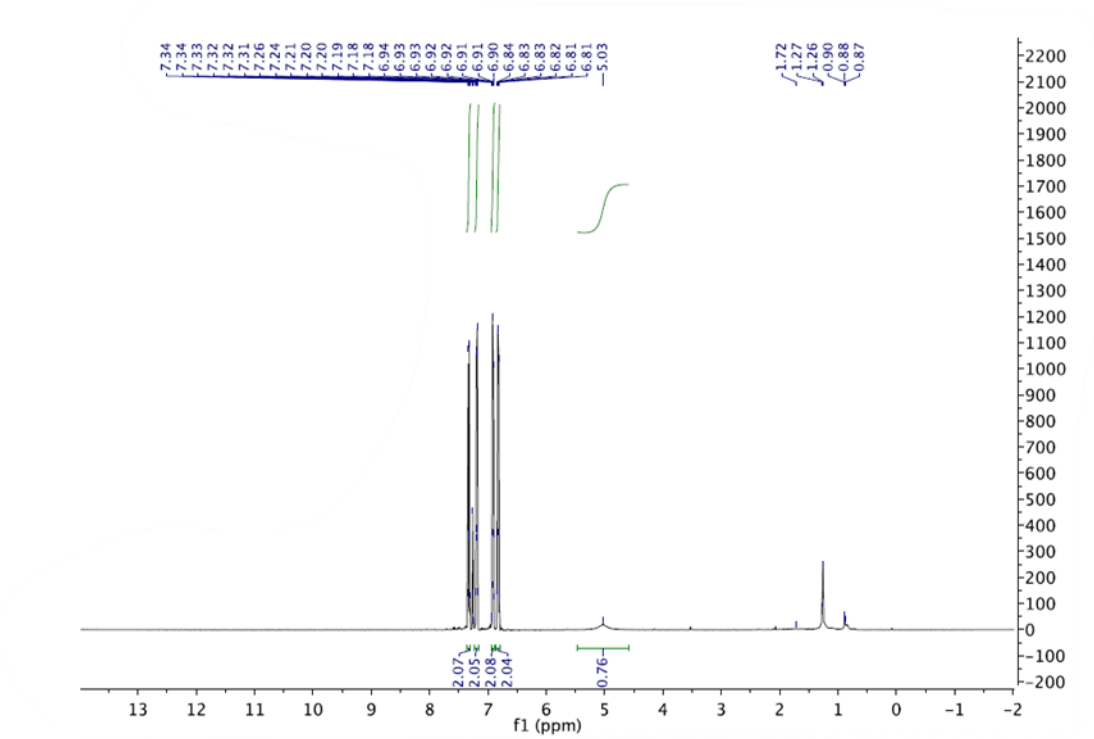

Figure 2-25 ^{1}H, $CDCl_3$, 500 MHz, (**13**)

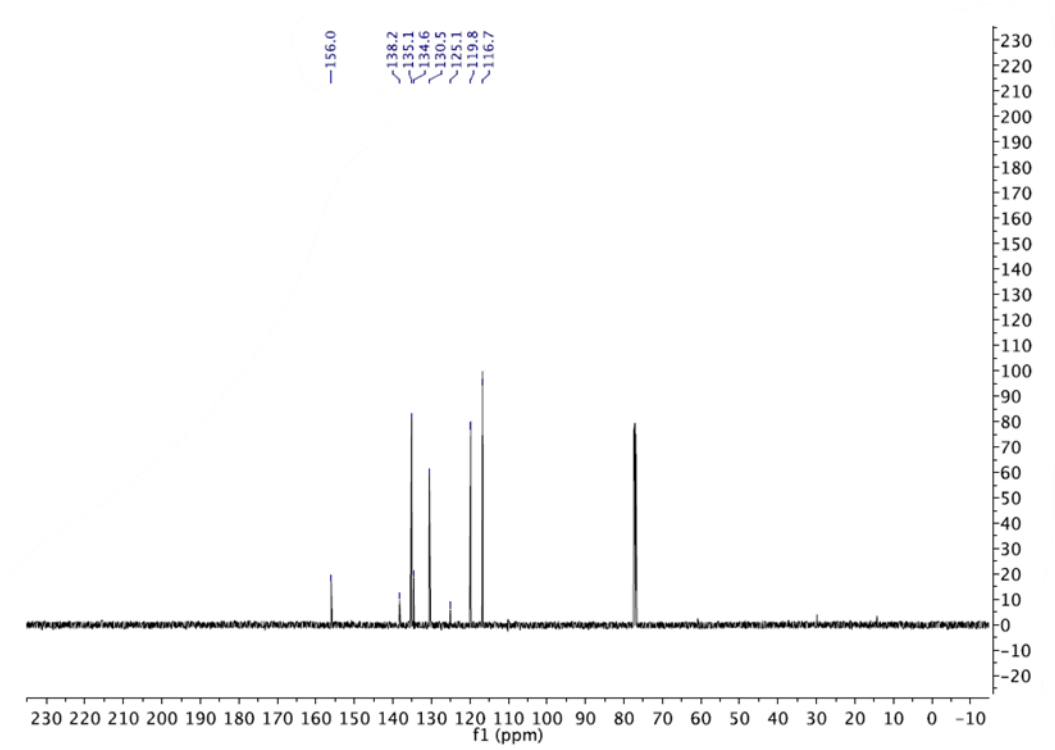

Figure 2-26 ^{13}C, $CDCl_3$, 126 MHz, (**13**)

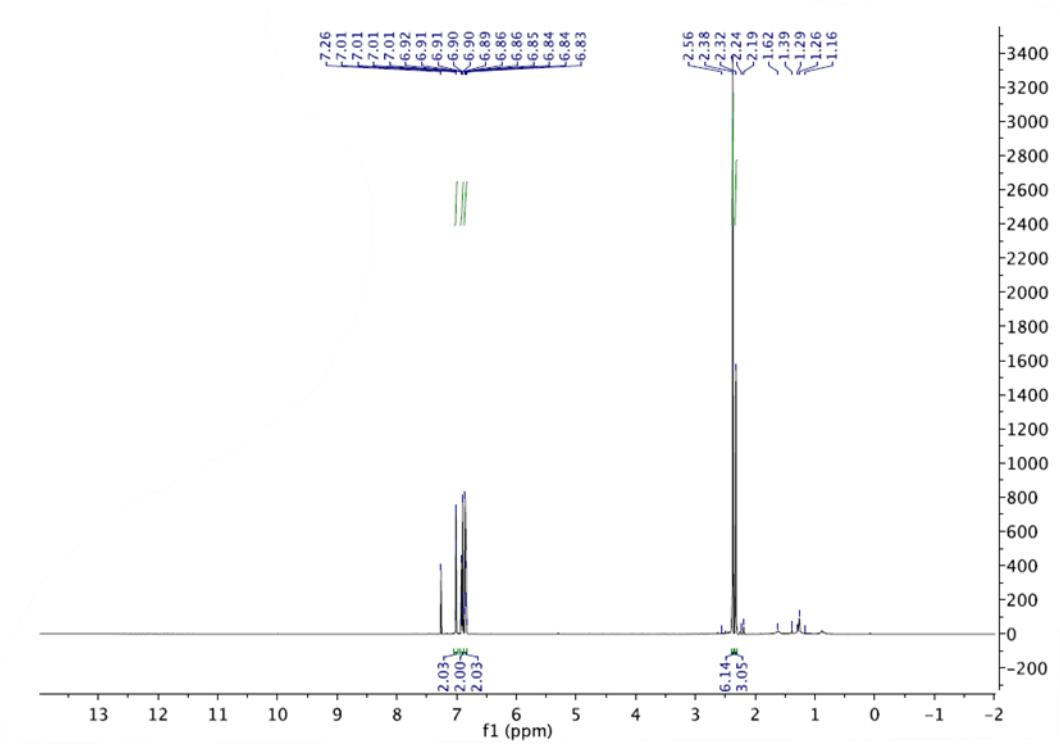

Figure 2-27 ^{1}H, $CDCl_3$, 500 MHz, (**14**)

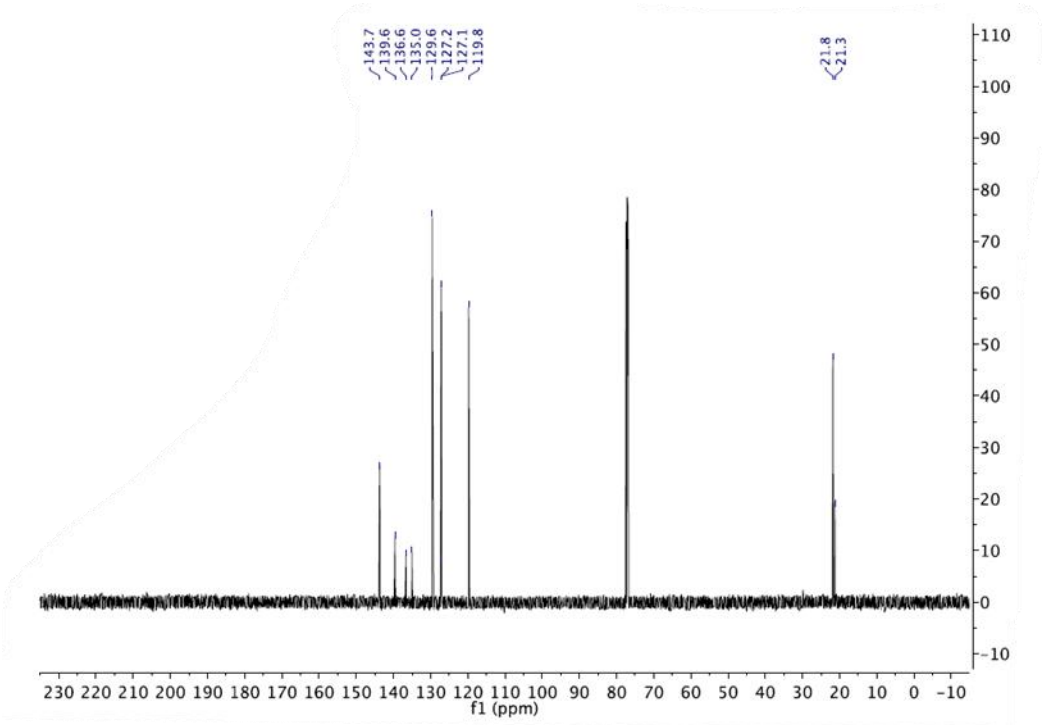

Figure 2-28 ^{13}C, $CDCl_3$, 126 MHz, (**14**)

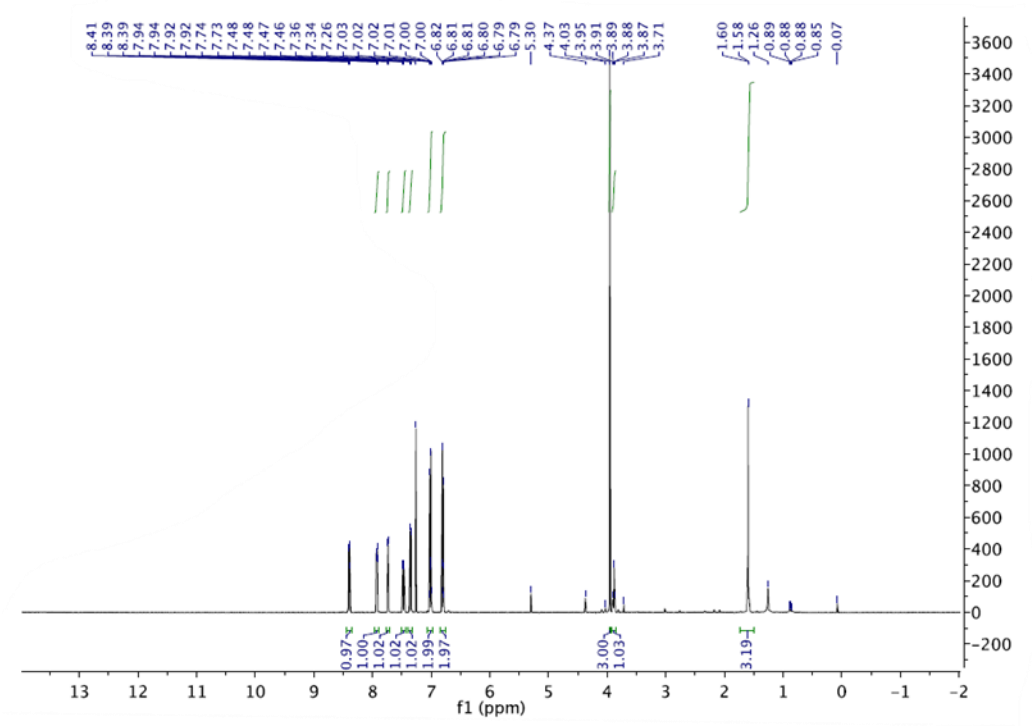

Figure 2-29 ^{1}H, $CDCl_3$, 500 MHz, (**15**)

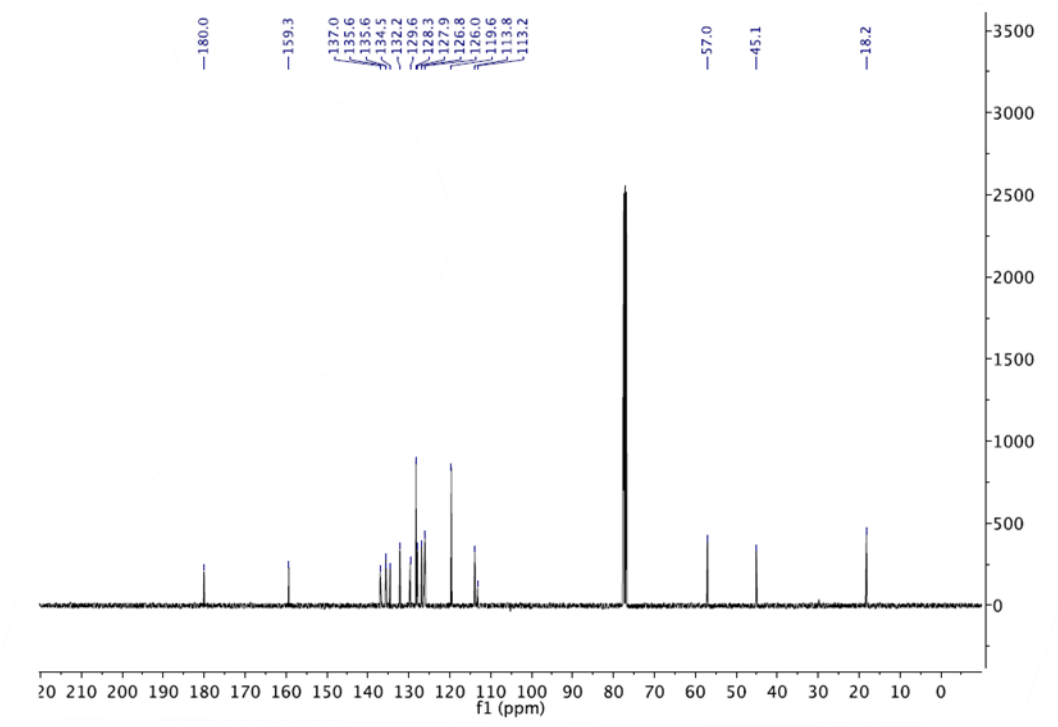

Figure 2-30 ^{13}C, $CDCl_3$, 101 MHz, (**15**)

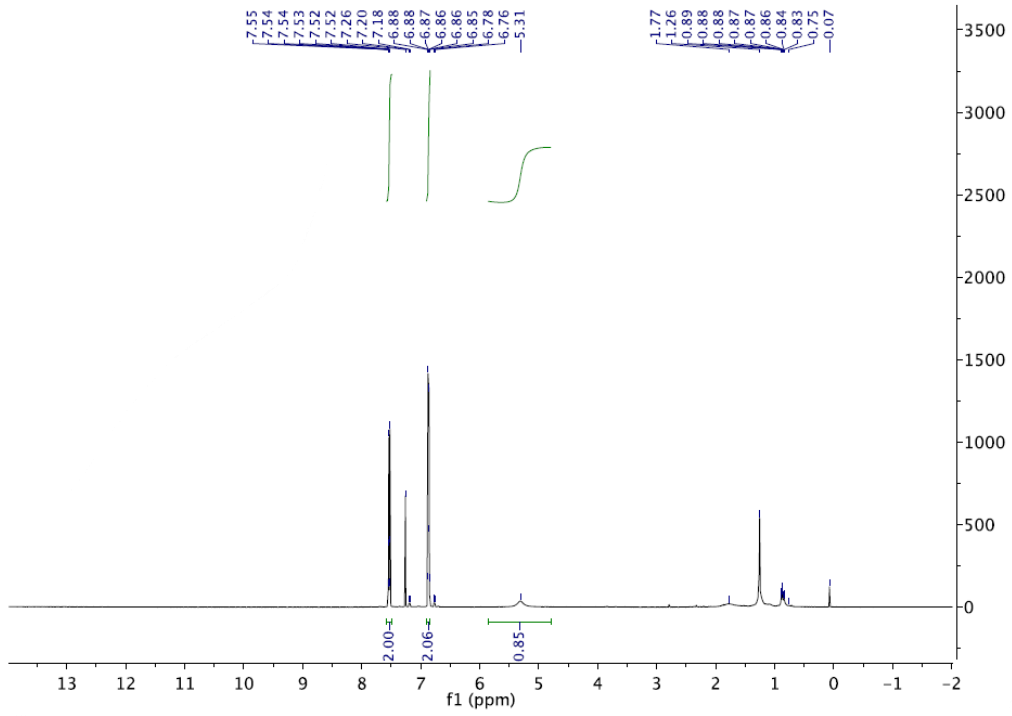

Figure 2-31 ^{1}H, $CDCl_3$, 500 MHz, (**16**)

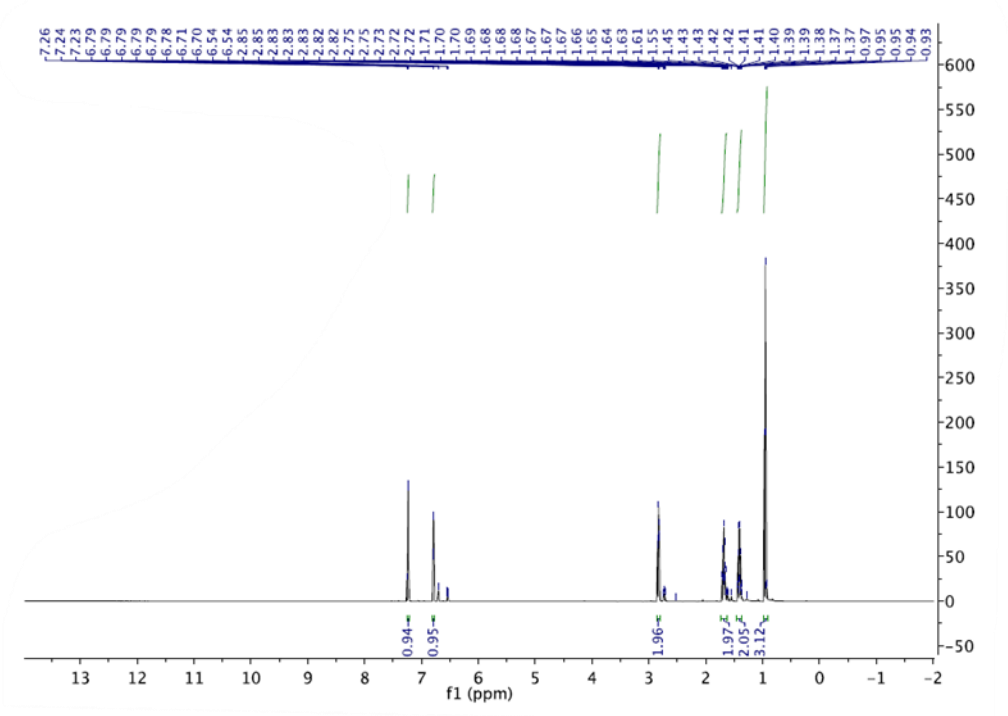

Figure 2-32 ^{1}H, $CDCl_3$, 400 MHz, (**17**)

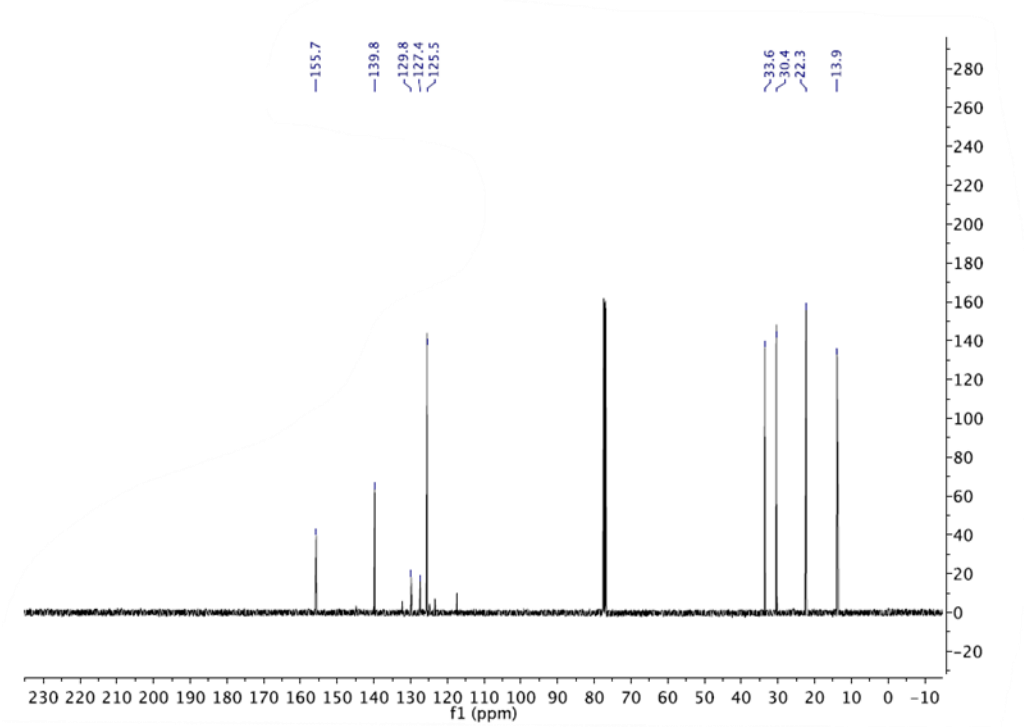

Figure 2-33 ^{13}C, $CDCl_3$, 126 MHz, (**17**)

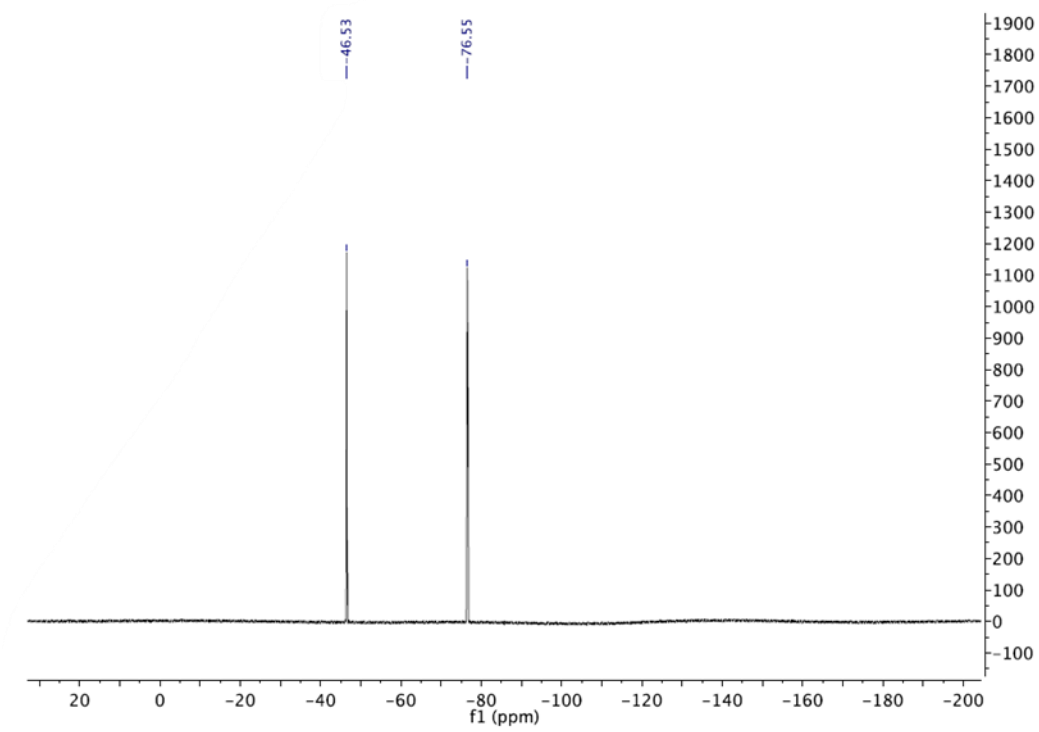

Figure 2-34 ^{19}F, $CDCl_3$, 376 MHz, (**17**)

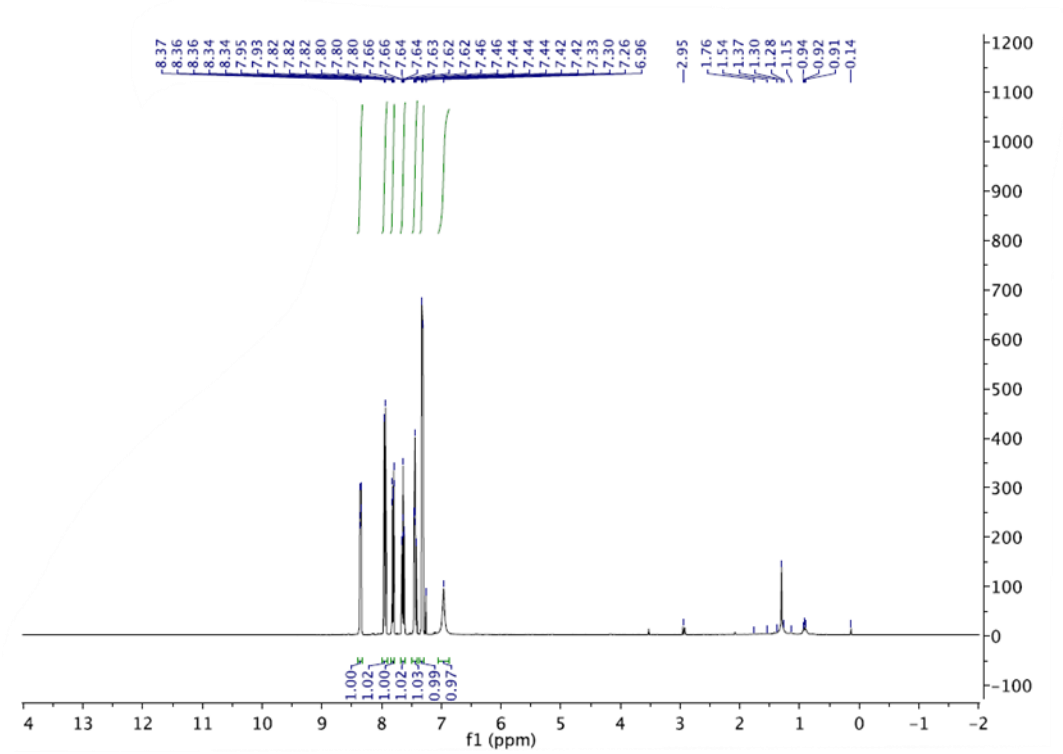

Figure 2-35 ^{1}H, $CDCl_3$, 500 MHz, (**18**)

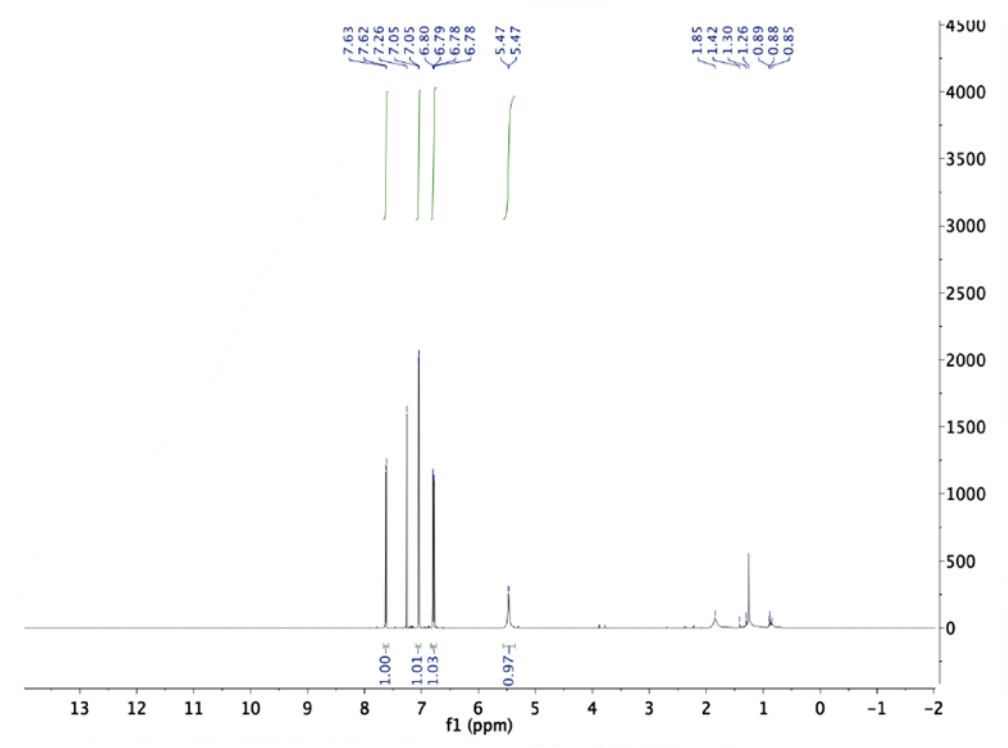

Figure 2-36 ^{1}H, $CDCl_3$, 500 MHz, (**19**)

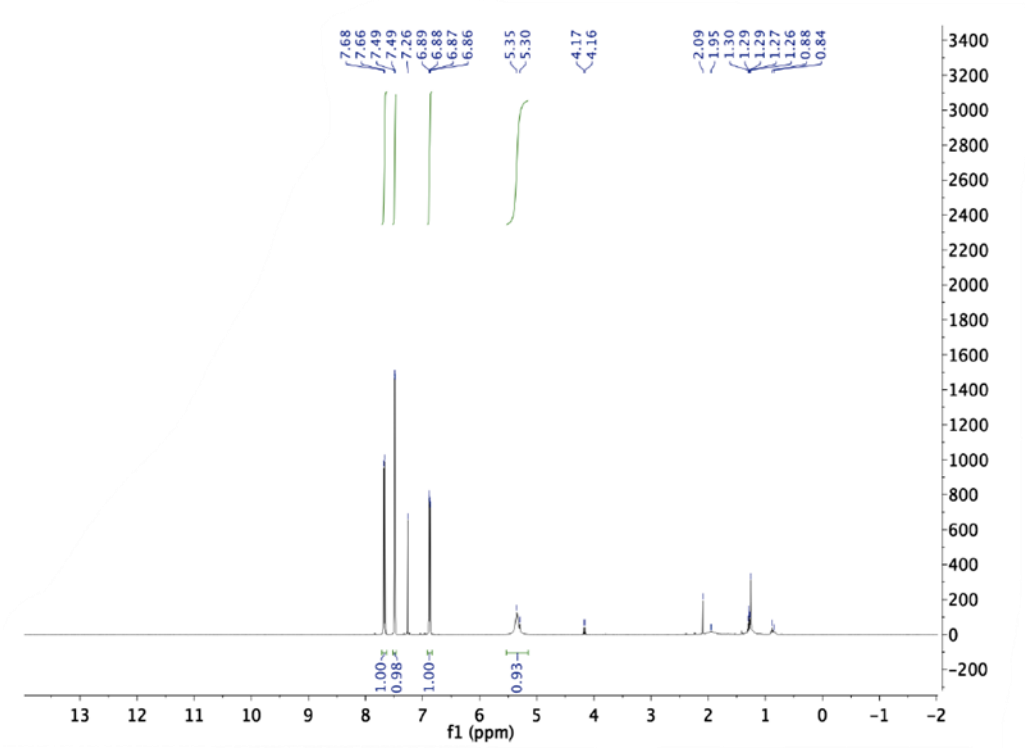

Figure 2-37 ^{1}H, $CDCl_3$, 500 MHz, (**20**)

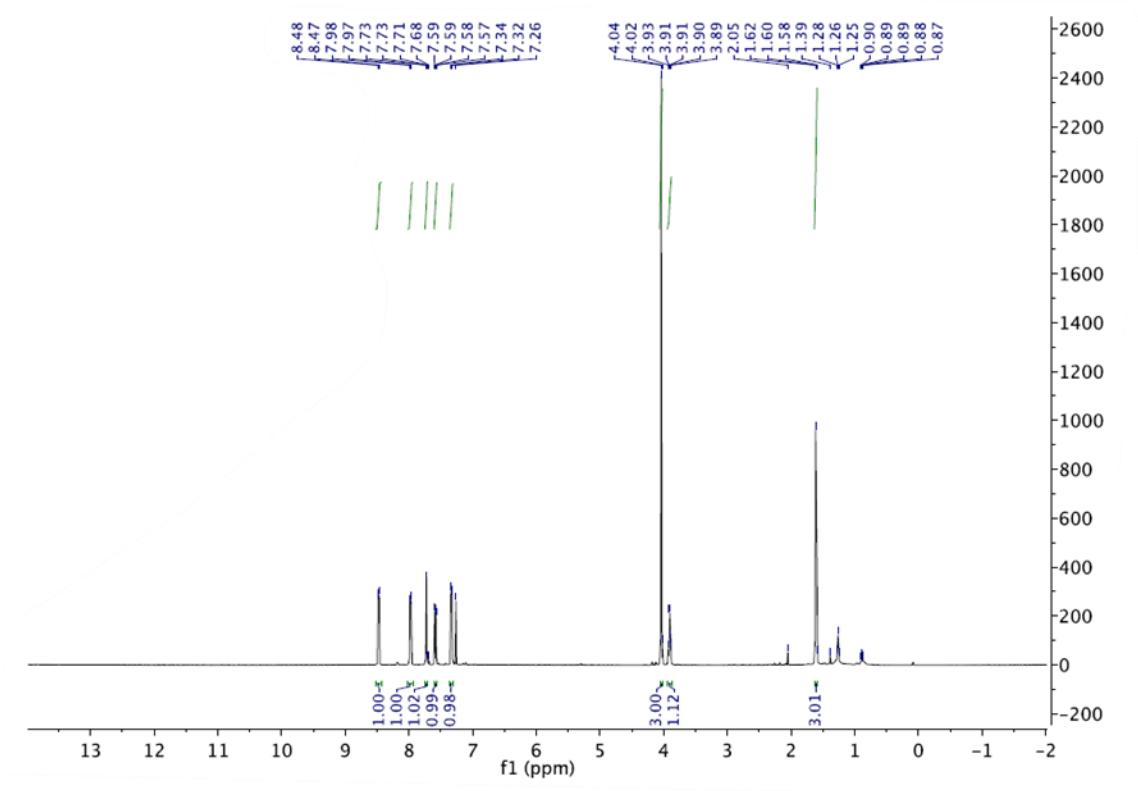

Figure 2-38 ^{1}H, $CDCl_3$, 500 MHz, (**21**)

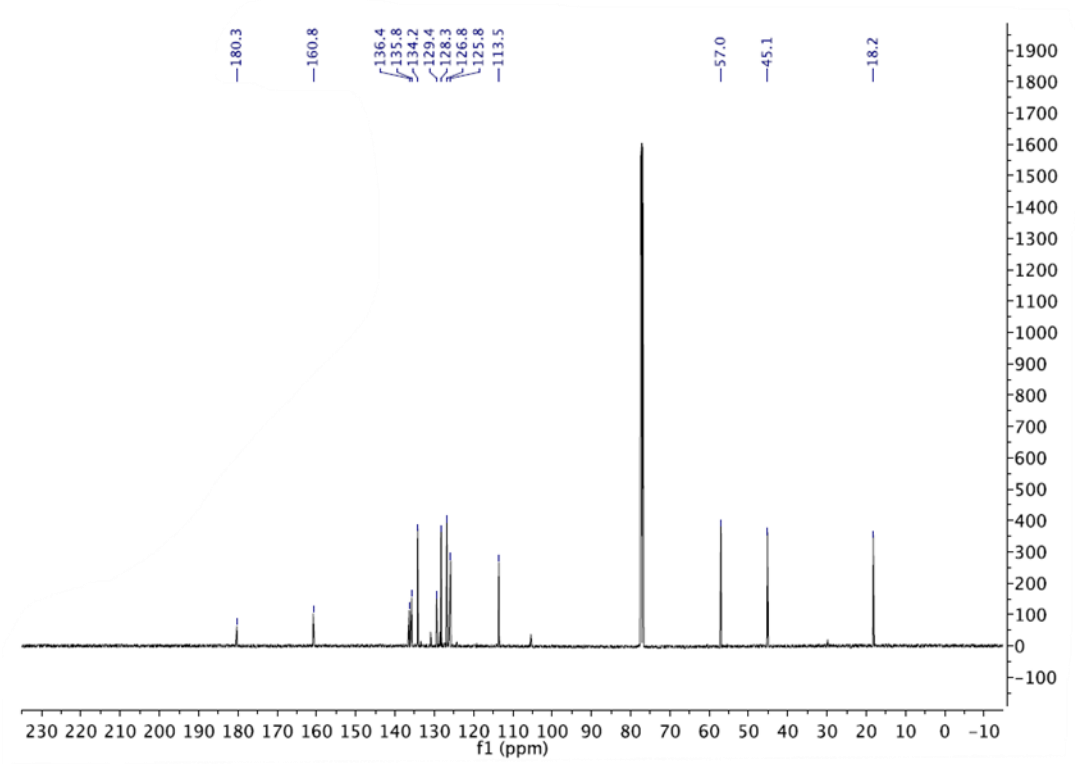

Figure 2-39 ^{13}C, $CDCl_3$, 126 MHz, (**21**)

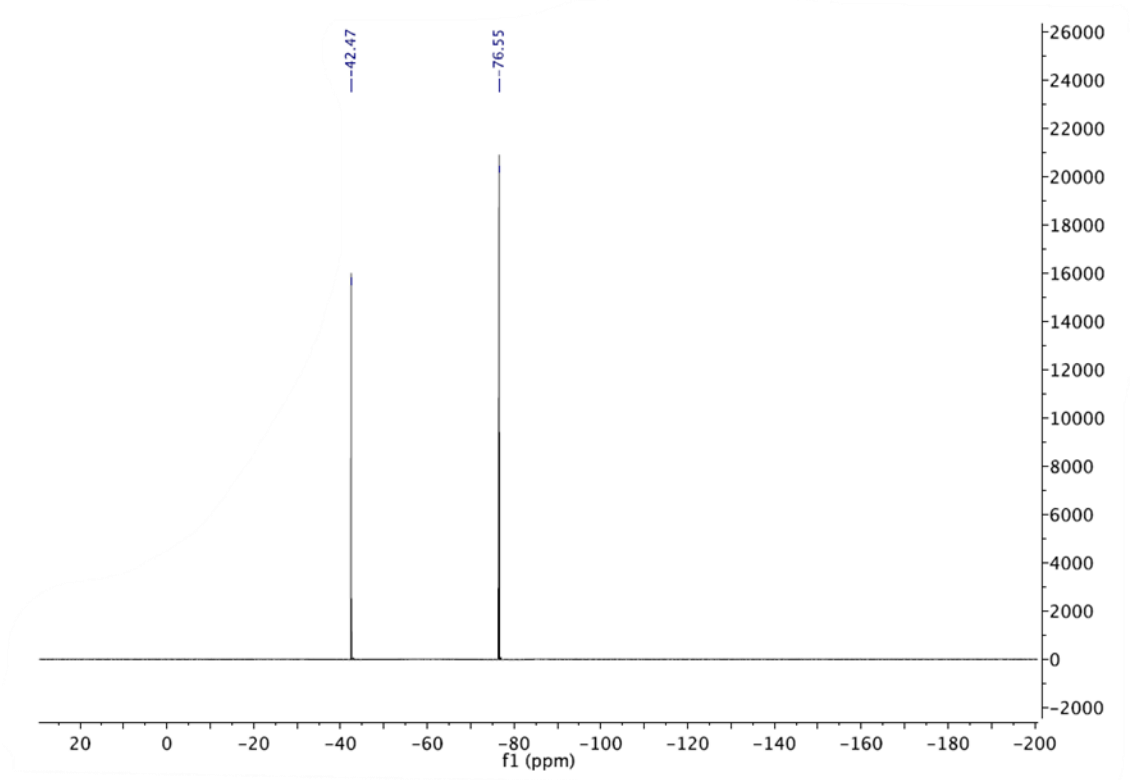

Figure 2-40 ^{19}F, $CDCl_3$, 470 MHz, (**21**)

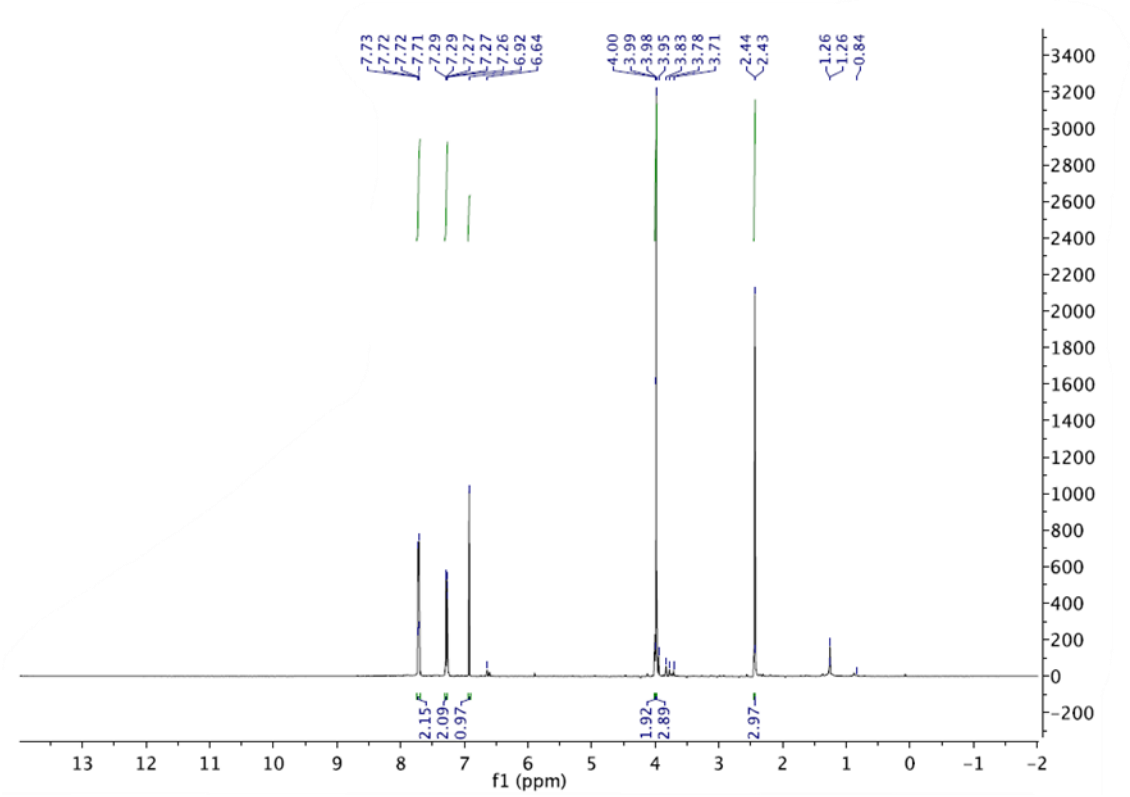

Figure 2-41 ^{1}H, $CDCl_3$, 500 MHz, (**22**)

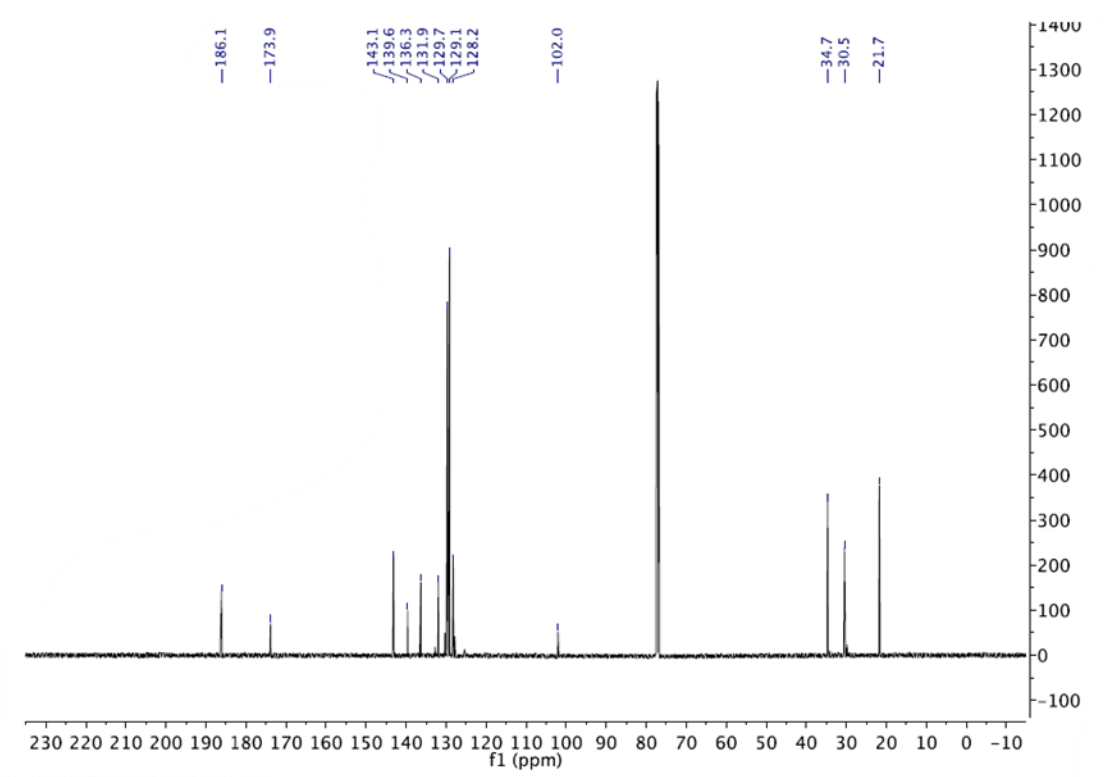

Figure 2-42 ^{13}C, $CDCl_3$, 126 MHz, (**22**)

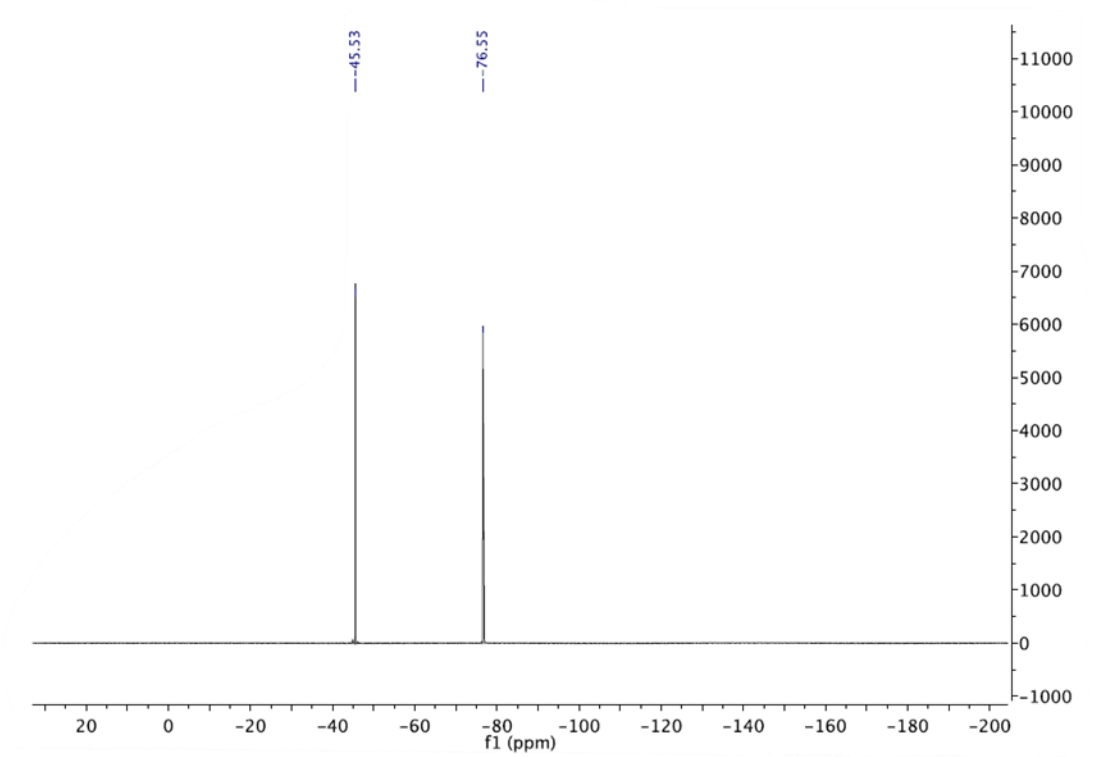

Figure 2-43 ^{19}F, $CDCl_3$, 376 MHz, (**22**)

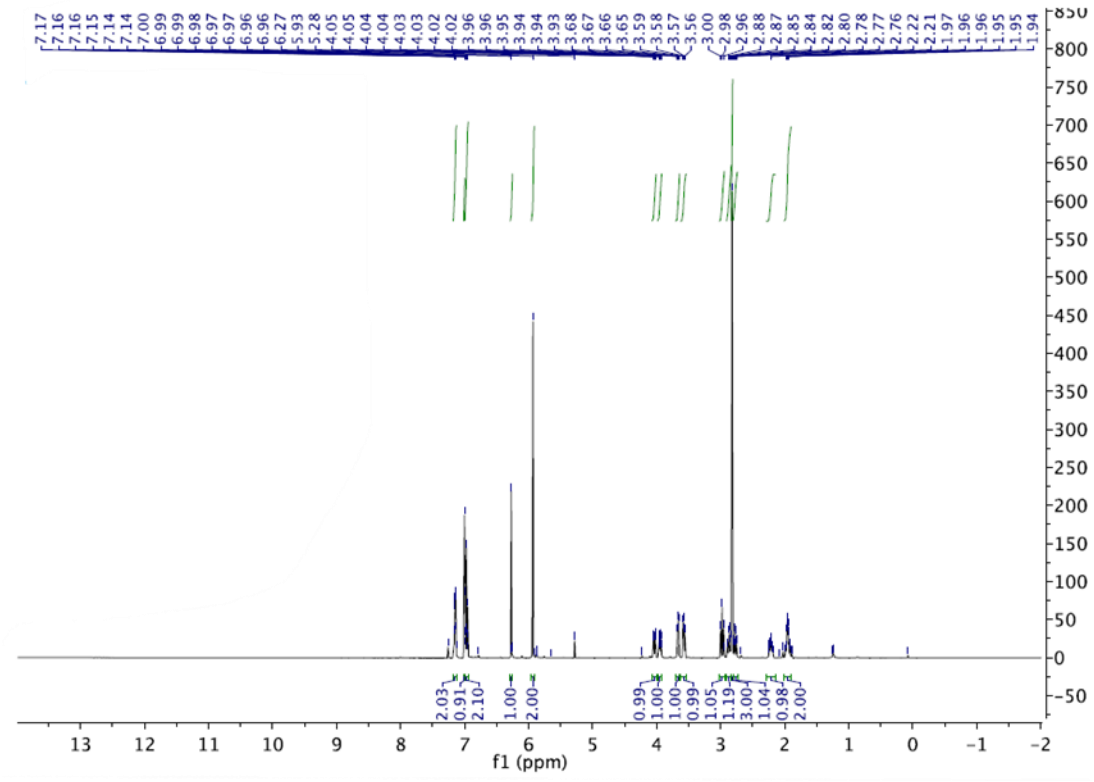

Figure 2-44 ^{1}H, $CDCl_3$, 500 MHz, (**23**)

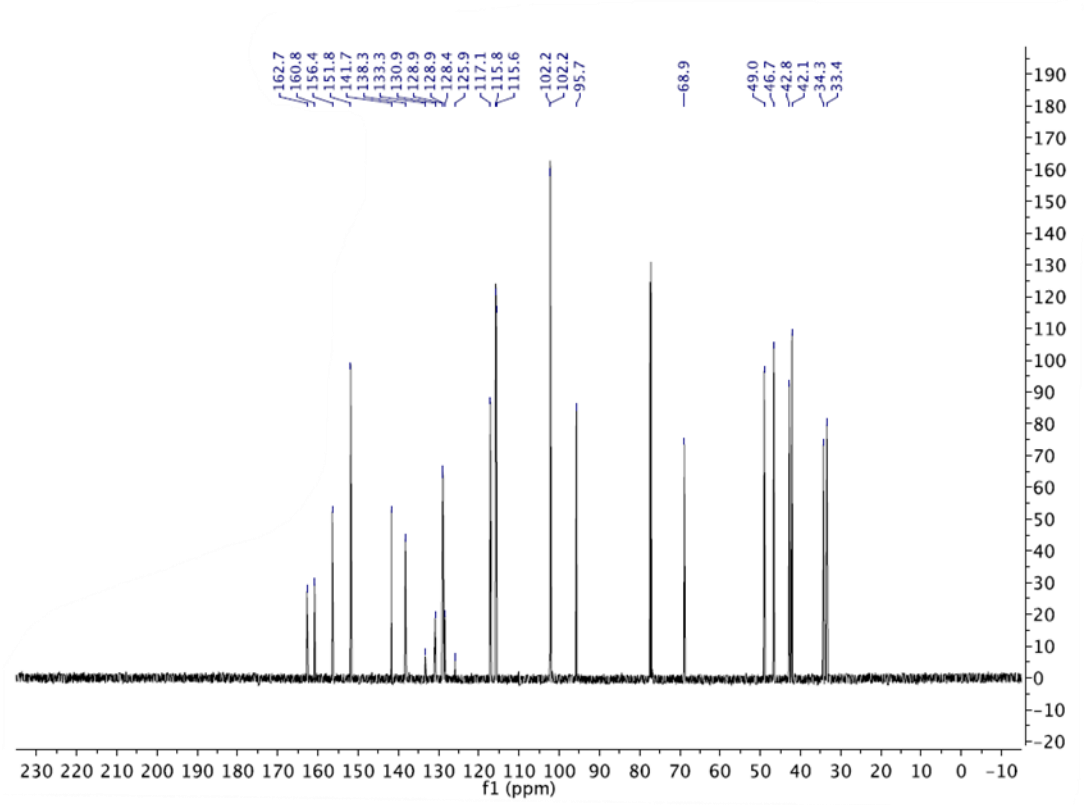

Figure 2-45 ^{13}C, $CDCl_3$, 126 MHz, (**23**)

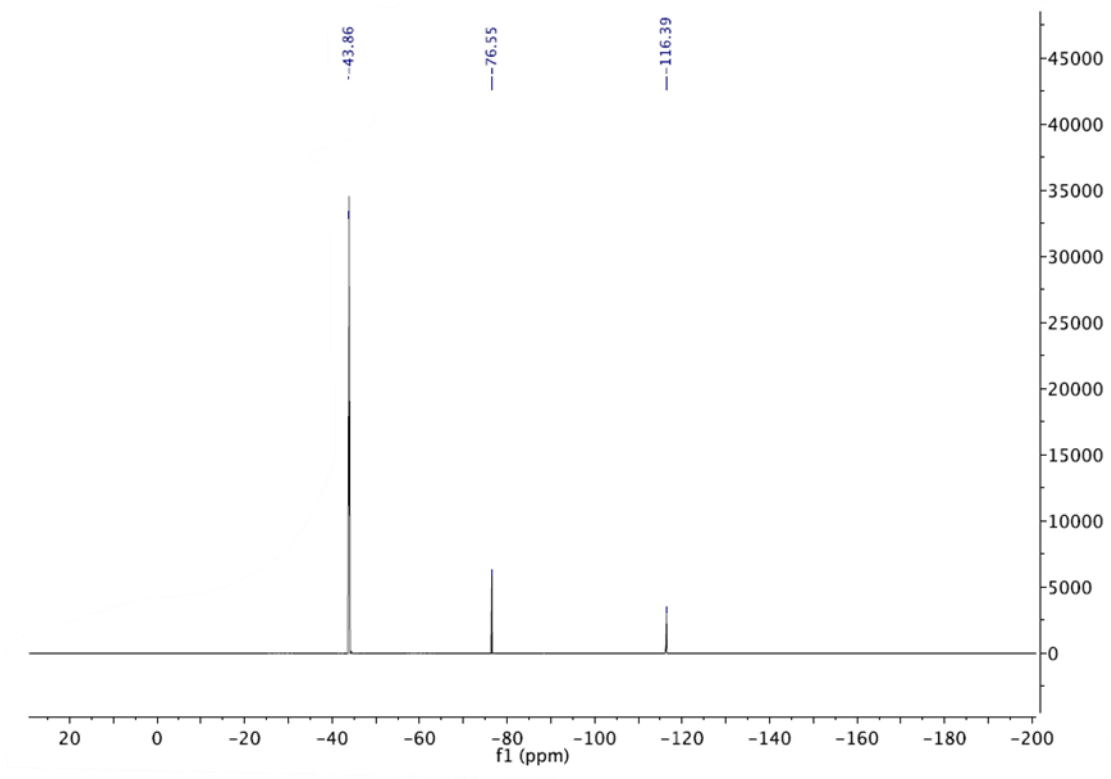

Figure 2-46 ^{19}F, $CDCl_3$, 376 MHz, (**23**)

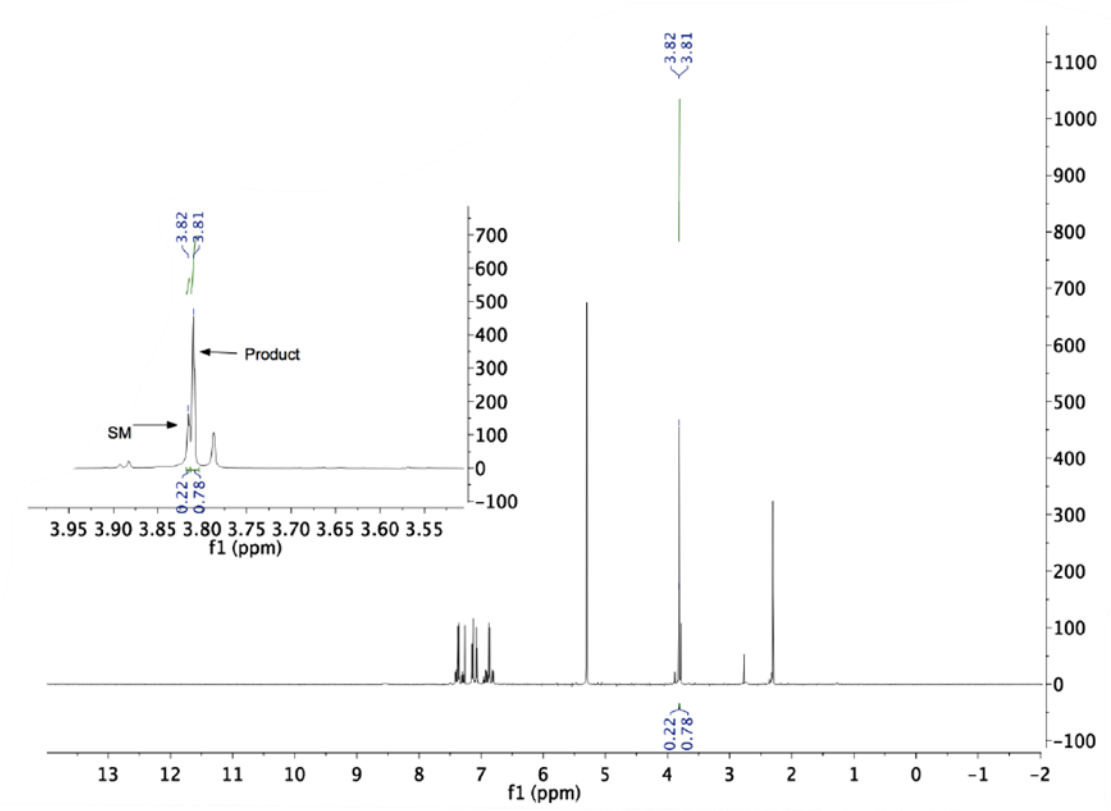

Figure 2-47 ^{1}H, $CDCl_3$, 500 MHz, (**4**) NMR conversion with catalyst **3**

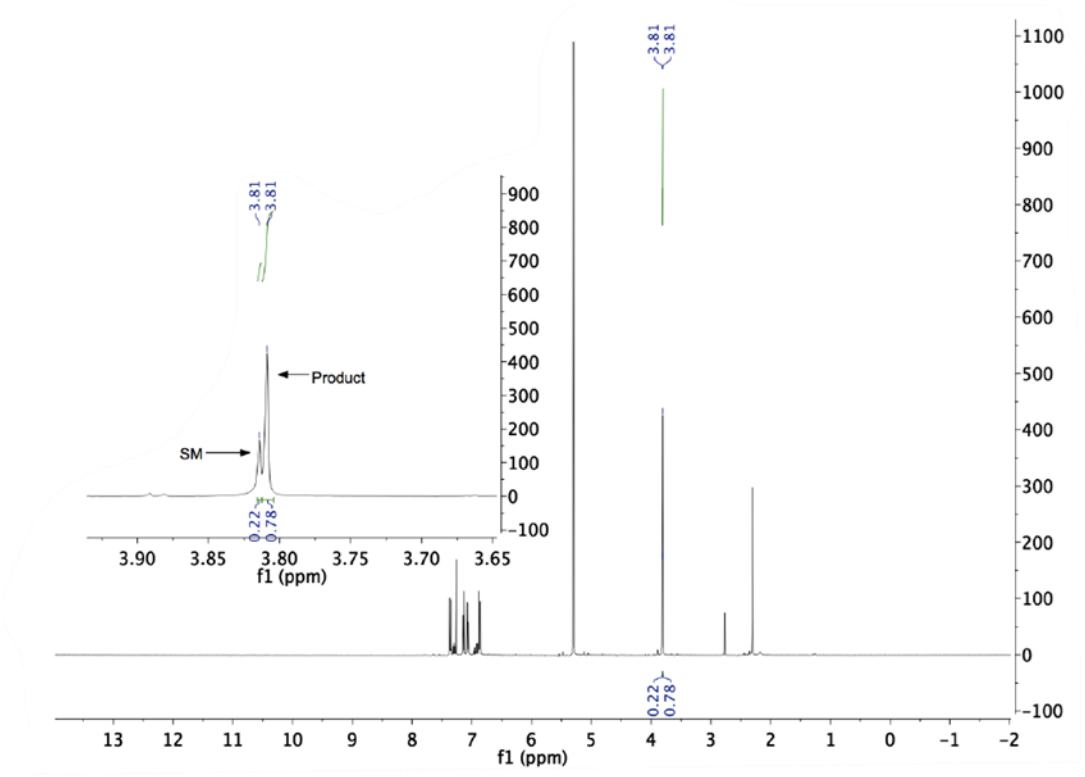

Figure 2-48 ^{1}H, $CDCl_3$, 500 MHz, (**4**) NMR conversion without catalyst **3**

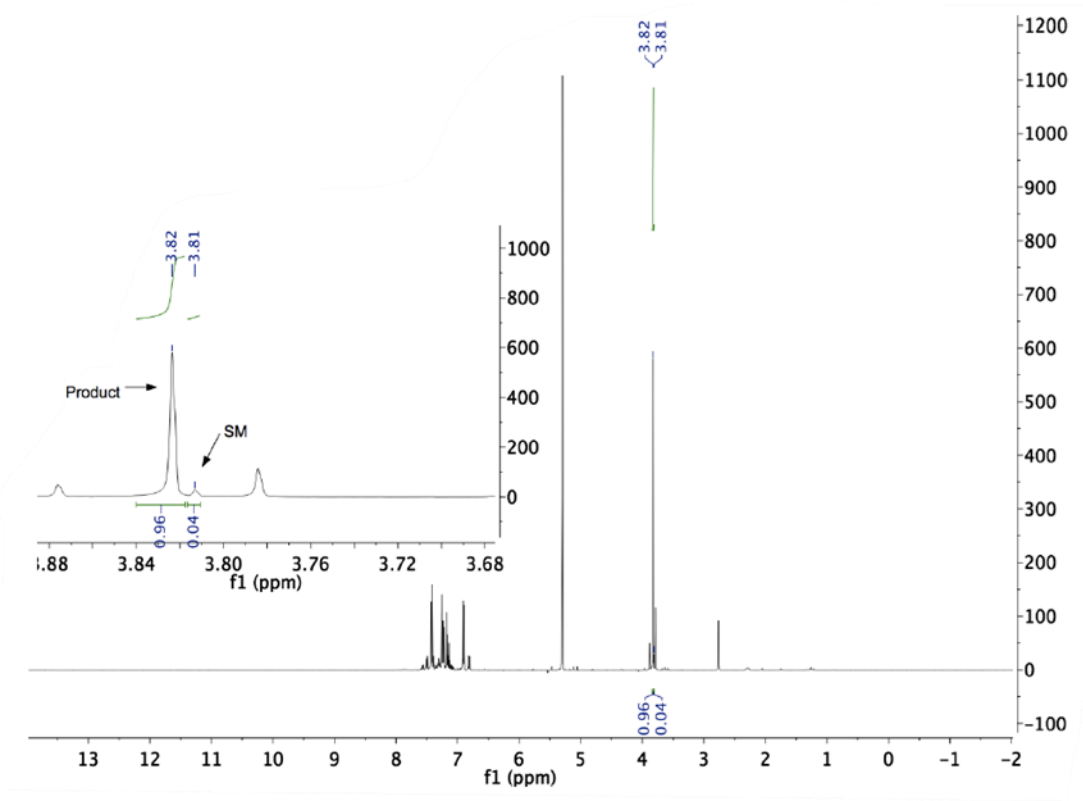

Figure 2-49 ^{1}H, $CDCl_3$, 500 MHz, (**9**) NMR conversion with catalyst **3**

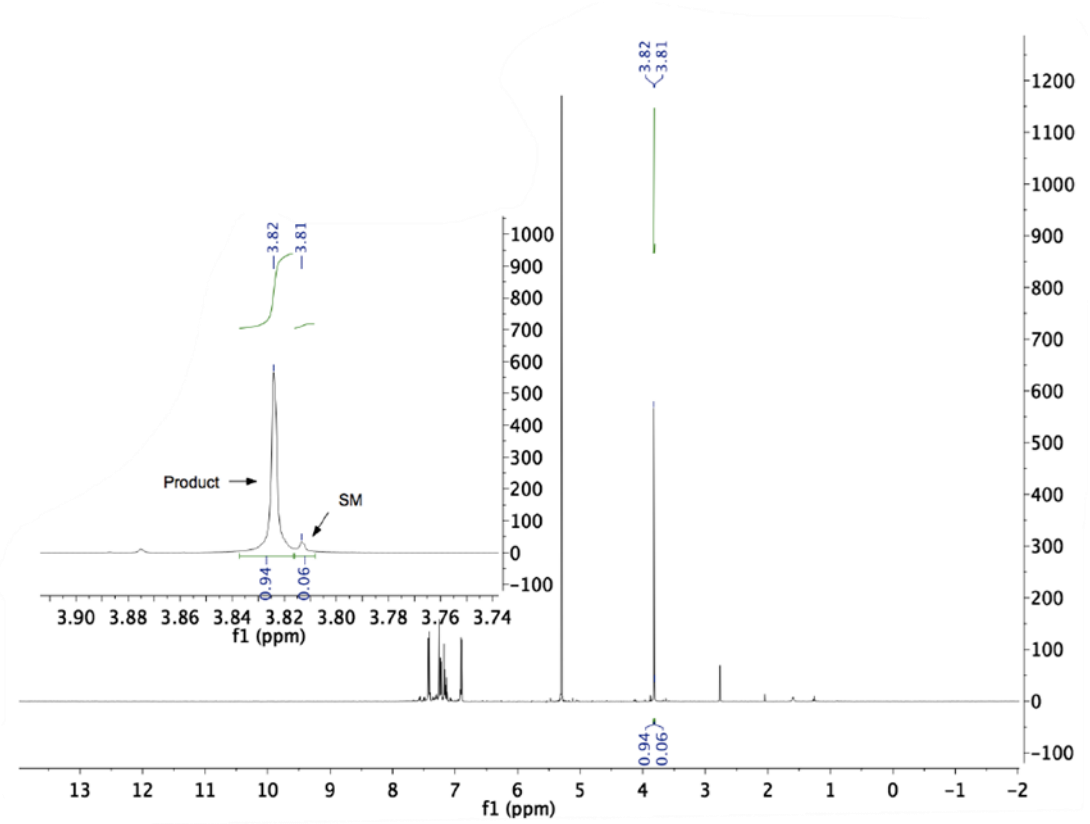

Figure 2-50 ^{1}H, $CDCl_3$, 500 MHz, (**9**) NMR conversion without catalyst **3**

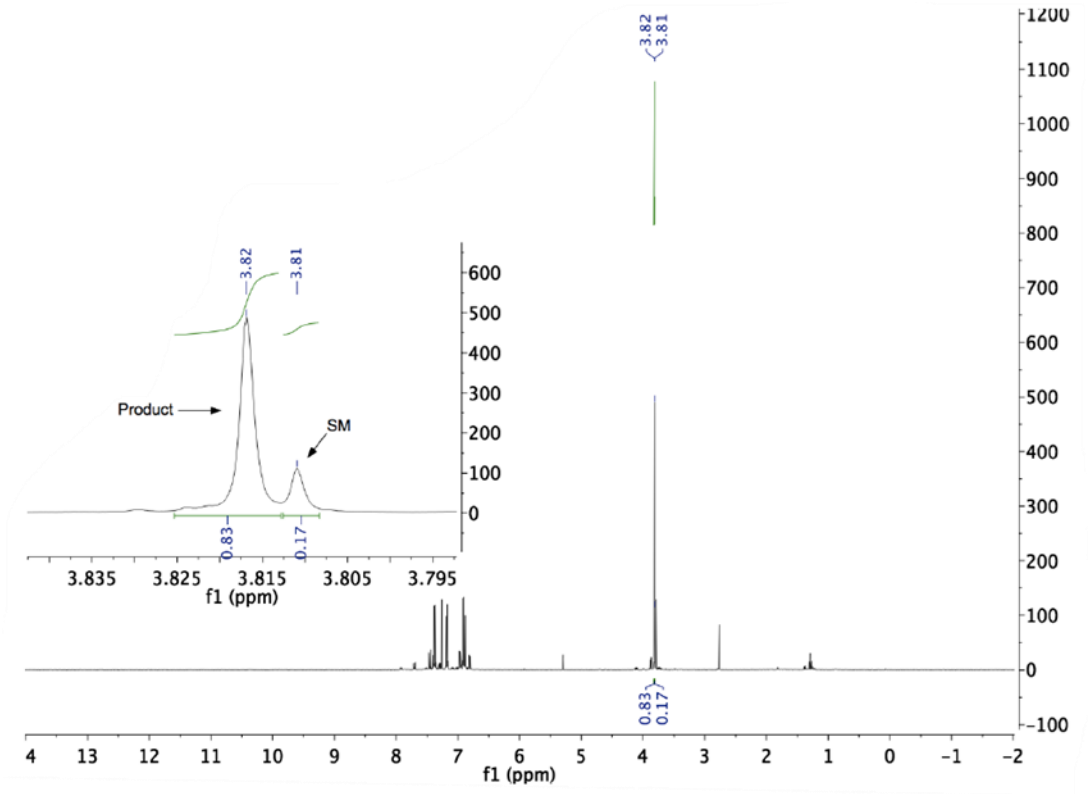

Figure 2-51 ^{1}H, $CDCl_3$, 500 MHz, (**10**) NMR conversion with catalyst **3**

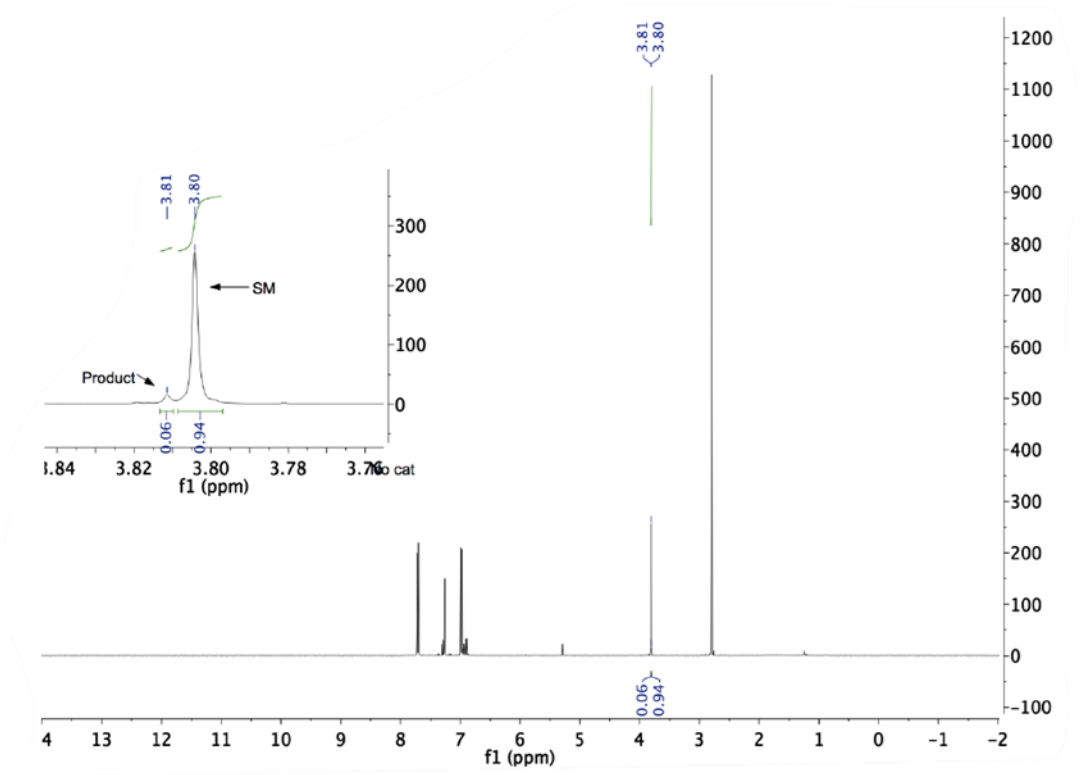

Figure 2-52 ^{1}H, $CDCl_3$, 500 MHz, (**10**) NMR conversion without catalyst **3**

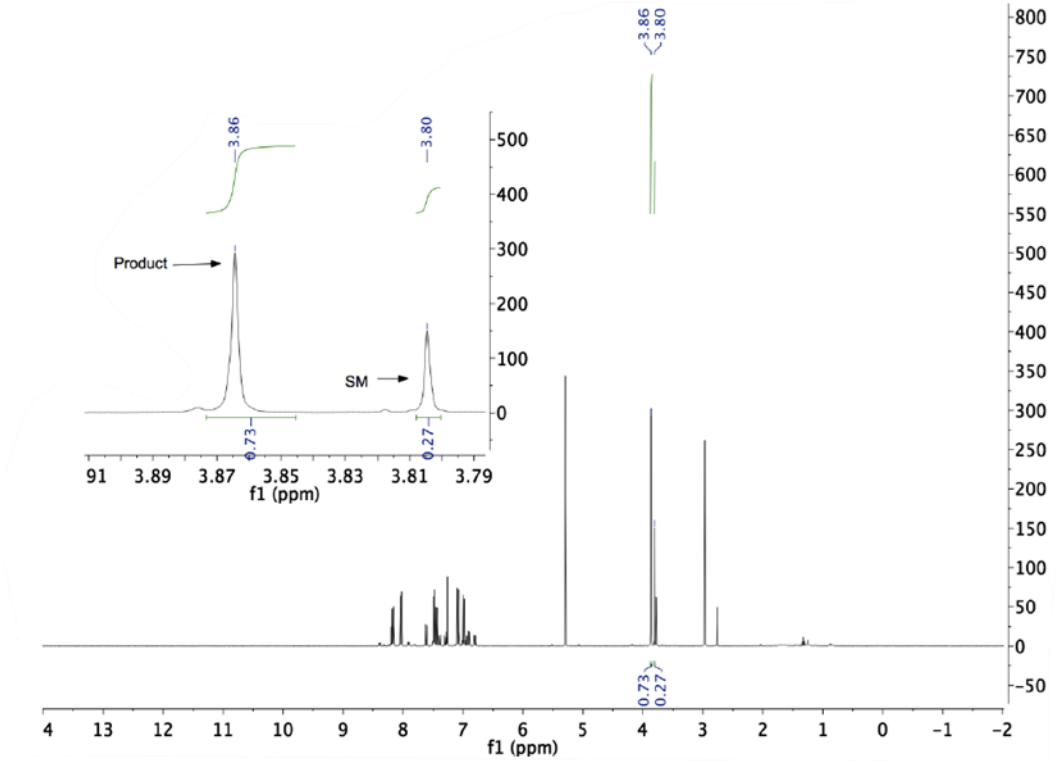

Figure 2-53 ^{1}H, $CDCl_3$, 500 MHz, (**11**) NMR conversion with catalyst **3**

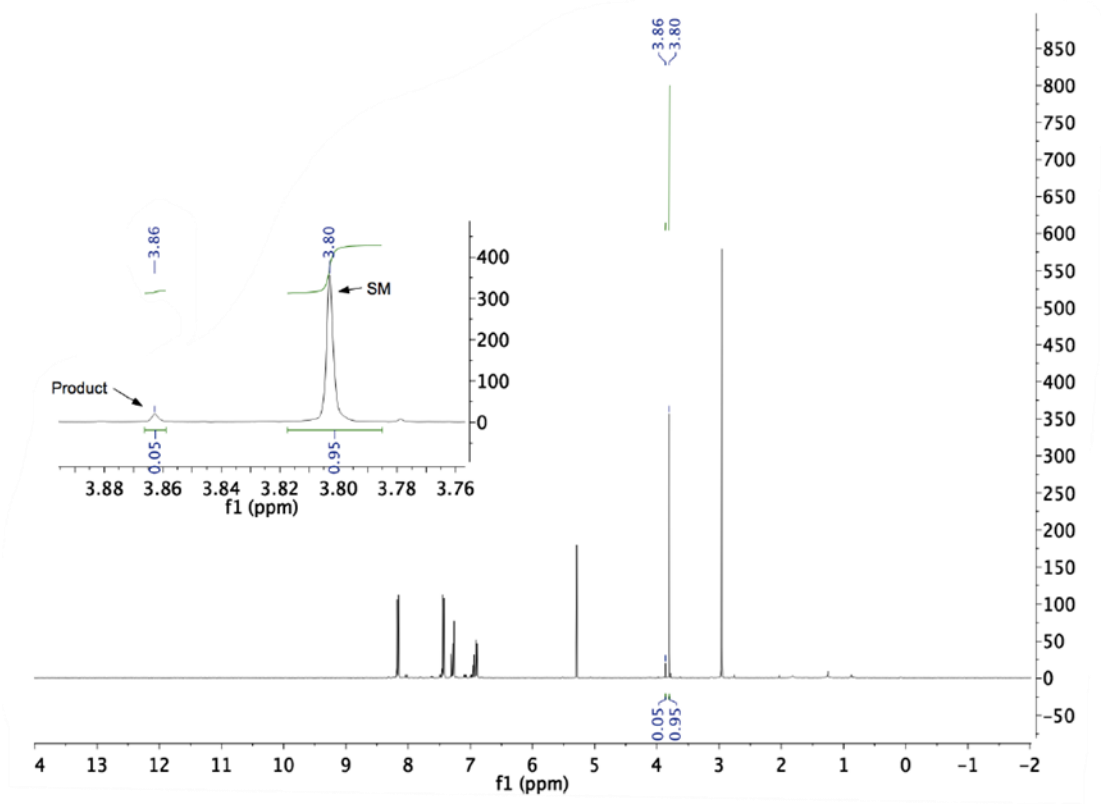

Figure 2-54 ^{1}H, $CDCl_3$, 500 MHz, (**11**) NMR conversion without catalyst **3**

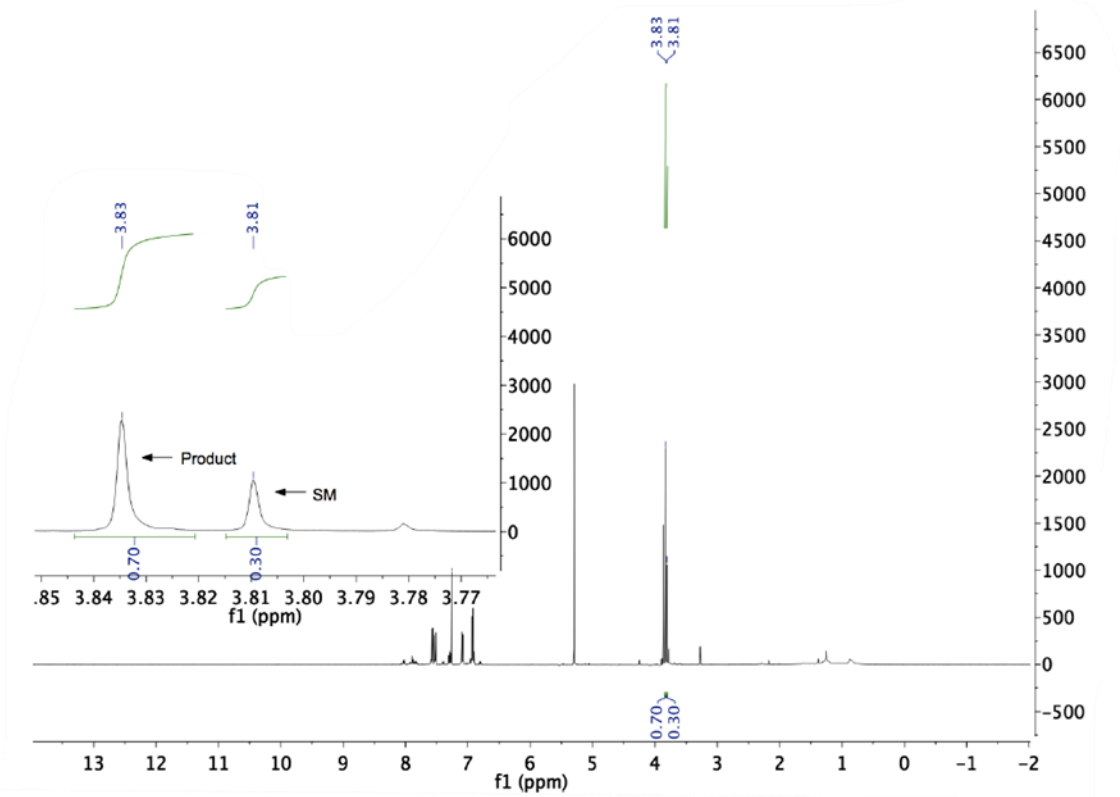

Figure 2-55 ^{1}H, $CDCl_3$, 500 MHz, (**12**) NMR conversion with catalyst **3**

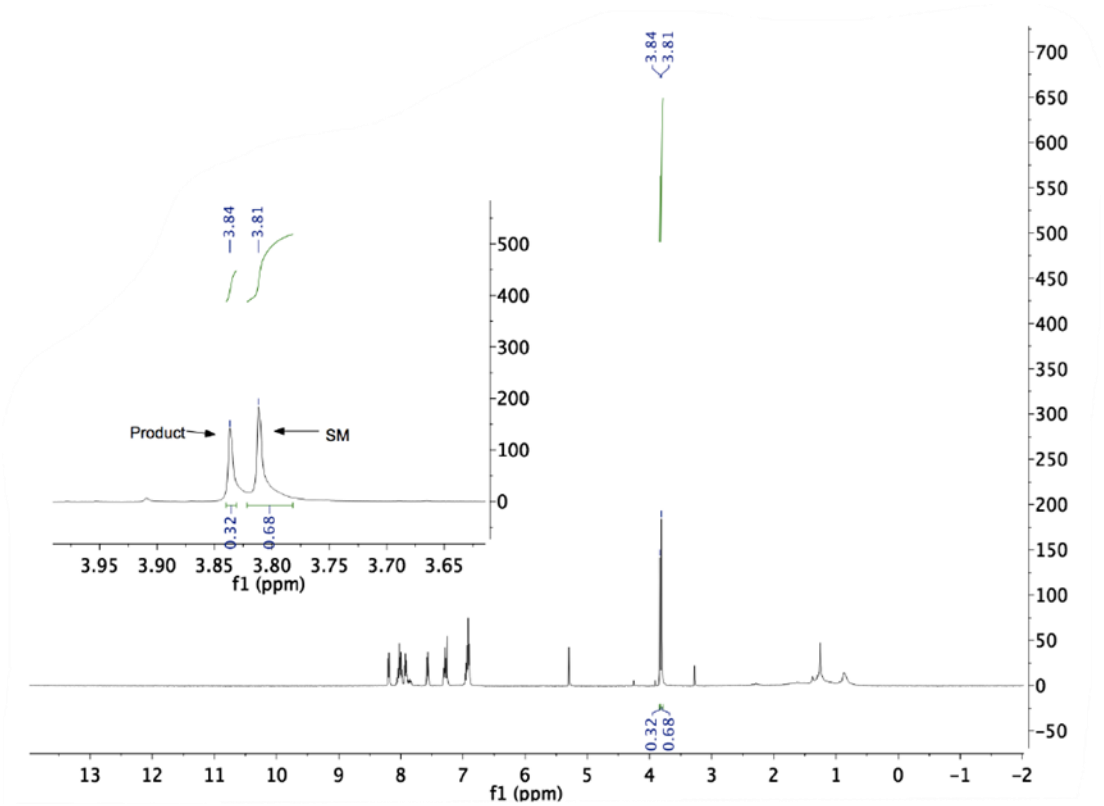

Figure 2-56 ^{1}H, $CDCl_3$, 500 MHz, (**12**) NMR conversion without catalyst **3**

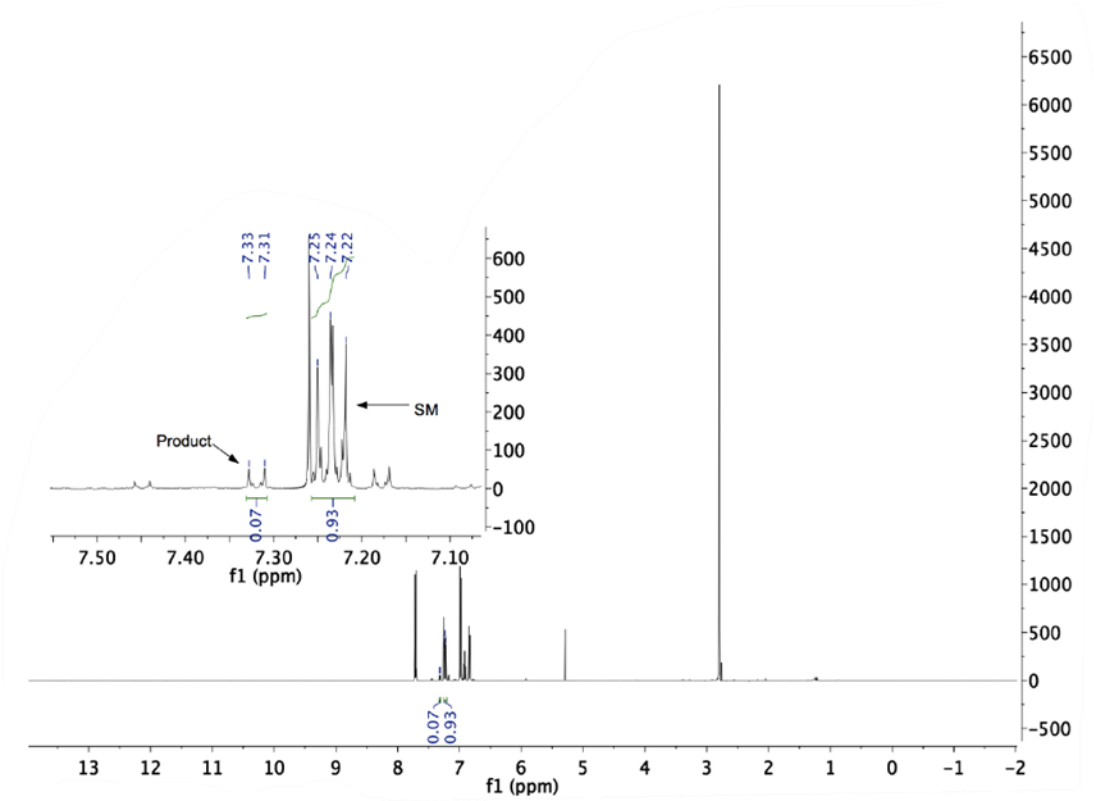

Figure 2-57 ^{1}H, $CDCl_3$, 500 MHz, (**13**) NMR conversion without catalyst **3**

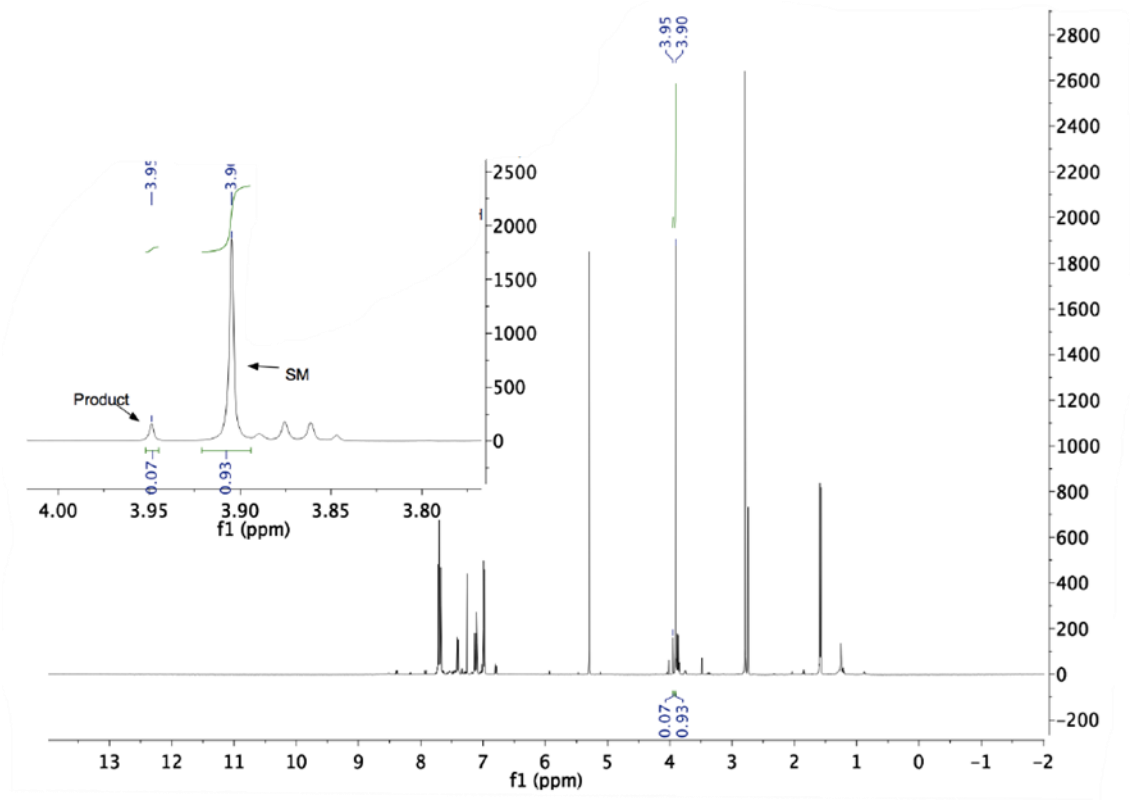

Figure 2-58 ^{1}H, $CDCl_3$, 500 MHz, (**15**) NMR conversion without catalyst **3**

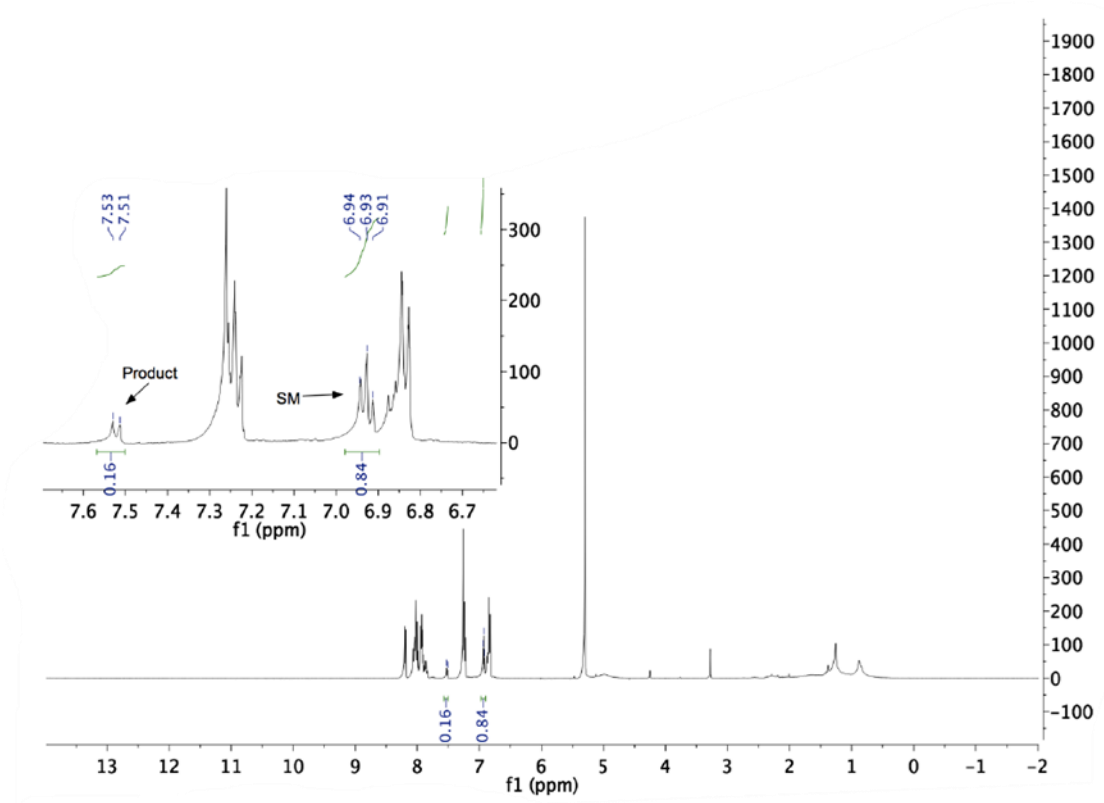

Figure 2-59 ^{1}H, $CDCl_3$, 500 MHz, (**16**) NMR conversion without catalyst **3**

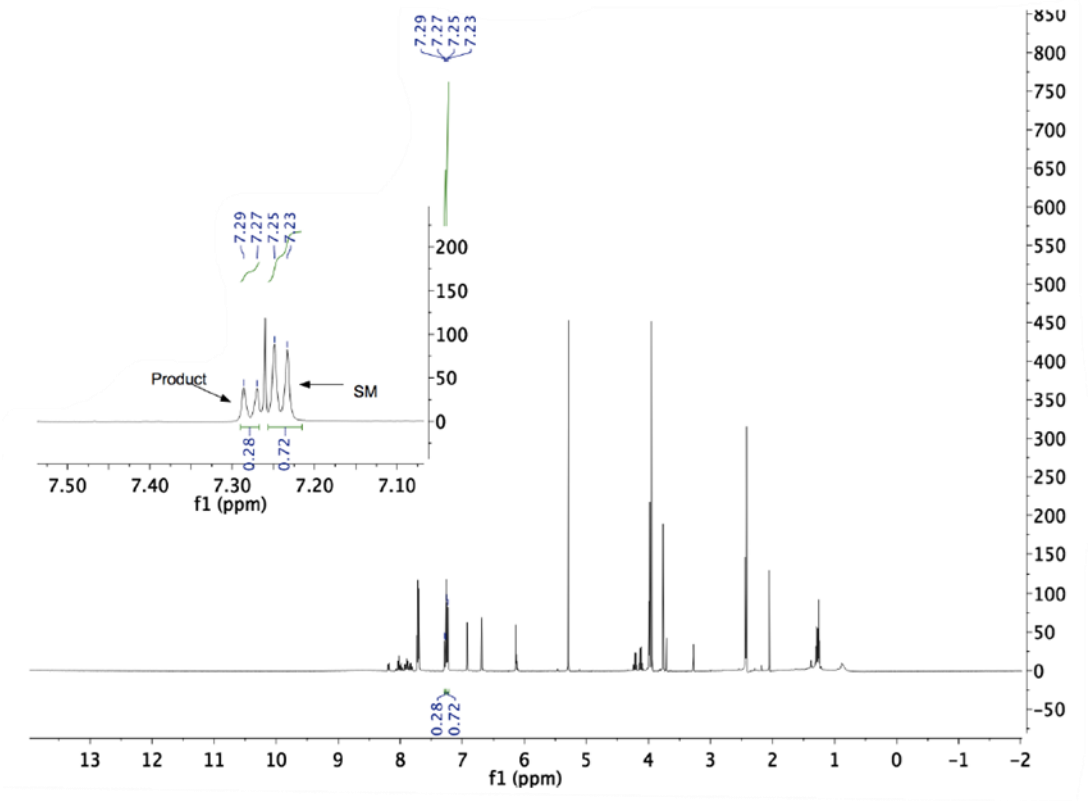

Figure 2-60 ^{1}H, $CDCl_3$, 500 MHz, (**22**) NMR conversion without catalyst **3**

J

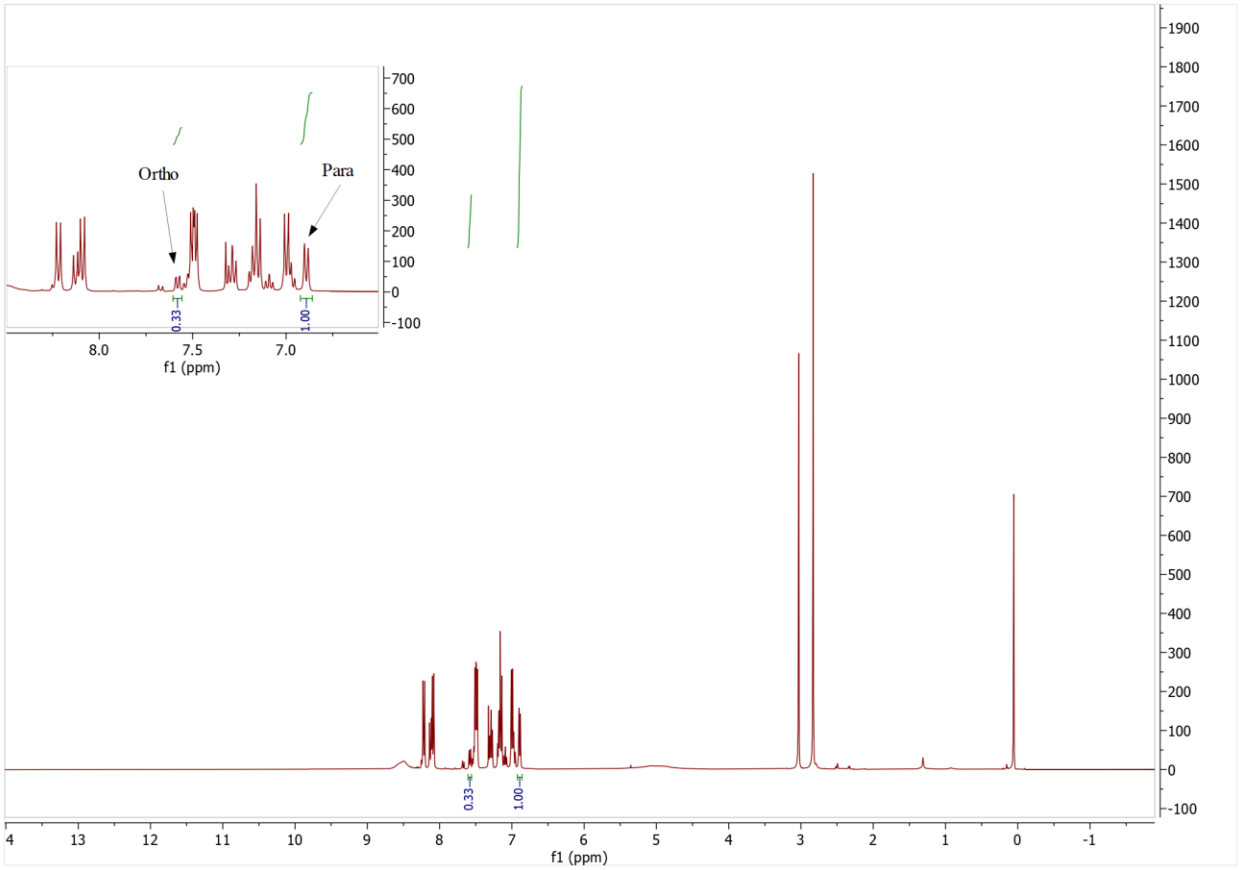

Figure 2-61 Crude ^{1}H NMR conversions for Table 2.2 entry 1

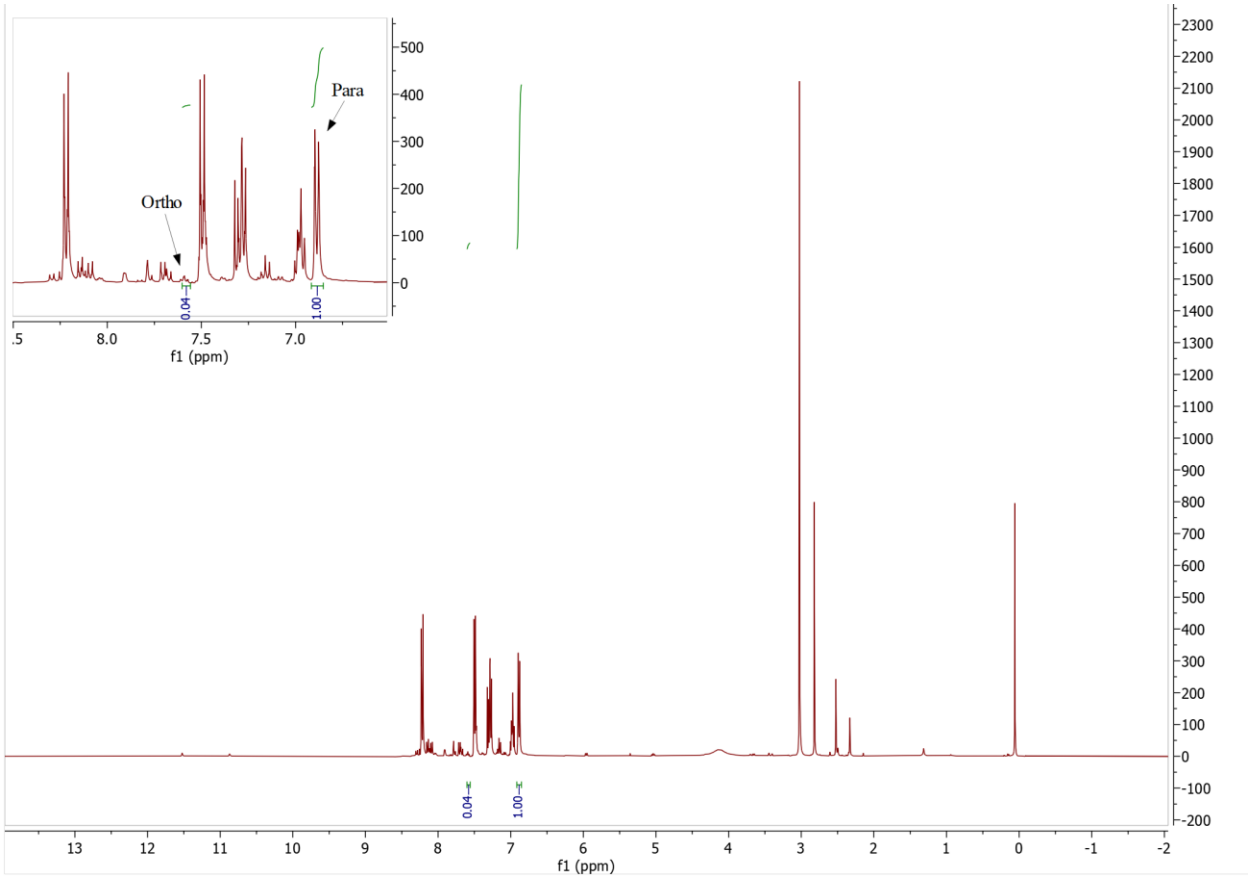

Figure 2-62 Crude ^{1}H NMR conversions for Table 2.2 entry 2

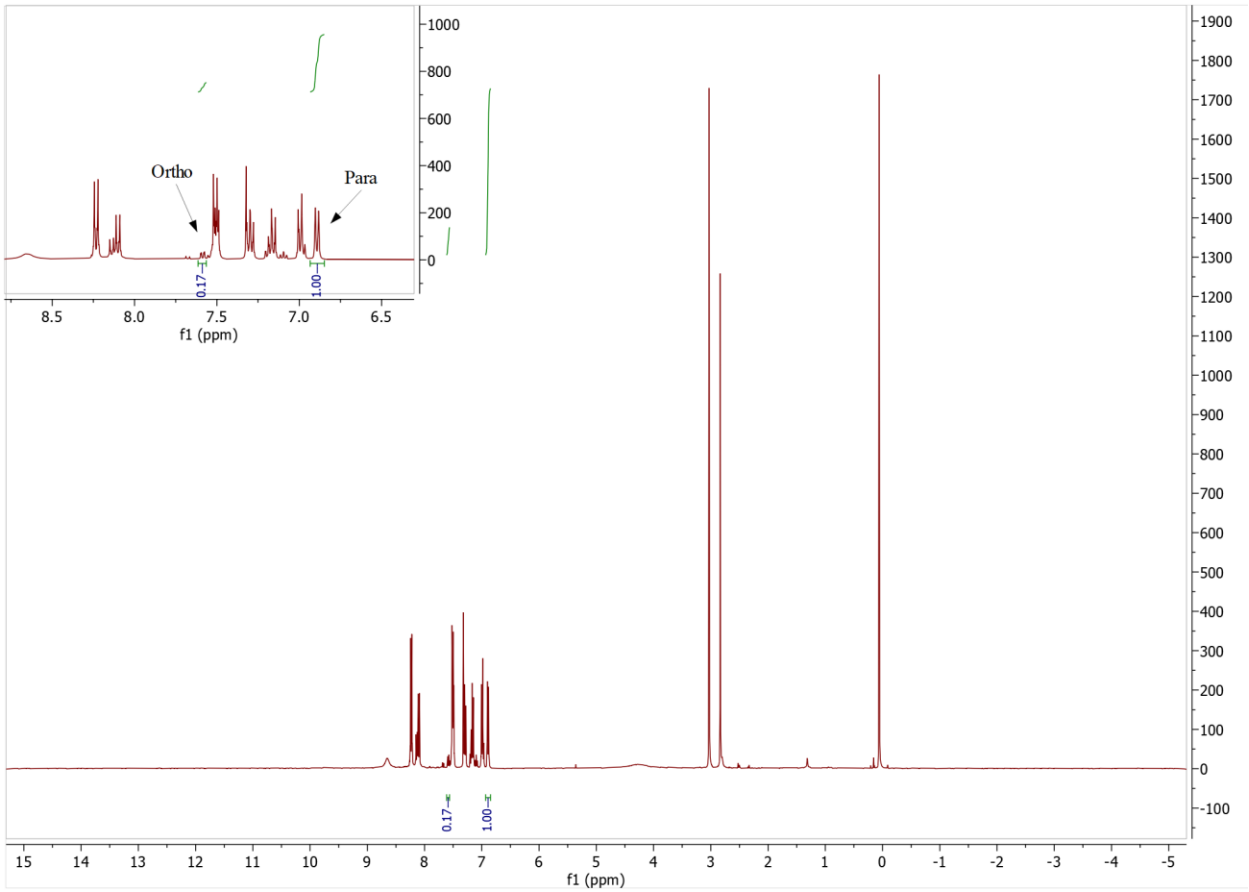

Figure 2-63 Crude ^{1}H NMR conversions for Table 2.2 entry 3

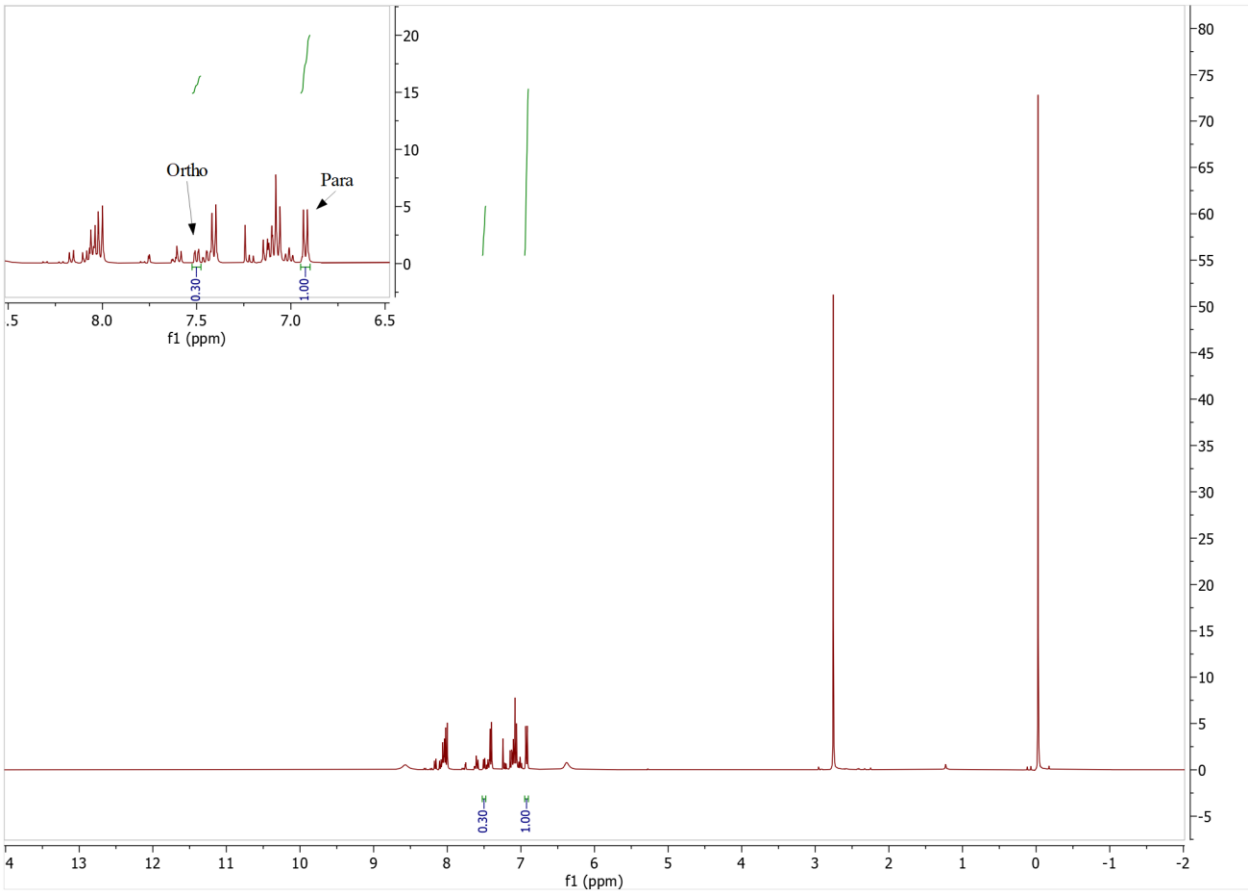

Figure 2-64 Crude ^{1}H NMR conversions for Table 2.2 entry 4

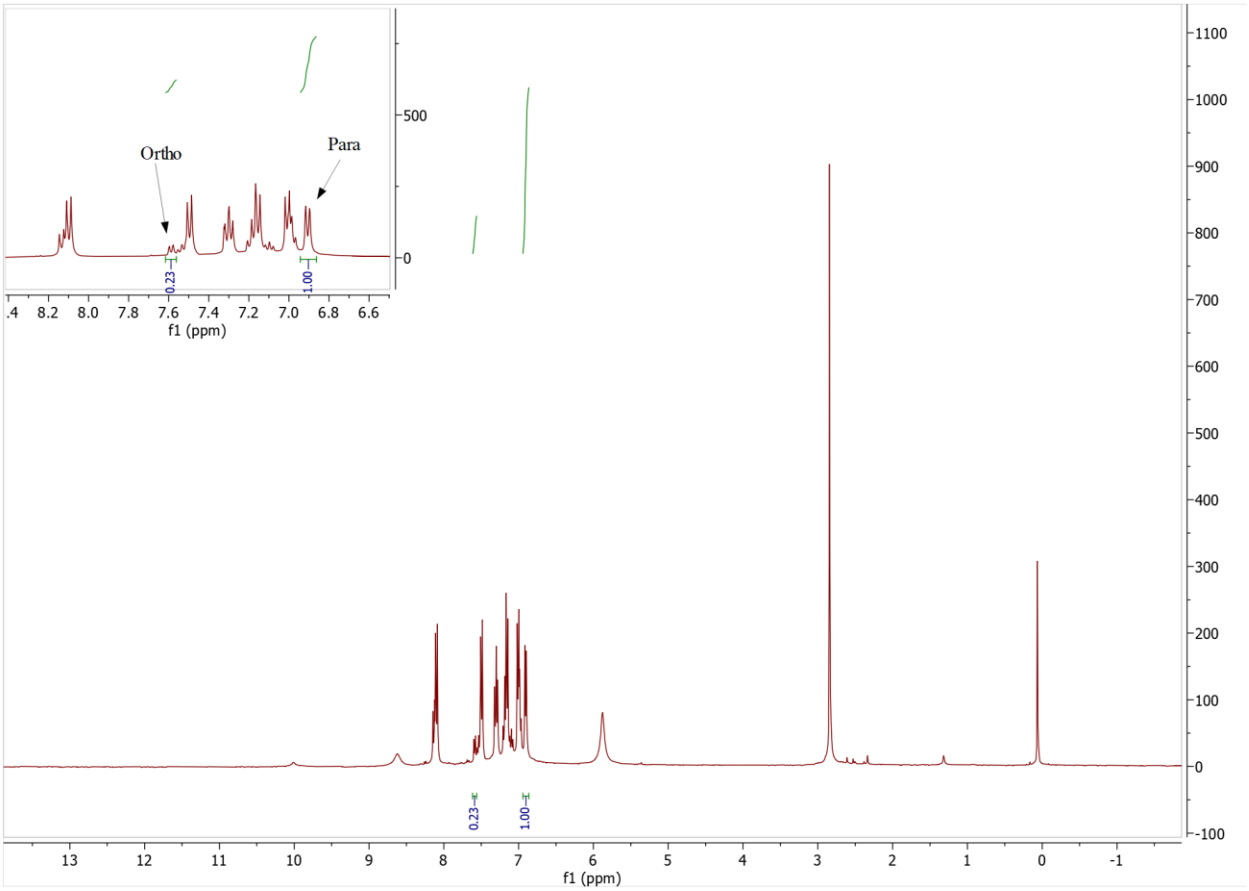

Figure 2-65 Crude ^{1}H NMR conversions for Table 2.2 entry 5

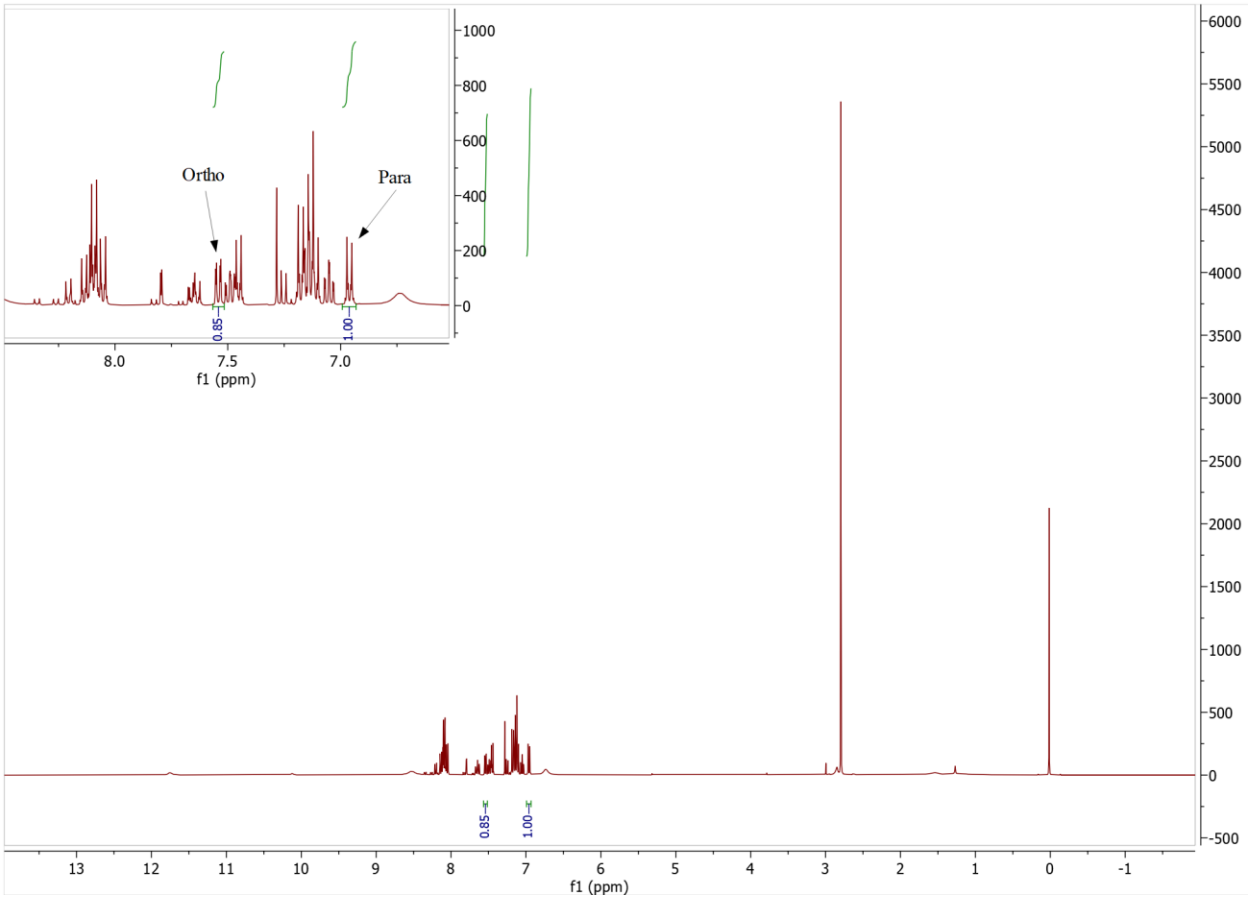

Figure 2-66 Crude ^{1}H NMR conversions for Table 2.2 entry 6

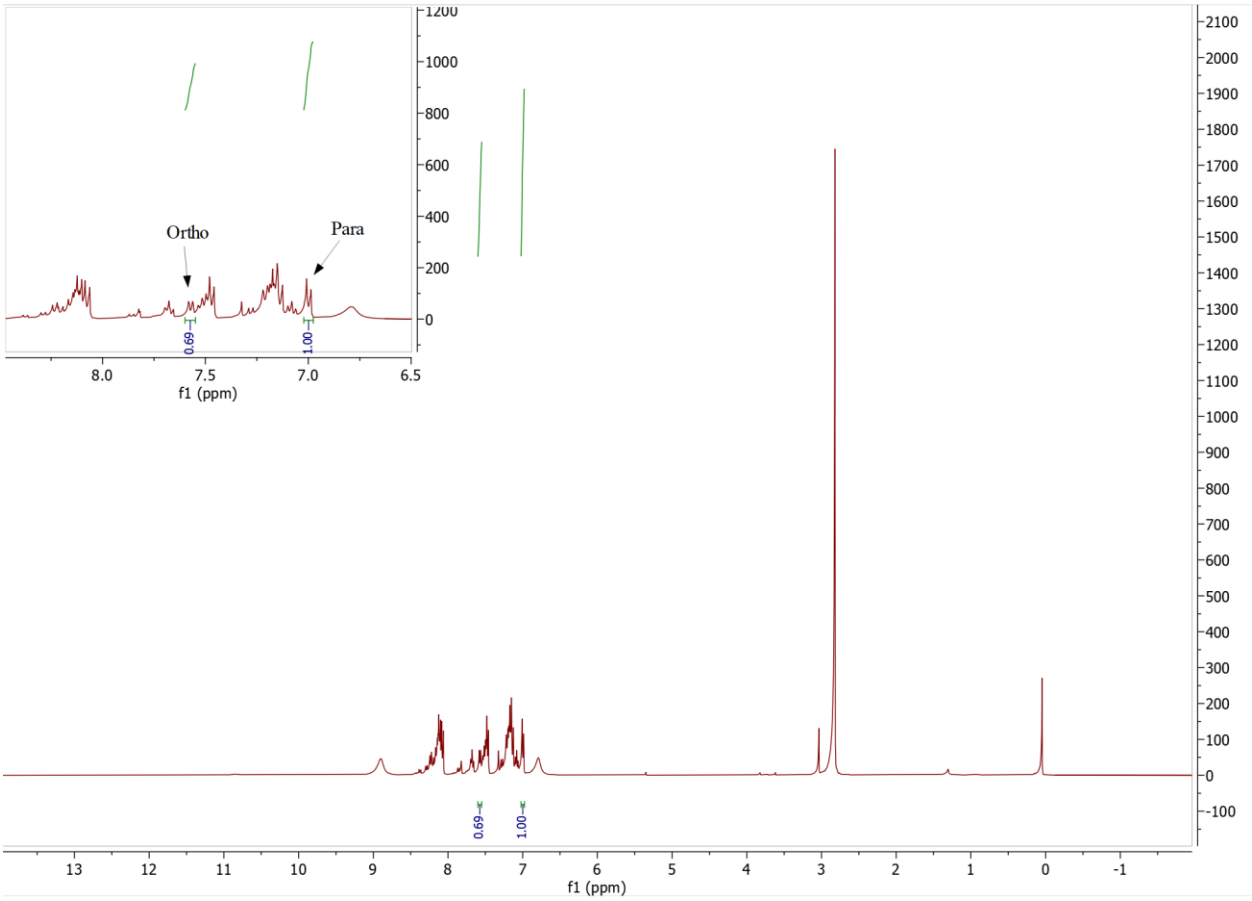

Figure 2-67 Crude ^{1}H NMR conversions for Table 2.2 entry 7

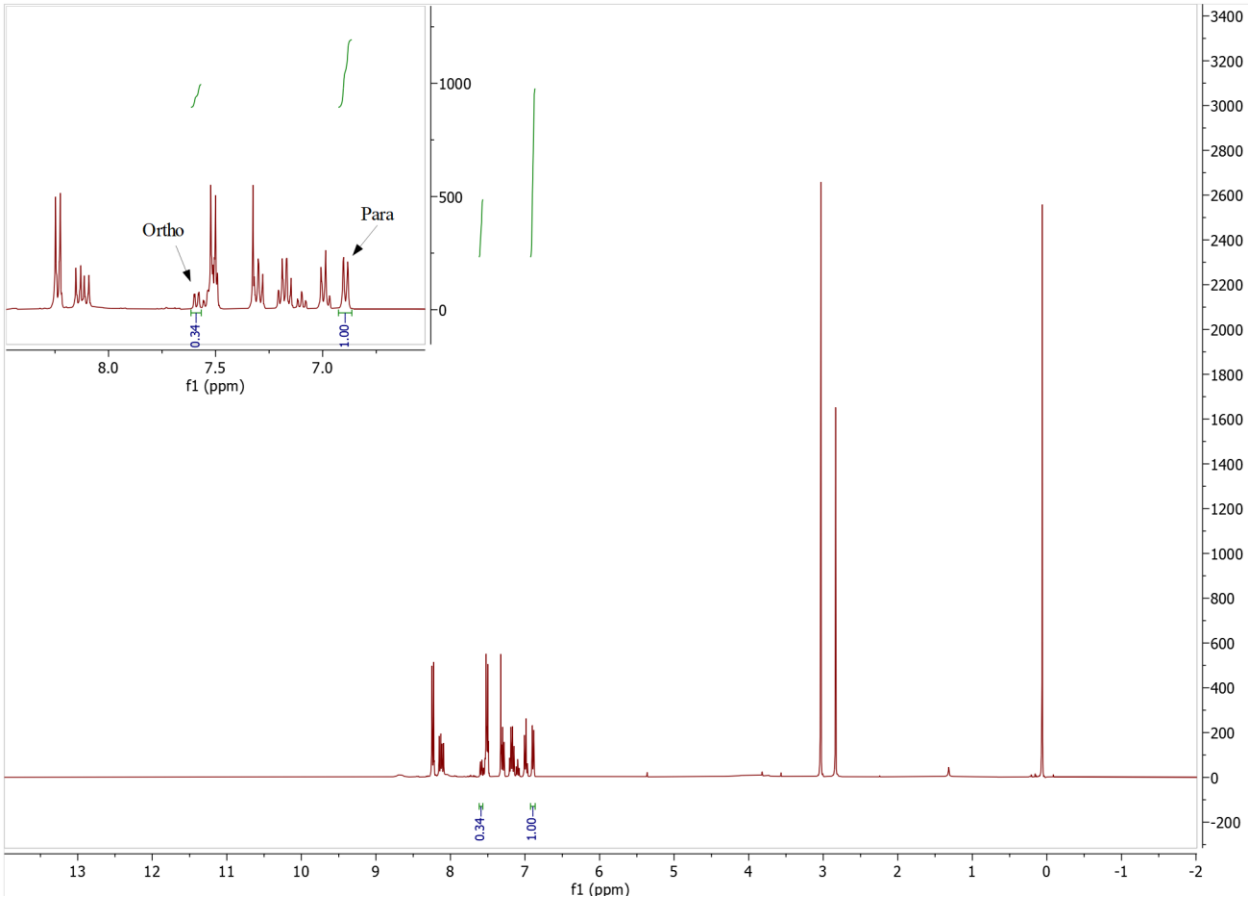

Figure 2-68 Crude ^{1}H NMR conversions for Table 2.2 entry 8

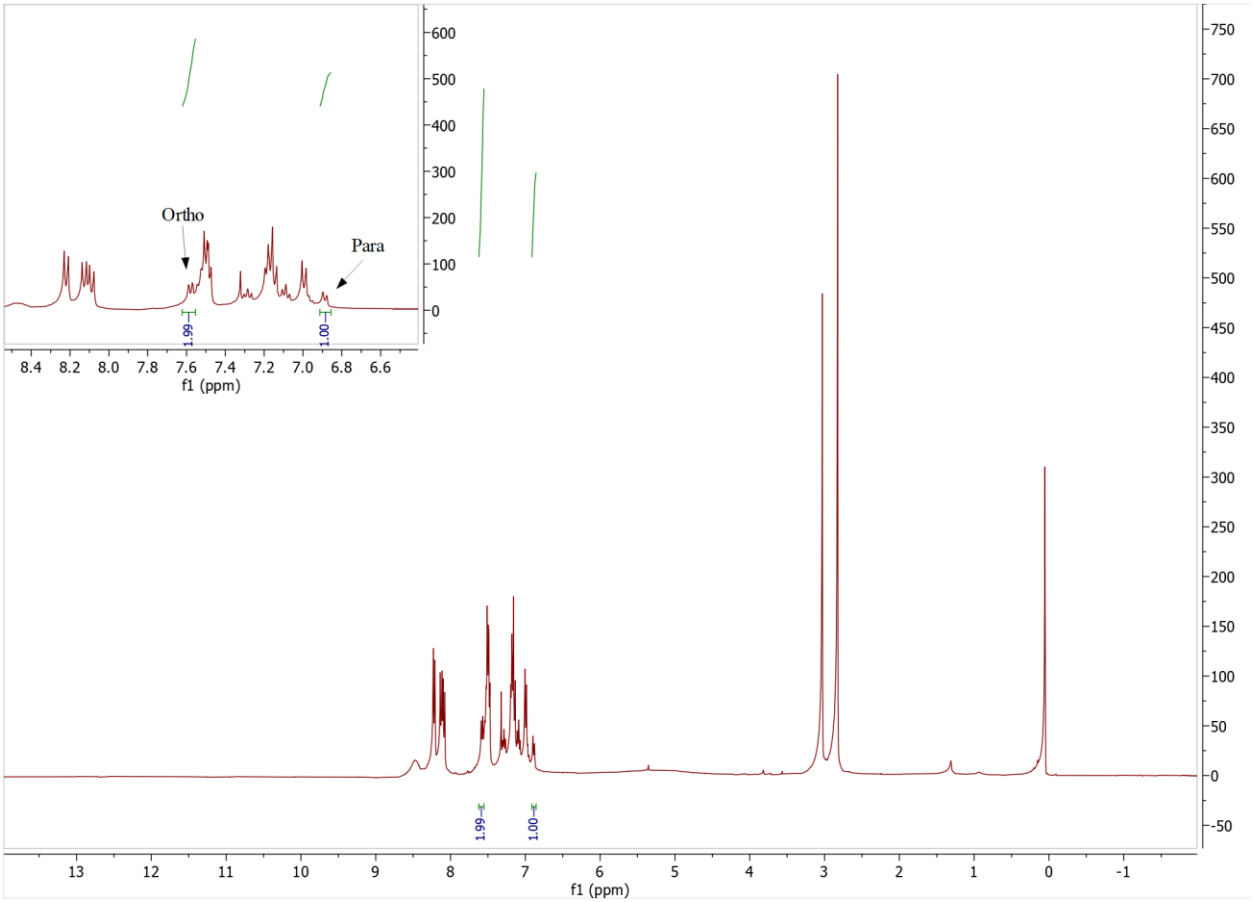

Figure 2-69 Crude ^{1}H NMR conversions for Table 2.2 entry 9

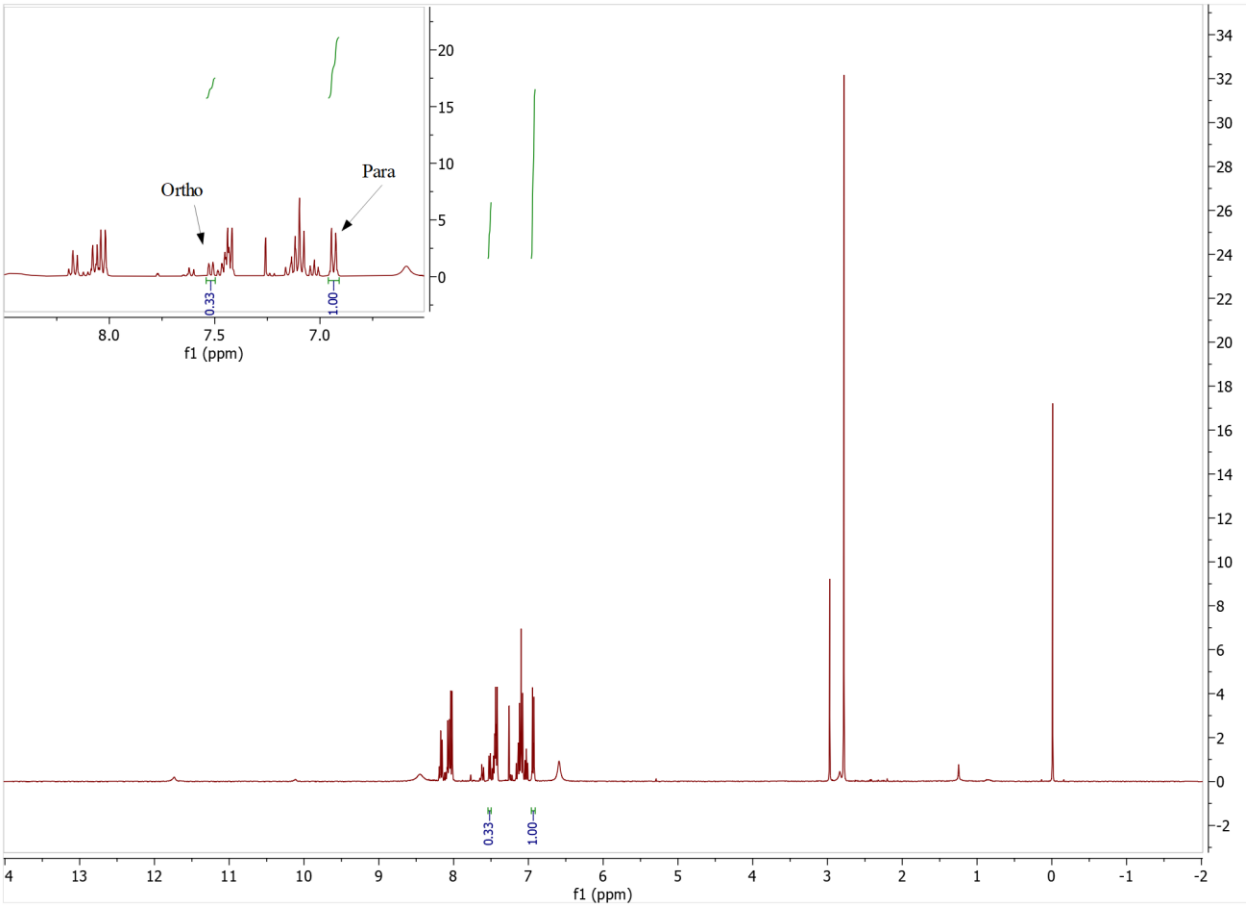

Figure 2-70 Crude ^{1}H NMR conversions for Figure 2.8 (**26**)

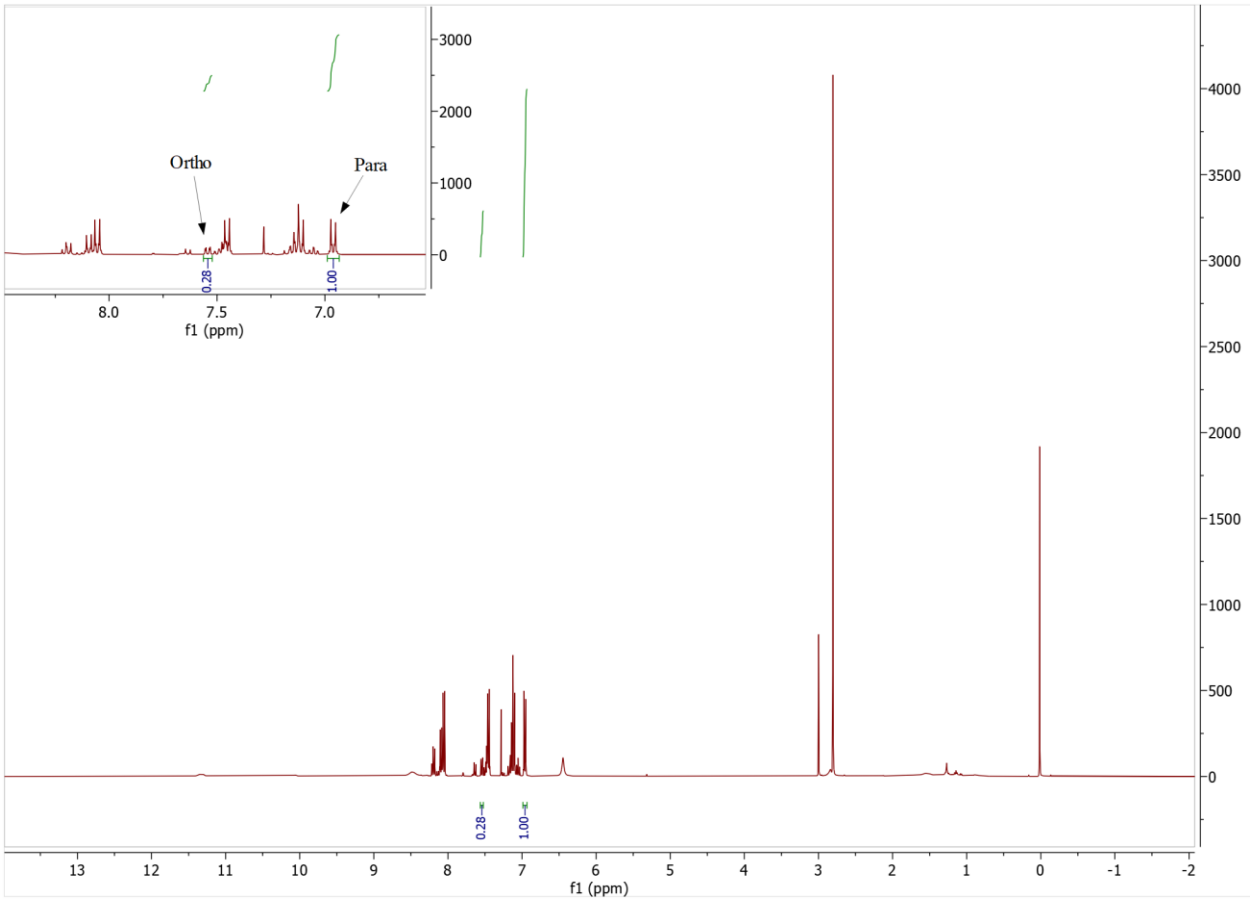

Figure 2-71 Crude ^{1}H NMR conversions for Figure 2.8 (**27**)

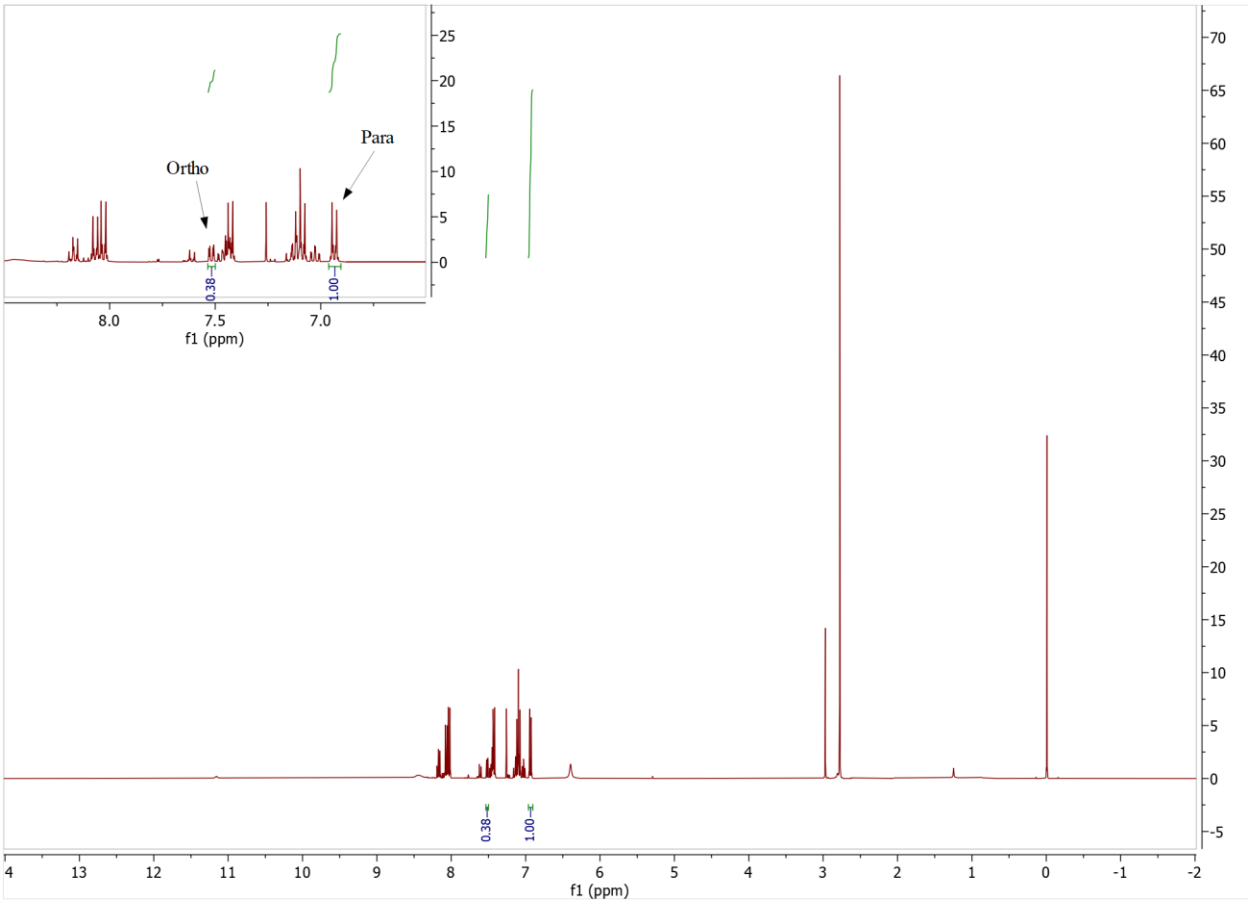

Figure 2-72 Crude ^{1}H NMR conversions for Figure 2.8 (**28**)

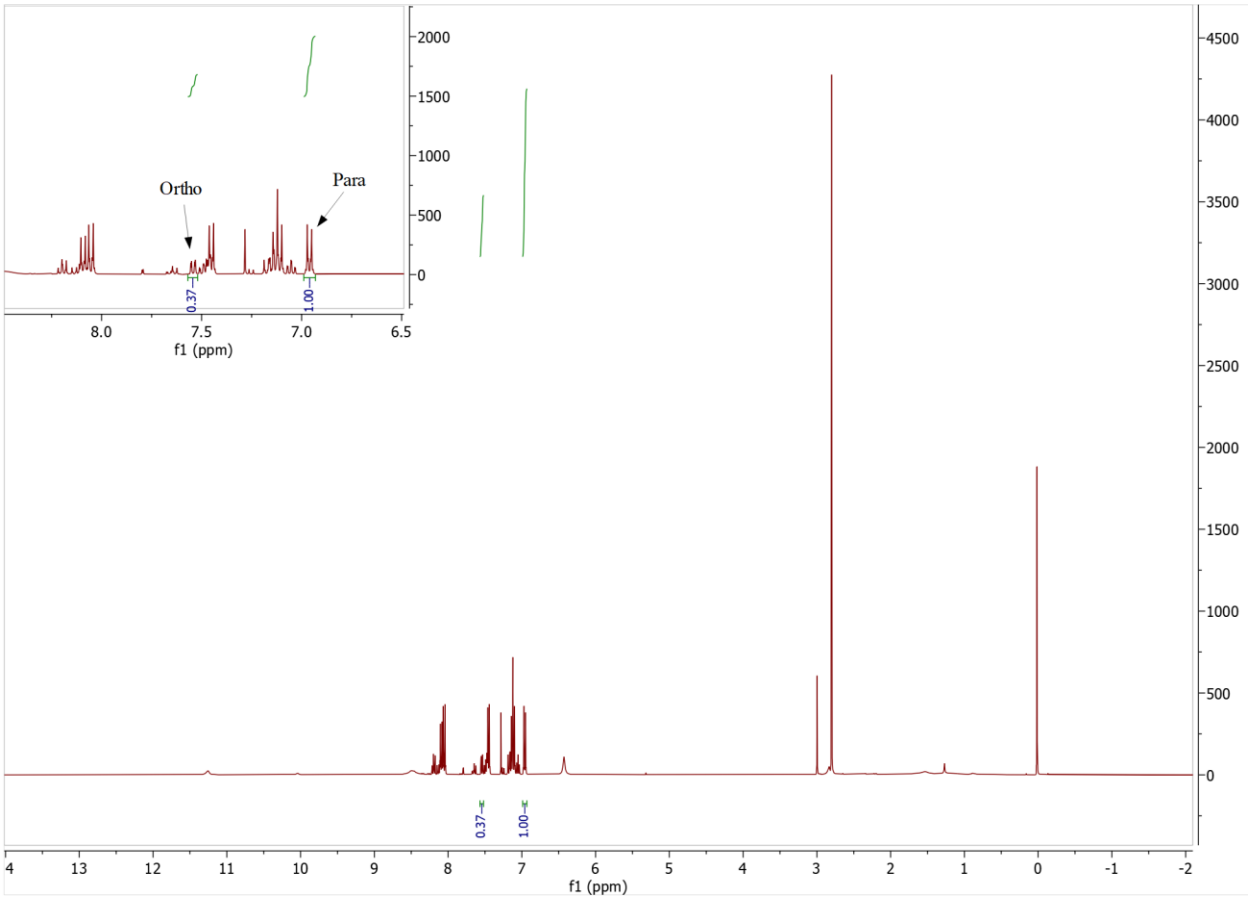

Figure 2-73 Crude ^{1}H NMR conversions for Figure 2.8 (**29**)

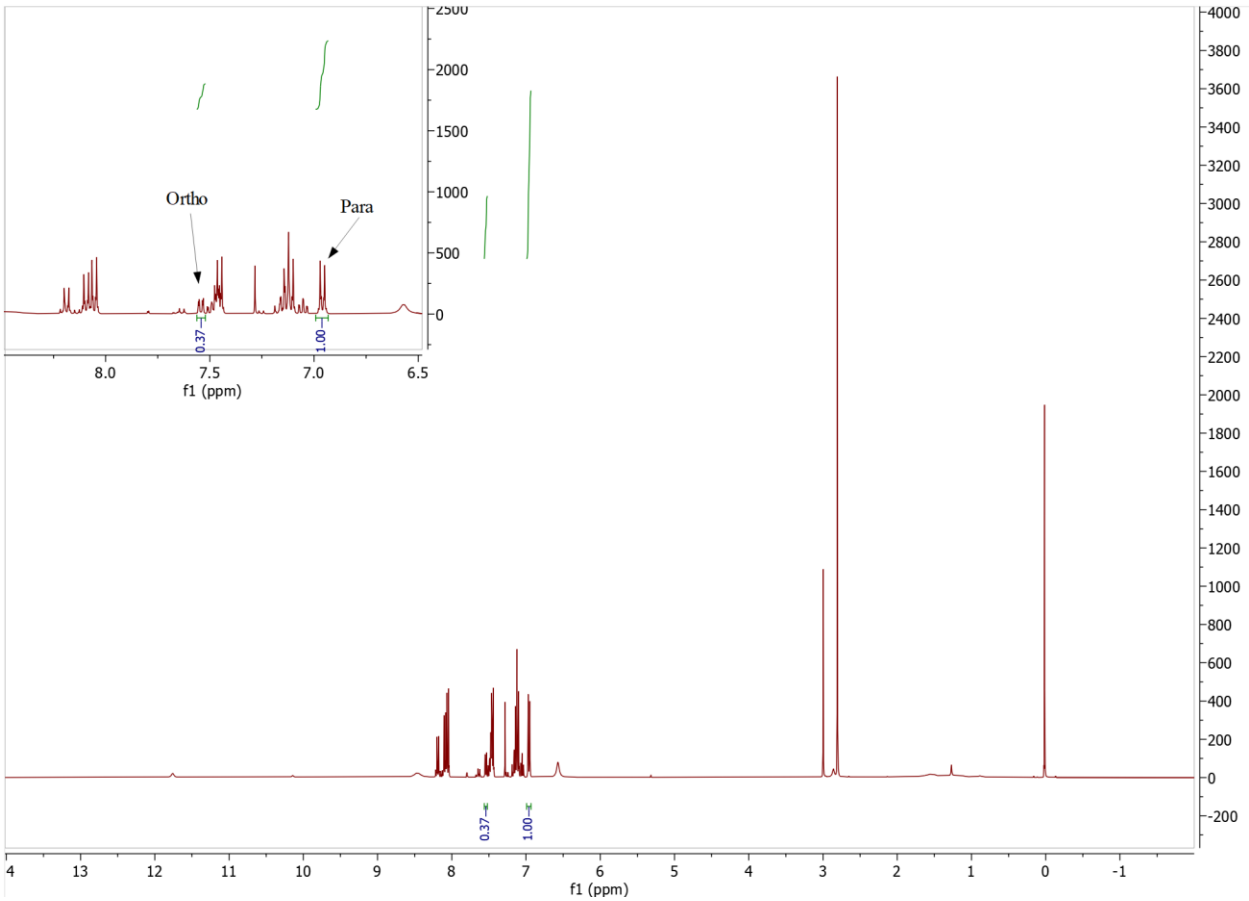

Figure 2-74 Crude ^{1}H NMR conversions for Figure 2.8 (**30**)

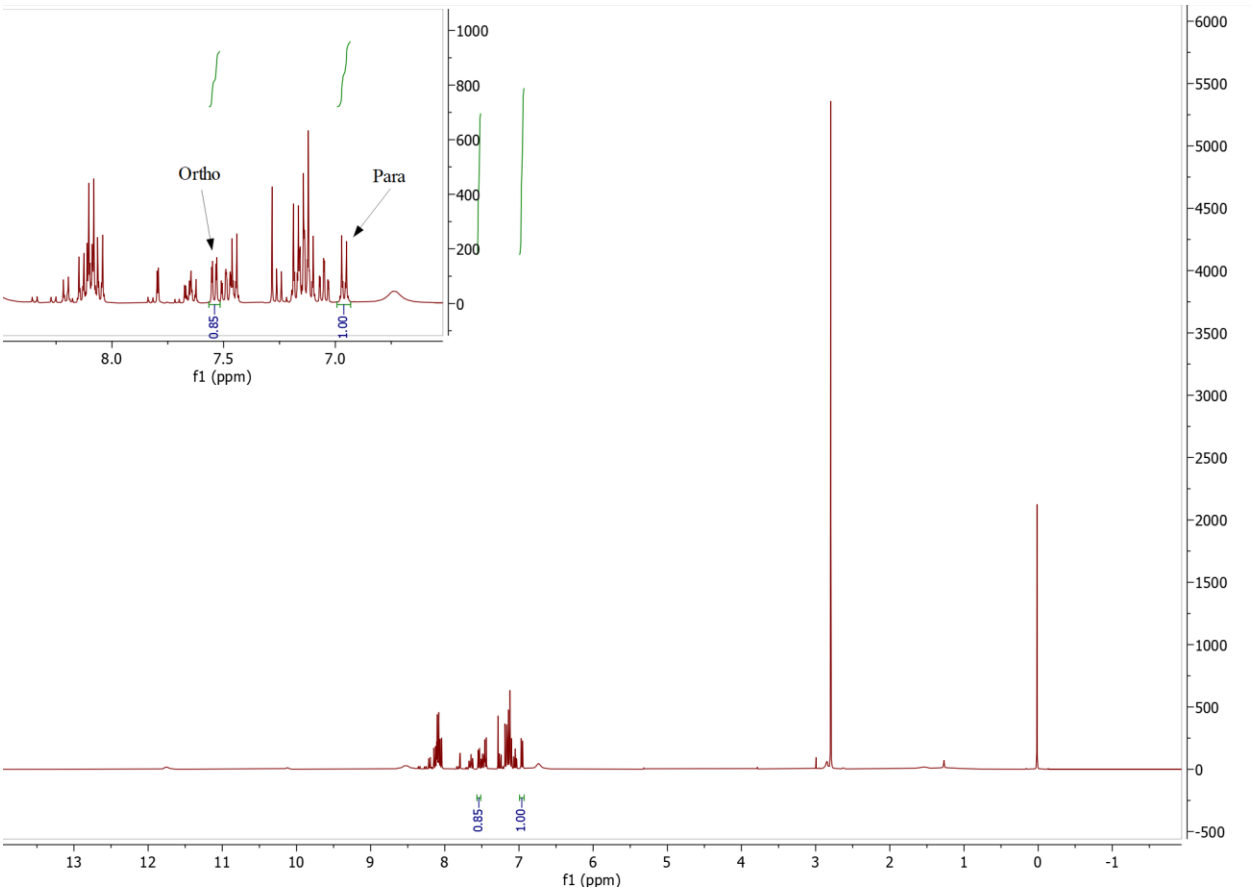

Figure 2-75 Crude ^{1}H NMR conversions for Figure 2.8 (**31**)

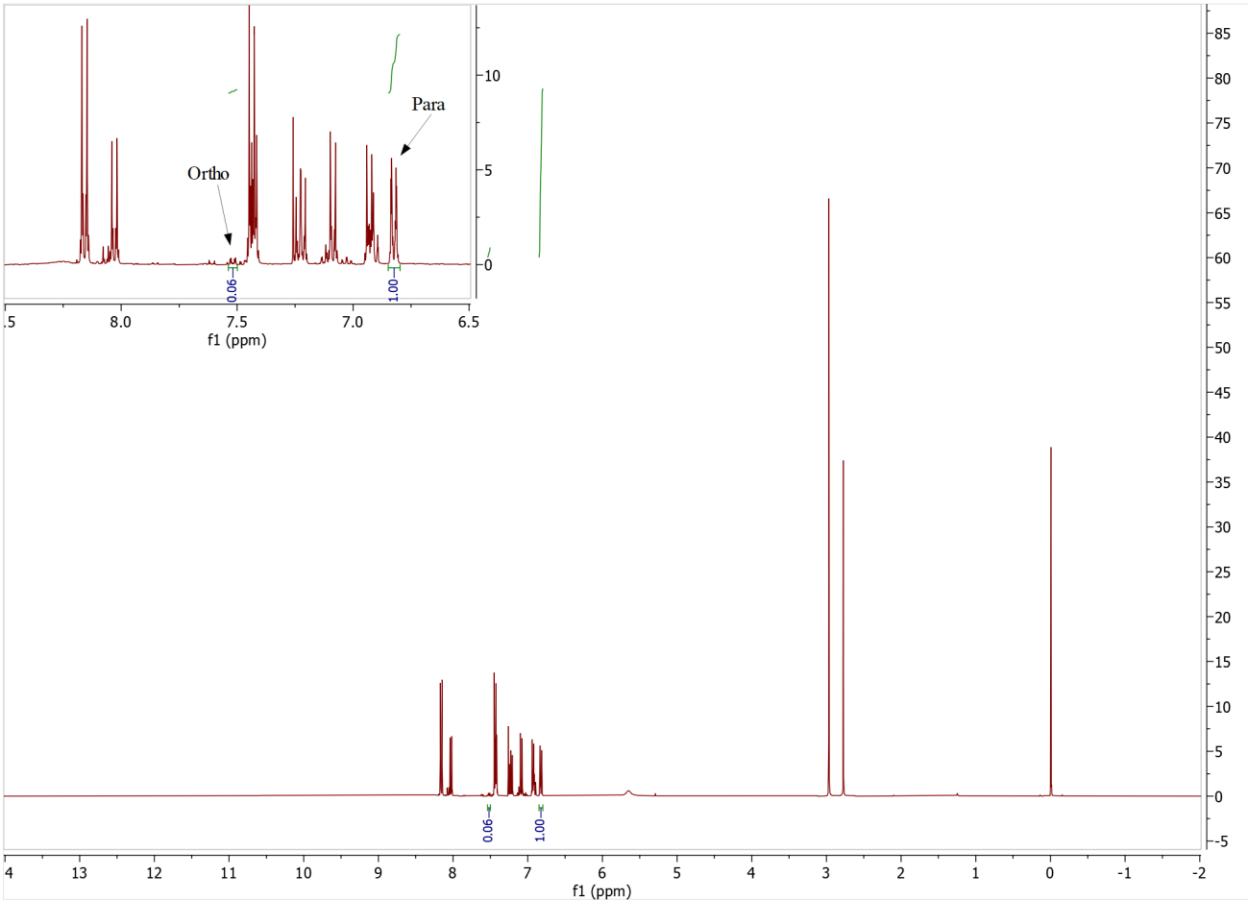

Figure 2-76 Crude ^{1}H NMR conversions for Figure 2.8 (**32**)

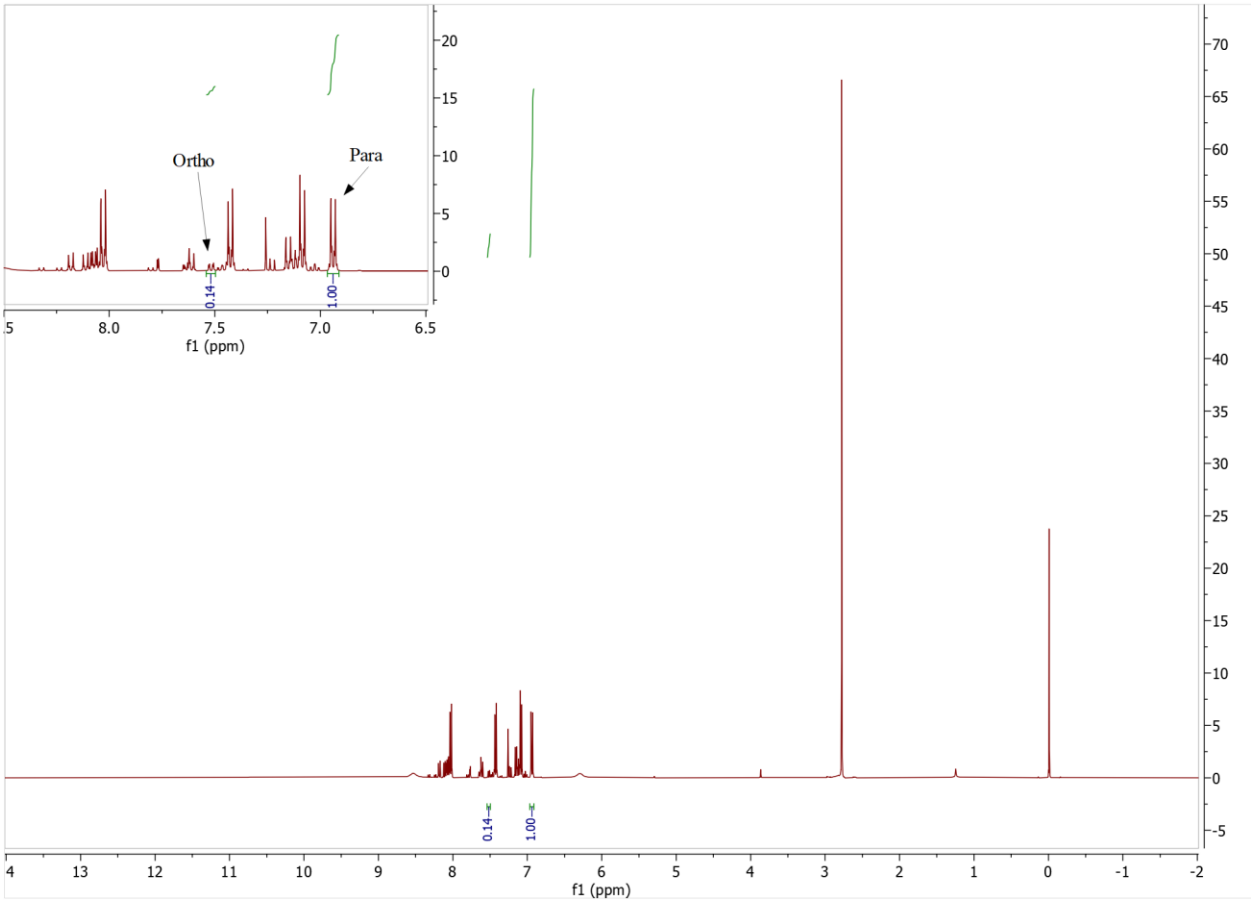

Figure 2-77 Crude ^{1}H NMR conversions for Figure 2.8 (**3**)

2.8 Acknowledgements

Chapter 2, in part, is a reformatted reprint of the material as it appears in the following manuscript: Nalbandian, C. J.; Brown, Z. E.; Alvarez, E.; Gustafson, J. L Lewis Base/Bronsted Acid Dual-Catalytic C-H Sulfenylation of Aromatics *Org. Lett.* **2018**, *20* (11), 3211-3214. The dissertation author was the secondary investigator and author of this paper. Chapter 2 in part, contains unpublished material in which the dissertation author is the primary investigator and author of this material.

Chapter 3

Peptide Stapling Via Tryptophan Selective Sulfenylation

3.1 Abstract

Peptide stapling has emerged as a powerful strategy for stabilizing α-helical structures and enabling the modulation of protein–protein interactions (PPIs) that are difficult to target with traditional small molecules. Despite substantial progress, most stapling chemistries rely on noncanonical amino acids, transition-metal catalysts, or residues such as cysteine that are not always compatible with complex peptide environments. Here we report a fundamentally new stapling platform based on Lewis base/Brønsted acid dual-catalyzed C2 sulfenylation of tryptophan, an underexploited yet highly conserved residue at many PPI interfaces. Using tunable N-thiosuccinimide PEG linkers, we demonstrate selective *i,i+4* macrocyclization under mild, metal-free conditions without perturbing sensitive functional groups such as free cysteine or lysine. Initial model studies validated the formation of Trp–Trp staples, and subsequent application to both established (BID–BCL-2, Axin–β-catenin) and unexplored (NHE-1, NF-κB p50) targets revealed robust helicity enhancement and sequence-dependent tunability. Circular dichroism analyses indicate that the tetra-PEG linker provides optimal helix stabilization, achieving helicity levels comparable to hydrocarbon-stapled analogs while offering improved synthetic accessibility. This work establishes tryptophan as a viable and strategic anchoring site for peptide macrocyclization and expands the chemical toolbox available for stabilizing α-helices and interrogating challenging PPIs.

3.2 Introduction

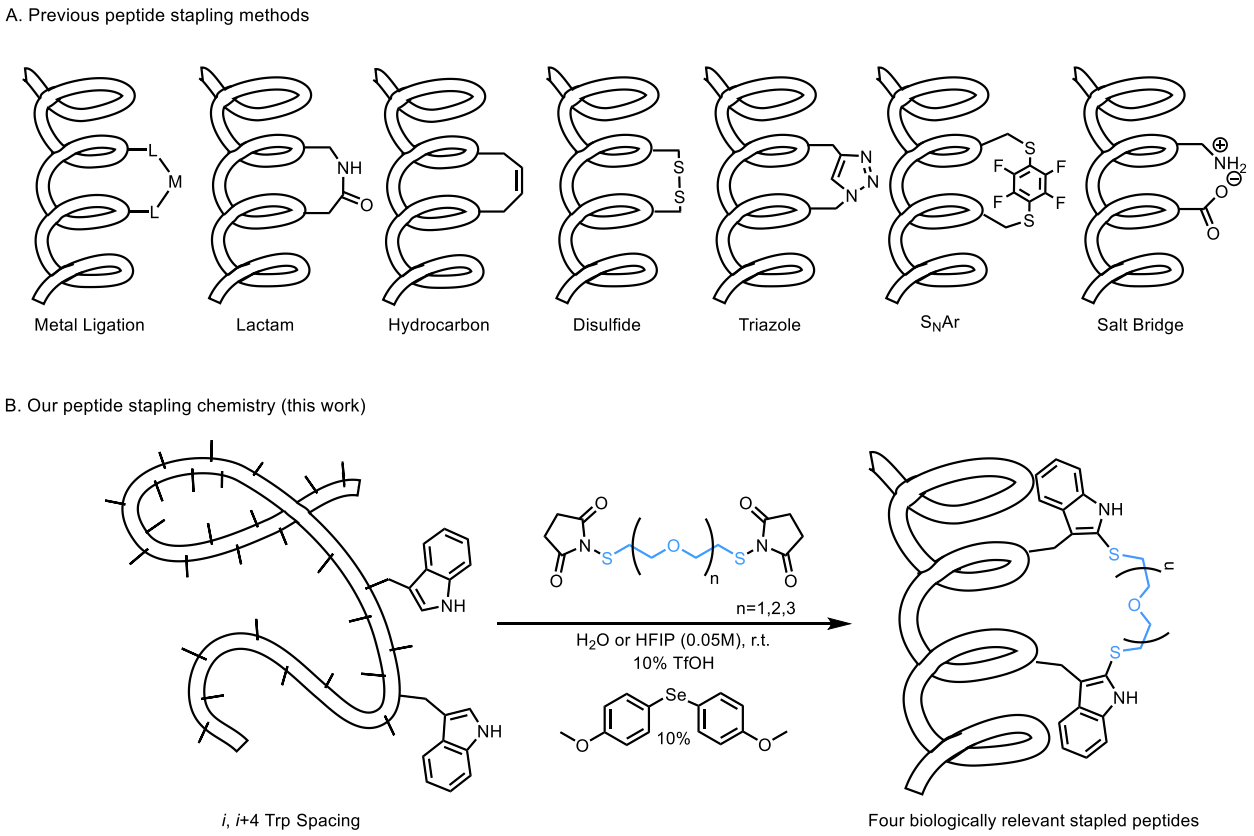

Figure 3-1 A.) Examples of current peptide stapling techniques. B.) Our peptide stapling chemistry.

Peptides represent a powerful class of molecules capable of engaging protein–protein interactions, PPIs, that are often inaccessible to small molecules[1,2]. Despite their promise, linear peptides typically suffer from low stability[3,4], poor pharmacokinetics[5,6], and limited cell permeability[7,8]. The introduction of side-chain cross-links, or "staples," has proven to be an elegant solution to these challenges, locking peptides into their bioactive helical conformations and improving biological function[9,10]. Among the pioneering contributions to this field was the introduction of hydrocarbon stapling by Verdine and Walensky[11], in which noncanonical olefin-bearing amino acids are incorporated into peptides and subjected to ruthenium-catalyzed ring-closing metathesis[12,13]. This approach remains the most widely recognized and has set the

benchmark for peptide stapling. Nevertheless, it requires the use of non-natural building blocks and organometallic catalysts, complicating both synthesis and potential therapeutic translation[14].

Alternative methods such as azide–alkyne cycloaddition, "click" chemistry, have provided orthogonal means of generating triazole-stapled peptides[15,16]. These strategies, while efficient, also rely on noncanonical amino acids and copper catalysis. Cysteine-based methods have attracted considerable attention because of the high nucleophilicity of the thiol side chain[17]. Perfluoroaryl-based nucleophilic aromatic substitution and bis-alkylation with alkyl halides are among the more common cysteine-directed approaches[18,19]. While selective in certain contexts, cysteine stapling is not universally applicable, particularly when multiple cysteines are present in the peptide. More generally, many of the current methods suffer from three key limitations: the need for noncanonical amino acids, selectivity issues that arise in more complex sequences, and the reliance on transition metal catalysts that may complicate downstream applications[20,21].

The impact of peptide stapling has been most clearly demonstrated in systems such as BH3-domain peptides[22], where stabilized helices targeting BCL-2 family proteins regulate apoptosis, and in the Wnt/β-catenin signaling axis[23], where stapled Axin-derived peptides have provided insights into oncogenic signaling. Additional studies have highlighted improved stability, protease resistance, and serum half-life of stapled peptides in vivo[24]. These examples illustrate the power of stapling but also highlight the lack of methods that combine efficiency, selectivity, and broad applicability to novel targets. For this reason, there remains a significant need for new chemistry that avoids the pitfalls of existing techniques while expanding the scope of PPIs that can be addressed.

In pursuit of such an approach, we developed a Lewis base/Brønsted acid-catalyzed sulfenylation of tryptophan using *N*-thiosuccinimide polyethylene glycol, PEG, linkers. Unlike

cysteine, which has been heavily leveraged in stapling chemistry, tryptophan is rarely targeted despite its unique reactivity[25,26]. The indole side chain possesses nucleophilicity at the C2 position that can undergo selective functionalization, making it an attractive anchor for covalent modification. Moreover, tryptophan residues are highly conserved at protein–protein interfaces[27], suggesting that they may serve as natural anchoring sites for stapling strategies. Our method exploits this reactivity under mild, metal-free conditions and allows *i,i+4* stapling through tunable PEG-based linkers, affording high selectivity without perturbing cysteine or lysine residues.

3.3 Results and Discussion

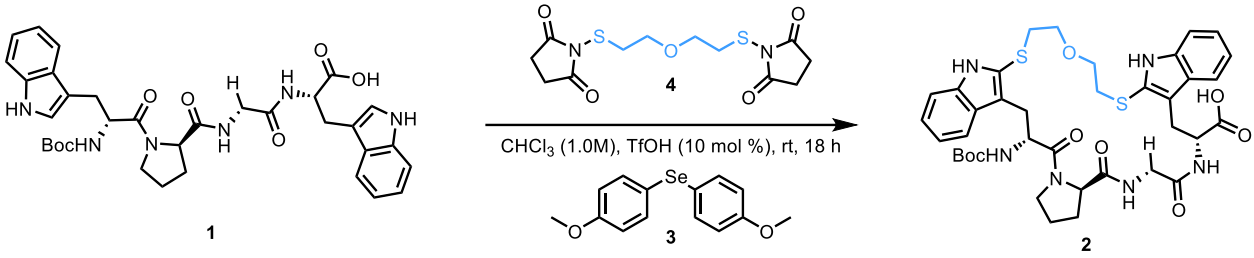

Figure 3-2 Sulfenylation of a short 4 amino acid peptide using our diethylene glycol based sulfenylating reagent

We began with synthesizing a short 4 amino acid peptide to establish proof of concept that we can tether two tryptophans on the same peptide together with a polyethylene glycol-based linker, Figure 3.2. The short peptide (**1**) contained two tryptophans at an *i, i + 4* configuration with glycine and proline in between. We started with the diethylene glycol based sulfenylating linker (**4**) with Lewis base catalyst (**3**) and triflic acid as our Bronsted Acid co-catalyst. The reaction was performed in chloroform at (1.0M) at room temperature and was monitored by matrix assisted laser desorption ionization, MALDI, mass spectrometry. This form

of mass spectrometry is useful in getting quick qualitative information about a reaction by allowing us to quickly spot an aliquot of our reaction on a plate and get instant mass analysis. This reaction proved successful by MALDI mass spectroscopy and gave us the evidence we needed to move forward with the project. We theorize the electrophilicity of the N-thiosuccinimide moiety is activated by a dual catalytic system. Initial activation occurs via triflic acid, which protonates the carbonyl oxygen and withdraws electron density from the adjacent sulfur atom. This enhanced polarization facilitates nucleophilic engagement by the selenide catalyst, which inserts into the sulfur with displacement of the succinimide leaving group. The resulting seleno-sulfur intermediate exhibits a well-defined affinity for the indole within tryptophan, enabling selective electrophilic aromatic substitution at the C2 position.

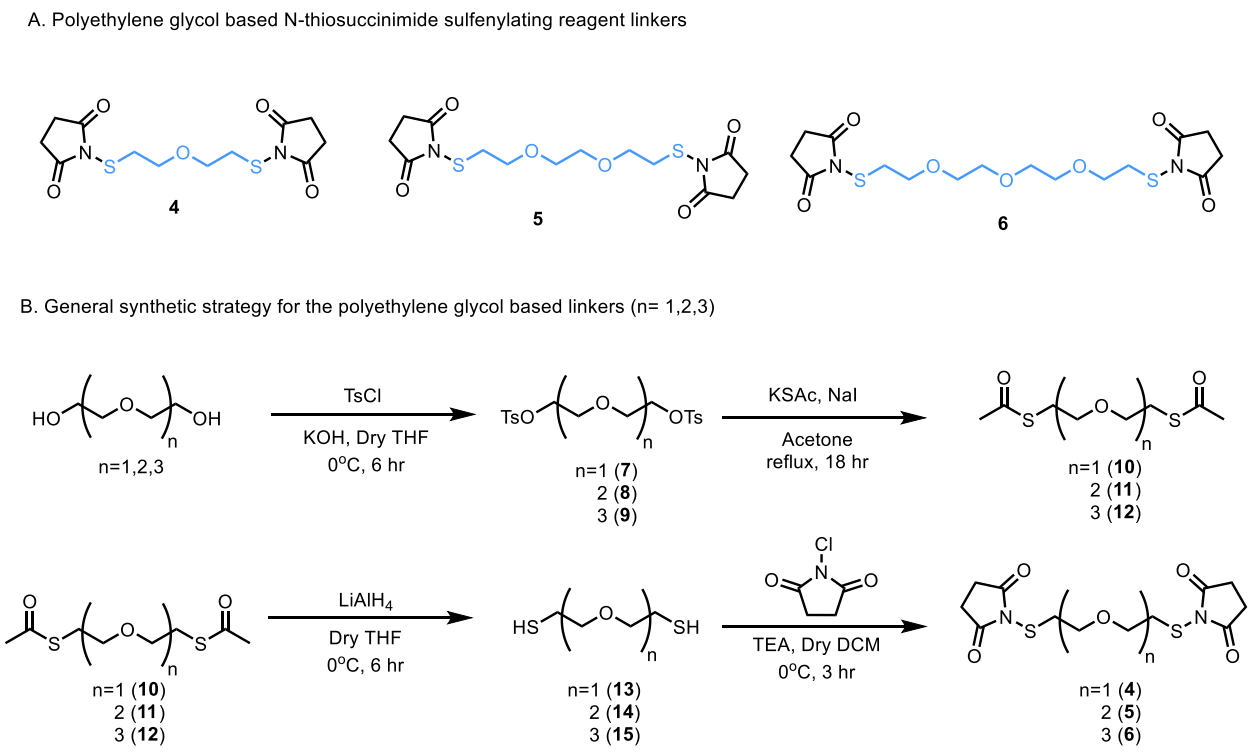

Figure 3-3 A.) Polyethylene glycol based sulfenylating reagents that we used to staple our tryptophan-containing peptides. B.) The synthetic strategy for our various length polyethylene glycol based sulfenylating reagents.

We then synthesized a series of PEG linkers to evaluate the optimal length for promoting α-helical stabilization. Straightforward derivatization of commercially available polyethylene glycols furnished the corresponding N-thiosuccinimide PEG linkers di- (**4**), tri- (**5**), and tetra- (**6**), as illustrated in Figure 3.3. PEG linkers have been shown to be an effective tool in modern bioconjugation as their lengths are highly tunable, they have low toxicity, and they offer high solubility in a biological environment[28]. We started with reacting cheap and readily available polyethylene glycol with p-toluene sulfonyl chloride, TsCl, to create tosylates, (**7**), (**8**), and (**9**). The new tosylate groups are great leaving groups and allow for thioacetate to attack and replace the tosylates to afford thioacetates (**10**), (**11**), and (**12**). To generate thiols (**13**), (**14**), and (**15**) we reduced our thioacetates with lithium aluminum hydride, LAH. N-chlorosuccinimide is then used as an electrophilic chlorine source to chlorinate the thiols. The chlorinated thiols are then attacked by deprotonated succinimide displacing the chloring leaving group to yield our sulfenylating linkers (**4**), (**5**), and (**6**).

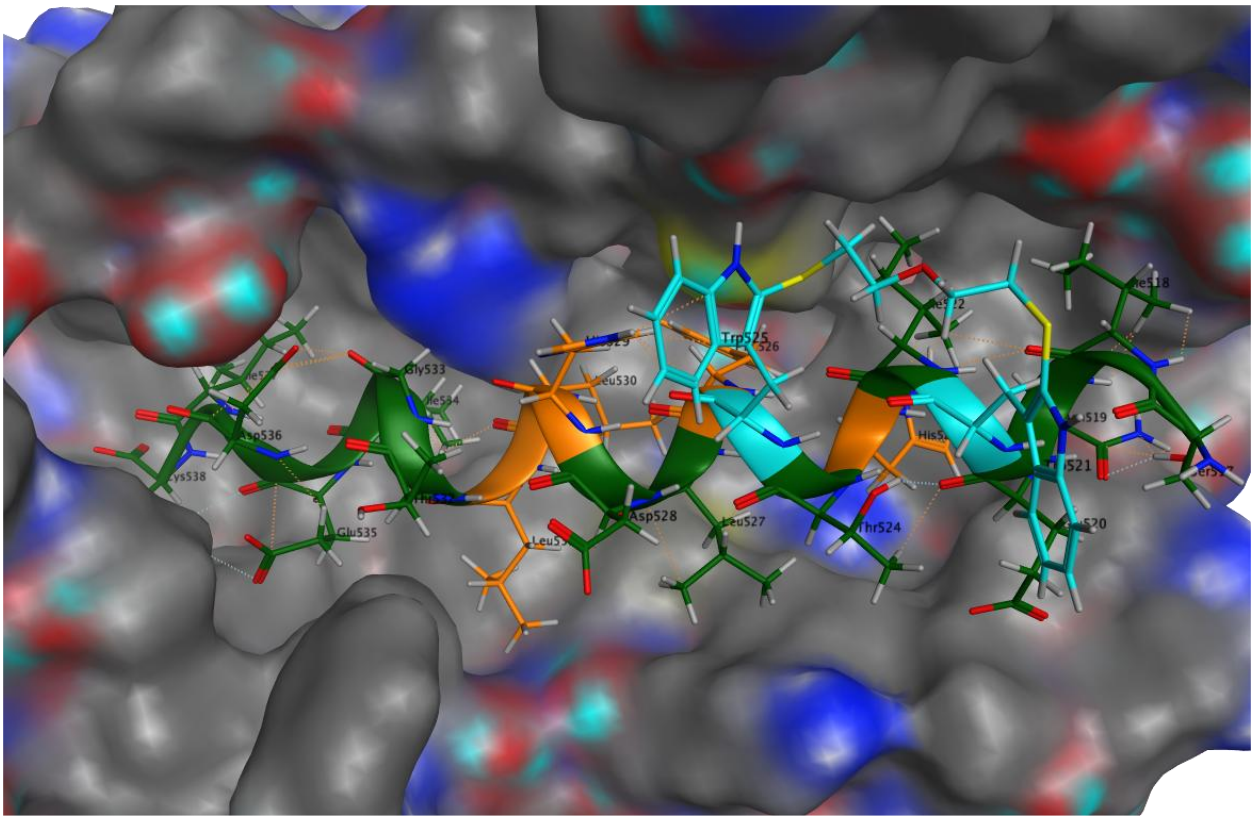

Figure 3-4 Molecular docking of peptide CHP with binding partner NHE-1. "Hot spot" residues highlighted in orange. Tryptophan amino acids and diethylene glycol based linker (**4**) highlighted in teal.

When investigating novel peptide stapling targets one approach is to dock the helical peptide with its binding partner to determine the binding face and "hot spot" residues. Bobby Aurora coined this term which means residues that are most responsible for the binding affinity of the peptide to its binding target[30]. Altering or replacing these "hot spot" residues can lead to a decrease in binding affinity so when designing a peptide stapling target, we want to place our amino acid targets on the opposite face of these residues. This ensures that the "staple" or linker does not interfere with the peptide-protein interaction. Figure 3.4 illustrates the molecular binding of a peptide derived from CHP and its binding target NHE-1. This PPI is well studied by Joseph Provost[31] but is a novel target for peptide stapling. This PPI is involved in regulating extracellular pH. Inbalance in this PPI can increase cancer metastasis. Figure 3.4 shows the "hot

spot" residues highlighted in orange with the tryptophan on the opposite face bound together by linker (**4**) highlighted in teal.

Our other peptide stapling target interactions are BID-BH3/BCL-2, Axin/Wnt, and NF-κB p50/IκBζ. The BID-BH3/BCL-2 PPI is arguably to most studied peptide stapling target and is involved in inducing apoptosis[22]. In some types of cancer, this PPI is improperly regulated and allows for increased cancer cell proliferation. Axin/Wnt is another famous peptide stapling target and involves regulation of the Wnt/β-catenin pathway which is a crucial cell signaling pathway that regulates key processes like cell proliferation, differentiation, and embryonic development[23]. The NF-κB p50/IκBζ PPI is responsible for controlling the expression of specific inflammatory genes in activated immune cells like macrophages[32]. For the well-studied targets we used the optimized amino acids locations (*i, i +4*) from literature to install our tryptophan residues where the artificial alkene containing amino acids would be located in the case of the RCM method used to study these PPIs. For the novel targets we placed our target Tryptophan residues on the opposite side of the binding face while not disturbing the "hot spot" residues.

Upon initial reactivity testing of these peptides with water as the solvent. The p50 peptide was the only peptide that showed reactivity. This peptide was used for initial optimization as shown in Table 3.1. Initially we were getting inconsistent results with the reactivity in which some experiments would produce inconsistent quantities of the dimer product shown in Table 3.1. This dimer product is a result of two peptides being bound together with one equivalence of the linker. We found that the order of addition for the reaction influenced this inconsistency. To deliver consistent results the peptide needs to be first dissolved and stirred in solvent to help distribute the peptide and then the Lewis base and sulfenylating reagent can be added. The

.

Table 3-1 Optimization table for our peptide stapling technique.

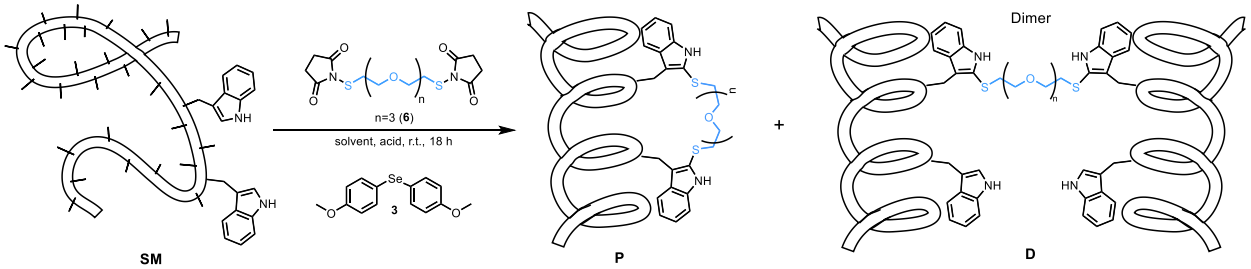

entry	peptide	solvent	molarity, M	cat **3** load	acid (equiv)	linker **4** equiv	conversion (SM:D:P)[a]
1	P50	Water	0.01M	0.1	TfOH (0.1)	1	(0:75:**25**)
2	P50	Water	0.005M	0.1	TfOH (0.1)	1	(0:5:**95**)
3	P50	Water	0.0025M	0.1	TfOH (0.1)	1	(1:98:**1**)
4	P50	Water	0.00125M	0.1	TfOH (0.1)	1	(0:80:**20**)
5	P50	Water	0.005M	0.1	No Acid	1	(0:90:**10**)
6	P50	Water	0.005M	0.1	HCl (0.1)	1	(0:80:**20**)
8	P50	Water	0.005M	0.1	HCl (100)	1	(0:60:**40**)
9	P50	Water	0.005M	0.2	TfOH (0.1)	1	(0:90:**10**)
10	P50	Water	0.005M	0	TfOH (0.1)	1	(95:5:**0**)
11	BID	Water	0.005M	0.1	TfOH (0.1)	1	(100:0:**0**)
12	BID	ACN	0.005M	0.1	TfOH (0.1)	1	(100:0:**0**)
13	BID	IPA	0.005M	0.1	TfOH (0.1)	1	(100:0:**0**)
14	BID	HFIP	0.005M	0.1	TfOH (0.1)	1	(52:2:**46**)
15	BID	HFIP	0.005M	0.1	TfOH (0.1)	1.5	(18:6:**76**)
16	BID	HFIP	0.005M	0.1	TfOH (0.1)	2	(5:8:**87**)
17	BID	HFIP	0.005M	0.1	TfOH (0.1)	3	(5:25:**70**)
18	BID	HFIP	0.005M	0.1	TFA (1)	2	(12:5:**83**)
19	NHE	HFIP	0.005M	0.1	TfOH (0.1)	2	(0:29:**71**)
20	AXIN	HFIP	0.005M	0.1	TfOH (0.1)	2	(0:42:**58**)

[a]Conversions were measured through LCMS analysis.

reaction is stirred again before the Bronsted acid was added. Table 3.1 shows the results of optimization using this proper order of addition. To start the optimization, we wanted to dissolve the peptide at a low concentration to reduce the proximity of the peptides to each other in solution. We found that the best concentration for this reaction is 0.005M found in Table 3.1 entry 2. This condition proved to be the most effective at generating our desired stapled product (**P**) with 95% conversion. We then applied this optimized condition to the BID peptide in Table 3.1 entry 11. Under these conditions the peptide was not soluble in water and showed zero conversion to either of the products. We found that the peptide was soluble in isopropyl alcohol

but still showed zero conversion, Table 3.1 entry 13. After testing several different solvents we found 46% conversion for BID peptide from the use of hexafluoroisopropyl alcohol, Table 3.1 entry 14. We found that increasing the equivalence of the linker gave us increased conversion with only slight increase in the dimer product. Ultimately, we found that with 2 equivalence of the linker showed the best results for the water insoluble peptide BID with 87% conversion to our desired stapled peptide product **P**, Table 3.1 entry 16. We applied this condition to NHE and Axin and got 71% and 58% respectively, Table 3.1 entries 19 and 20.

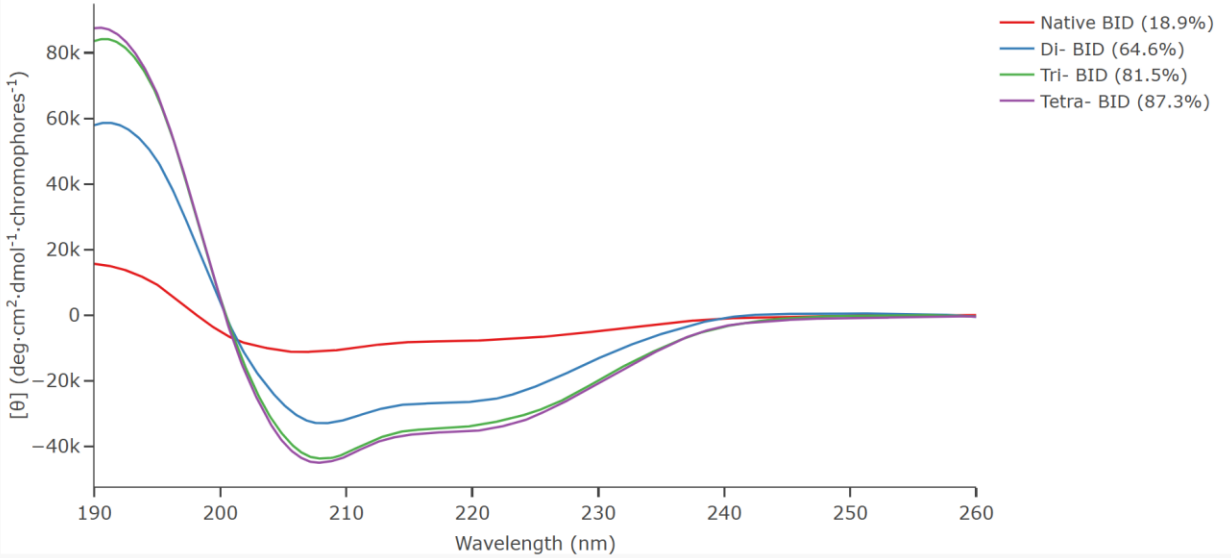

Figure 3-5 Circular dichroism spectra of the native BID peptide and the three different length linkers and their respective helicities.

Using di-(**4**), tri-(**5**), and tetra-(**6**) PEG N-thiosuccinimide linkers and our optimized condition, we evaluated the ability of our method to induce α-helicity. Circular dichroism analysis of the stapled BID peptides in Figure 3.5 revealed that the tetra-PEG linker provided the optimal spacing for *i,i+4* Trp-stapling. Achieving helicity comparable to that of RCM-stapled analogs at 87.3% helicity. The Di- had the lowest helicity at 64.6% and is likely due to its tighter

constraint on the peptide which could potentially cause contortion of its three-dimensional shape. The Tri- showed very similar helicity to the Tetra- with 81.5% helicity. The native BID peptide showed 18.9% helicity which is higher than typically seen from the BID alkene integrated residues used for the RCM method. Nonetheless, we see an increase in helicity by greater than 4 times with our tetra linker when compared to the native peptide.

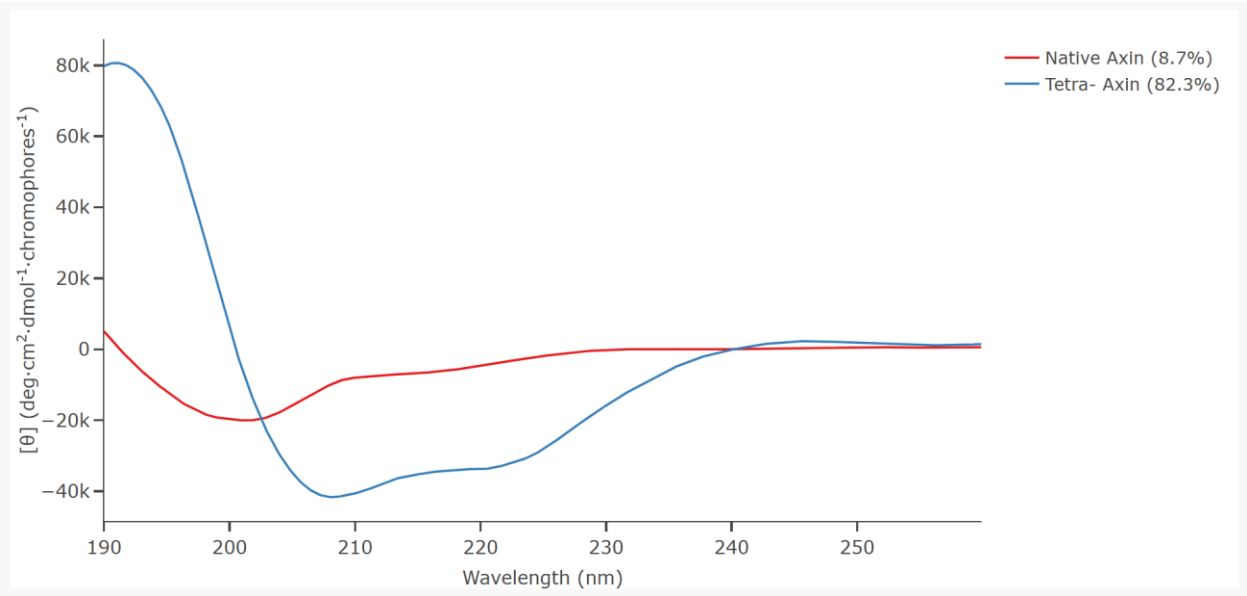

Figure 3-6 Circular dichroism spectra of native Axin peptide and the tetra stapled Axin peptide and their respective helicities.

Having established optimal length, we next applied the optimized tetra-PEG stapling conditions to our Axin-derived peptide, Figure 3.6. Similarly to the BID peptide we see greatly enhanced helicity with the introduction of our tetra linker, 82.3%, confirming that our approach is generalizable beyond BID peptides and validating its application to established stapled-peptide targets. Encouraged by these results, we turned to our unexplored peptide stapling targets, NHE and p50. We see helicity of NHE-1 up to 38.9% compared to its native 8.7%, Figure 3.7. The stapled p50 peptide saw helicity up to 64.1% compared to its native 16.5%. Our chemistry successfully stapled these novel targets but did not induce the same level of helicity as the well-

studied targets. As shown in peptide stapling literature, the same stapling chemistry can range from 10-80% helicity with just a change of staple location on the same peptide[34]. This positional dependence is a known hallmark of helix stabilization and must be accounted for in the design of tryptophan-based staples[35]. More research needs to be done on these novel targets to optimize the location of the staple within the peptide.

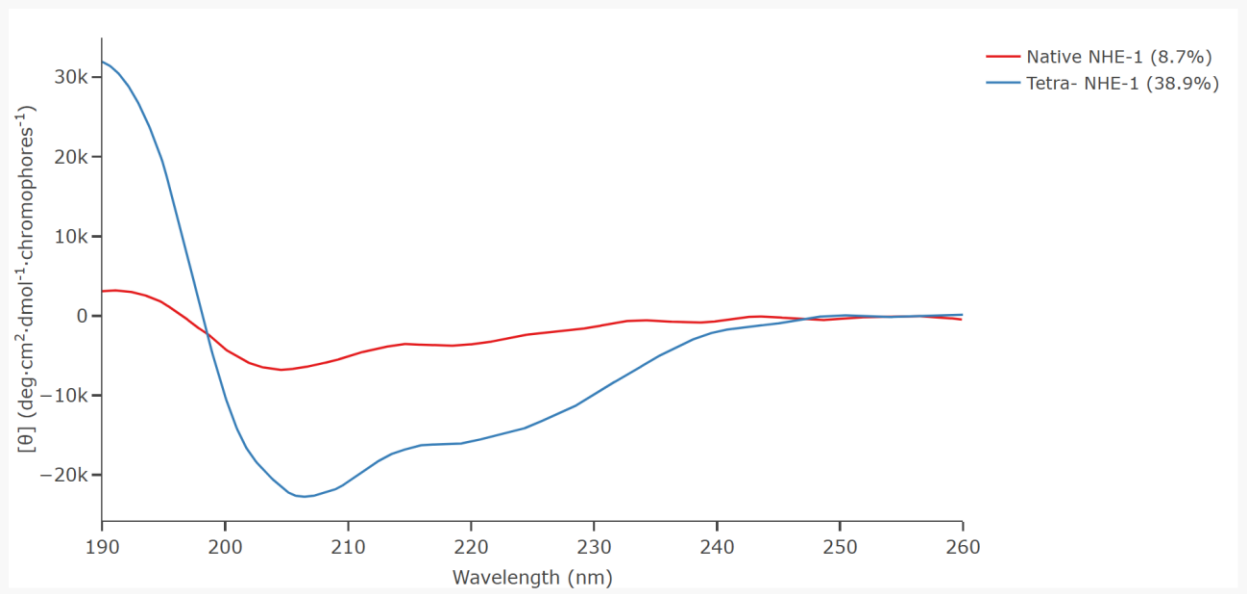

Figure 3-7 Circular dichroism spectra of native NHE-1 peptide and the tetra stapled NHE-1 peptide and their respective helicities.

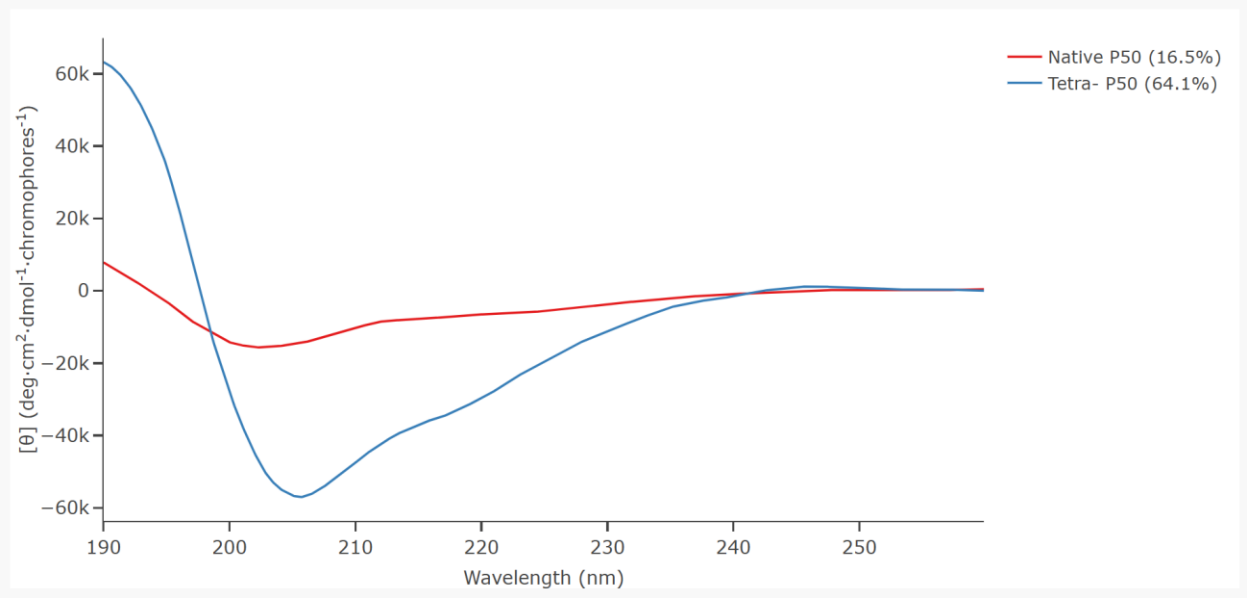

Figure 3-8 Circular dichroism spectra of native p50 peptide and the tetra stapled p50 peptide and their respective helicities.

3.4 Conclusions

In summary, we have established a tryptophan-selective, metal-free stapling strategy that expands the chemical repertoire available for stabilizing α-helical peptides. By harnessing the unique reactivity of the indole side chain toward N-thiosuccinimide PEG linkers under Lewis base/Brønsted acid dual catalysis, we achieved efficient *i,i+4* cross-linking without the need for noncanonical amino acids or transition metals. Benchmarking on the BID BH3 helix demonstrated that our tetra-PEG staple can induce helicity on par with the well-established RCM approach, while offering a more streamlined and biocompatible synthesis. The successful extension of this methodology to Axin peptides further underscores its generalizability to known stapling targets. Importantly, our application of this chemistry to the NHE/CHP-1 and NF-κB p50/IκBζ interfaces introduces two previously untapped systems into the stapled peptide landscape, illustrating its potential to broaden the range of biologically relevant PPIs that can be

addressed. Although further work is required to refine staple positioning in these novel contexts, the ability to access high yields and enhanced helicity across multiple targets highlights the promise of this approach. Taken together, these results provide both a new chemical strategy for peptide stapling and a foundation for future exploration of therapeutically important protein interactions using Tryptophan targeted macrocyclization.

3.5 Abbreviations

PPI, protein-protein interactions; PEG, polyethylene glycol; TFA, CF_3O_2H, trifluoroacetic acid; S_EAr, Electrophilic aromatic substitution; IPA, isopropyl alcohol; HFIP, hexafluoroisopropyl alcohol; CD, circular dichroism; MALDI, matrix assisted laser desorption ionization; NMR, nuclear magnetic resonance; EDG, electron donating group; EWG, electron withdrawing group; TfOH, trifilic acid, trifluoromethanesulfonic acid; eq., equivalence; $CHCl_3$, chloroform; Me, methyl; H, hydrogen; OMe, methoxy; RPM, revolutions per minute.

3.6 References

(1) Arkin, M. R.; Wells, J. A. Small-Molecule Inhibitors of Protein–Protein Interactions: Progressing Toward the Reality. *Nat. Rev. Drug Discov.* **2004**, *3*, 301–317.

(2) Scott, D. E.; Bayly, A. R. Small-Molecule Protein–Protein Interaction Inhibitors: Challenges and Opportunities. *Nat. Rev. Drug Discov.* **2016**, *15*, 533–550.

(3) Otaka, A.; Fujii, N. Strategies for the Conformational Stabilization of Bioactive Peptides. *Biopolymers* **2010**, *94*, 763–771.

(4) Adessi, C.; Soto, C. Strategies to Improve the Stability and Bioavailability of Peptide Drugs. *Curr. Med. Chem.* **2002**, *9*, 963–978.

(5) Fosgerau, K.; Hoffmann, T. Peptide Therapeutics: Current Status and Future Directions. *Drug Discov. Today* **2015**, *20*, 122–128.

(6) Chiu, H.-C.; Prenner, E. J. Peptide Pharmacokinetics: Challenges and Opportunities. *Ther. Delivery* **2011**, *2*, 1305–1320.

(7) Walensky, L. D.; Bird, G. H. Hydrocarbon-Stapled Peptides: Principles, Practice, and Progress. *J. Med. Chem.* **2014**, *57*, 6275–6288.

(8) Qian, Z.; Liu, T. Cell-Penetrating Peptides for Intracellular Delivery. *Adv. Drug Delivery Rev.* **2016**, *110–111*, 1–2.

(9) Davis, J. M.; Carvalho, M. A. The Importance of Peptide Helicity for Biological Function. *J. Biol. Chem.* **2009**, *284*, 34135–34143.

(10) Schafmeister, C. E.; Po, J.; Verdine, G. L. An All-Hydrocarbon Cross-Linking System for Enhancing the Helicity and Biological Stability of Peptides. *J. Am. Chem. Soc.* **2000**, *122*, 5891–5892.

(11) Walensky, L. D.; Kung, A. L. Activation of Apoptosis In Vivo by a Hydrocarbon-Stapled BH3 Helix. *Science* **2004**, *305*, 1466–1470.

(12) Blackwell, H. E.; Grubbs, R. H. Highly Efficient Synthesis of Covalently Cross-Linked Peptide Helices by Ring-Closing Metathesis. *Angew. Chem., Int. Ed.* **1998**, *37*, 3281–3284.

(13) Miller, S. J.; Grubbs, R. H. Olefin Metathesis for Peptide Macrocyclization. *J. Am. Chem. Soc.* **1995**, *117*, 5855–5856.

(14) Azzarito, V.; Long, K. New Peptide Macrocyclization and Stapling Strategies for Drug Development. *Chem. Soc. Rev.* **2013**, *42*, 3410–3421.

(15) Cantel, S.; Scrima, M. Synthesis and Conformational Analysis of Triazole-Stapled Peptides via Copper(I)-Catalyzed Azide–Alkyne Cycloaddition. *Angew. Chem., Int. Ed.* **2008**, *47*, 3490–3493.

(16) Angell, Y. L.; Burgess, K. Ring-Closing Metathesis and CuAAC for Turn Mimetics in Peptides. *J. Org. Chem.* **2005**, *70*, 9595–9598.

(17) Zhang, H.; Wang, P. Cysteine-Specific Peptide Macrocyclization Strategies. *ChemBioChem* **2017**, *18*, 1359–1363.

(18) Spokoyny, A. M.; Zou, Y. A Perfluoroaryl-Cysteine SNAr Chemistry Approach to Unprotected Peptide Stapling. *J. Am. Chem. Soc.* **2013**, *135*, 5946–5949.

(19) Raj, M.; Khurana, R. Bis-Alkylation of Cysteines for Peptide Macrocyclization. *J. Org. Chem.* **2013**, *78*, 1379–1383.

(20) Lau, Y. H.; de Andrade, P. Functionalized Stapled Peptides via Oxidative Stapling. *Chem. Soc. Rev.* **2015**, *44*, 91–102.

(21) Cromm, P. M.; Spiegel, J.; Grossmann, T. N. Stapled Peptides as Tools for Modulating Protein–Protein Interactions. *ACS Chem. Biol.* **2015**, *10*, 1362–1375.

(22) LaBelle, J. L.; Katz, S. G. A Stapled BIM BH3 Peptide Directly Activates BAX. *Nat. Rev. Cancer* **2012**, *12*, 152–160.

(23) Takada, K.; Zhu, D. Targeting Wnt Signaling Using Stabilized Helical Peptides Derived from Axin. *Nat. Chem. Biol.* **2012**, *8*, 616–624.

(24) Bird, G. H.; Mazzola, E. Hydrocarbon-Stapled Peptides Increase Stability and Serum Half-Life In Vivo. *Nat. Chem. Biol.* **2016**, *12*, 147–152.

(25) Bloom, S.; Liu, C. Decarboxylative Alkylation for Tryptophan-Selective Bioconjugation. *Nat. Chem.* **2018**, *10*, 205–211.

(26) Sato, S.; Nakamura, H. Chemical Modification of Tryptophan Residues in Peptides and Proteins. *Angew. Chem., Int. Ed.* **2013**, *52*, 8681–8684.

(27) Pal, D.; Chakrabarti, P. Aromatic Interactions in Protein–Protein Interfaces: The Role of Tryptophan. *J. Mol. Biol.* **1999**, *294*, 271–288.

(28) Knop, K.; Hoogenboom, R. Poly(ethylene glycol) in Drug Delivery: Advantages and Limitations. *Angew. Chem., Int. Ed.* **2010**, *49*, 6288–6308.

(29) Veronese, F. M.; Pasut, G. PEGylation: Recent Achievements and Perspectives. *Drug Discov. Today* **2005**, *10*, 1451–1458.

(30) Clackson, T.; Wells, J. A. A Hot Spot of Binding Energy in a Hormone–Receptor Interface. *Science* **1995**, *267*, 383–386.

(31) Donowitz, M.; Tse, C. M.; Fuster, D. SLC9/NHE Family of Na+/H+ Exchangers. *Physiol. Rev.* **2013**, *93*, 803–827.

(32) Renner, F.; Schmitz, M. L. Autoregulatory Feedback Loops in NF-κB Signaling. *Biochim. Biophys. Acta* **2009**, *1793*, 145–154.

(33) Henriques, S. T.; Castanho, M. A. R. B. Cell-Penetrating Stapled Peptides in Transcriptional Regulation. *FEBS J.* **2016**, *283*, 2547–2571.

(34) Henchey, L. K.; Jochim, A. L.; Arora, P. S. Contemporary Strategies for Stabilizing the α-Helical Conformation in Peptides. *Curr. Opin. Chem. Biol.* **2008**, *12*, 692–697.

(35) Walensky, L. D.; Bird, G. H. Optimizing Staple Position for α-Helix Stabilization. *Methods Enzymol.* **2014**, *544*, 1–30.

3.7 Supplemental Information

Synthesis of the Stabilized Alpha Helical Peptides

Peptides were synthesized by Biomatik and GenScript with Tryptophan flanking three amino acids in the *i, i+4* positions within the peptide. BID peptide sequence: Ac-EDIIRNIARHLA**W**VGD**W**MDRSI-OH. P50 peptide sequence: Ac-KDKEEV**W**RKR**W**KLMP-OH. NHE peptide sequence: Ac-**W**IHT**W**FLDHLLTGIE-OH. Axin peptide sequence: Ac-ENPE**W**ILD**W**HVQRVM-OH. Each peptide (0.005 mmol) was added to a clear GC vial and dissolved in solvent. A micro stir bar was added. Stock solutions of the Lewis base catalyst in $CHCl_3$ (0.04mg/mL) and the sulfenylating reagent in DCM (0.06mg/mL) were added. The reaction was stirred for 2 minutes then the acid stock solution in was added. The acid stock solution was made immediately before each reaction and the solvent and concentration depended on the acid being used. HCl solution was made in water and TfOH (0.005μL/mL) and TFA (0.1μL/mL) solutions were made in $CHCl_3$. Acid stock solutions were mixed by drawing the solution up and down in a glass Pasteur pipette repeatedly. TfOH stock solution would become cloudy upon mixing. The reaction was stirred overnight at room temperature then analyzed by LC/MS. The reaction was purified by reverse phase HPLC using an Agilent Zorbax SB C-18 column. The resulting fractions were lyophilized and analyzed by CD spectrometry.

Circular Dichroism

Compounds were dissolved in a 70:30 water:acetonitrile solution to concentrations of 25-50 μM. CD spectra were obtained on a Jasco J-110 spectropolarimeter at 20^{o}C using the

following standard measurement parameters: wavelength, 190-260 nm; step resolution, 0.5 nm; speed, 1000 nm/min; accumulations, 10; response, 1 sec; bandwidth, 1 nm; path length, 0.1 cm. The α-helical content of each peptide was calculated by dividing the mean residue ellipticity [φ]222obs by the reported [φ]222obs for a model helical decapeptide.

Linker Synthesis

2,2′-oxybis-, 1,1′-bis(4-methylbenzenesulfonate) (7)

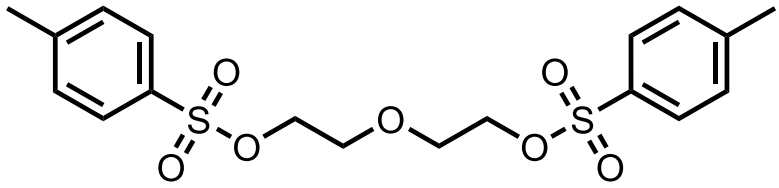

Diethylene Glycol (2.43g, 22.9mmol) and crushed potassium hydroxide (8 eq) were added to a round bottom flask under argon gas and dissolved in dry THF (0.6 M) stirred for 10 minutes. Solution becomes cloudy and p-toluenesulfonic acid (2.2 eq) was added at 0°C, allowed to warm to room temperature and stirred for 18 hours. The resulting solution is diluted and vacuum filtered. Filtrate is dried over sodium sulfate and evaporated to yield a white solid (8.90g, 93.6% yield). The spectral data is in agreement with the reported literature: Roy, R.K. and Ramakrishnan, S. **2013**, *Polym. Chem*., 51: 4125-4135. **^{1}H NMR** (400 MHz, $CDCl_3$) δ 7.787 (d, J = 7.23 Hz, 4H), 7.39 (d, J = 7.86 Hz, 4H), 4.08 (d, J = 5.80 Hz, 4H), 3.60 (d, J = 5.17, 4H), 2.45 (s, 6H).

***S*,*S*′-(oxydi-2,1-ethanediyl) ester (10)**

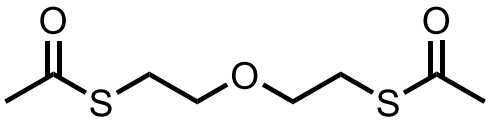

Added to a round bottom flask was Compound (**7**) (8.90g, 21.5mmol), potassium thioacetate (5 eq), and sodium iodide (0.1 eq) dissolved in acetone (0.1M). Solution thickens upon heating and becomes a cloudy brown. Stirred and refluxed for 18 hours. Solution is evaporated. Dissolved in water and extracted with DCM. DCM fractions combined and washed with brine solution. Dried over sodium sulfate and evaporated to yield a dark red oil. Product smells strongly of sulfur (4.16g, 87% yield). The spectral data is in agreement with the reported literature: Scullion, L. E.; Leary, E.; Higgins, S. J.; Nichols, R. J. *J. Phys.-Condens. Mat.* **2012**, *24*, 164211–164219. **^{1}H NMR** (400 MHz, $CDCl_3$): δ = 3.56 (t, J = 6.4 Hz, 4 H), 3.05 (t, J = 6.4 Hz, 4 H), 2.32 (s, 6 H)

2,2′-Oxydi-1-ethanethiol (13)

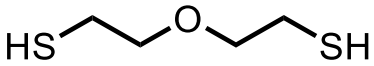

Compound (**10**) (3.23g, 14.5 mmol) was measured into a vial under Argon then diluted with dry THF (1.8M). Lithium aluminum hydride (4 eq) was added to a round bottom flask and suspended in dry THF (0.6M). Suspended LAH was cooled to 0ºC and solution of compound (**10**) was added dropwise and stirred overnight at room temperature. The reaction was then cooled to 0ºC in an ice bath and quenched with a saturated sodium sulfate water solution until no more gas is produced. To the quenched reaction 10 mL 1M HCl was added and stirred for 5 minutes. Reaction mixture was added to a separatory funnel along with 50mL 1M HCl solution. The mixture was extracted with DCM, dried over sodium sulfate, and evaporated to yield a crude dark red oil. The crude oil was purified by flash column chromatography to yield a light orange

oil (1.71g, 85.1% yield). The spectral data is in agreement with the reported literature: Roy, R.K. and Ramakrishnan, S. **2013**, *Polym. Chem*., 51: 4125-4135. **^{1}H NMR** (400 MHz, $CDCl_3$): 1.7 (t, J = 8.28 Hz, 2H); 2.70 (q, J = 7.25 Hz, 4H), 3.61 (t, J = 7.59 Hz, 4H)

1,1′-[Oxybis(2,1-ethanediylthio)]bis[2,5-pyrrolidinedione] (4)

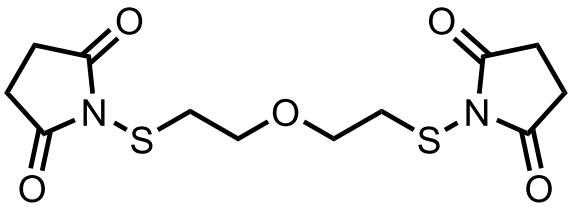

Compound (**13**) (225.3mg, 1.630 mmol) was measured into a vial under argon. N-Chlorosuccinimide (2.2 eq) was added to a round bottom flask and suspended in dry DCM (0.4 M) cooled in an ice bath to 0^{o}C. Compound (**13**) was added dropwise to the solution of NCS at 0^{o}C and stirred for 20 minutes. Triethylamine (2.3 eq) was dissolved in dry DCM (2.8M) and added dropwise to solution of (**13**) and NCS at 0^{o}C. The reaction was allowed to warm to room temperature while it stirred for 2.5 hrs. The reaction was washed with brine solution four times. The organic layer was dried over sodium sulfate and evaporated to give a light orange/red oil. The crude oil was purified by flash column chromatography to yield a slightly yellow oil (137.8mg, 26.0% yield). The spectral data is in agreement with the reported literature: Jun Yoo, Denison J. Kuruvilla, Sheetal R. D'Mello, Aliasger K. Salem, and Ned B. Bowden, *Macromolecules* **2012** *45* (5), 2292-2300. **^{1}H NMR** (400 MHz, $CDCl_3$): δ 2.81 (s, 8H), 2.91 (t, 4H, J = 5.9 Hz), 3.63 (t, 4H, J = 6.0 Hz)

1,8-Bis(tosyloxy)-3,6-dioxaoctane (8)

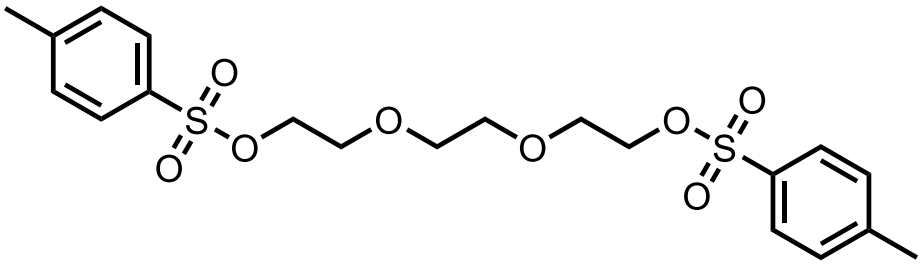

Triethylene Glycol (3.45g, 22.9mmol) and crushed potassium hydroxide (8 eq) were added to a round bottom flask under argon gas and dissolved in dry THF (0.6 M) stirred for 10 minutes. Solution becomes cloudy and p-toluenesulfonic acid (2.2 eq) was added at 0ºC, allowed to warm to room temperature and stirred for 18 hours. The resulting solution is diluted and vacuum filtered. Filtrate is dried over sodium sulfate and evaporated to yield a purple solid (10.09g, 96.0% yield). The spectral data is in agreement with the reported literature: Daniel J. Keddie, John B. Grande, Ferdinand Gonzaga, Michael A. Brook, and Tim R. Dargaville, *Organic Letters* **2011** *13* (22), 6006-6009. **^{1}H NMR** (400MHz, $CDCl_3$): δ 2.43 (6H, s), 3.55 (4H, s), 3.67 (4H, t, J = 4.1 Hz,), 4.14 (4H, t, J = 4.1 Hz,), 7.33 (4H, d, J = 7.6 Hz,), 7.78 (4H, d, J = 7.6 Hz,)

2,2′-(Ethylenedioxy)diethanethioacetate (11)

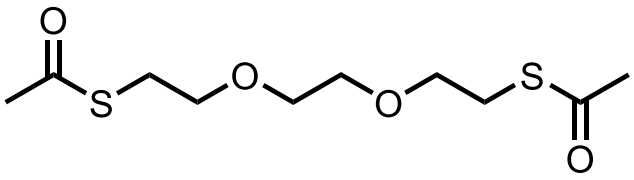

Added to a round bottom was Compound (**8**) (7.64g, 16.6mmol), potassium thioacetate (5 eq), and sodium iodide (0.1 eq) dissolved in acetone (0.1M). Solution thickens upon heating and becomes a cloudy brown. Stirred and refluxed for 18 hours. Solution is evaporated. Dissolved in water and extracted with DCM. DCM fractions combined and washed with brine solution. Dried

over sodium sulfate and evaporated to yield a dark red oil. Product smells strongly of sulfur (3.96g, 88.9% yield). The spectral data is in agreement with the reported literature: Daniel J. Keddie, John B. Grande, Ferdinand Gonzaga, Michael A. Brook, and Tim R. Dargaville, *Organic Letters* **2011** *13* (22), 6006-6009. **^{1}H NMR** (400MHz, $CDCl_3$): δ 2.28 (6H, s), 3.03 (4H, t, J = 6.3 Hz), 3.56- 3.67 (8H, m)

2,2′-(Ethylenedioxy)diethanethiol (14)

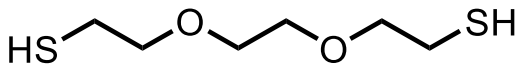

Compound (**11**) (5.26g, 19.7 mmol) was measured into a vial under Argon then diluted with dry THF (1.8M). Lithium aluminum hydride (4 eq) was added to a round bottom flask and suspended in dry THF (0.6M). Suspended LAH was cooled to 0^{o}C and solution of compound (**11**) was added dropwise and stirred overnight at room temperature. The reaction was then cooled to 0^{o}C in an ice bath and quenched with a saturated sodium sulfate water solution until no more gas is produced. To the quenched reaction 10 mL 1M HCl was added and stirred for 5 minutes. Reaction mixture was added to a separatory funnel along with 50mL 1M HCl solution. The mixture was extracted with DCM, dried over sodium sulfate, and evaporated to yield a crude dark red oil. The crude oil was purified by flash column chromatography to yield a light orange oil (3.16g, 87.8% yield). The spectral data is in agreement with the reported literature: Daniel J. Keddie, John B. Grande, Ferdinand Gonzaga, Michael A. Brook, and Tim R. Dargaville, *Organic Letters* **2011** *13* (22), 6006-6009. **^{1}H NMR** (400 MHz, $CDCl_3$): δ 1.59 (2H, t, *J* = 8.2 Hz), 2.69 (4H, dt, *J* = 6.3 and 8.2 Hz), 3.57-3.66 (12H, m)

1,1′-[Oxybis(2,1-ethanediylthio)]bis[2,5-pyrrolidinedione] (5)

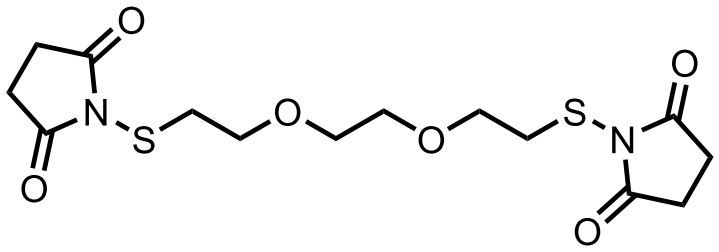

Compound (**14**) (223.5mg, 1.226 mmol) was measured into a vial under argon. N-Chlorosuccinimide (2.2 eq) was added to a round bottom flask and suspended in dry DCM (0.4 M) cooled in an ice bath to 0°C. Compound (**14**) was added dropwise to the solution of NCS at 0°C and stirred for 20 minutes. Triethylamine (2.3 eq) was dissolved in dry DCM (2.8M) and added dropwise to solution of (**14**) and NCS at 0°C. The reaction was allowed to warm to room temperature while it stirred for 2.5 hrs. The reaction was washed with brine solution four times. The organic layer was dried over sodium sulfate and evaporated to give a light orange/red oil. The crude oil was purified by flash column chromatography to yield a slightly yellow oil (112.5mg, 24.4% yield). **^{1}H NMR** (400 MHz, $CDCl_3$): δ 3.71 (t, J = 6.1 Hz, 4H), 3.51 (s, 4H), 3.00 (t, J = 6.1, 4H), 2.83 (s, 8H). **^{13}C NMR** (126 MHz, $CDCl_3$): δ 177.8, 77.4, 77.1, 76.7, 29.6, 28.7 **LC-HRMS (EI): Calculated** $C_{14}H_{20}N_2O_6S_2[M+Na]^+$ 399.0661 m/z **Found:** 399.0672 m/z.

1,8-Bis(tosyloxy)-3,6-dioxaoctane (9)

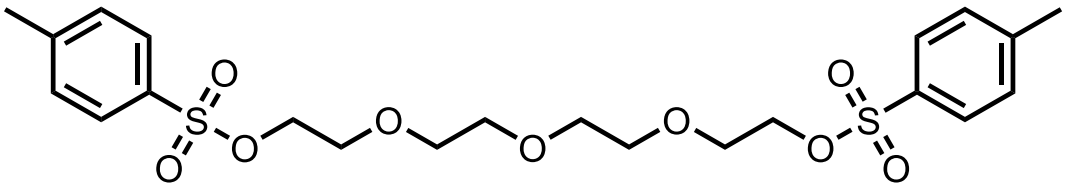

Tetraethylene Glycol (4.06g, 20.9mmol) and crushed potassium hydroxide (8 eq) were added to a round bottom flask under argon gas and dissolved in dry THF (0.6 M) stirred for 10

minutes. Solution becomes cloudy and p-toluenesulfonic acid (2.2 eq) was added at 0ºC, allowed to warm to room temperature and stirred for 18 hours. The resulting solution is diluted and vacuum filtered. Filtrate is dried over sodium sulfate and evaporated to yield a white solid (9.53g, 90.1% yield). The spectral data is in agreement with the reported literature: Bonger, K. M.; van den Berg, R. J. B. H. N.; Heitman, L. H.; IJzerman, A. P.; Oosterom, J.; Timmers, C. M.; Overkleeft, H. S.; van der Marel, G. A. *Bioorgan. Med. Chem.* **2007**, *15*, 4841–4856. **^{1}H NMR** (400 MHz, $CDCl_3$): δ = 7.76 (d, *J* = 8.3 Hz, 4 H,), 7.31 (d, *J* = 8.6 Hz, 4 H), 4.08 (t, *J* = 4.8 Hz, 4 H), 3.68 (t, *J* = 9.6 Hz, 4H), 3.48 (s, 12 H,), 2.42 (s, 6 H)

2,2′-(Ethylenedioxy)diethanethioacetate (12)

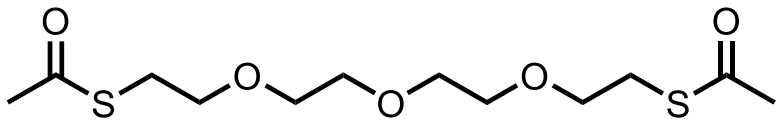

Added to a round bottom was Compound (**9**) (10.53g, 20.9mmol), potassium thioacetate (5 eq), and sodium iodide (0.1 eq) dissolved in acetone (0.1M). Solution thickens upon heating and becomes a cloudy brown. Stirred and refluxed for 18 hours. Solution is evaporated. Dissolved in water and extracted with DCM. DCM fractions combined and washed with brine solution. Dried over sodium sulfate and evaporated to yield a dark red oil. Product smells strongly of sulfur (4.78g, 73.4% yield). The spectral data is in agreement with the reported literature: Keddie, D. J.; Grande, J. B.; Gonzaga, F.; Brook, M. A.; Dargaville, T. R. *Org. Lett.* **2011**, *13*, 6006–6009. **^{1}H NMR** (400 MHz, $CDCl_3$): δ 3.63–3.55 (m, 12 H), 3.05 (t, *J* = 6.5 Hz, 4 H), 2.30 (s, 6 H)

2,2′-(Ethylenedioxy)diethanethiol (15)

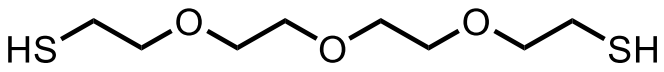

Compound (**12**) (4.77g, 15.4 mmol) was measured into a vial under Argon then diluted with dry THF (1.8M). Lithium aluminum hydride (4 eq) was added to a round bottom flask and suspended in dry THF (0.6M). Suspended LAH was cooled to 0°C and solution of compound (**12**) was added dropwise and stirred overnight at room temperature. The reaction was then cooled to 0°C in an ice bath and quenched with a saturated sodium sulfate water solution until no more gas is produced. To the quenched reaction 10 mL 1M HCl was added and stirred for 5 minutes. Reaction mixture was added to a separatory funnel along with 50mL 1M HCl solution. The mixture was extracted with DCM, dried over sodium sulfate, and evaporated to yield a crude dark red oil. The crude oil was purified by flash column chromatography to yield a light orange oil (3.18g, 91.0% yield). The spectral data is in agreement with the reported literature: Keddie, D. J.; Grande, J. B.; Gonzaga, F.; Brook, M. A.; Dargaville, T. R. *Org. Lett.* **2011**, *13*, 6006–6009. **^{1}H NMR** (400 MHz, $CDCl_3$): δ 3.68–3.57 (m, 12 H), 2.68 (dt, J = 8.1, 6.4 Hz, 4 H), 1.59 (t, J = 8.1 Hz, 2 H)

1,1′-[Oxybis(2,1-ethanediylthio)]bis[2,5-pyrrolidinedione] (6)

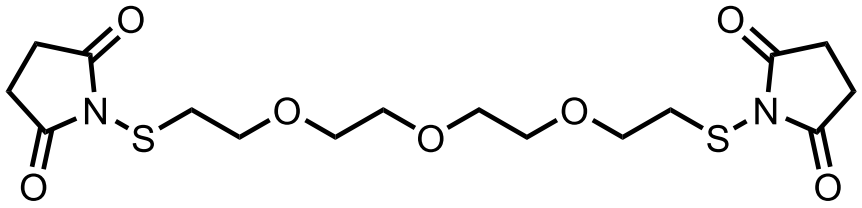

Compound (**15**) (224.7mg, 0.9927 mmol) was measured into a vial under argon. N-Chlorosuccinimide (2.2 eq) was added to a round bottom flask and suspended in dry DCM (0.4 M) cooled in an ice bath to 0°C. Compound (**15**) was added dropwise to the solution of NCS at 0°C and stirred for 20 minutes. Triethylamine (2.3 eq) was dissolved in dry DCM (2.8M) and

added dropwise to solution of (**15**) and NCS at 0ºC. The reaction was allowed to warm to room temperature while it stirred for 2.5 hrs. The reaction was washed with brine solution four times. The organic layer was dried over sodium sulfate and evaporated to give a light orange/red oil. The crude oil was purified by flash column chromatography to yield a slightly yellow oil (113.9mg, 27.3% yield). **^{1}H NMR** (400 MHz, $CDCl_3$): δ 3.71 (t, J = 6.2 Hz, 4H), 3.54 (s, 8H), 2.99 (t, J = 6.7, 4H), 2.81 (s, 8H). **^{13}C NMR** (126 MHz, $CDCl_3$): δ 177.3, 77.4, 77.1, 76.8, 70.8, doublet (70.5, 70.4), 37.1, 28.6. **LC-HRMS (EI): Calculated** $C_{16}H_{24}N_2O_7S_2[M+Na]^+$ 443.09171 m/z **Found:** 443.0938 m/z.

NMR Spectra

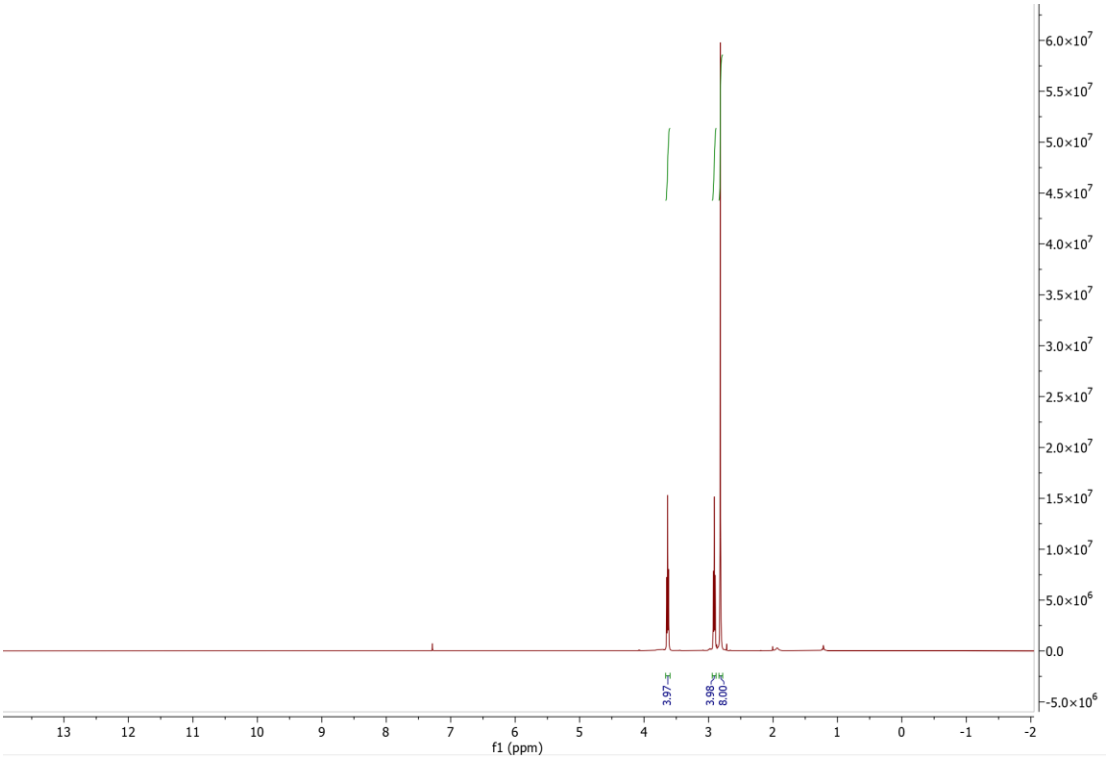

Figure 3-9 ^{1}H, ($CDCl_3$), 400 MHz (**4**)

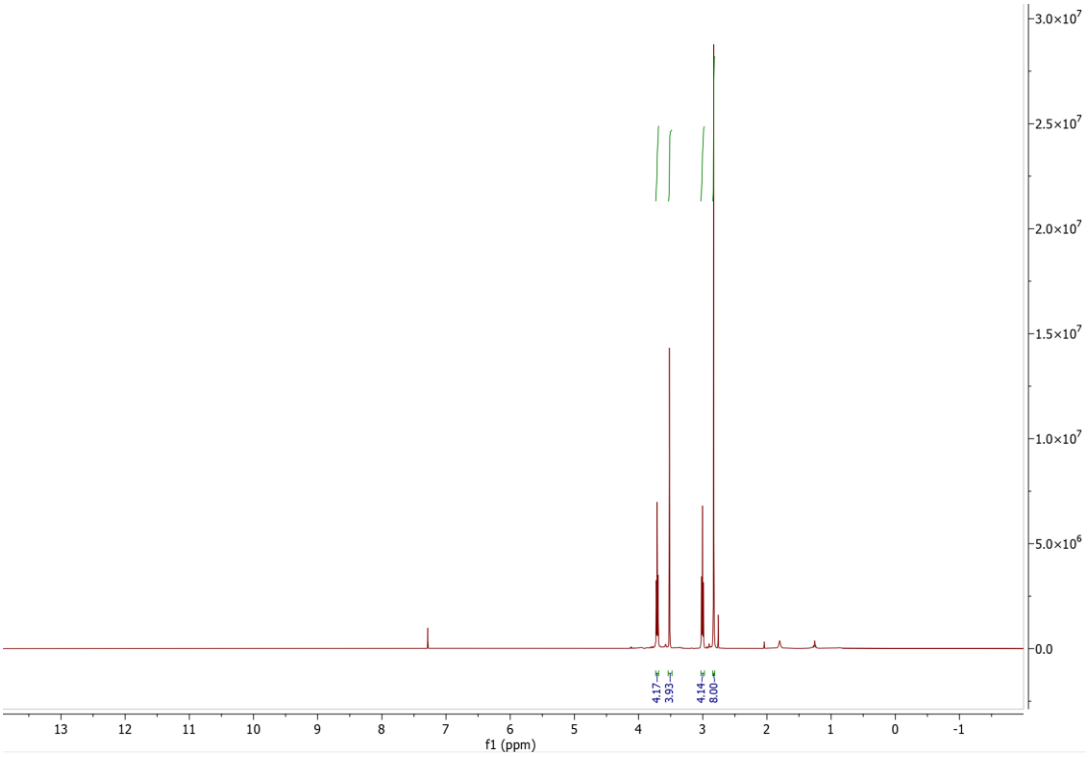

Figure 3-10 ^{1}H, ($CDCl_3$), 400 MHz (**5**)

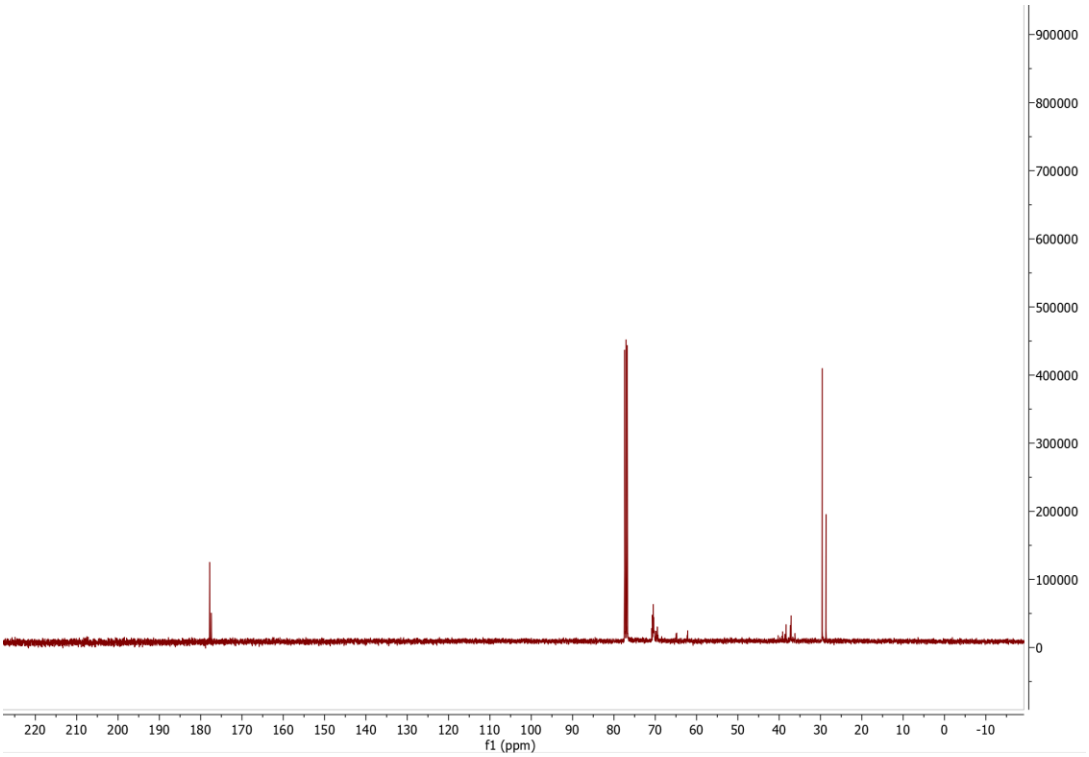

Figure 3-11 ^{13}C, ($CDCl_3$), 400 MHz (**5**)

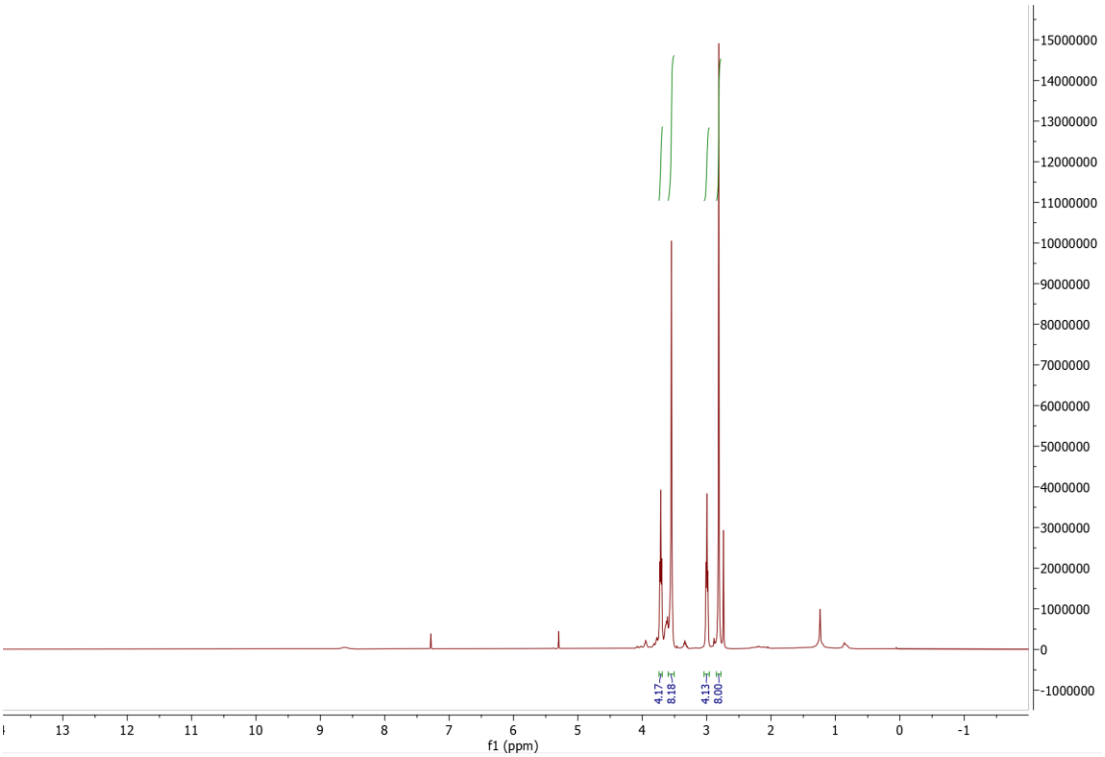

Figure 3-12 ^{1}H, ($CDCl_3$), 400 MHz (**6**)

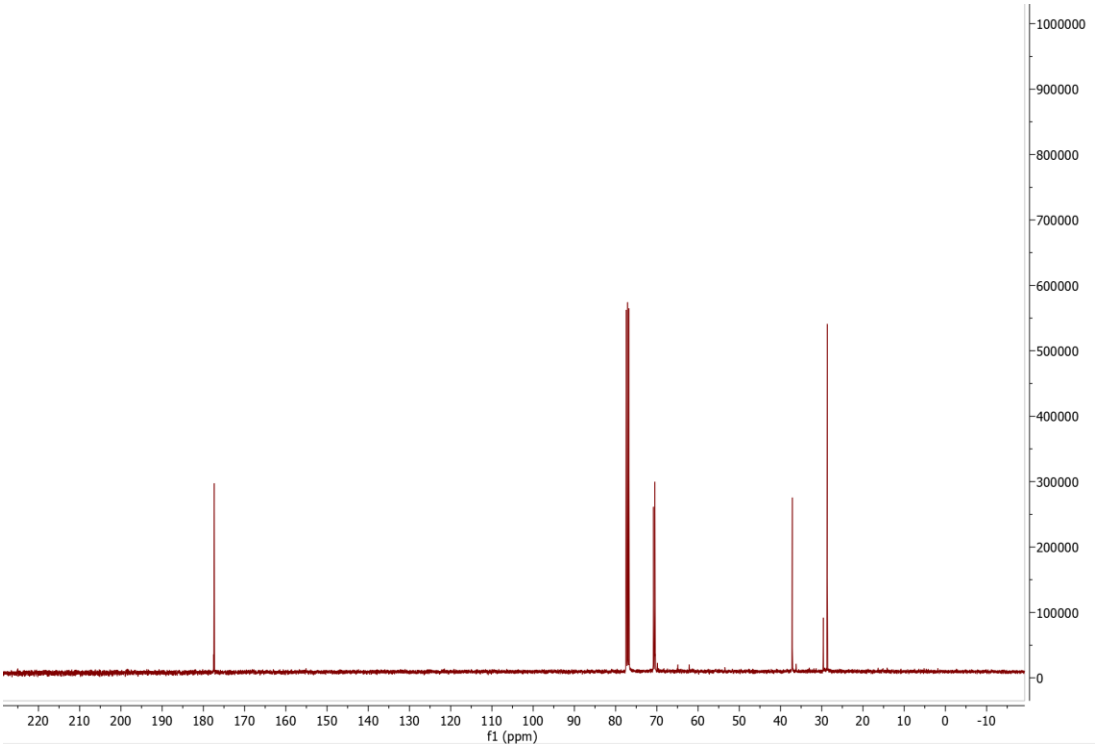

Figure 3-13 ^{13}C, ($CDCl_3$), 400 MHz (**6**)

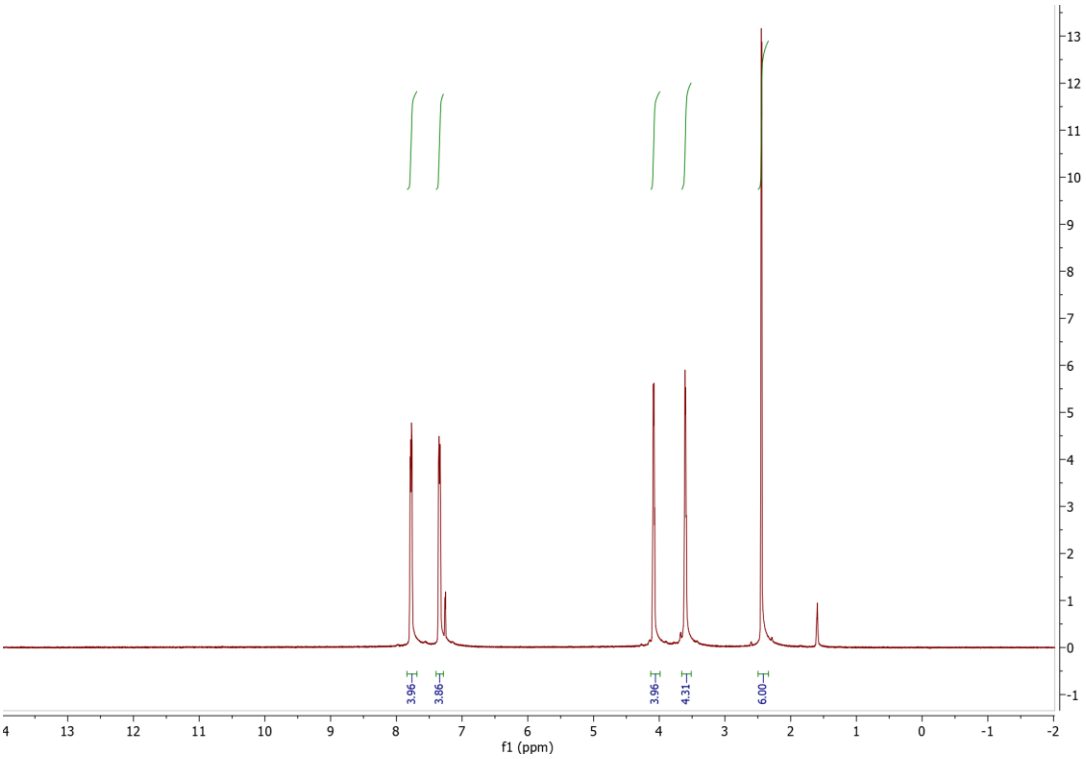

Figure 3-14 ^{1}H, ($CDCl_3$), 400 MHz (**7**)

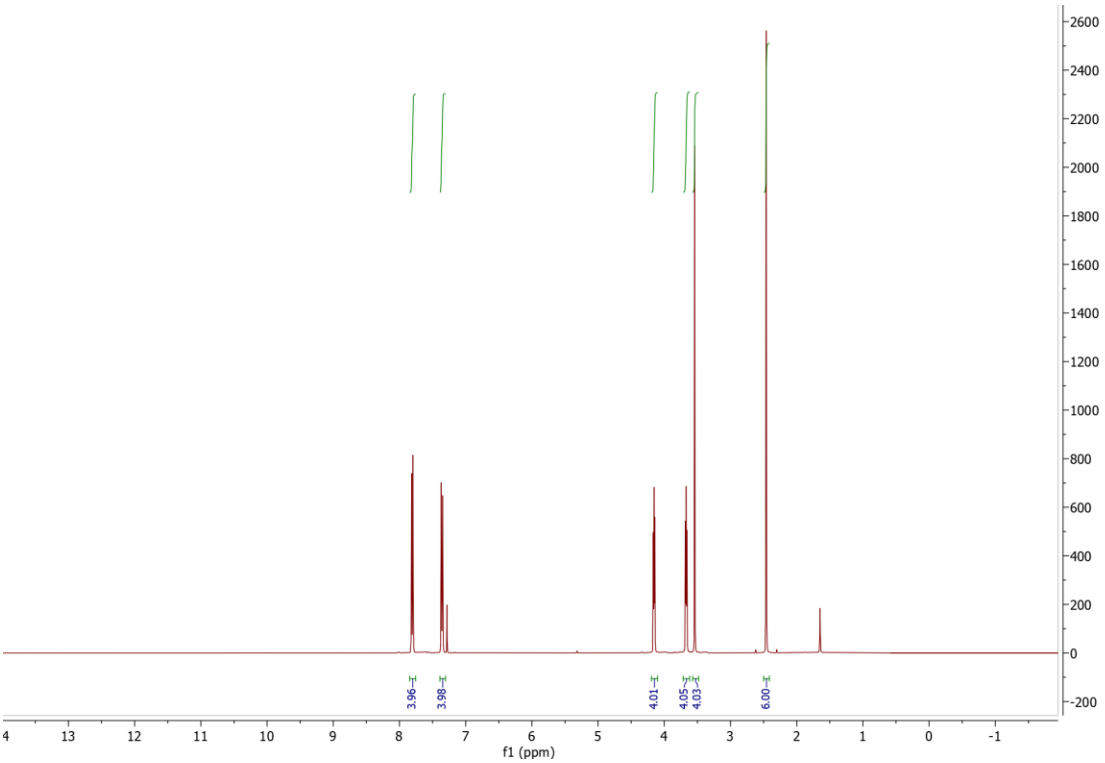

Figure 3-15 ^{1}H, ($CDCl_3$), 400 MHz (**8**)

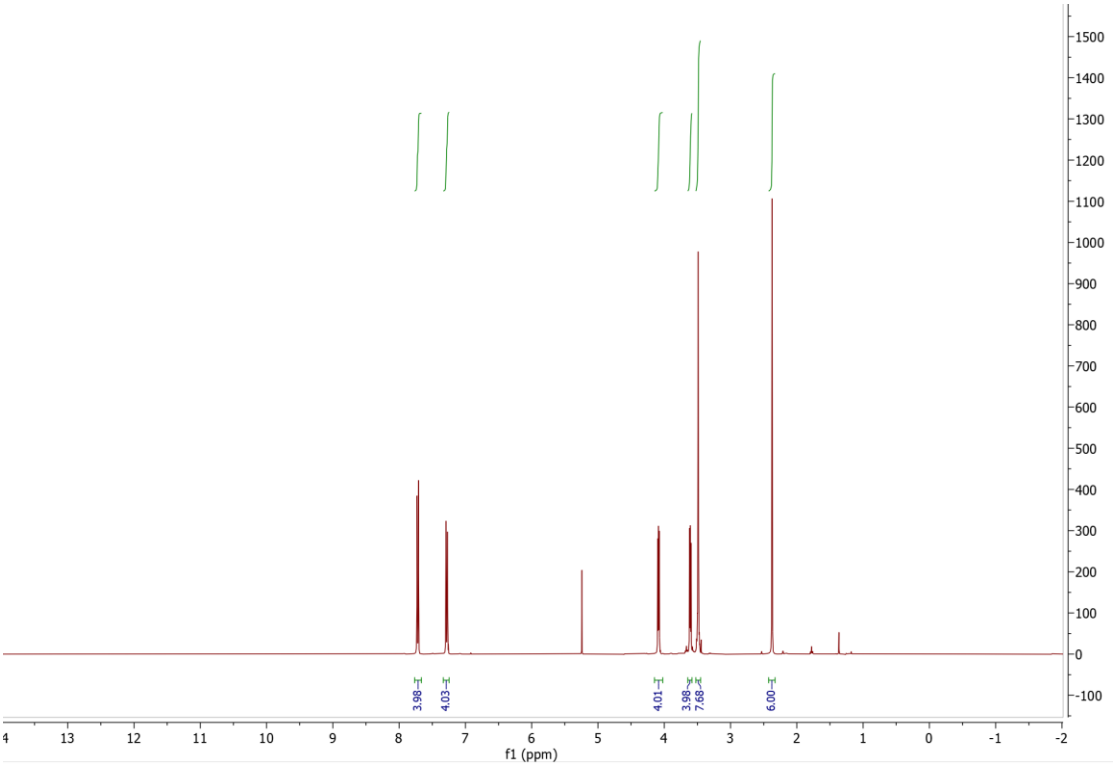

Figure 3-16 ^{1}H, ($CDCl_3$), 400 MHz (**9**)

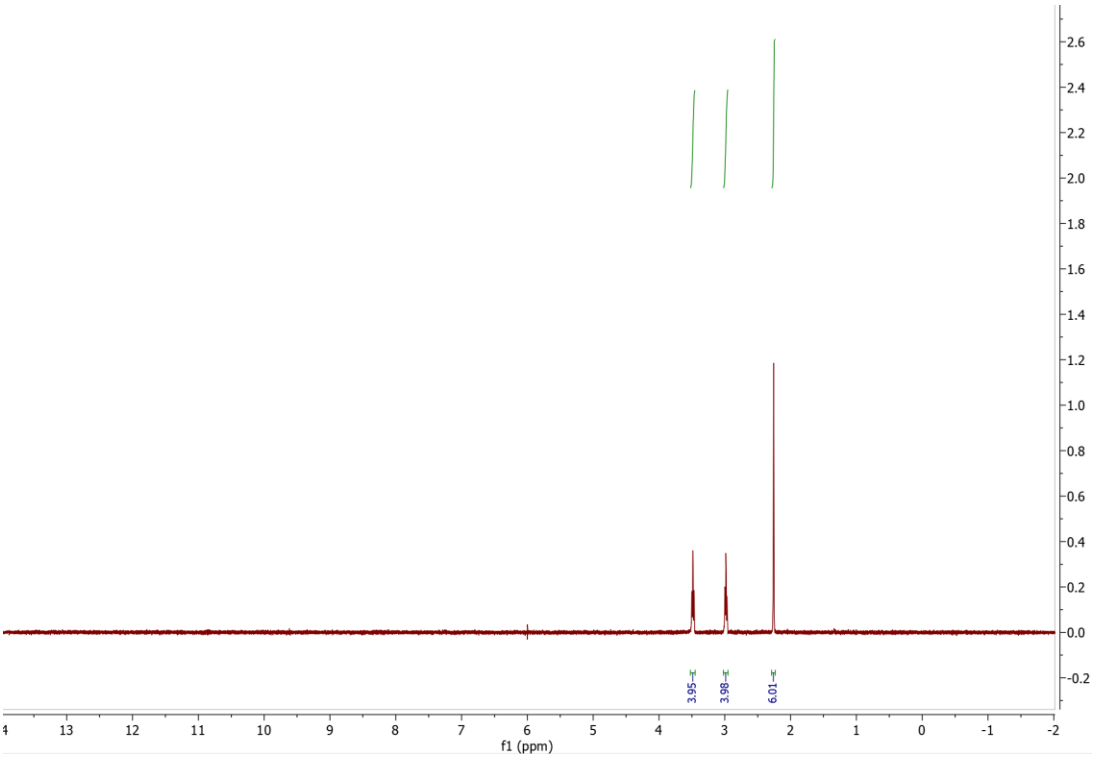

Figure 3-17 ^{1}H, ($CDCl_3$), 400 MHz (**10**)

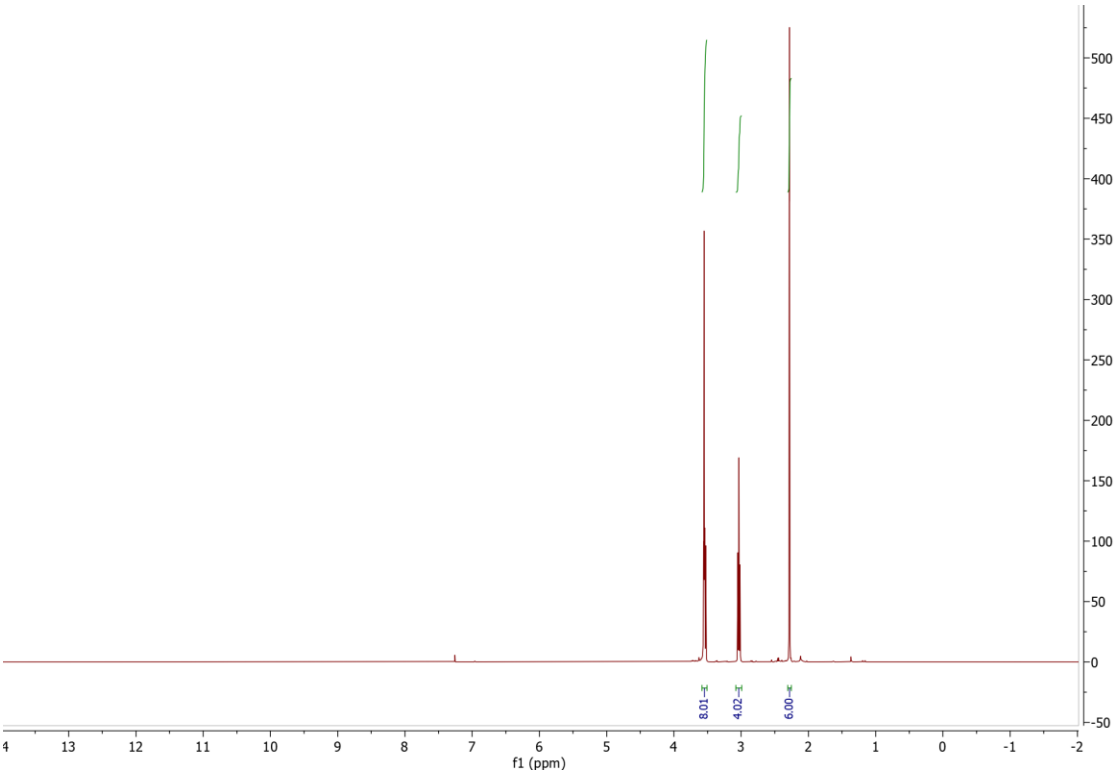

Figure 3-18 ^{1}H, ($CDCl_3$), 400 MHz (**11**)

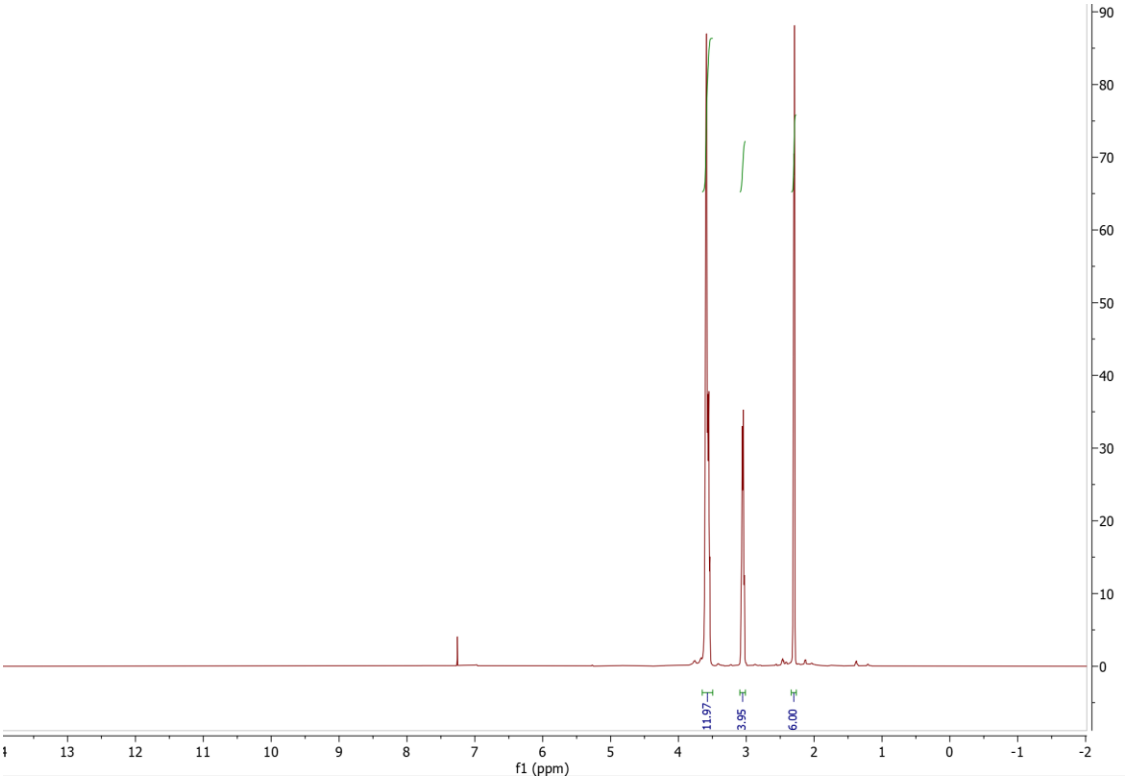

Figure 3-19 ^{1}H, ($CDCl_3$), 400 MHz (**12**)

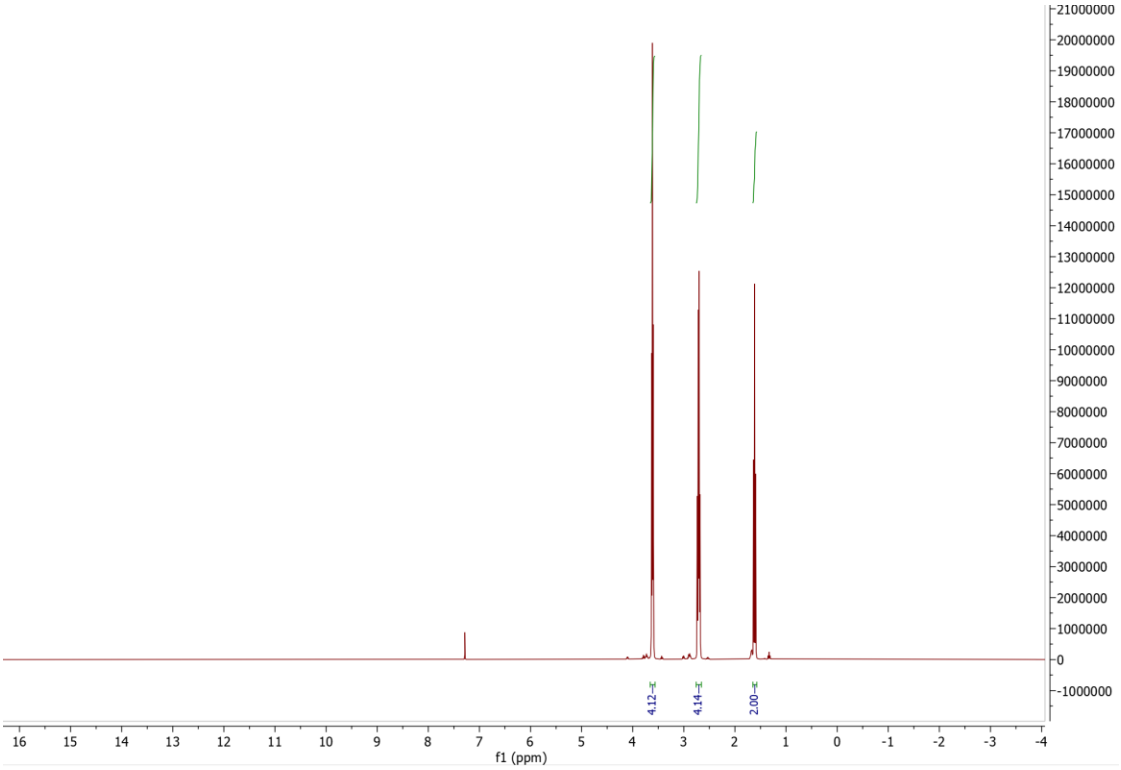

Figure 3-20 ^{1}H, ($CDCl_3$), 400 MHz (**13**)

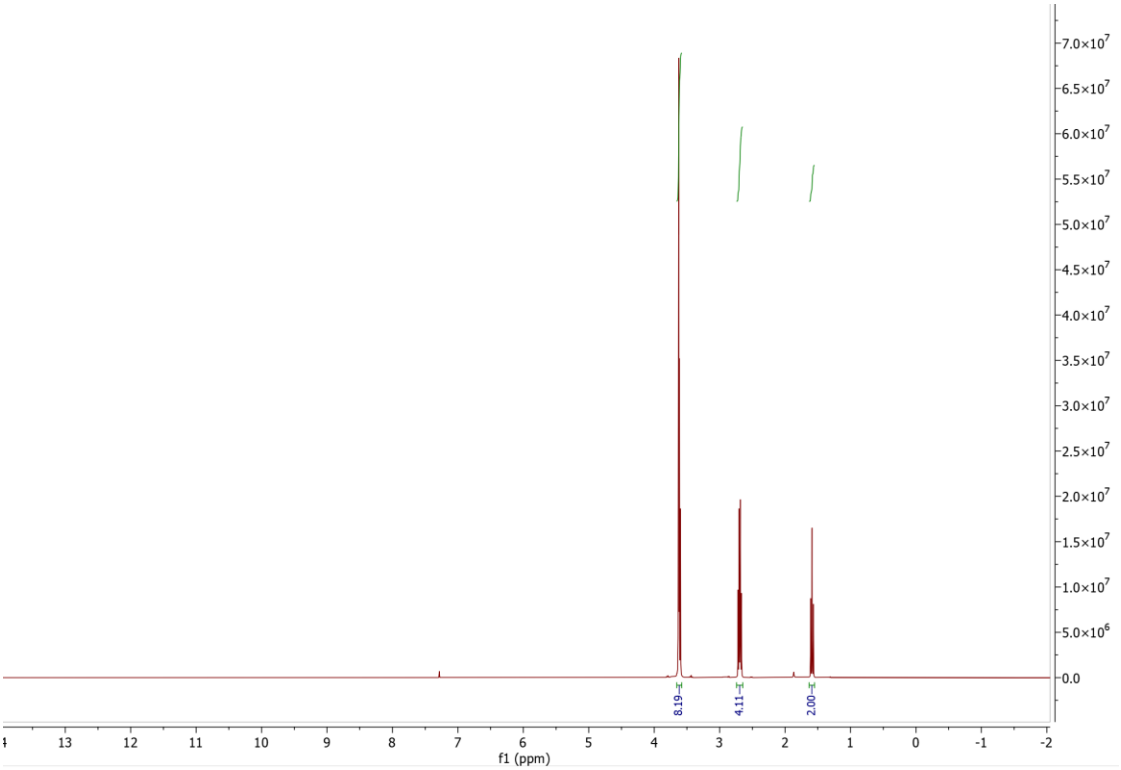

Figure 3-21 ^{1}H, ($CDCl_3$), 400 MHz (**14**)

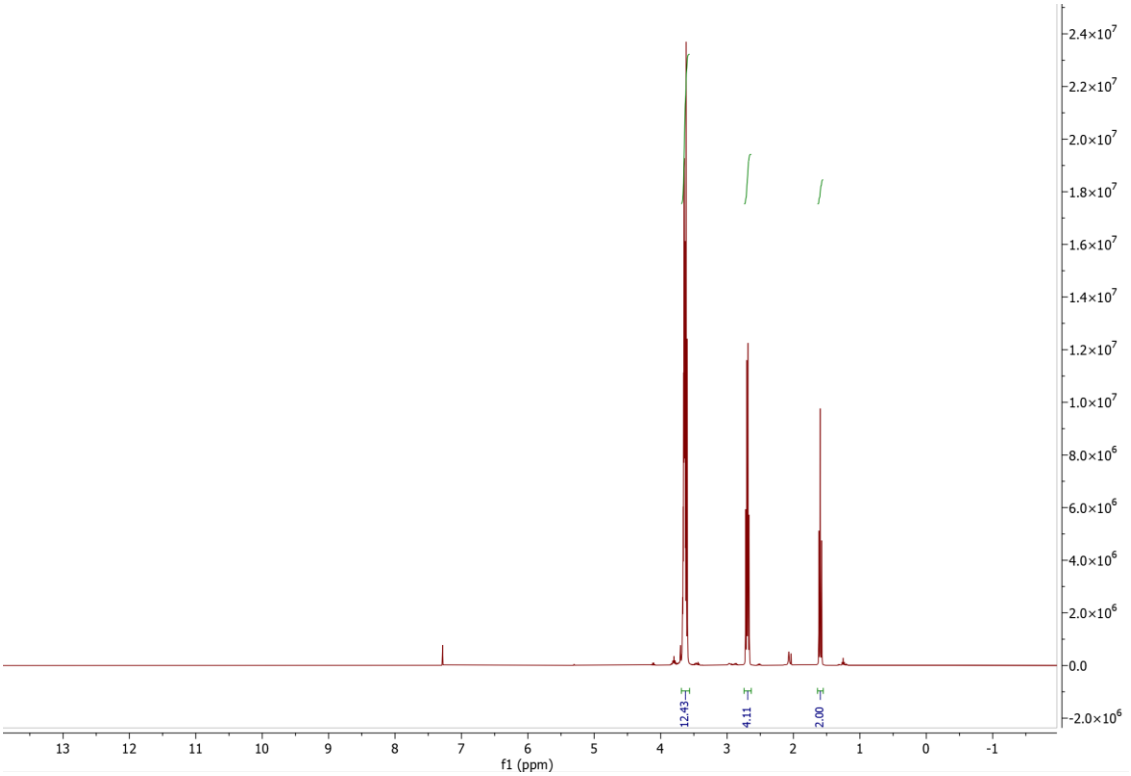

Figure 3-22 ^{1}H, ($CDCl_3$), 400 MHz (**15**)

HPLC Traces

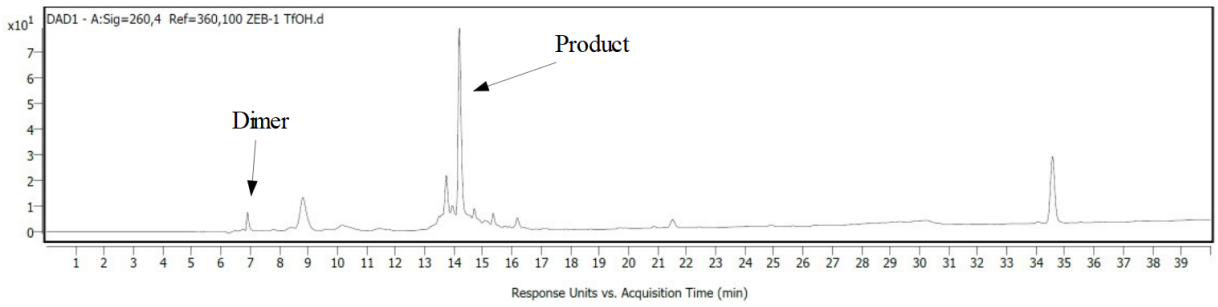

Figure 3-23 HPLC trace for p50, Table 3.1 entry 2

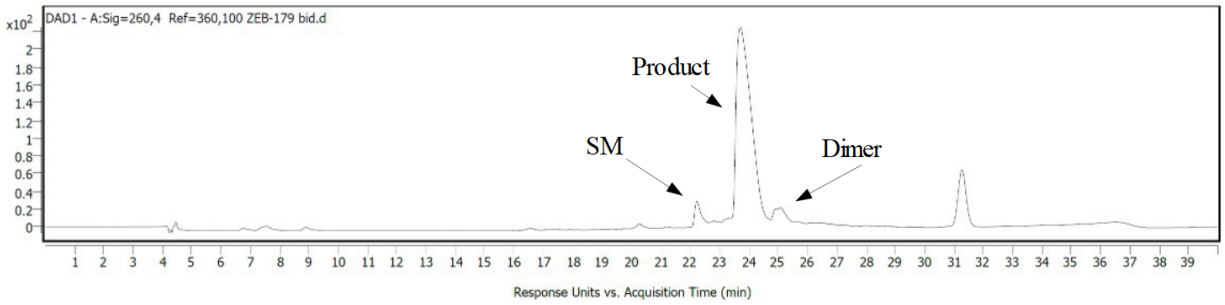

Figure 3-24 HPLC trace for BID, Table 3.1 entry 16

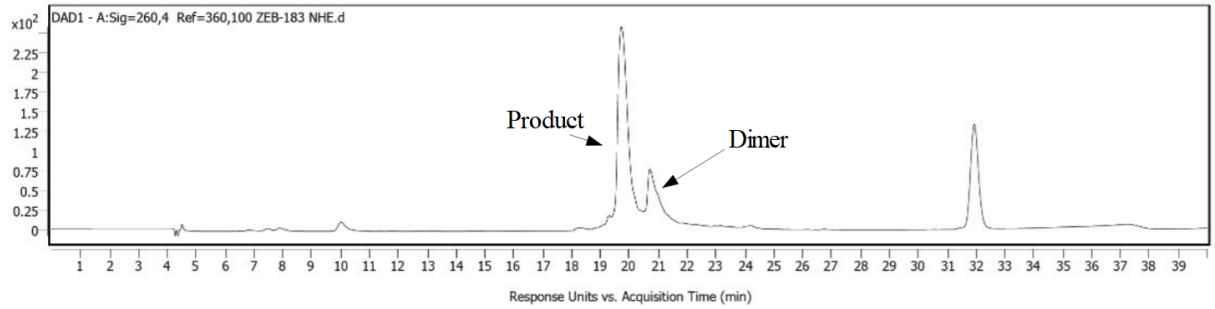

Figure 3-25 HPLC trace for NHE, Table 3.1 entry 19

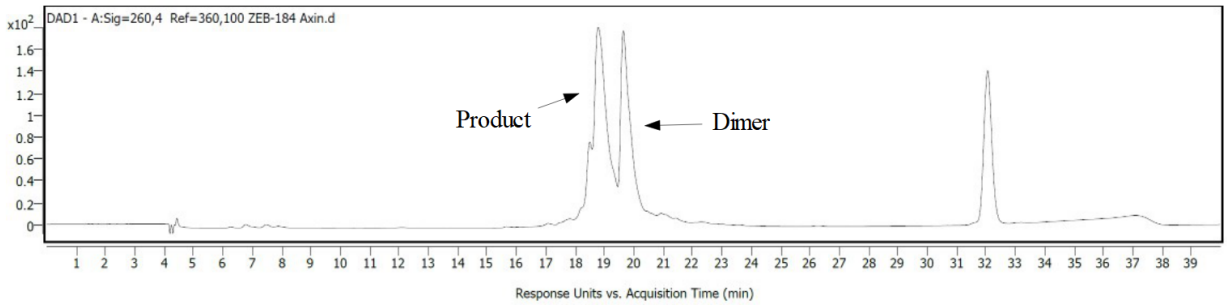

Figure 3-26 HPLC trace for Axin, Table 3.1 entry 20

3.8 Acknowledgements

Chapter 3, in full is currently being prepared for submission for publication of the material. Brown, Z. E.; Elliott, G.; Gustafson, J. L. Peptide Stapling Via Selective Sulfenylation of Tryptophan. The dissertation author was the primary researcher and author of this material.